Roles of α-neurexins in synapse stabilization and Ca^{2+}-dependent endocrine secretion

PhD Thesis

in partial fulfillment of the requirements
for the degree "Doctor of Philosophy (PhD)"
in the Neuroscience Program
at the Georg August University Göttingen,
Faculty of Biology

submitted by

Irina Dudanova

born in

Petrozavodsk, the Russian Federation

2007

Declaration

This thesis has been written independently, with no other sources and aids than quoted, and presents a description of my own work.

Irina Dudanova

Göttingen, March 19, 2007

Table of contents

Abbreviations

ACTH	adrenocorticotrophic hormone
AMPA	α-amino-3-hydroxy-5-methyl-4-isoxazolepropionic acid
bp	base pair
BSA	bovine serum albumine
CA	*Cornu ammonis*, hippocampus
CASK	Ca^{2+}/Calmodulin-dependent serine protein kinase
cDNA	complementary DNA
DAB	diaminobenzidine
DEPC	diethylpyrocarbonate
dH_2O	distilled water
DKO	double knockout
DMEM	Dulbecco's modified Eagle medium
DMSO	dimethylsulfoxide
DNA	deoxyribonucleic acid
dNTP	deoxynucleotide triphosphate
D-PBS	Dulbecco's phosphate-buffered saline
DTT	dithiothreitol
E	embryonic day
E. coli	*Escherichia coli*
EDTA	ethylenediaminetetraacetic acid
EGF	epidermal growth factor
ES cells	embryonic stem cells
FCS	fetal calf serum
FSH	follicle-stimulating hormone
GABA	γ-aminobutyric acid
GAD	glutamic acid decarboxylase
GH	growth hormone
HBSS	Hank's buffer salt solution
HVA	high voltage-activated
IRP	immediately releasable pool
kb	kilobase pair
kDa	kilodalton

KO	knockout
LB medium	Luria-Bertani bacterial growing medium
LB agar	Luria-Bertani bacterial growing agarose
LH	luteinizing hormone
LIF	leukemia inhibitory factor
LNS	Laminin/Neurexin/Sex hormone-binding globulin domain
LTP	long-term potentiation
Mb	Megabase pair
MEF cells	mouse embryonic fibroblasts
MEM	modified Eagle's medium
mEPSC	miniature excitatory postsynaptic current
mIPSC	miniature inhibitory postsynaptic current
MRI	magnetic resonance imaging
α-MSH	α-melanocyte-stimulating hormone
NCAM	neural cell adhesion molecule
NGS	normal goat serum
NMDA	N-methyl-D-aspartate
Nrxn	neurexin
OD	optical density
P	postnatal day
PB	phosphate buffer
PBS	phosphate-buffered saline
PCR	polymerase chain reaction
PDZ	postsynaptic density 95/Discs large/ZO-1 domain
PFA	paraformaldehyde
POMC	proopiomelanocortin
PRL	prolactin
PSD	postsynaptic density
RIM	Rab3-interacting molecule
RNA	ribonucleic acid
RNAi	RNA interference
RT	room temperature
RT-PCR	reverse transcriptase – polymerase chain reaction
SDS	sodium dodecyl sulfate

Sema	semaphorin
SKO	single knockout
SNARE	soluble N-ethylmaleimide-sensitive factor attachment protein receptor
tk	thymidine kinase
TKO	triple knockout
TTH	thyrotrophic hormone
UV	ultraviolet
VGAT	vesicle GABA transporter
VGlu	vesicle glutamate transporter
WT	wild type

1. Introduction

Regulated Ca^{2+}-triggered release of messenger substances represents the basis of several vitally important processes in multicellular organisms. For example, it underlies the extremely fast and highly localized transmission of signals from neurons to other neurons, muscle fibers and endocrine cells. Complex processes like sensation and motor control, as well as higher cognitive functions represent an integrated outcome of this intercellular communication. In addition, the much slower release of hormones and modulatory substances from peptidergic neuronal terminals and from endocrine cells also occurs by Ca^{2+}-triggered exocytosis. These signals are not directed to one specific cell, but act with a longer delay on more remote targets at the level of the surrounding tissue or even the whole organism, controling processes such as growth and homeostasis.

1.1. Synapses are sites of interneuronal communication

Communication between neurons occurs at specialized contacts termed synapses, which are highly elaborate structures equipped with the machinery for fast information transfer. The majority of synapses in the nervous system are of a chemical nature and transmit information in the form of neurotransmitter substances which diffuse through the narrow cleft between the cells.

A typical chemical synapse is a polarized junction consisting of a presynaptic compartment, which harbors mitochondria and numerous small clear-core synaptic vesicles; a postsynaptic compartment with an electron-dense thickening under the membrane; and a thin synaptic cleft which separates the synaptic membranes (Palay 1956) (Fig. 1A). Although the general structure of synaptic contacts has been known for half a century, only recently have we begun to gain insights into their molecular composition and the mechanisms underlying their formation, function and plastic changes.

The presynaptic side of a synapse typically represents an axonal terminal containing neurotransmitter-filled synaptic vesicles and an inventory of proteins involved in their maturation, regulated exocytosis, subsequent endocytosis and recycling (Murthy and De Camilli 2003; Sudhof 2004). The release of neurotransmitter from vesicles is triggered by a Ca^{2+} influx through high voltage-activated (HVA) Ca^{2+} channels, which are opened when the membrane is depolarized by the arrival of an action potential (Katz 1969). The fusion of vesicles occurs at a specialized region of the presynaptic terminal called the active zone, which appears on electron micrographs as an electron-dense structure adjacent to the presynaptic membrane (Gray 1963), and contains protein complexes mediating the docking,

priming and fusion of synaptic vesicles (Rosenmund et al. 2003; Jahn et al. 2003). Neurotransmitter is then released into the synaptic cleft where it can bind to specific receptors at the postsynaptic membrane of the receiving cell, leading to local depolarization and/or activation of signaling pathways. The electron-dense structure adjacent to the postsynaptic membrane, the postsynaptic density (PSD), consists of scaffolding and signaling proteins which anchor neurotransmitter receptors opposite to the release sites and mediate signal transduction in the postsynaptic cell (Kennedy 2000; Boeckers 2006).

For the spatial precision of interneuronal signaling, it is important that the pre- and postsynaptic compartments are tightly coordinated so that the neurotransmitter release machinery and the neurotransmitter receptors are correctly apposed to each other. This close apposition of pre- and postsynaptic membranes has recently been shown to be achieved by cell adhesion molecules which bridge the synaptic cleft and are anchored to scaffolding proteins and the cytoskeleton on both sides of the synapse. Early in development, these molecules are believed to mediate cell recognition and establishment of appropriate synaptic contacts between neurons and their partner cells (Dalva et al. 2007; Piechotta et al. 2006; Waites et al. 2005; Yamagata et al. 2003). Once the initial contacts are established, these molecules induce the coordinated assembly of the pre- and postsynaptic compartments, resulting in a mature junction with precisely aligned synaptic membranes, where the inventory of postsynaptic receptors matches the presynaptic neurotransmitter phenotype. Later in life, synaptic adhesion molecules serve to stabilize mature synapses, on the one hand, and mediate their dynamic changes in the course of synaptic plasticity, on the other.

1.2. Ca^{2+}-triggered exocytosis at synapses and in endocrine cells: Similarities and differences

Regulated Ca^{2+}-dependent exocytosis does not only operate in neurons. Endocrine cells rely on a largely similar mechanism for the release of peptide hormones (Morgan and Burgoyne 1997). In both cases, secretory vesicles undergo sequential maturation steps, including docking and priming, which renders them fusion-competent. In both cell types, the elevation of the Ca^{2+} concentration and its recognition by a Ca^{2+} sensor serves as a trigger for exocytosis, leading to the release of vesicle contents into the extracellular space (Sudhof 2004; Thomas et al. 1990).

However, a number of differences exist between regulated secretion at synapses and in endocrine cells. In the case of synaptic exocytosis, neurotransmitters are typically found in small clear-core vesicles (Fig. 1A). These vesicles dock at the active zone, where Ca^{2+}

channels and proteins of the exocytotic machinery are located in close spatial proximity (Rosenmund et al. 2003). When Ca^{2+} channels open upon membrane depolarization, the Ca^{2+} concentration is rapidly elevated near the entry sites, while the diffusion of Ca^{2+} out of these "microdomains" is largely restricted by intracellular buffers, resulting in a highly inhomogoneous distribution of Ca^{2+} (Neher 1998). Within the microdomains the Ca^{2+} concentration is sufficiently high to trigger vesicle fusion. Due to this tight coupling of Ca^{2+} channels and docking sites at the active zone, neurotransmitter release is very fast and strictly localized, occuring just opposite the postsynaptic receptors clusters (Rosenmund et al. 2003).

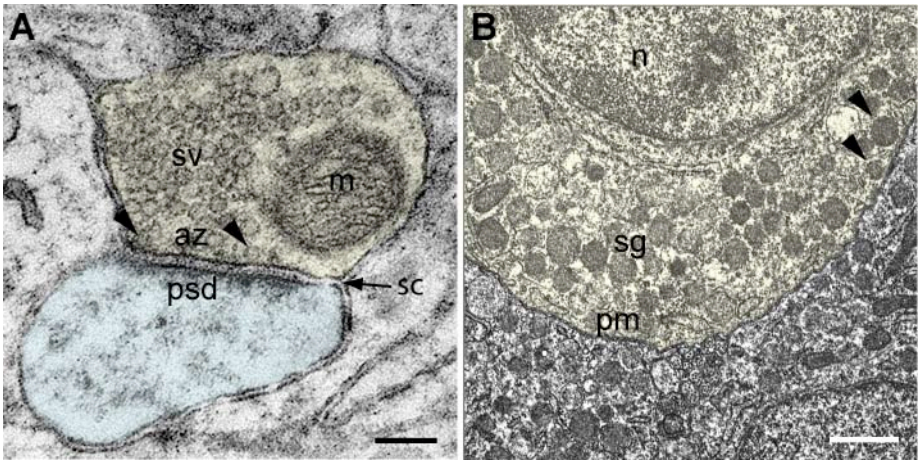

Figure 1. Ultrastructure of a synapse and an endocrine cell. **A**: A synapse consists of a presynaptic terminal (yellow) and a postsynaptic compartment (blue), separated by a narrow synaptic cleft (sc). The presynaptic terminal is filled with small clear-core synapic vesicles (sv), some of which are docked (arrowheads) at the active zone (az). The pre- and postsynaptic membranes are precisely aligned parallel to each other. Opposite the active zone, the postsynaptic density (psd) can be seen as a thickening of the postsynaptic membrane. **B**: An endocrine cell (here a melanotroph from the intermediate lobe of the pituitary gland, yellow) has no postsynaptic partner and no specialized sites for vesicle release. The cytoplasm of the cell is filled with large (note the difference in scale between A and B) electron-dense secretory granules (sg), with some of them docked (arrowheads) at the plasma membrane (pm). The nucleus of the cell can also be seen (n). Scale bars: 100 nm in A, 300 nm in B.

Peptide release, on the other hand, does not require such temporal and spatial precision. Secreted peptides are stored in electron-dense secretory granules, which are much bigger than synaptic vesicles (Fig. 1B). These granules can be docked anywhere along the plasma membrane and require a lower Ca^{2+} concentration for fusion than synaptic vesicles (Thomas et al. 1993b; Heidelberger et al. 1994). The absence of specialized docking sites in endocrine cells explains the slower release kinetics of secretory granules compared to synaptic vesicles, as greater distances between granules and Ca^{2+} channels result in a considerable delay between Ca^{2+} entry and fusion (Klingauf and Neher 1997; Neher 1998).

However, there is some evidence that the sites of fusion are not completely random. For example, simultaneous visualization of Ca^{2+} influx and vesicle fusion by dual-color evanescent field microscopy demonstrated that in endocrine cells the sites of vesicle exocytosis also colocalize with Ca^{2+} entry sites, as granules preferentially dock and undergo fusion within Ca^{2+} microdomains (Becherer et al. 2003). Such findings have led to the notion of "hot spots" of release in endocrine cells. Supposing these preferential sites exist, they still seem to have quite a loose organization, compared to the highly specialized, morphologically distinct structure of the synaptic active zones.

Another difference between synapses and endocrine cells concerns the type of Ca^{2+} currents that trigger release. Ca^{2+} influx at synapses is mostly provided by N- and P/Q-type HVA Ca^{2+} channels, whereas in endocrine cells the relative contribution of Ca^{2+} channels varies considerably depending on the cell type: chromaffin cells largely rely on L-type channels, pancreatic β-cells on L- and P/Q-channels, while in melanotrophs there is no preferential coupling of a particular channel type to secretion (Mansvelder and Kits 2000; Sedej et al. 2004).

These differences acknowledged, the processes of neurotransmitter release from small synaptic vesicles and hormone release from secretory granules are still essentially similar. Importantly, they are mediated by largely the same ensemble of proteins responsible for docking, priming, Ca^{2+} sensing, fusion and modulation of release (Morgan and Burgoyne 1997; Neher 2006). Many proteins of the presynaptic exocytotic apparatus such as syntaxin 1, synaptobrevin 2, SNAP25, synaptotagmin 1, and Munc18 have also been found in the endocrine cells of the pituitary gland, adrenal medulla and pancreatic islets (Jacobsson et al. 1994; Jacobsson and Meister 1996; Marqueze et al. 1995). In most cases, these proteins have conserved functions in both types of release. This makes endocrine cells, with their large size, round shape and amenability to capacitance measurements, a very convenient model for electrophysiological studies addressing the functions of synaptic molecules involved in regulated exocytosis (Rettig and Neher 2002). Such experiments are technically difficult to perform in neurons, and in most cases presynaptic processes can only be studied indirectly, by measuring postsynaptic responses, since the majority of presynaptic endings are too small for electrophysiological measurements. Therefore experiments on endocrine cells have provided many useful insights into the functions of presynaptic proteins.

1.3. Molecular structure and interaction partners of neurexins

Among the various protein families involved in presynaptic functions are neurexins, transmembrane molecules which have been implicated in initiating synapse assembly, promoting synaptic differentiation and regulating exocytosis at synapses. The family of vertebrate neurexin (Nrxn) genes comprises three genes (*Nrxn1*, *Nrxn2* and *Nrxn3*), each of them with two independent promoters, giving rise to the longer α-isoforms and shorter β-isoforms (reviewed in Missler et al. 1998; Missler and Sudhof 1998). These six principal transcripts undergo extensive alternative splicing at several conserved sites (five sites in each α-neurexin and the last two of them in the respective β-neurexin (Fig. 2)), potentially resulting in an enormous variety of protein isoforms with different, though partly overlapping expression patterns in the brain (Rowen et al. 2002; Tabuchi and Sudhof 2002; Ullrich et al. 1995). An *in situ* hybridization study demonstrated, for example, that all six principal isoforms are found in the cortex, but different cortical layers display specific combinations of neurexin variants, e.g., in layer II all isoforms are present, while layer V lacks Nrxn2α, 3α and 1β (Ullrich et al. 1995).

α-Neurexins consist of six extracellular LNS (Laminin/Neurexin/Sex hormone-binding globulin) domains with three epidermal growth factor (EGF)-like sequences interspersed between them. In addition, they contain an O-glycosylation sequence, a single transmembrane region and a short cytoplasmic sequence ending with a C-terminal PDZ-binding motive (Fig. 2). In contrast, β-neurexins have considerably smaller extracellular sequences and contain only the last one of the six LNS domains, preceeded by a stretch of several β-specific amino acids, while their transmembrane and cytoplasmic regions are identical to their respective regions of α-neurexins (Missler and Sudhof 1998; Ushkaryov et al. 1992; 1994).

Neurexins were originally discovered as receptors for α-latrotoxin, a presynaptically acting neurotoxin, which elicits massive neurotransmitter release (Geppert et al. 1992; Ushkaryov et al. 1992; Tzeng et al. 1978). The synaptic localization of neurexins was further supported by immunolabeling experiments (Dean et al. 2003; Ushkaryov et al. 1992) and subcellular fractionation (Butz et al. 1998), and by the phenotype of α-neurexin knockout (KO) mutants, which showed a severe impairment of neurotransmitter release (Missler et al. 2003).

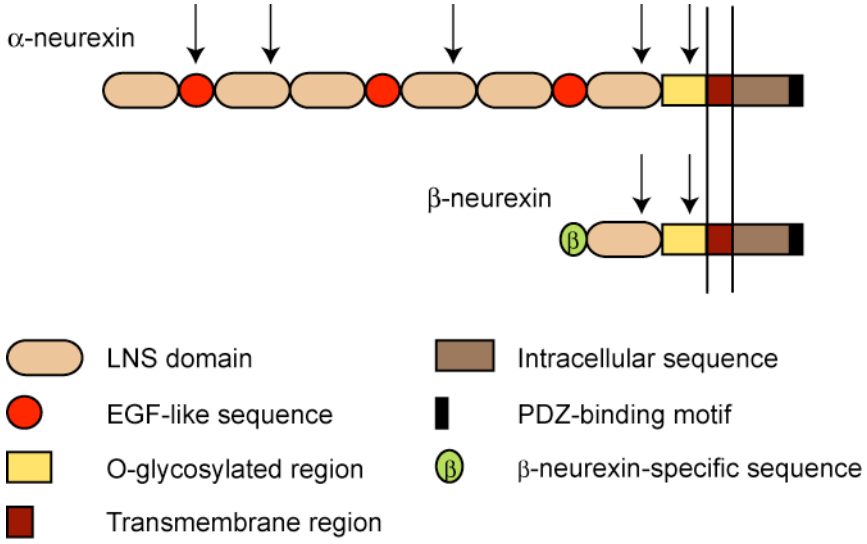

Figure 2. Domain structure of neurexins. α-Neurexins contain 3 extracellular repeats, each comprised of 2 LNS domains and an epidermal growth factor (EGF)-like sequence between them. β-Neurexins contain a short β-specific sequence at the N-terminus and the last one of the LNS domains. The C-terminal part is common to the α- and β-isoforms: The last LNS domain is followed by an O-glycosylation sequence, a transmembrane region and a cytoplasmic tail with a PDZ-binding motif at the end. Arrows mark the location of alternative splice sites.

The endogenous ligands of neurexins include the transmembrane proteins neuroligins and dystroglycan, and the secreted molecules neurexophilins, the latter only binding to α-neurexins (Petrenko et al. 1996; Missler and Sudhof 1998). Similar to neurexins, neuroligins constitute a family of alternatively spliced neuronal transmembrane molecules, but with a postsynaptic localization (Song et al. 1999; Rosales et al. 2005). They were initially discovered as extracellular ligands of β-neurexins, whose binding is dependent on Ca^{2+} (Ichtchenko et al. 1995, 1996). Later Boucard et al. (2005) reported that α-neurexins are also able to interact with neuroligins, though only with particular splice variants. Neuroligins are alternatively spliced at 2 positions (Ichtchenko et al. 1995, 1996), and the pattern of splicing of both neurexins and neuroligins determines the specificity of interactions between the two families (Boucard et al. 2005; Comoletti et al. 2006). Dystroglycan, a transmembrane protein associated with GABAergic synapses (Levi et al. 2002) is another ligand common to α- and β-isoforms, whose binding is also regulated by the alternative splicing of neurexins (Sugita et al. 2001).

At the intracellular side, the C-termini of both α- and β-neurexins interact with the PDZ-domain proteins CASK (Hata et al. 1996) and Mint 1 and 2 (Biederer and Sudhof 2000). An interaction between neurexins and the synaptic vesicle protein synaptotagmin has also been reported (Perin 1994). Both CASK and Mint 1, which are found in a complex with

another PDZ-domain protein Veli (Butz et al. 1998), have binding sites for the pore-forming subunit of N-type Ca^{2+} channels (Maximov et al. 1999). Mint 1 and 2 are also known to bind Munc18-1 (Okamoto and Sudhof 1997), a protein required for synaptic exocytosis, while CASK interacts with the active zone proteins α-liprins (Olsen et al. 2005). Thus, via multiple adaptor proteins neurexins may be connected to both Ca^{2+} channels as well as the vesicle release machinery, therefore representing a potential focus point for coordinating the positioning of Ca^{2+} channels at the active zone.

1.4. Roles of neurexins: From synaptic structure to synaptic function

Based on their receptor-like structure, outstanding variability, synaptic localization and differential distribution in the brain, neurexins were proposed to function as synaptic cell adhesion/recognition molecules, possibly involved in synapse formation (Ushkaryov et al. 1992). Together with their postsynaptic binding partners neuroligins, they have recently attracted much attention as promising candidates for mediating synaptogenesis, due to the heterophilic nature of this complex, which mirrors the asymmetric structure of a synapse, and due to the intracellular interactions of both partners with modular adaptor proteins. While neurexins interact with CASK and Mints, neuroligins bind the postsynaptic scaffolding protein PSD-95, which is known to recruit NMDA and AMPA receptors and K^+ channels to postsynaptic sites (Irie et al. 1997; Kim et al. 1995; Kornau et al. 1995; Leonard et al. 1998). These interactions make the neurexin-neuroligin complex a potential nucleation site for the assembly of the pre- and postsynaptic apparatus. The synaptogenic potential of neurexins and neuroligins has been therefore intensively investigated *in vitro* (Chih et al. 2005, 2006; Dean et al. 2003; Graf et al. 2004; Sara et al. 2005; Scheiffele et al. 2000).

In a co-culture assay first used by Scheiffele and colleagues (2000), neuroligins presented on the surface of non-neuronal cells instigated the clustering of synapsin and the accumulation of synaptic vesicles in overlying axons. Neuroligin-induced terminals had a typical presynaptic ultrastructure and displayed neurotransmitter release and vesicle recycling (Fu et al. 2003; Scheiffele et al. 2000). This synaptogenic activity of neuroligin was shown to depend on the presynaptic β-neurexins (Dean et al. 2003; Scheiffele et al. 2000). Heterologously expressed β-neurexins, in turn, were reported to trigger excitatory and inhibitory postsynaptic differentiation in contacting dendrites via their interaction with neuroligins (Graf et al. 2004; Nam and Chen 2005), implying bidirectional signaling by this transsynaptic complex at both types of synapses. Neurexin-induced postsynaptic sites were equipped with scaffolding molecules and neurotransmitter receptors. In contrast, numerous

other adhesion molecules, such as N-cadherin, EphrinB1, TAG-1, agrin and L1, did not initiate synaptic differentiation when tested in similar co-culture assays (Graf et al. 2004; Nam and Chen 2005; Scheiffele et al. 2000).

Neuroligins were also reported to act as potent synapse inducers in neuronal cultures, where they significantly increased the number and size of synaptic contacts when mildly overexpressed (Chih et al. 2005; Prange et al. 2004; Sara et al. 2005). In contrast, a high degree of neuroligin overexpression caused disruption of synaptic contacts and reduced synaptic activity, presumably by sequestering other synaptic proteins at nonsynaptic sites (Graf et al. 2004). RNAi knockdown of neuroligins also reduced the number of synapses formed between neurons and led to a decrease of synaptic activity (Chih et al. 2005). In addition, evidence has emerged for a role of neuroligins and their intracellular binding partners in determining the balance between the number of excitatory and inhibitory synapses (Prange et al. 2004; Levinson et al. 2005; Levinson and El-Husseini 2005).

In all initial reports about synaptogenic acitivity, only β-neurexins were considered as binding partners of neuroligins. Then a study by Boucard et al. (2005) described an interaction of α-neurexins with particular splice isoforms of neuroligins. Since α-neurexin molecules contain almost the entire β-neurexin sequences and share common extra- and intracellular interaction partners, it seemed plausible that α-neurexins should show a similar synapse-promoting activity as observed for the β-isoforms *in vitro*. In the same study, overexpression of the α-neurexin-binding isoform of neuroligin 1 in neurons resulted in the strengthening and enlargement of synaptic contacts, without a significant increase in their number (Boucard et al. 2005). Furthermore, Chih et al. (2006) observed *de novo* formation of synapses triggered by heterologously expressed α-neurexins. In addition, based on the activity of different isoforms in the co-culture assay and on blocking experiments with soluble neurexins, the authors suggested a functional specialization of neurexin isoforms. Thus, expression in COS cells of α-variants and β-variants with an insert in splice site 4 resulted exclusively in the induction of GABAergic synapses in contacting neurons, and these neurexin isoforms were therefore proposed to be inhibitory synapse-specific. Insert 4-negative β-neurexin, on the other hand, proved capable of inducing both types of synaptic specializations (Chih et al. 2006). Since these functionally distinct isoforms of neurexins were shown to interact with particular neuroligin splice isoforms (Boucard et al. 2005), which are also preferably localized at excitatory or inhibitory synapses (Chih et al. 2006), this has given rise to a hypothesis about a neurexin-neuroligin splice code for determining synapse-type

differentiation, a surprising scenario in view of the wide and overlapping expression patterns of α- and β-isoforms in both excitatory and inhibitory neurons (Ullrich et al. 1995).

Along this line, it should be noted that the phenomena observed in cell culture might not truly represent the physiological processes occuring *in vivo*. The role of neuroligins in promoting synapse formation was recently called into question by the findings in neuroligin KO mice. Mutants lacking multiple neuroligin genes show very subtle changes in the ratio of inhibitory vs. excitatory synapses without any reduction in the total number of contacts, and display much more pronounced defects in synaptic transmission (Varoqueaux et al. 2006).

In addition to the proposed function of both α- and β-neurexins in synaptogenesis, a specific role for α-isoforms in synaptic vesicle exocytosis was revealed by the analysis of α-neurexin KO mice (Missler et al. 2003). Animals deficient in multiple α-neurexins display very poor survival rates: all triple knockout (TKO) and most of the double knockout (DKO) mutants die early postnatally from a respiratory dysfunction. Only 5-10% of neurexin 1α/2α DKOs and ~40% of neurexin 2α/3α DKOs (DKO1/2 and DKO2/3, respectively) reach the age of 1 month (Fig. 3A). The few surviving DKOs mice are hypomorphic, their body weight reaching only ~60% of littermate controls (Fig. 3B).

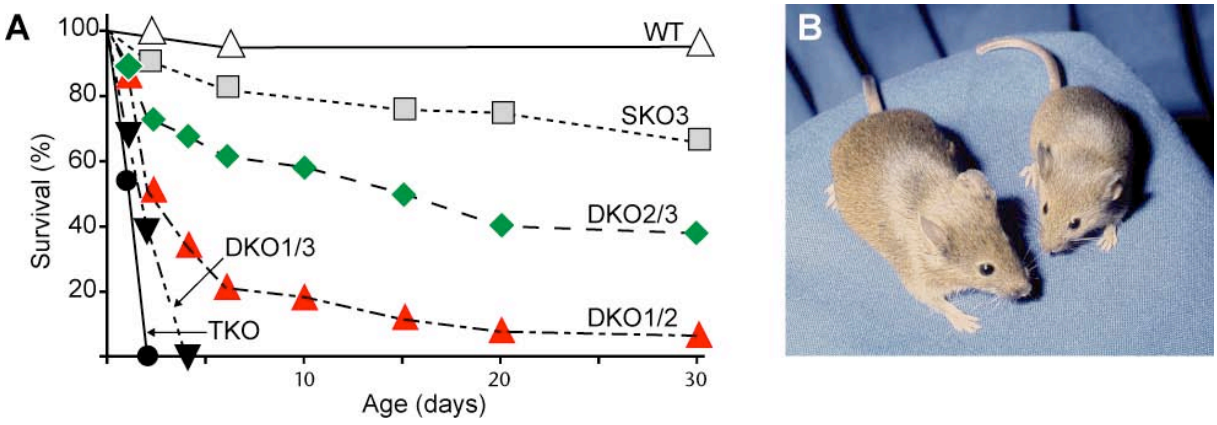

Figure 3. Deletion of α-neurexins causes impaired survival rates and hypomorphic phenotype of the mutants. **A**: Survival plot of α-neurexin knockout mutants. All TKOs (black circles) die within several hours after birth, and all neurexin 1α/3α DKOs (DKO1/3, black triangles) perish within a few days. Only ~5-10% of DKO1/2 mice (red triangles) and ~40% of DKO2/3 mice (green diamonds) reach the age of 1 month. Even the survival of 3α SKO mice (SKO3, grey squares) is significantly decreased as compared to wild type (WT, white triangles). *Adapted from Missler et al. 2003*. **B**: Hypomorphic phenotype of α-neurexin mutants. Adult DKO mice (right) are significantly smaller in size than their SKO littermates. The photo was made by M. Missler.

The most prominent feature of the KO phenotype is the severely reduced spontaneous and evoked neurotransmitter release, observed at both excitatory and inhibitory synapses. Based on the weaker effect of HVA Ca^{2+} channel blockers, notably N-type-specific toxins, on synaptic transmission in the KOs, and on the reduced whole-cell HVA Ca^{2+} currents measured in the brainstem neurons, it was proposed that the impaired activity of HVA Ca^{2+} channels underlies the decrease in neurotransmitter release in α-neurexin mutants. In addition to the presynaptic defect, a reduced ratio of NMDA/AMPA receptor-mediated currents was observed in the mutant cortical neurons (Kattenstroth et al. 2004). In spite of the dramatic functional impairments, light microscopic analysis of brain structure in the KOs did not reveal any obvious alterations. An electron microscopic study demonstrated normal synaptic ultrastructure and an ~50% decrease in the density of type II (presumably inhibitory) synapses in newborn TKO mice (Missler et al. 2003).

Transgenic expression of Nrxn1α on the null mutant background resulted in partial rescue of the neurotransmission deficit and of N- and P/Q-type Ca^{2+} channel activity, demonstrating functional redundancy of α-neurexin isoforms and further suggesting a selective regulation of these Ca^{2+} channel types by α-neurexins. In contrast, expression of Nrxn1β could not rescue the KO phenotype, pointing to the importance of the α-neurexin-specific extracellular sequences, not present in the β-isoforms, for regulating synaptic vesicle exocytosis (Zhang et al. 2005). At the peripheral neuromuscular synapse, the deletion of α-neurexins resulted in impaired neurotransmission and disturbed Ca^{2+}-dependent homeostasis. In addition, minor structural changes were found at some of the junctions in adult DKO mice, which were most likely a long-term consequence of the functional defects (Sons et al. 2006). Taken together, the findings in KO animals established the essential and unique role of α-neurexins in the exocytosis of synaptic vesicles.

It is worth noting that mutations in neuroligin and neurexin genes have been found in a number of patients with autism spectrum disorders (Jamain et al. 2003; Laumonnier et al. 2004; Feng et al. 2006; Szatmari et al. 2007), supporting the role of these proteins in normal brain function. Furthermore, there is evidence that autism-related diseases may arise from imbalance between excitation and inhibition, consistent with a role of the neurexin-neuroligin complex in the pathogenesis of these disorders (Polleux and Lauder 2004).

1.5. Objectives of the study

While α-neurexins do not greatly influence the initial brain assembly (Missler et al. 2003), an involvement of these molecules in shaping brain structure at later developmental stages

remained a possibility. Furthermore, *in vitro* data also suggested a more prominent role for α-neurexins in synaptogenesis. In order to assess the contribution of α-neurexins to the formation and long-term maintenance of synapses *in vivo*, here I performed an extensive morphological analysis of the brains of adult α-neurexin mutants. Because of the premature death of the TKO animals, we focused on the surviving group of DKO1/2 and DKO2/3 mutants, which reach an adult age.

In addition, while neurexins are clearly essential for neurotransmitter release at synapses, it remained unclear whether they play a similar role in endocrine release, where the basic components of the synaptic exocytotic machinery are also engaged (Morgan and Burgoyne 1997; Rettig and Neher 2002). To test if α-neurexins belong to the general players in different types of Ca^{2+}-triggered release, and to get further insights into the mechanism of their action, we investigated the expression of neurexins and the consequences of their deletion in the endocrine cells of the pituitary gland.

2. Materials and Methods

2.1. Materials

2.1.1. Solutions for morphological methods

Phosphate buffer (PB), pH 7.4 (for 1 L)

196 ml 0.2 M NaH_2PO_4, 804 ml 0.2 M Na_2HPO_4

Phosphate-buffered saline (PBS)

0.1 M PB, 0.9% NaCl

4% Paraformaldehyde (PFA) in 0.1 M PB

8 g Paraformaldehyde in 100 ml dH_2O was heated to 60°C whilst stirring, and 1-2 drops of concentrated NaOH were added. Once clear, the solution was mixed with 100 ml 0.2 M PB, filtered and stored at 4°C for up to 1 week.

2.5% PFA, 2.5% glutaraldehyde in 0.1 M PB (for 300 ml)

7.5 g PFA in 120 ml dH_2O was heated to 60°C whilst stirring, and 2 drops of concentrated NaOH were added. Once clear, the solution was allowed to cool down, then mixed with 30 ml 25% glutaraldehyde and 150 ml 0.2 M PB and filtered.

25% Sucrose

50 g Sucrose was dissolved in 100 ml dH_2O, then mixed with 100 ml 0.2 M PB and stored at 4°C.

Cresyl violet solution

0.1% cresyl violet in 1% glacial acetic acid in dH_2O

Eosin solution

0.1% Eosin, 0.16% glacial acetic acid in dH_2O. The solution was filtered before use.

Lead citrate

0.01g Lead citrate in 10 ml dH_2O, 100μl 10N NaOH

2.1.2. Solutions and media for molecular biology

TAE buffer 50x (for 1 L)

242.28 g Tris, 18.61 g EDTA·Na_2, 40 ml acetic acid, pH 8.5

10x DNA loading buffer

100 mM Tris (pH 8.0), 10 mM EDTA (pH 8.0), 57% glycerol, bromophenol blue

LB medium

20 g LB broth base powder (1% SELECT peptone 140, 0.5% SELECT yeast extract, 0.5% NaCl) was dissolved in 1 L dH_2O, autoclaved and kept at room temperature.

LB agar plates

32 g LB agar powder (1% SELECT peptone 140, 0.5% SELECT yeast extract, 0.5% NaCl, 1.2% SELECT agar) was dissolved in 1 L dH_2O and autoclaved. The solution was allowed to cool while stirring until hand-warm, then Ampicillin was added to 50 μg/ml final concentration, and the mixture was poured into 100 mm plates. After agar became solid, the plates were stored at 4°C.

STET buffer

8% sucrose, 0.5% Triton X100, 10 mM Tris pH 8.0, 50 mM EDTA

TE buffer

10 mM Tris (pH 8.0), 1 mM EDTA (pH 8.0)

DEPC water

1 ml Diethylpyrocarbonate was dissolved in 1 L dH_2O, and the mixture was autoclaved.

<u>For Southern blot and colony hybridization</u>

Denaturing buffer

1.5 M NaCl, 0.5 M NaOH

Neutralizing buffer

1.5 M NaCl, 1 M Tris

20x SSC buffer

0.3 M Trisodium citrate dihydrate, 3 M NaCl, pH 7.0 with HCl

20x SSPE buffer

3 M NaCl, 0.2 M NaH_2PO_4-H_2O, 0.02 M EDTA, pH 7.0-7.4

2.1.3. Solutions and media for embryonic stem (ES) cell culture

DMEM

13.38 g DMEM powder, 2.3 g $NaHCO_3$, 1.08 L cell culture grade H_2O. The solution was filtered and stored in 500 ml bottles at 4°C for up to 2 weeks.

Complete ES cell medium

500 ml	DMEM
95 ml	FCS
6 ml	MEM non-essential amino acids
6 ml	β-mercaptoethanol solution (7 µl β-mercaptoethanol in 10 ml PBS)
6.6 ml	penicillin (5000 u/ml)/streptomycin (5000 µg/ml)
63 µl	LIF stock (ESGRO) 10^7 units

The medium was stored at 4°C for up to 1 week.

2x Freezing medium

30 ml complete ES cell medium, 10 ml FCS, 10 ml DMSO. The solution was filtered and stored in aliquots at -20°C.

Lysis buffer

10 mM Tris, pH 7.5, 10 mM EDTA, 10 mM NaCl, 0.5% N-lauroylsarcosine. Proteinase K was added to a final concentration of 1 mg/ml just before use.

2.1.4. DNA material

2.1.4.1. Vectors

pBluescript II SK	Stratagene, La Jolla, California, USA
pcDNA5/FRT	Invitrogen, Groningen, the Netherlands

pFRT/LacZeo	Invitrogen, Groningen, the Netherlands
pTKNeoLox	Kindly provided by Dr. T.C. Südhof, UTSW, Dallas, Texas, USA

2.1.4.2. Genomic clones

pmNx1-5c	Genomic clone of the 3' end of the mouse *Nrxn1* gene, cloned into the pBluescript vector. Contains the last coding exon (exon 24) of *Nrxn1*. From mouse SV129 genomic library, Stratagene, La Jolla, California, USA
pmNx1-8a	Genomic clone of the 3' end of the mouse *Nrxn1* gene, cloned into the pBluescript vector. Contains exon 21 of the *Nrxn1* gene. From mouse SV129 genomic library, Stratagene, La Jolla, California, USA
Nrxn1-5' targeting vector	Conditional knockout vector, containing exon 1 of the *Nrxn1* gene with the surrounding intronic sequences, a Neomycin resistance gene, a 2x*tk* cassette, and two LoxP sites for excision of exon 1 and the Neomycin gene by Cre-mediated recombination. Generated in the laboratory by M. Ahmad
Nrxn1-3'Neo targeing vector	Conditional knockout vector, containing exon 24 of the *Nrxn1* gene with the surrounding intronic sequences, a Neomycin resistance gene, a 2x*tk* cassette, and LoxP sites flanking the Neomycin gene. Generated in the laboratory during my lab rotation

2.1.4.3. Oligonucleotides for RT-PCR

Isoform-specific PCR primers for *RT-PCR* (designed by M. Ahmad) were placed in exons 8 and 9 for α-neurexins, and in the β-specific exon and the following exon for β-neurexins (exon 18 for Nrxn1β and exon 17 for Nrxn2β and 3β) (exon numbering according to Tabuchi and Sudhof (2002)).

Primer number	Primer sequence (5'→3')	Amplified cDNA
MM04-38	CCACAACGGGCTACACGCAAGAAG	Nrxn1α
MM04-39	CAGGATGAGGCCATTTGGCTCCG	
MM04-40	CTACCTTCTGCTGGACATGGGCTCC	Nrxn2α
MM04-41	CAGAAAGGAGCAACGCCCACAGCC	
MM04-42	GCACCATCAAAGTGAAGGCCACTC	Nrxn3α
MM04-43	CTGCTTGGCGCTCATGCGTGAAC	
MM04-44	CTGATCTGGATAGTCCCGCTCACC	Nrxn1β
MM04-45	GTGCAGCTCCAGGTAGTCACCCAG	

MM04-46	GTCTCGTCCAGCCTCAGCACCACC	Nrxn2β
MM04-47	CTCACGATGGCGTTGGGCTCATC	
MM04-48	CTCCGGGATCTCACTCTCAGCAGG	Nrxn3β
MM04-49	GTGAAGCTGGAGGAAGTCGCCAAG	
MM04-50	GCTGCCCCTATCACCACTGTTG	Synaptotagmin 1 (positive control)
MM04-51	GGGCTCCTCCTTTTCTTCTCCACT	

For *real-time PCR*, different pairs of primers were designed that were located in the same exons, but closer together in order to achieve a higher efficiency of amplification.

Primer number	Primer sequence (5'→3')	Amplified cDNA
MM04-38	CCACAACGGGCTACACGCAAGAAG	Nrxn1α
MM05-11	GCAAGTCGCGATAATTCCAGCCT	
MM04-40	CTACCTTCTGCTGGACATGGGCTCC	Nrxn2α
MM05-12	GCGTGCTGCGGCTGTTCACA	
MM04-42	GCACCATCAAAGTGAAGGCCACTC	Nrxn3α
MM05-13	GCCCAGATACATGTCCCCCTCCA	
MM05-14	CCATGGCAGCAGCAAGCATCATTCA	Nrxn1β
MM05-15	CGTGTACTGGGGCGGTCATTGGGA	
MM04-46	GTCTCGTCCAGCCTCAGCACCACC	Nrxn2β
MM05-16	CGTGTCATGGGCCGGTCATTGGGA	
MM04-48	CTCCGGGATCTCACTCTCAGCAGG	Nrxn3β
MM05-17	GATGAGGCCACCGCTTTTCCCAA	
MM05-03	CGTGCGTGACATCAAAGAGAAGCTG	β-actin (reference gene)
MM05-04	GGATGCCACAGGATTCCATACCCAAG	

2.1.4.4. Newly generated constructs

Neurexin 1 3'-targeting vector containing exon 24 (Nrxn1-3'Hygro)

The vector was designed to include the last exon of the *Nrxn1* gene (exon 24 according to exon numbering by Tabuchi and Sudhof (2002)), and the intronic sequences around it, which amounted to 6.2 kb genomic DNA from the genomic clone pmNx1-5c. The vector was constructed by replacing a Hygromycin for the Neomycin resistance gene in the Nrxn1-3'Neo targeting vector, which had been constructed earlier during my lab rotation and already contained the genomic sequences, as well as two LoxP sites on both sides of the resistance

gene to allow for Cre-mediated recombination, and a 2x*tk* cassette for negative selection against randon integration.

The Xba I – Sal I fragment of pcDNA5/FRT, containing the Hygromycin cassette and polyA region, was inserted into Xba I, Sal I sites of pBluescript for site-directed mutagenesis. The insertion was checked with an Nde I – Xba I digestion.

Sgf I site in the Hygromycin cassette was destroyed by site-directed mutagenesis. The mutated Hygromycin cassette with the polyA sequence was then taken out with Xba I, Apa I and inserted into the same sites of pFRT/LacZeo, downstream of the P_{SV40} promoter. The insertion was tested by an analytical digestion with Nde I.

The fragment containing the P_{SV40} promoter, Hygromycin resistance gene and polyA sequence was amplified by PCR, adding an Sgf I site at the 5' end and a loxP site and BamH I site at the 3' end. The PCR product was cloned into Sgf I, BamH I sites of pTKNeoLox, replacing the Neomycin cassette with the Hygromycin one. The final construct was confirmed by Xba I restriction digestion and by sequencing.

Neurexin 1 3'-targeting vector containing exon 21 (Nrxn1-3'Hygro (21))

The vector contained 6.2 kb genomic DNA, including exon 21 of the *Nrxn1* gene and the intronic sequences upstream and downstream of it. It was constructed by inserting the whole genomic fragment into the pTKNeoLox plasmid, which led to the loss of the Neomycin cassette and LoxP sites, and then introducing the Hygromycin resistance gene flanked by LoxP sites between the two homology arms.

The Spe I – Spe I fragment of pmNx1-8a genomic clone was ligated into Spe I, Nhe I sites of pTKNeoLox, taking advantage of the compatible ends of Spe I and Nhe I digestion sites. Colonies were screened by colony hybridization with the Sac I – EcoR I probe. Orientation of the insert was tested by an analytical digestion with BamH I and Cla I.

The Hygromycin resistance cassette (1.8 kb) was PCR-amplified from the Nrxn1-3'Hygro vector (see above), adding Nhe I and LoxP sites at the 5' end, and LoxP and Nhe I sites at the 3' end. The PCR fragment was ligated into Nhe I site in the genomic sequence. The orientation of the insert was checked with a BamH I digestion.

2.1.5. Eukaryotic cell lines

E14.1	Mouse embryonic stem cells, from male SV/129 mouse embryos. Derived by Prof. Klaus Rajewsky, University of Cologne

MEF, Neomycin resistant	Mouse embryonic fibroblasts. Genome systems, St. Louis, MO, USA
MEF, Hygromycin resistant	Mouse embryonic fibroblasts. Genome systems, St. Louis, MO, USA
DR4 cells	Mouse embryonic fibroblasts, resistant to Hygromycin, Neomycin, Puromycin and HAT; mitotically inactivated. Open Biosystems, Huntsville, AL, USA

2.1.6. Bacterial Strains

Escherichia coli XL1-Blue MRF´	Stratagene, La Jolla, CA, USA
Escherichia coli XL10-Gold	Stratagene, La Jolla, CA, USA

2.1.7. Apparatus

Autoclave	Fedegari, Pavia, Italy
CCD camera 2048x2048 Tietz TemCam 224A	TVIPS, Gauting, Germany
Cell culture hood	Kendro, Asheville, NC, USA
Centrifuges	Eppendorf, Hamburg, Germany; Kendro, Asheville, NC, USA; Beckman Coulter, Krefeld, Germany
Confocal laser scanning microscope LSM 510	Zeiss, Oberkochen, Germany
Diamond knives	Diatome, Biel, Switzerland
Digital camera AxioCam HRc	Zeiss, Oberkochen, Germany
Electron microscope Philips CM 120	Philips Inc., Eindhoven, the Netherlands
Electrophoresis chambers (for DNA)	Amersham Pharmacia Biotech, Little Chalfont, UK
Electrophoresis power supply	Biometra, Göttingen, Germany
Electroporators	Bio-Rad, Hercules, CA, USA
Epifluorescent microscope Axioscope 2	Zeiss, Oberkochen, Germany
Eraser	Raytest, Straubenhardt,Germany

Freezers	Sanyo, Gunma, Japan
Heat block	USA/Scientific Plastics (Europe), Milton Keynes, UK
Ice machine	Scotsman Ice Systems, Vernon Hills, IL, USA
Incubator, for bacterial culture	WTC binder, Tuttlingen, Germany
Incubator shaker, for bacterial culture	New Brunswick Scientific, Edison, NJ, USA
Incubator, for cell culture	Sanyo, Gunma, Japan
Instruments for dissection	Fine Science Tools, Heidelberg, Germany
Ligation chamber	Techne, Cambridge, UK
Magnetic stirring plates	Heidolph, Kelheim, Germany; H+P Labortechnik, Oberschleißheim/München, Germany
Microtome	Leica, Nussloch, Germany
Microwave oven	Bosch, Stuttgart, Germany
Multichannel pipette	Brand, Wertheim/Main, Germany
Oligonucleotide synthesizer	Applied Biosystems, Foster City, CA, USA
PCR machines	Biometra, Göttingen, Germany
Perfusion pump	Bio-Rad, Hercules, CA, USA
pH-meter	WTW-inoLab, Weilheim, Germany
Phosphoimager FLA-3000	Fujifilm, Tokyo, Japan
Pipettes	Brand, Wertheim/Main, Germany; Gilson, Villiers-le-Bel, France
Pipetting device	Brand, Wertheim/Main, Germany
Radioactivity counter	Perkin-Elmer, Boston, MA, USA
Real-time PCR cycler ABI SDS-7000	Applied Biosystems, Foster City, CA, USA
Refrigerators	Sanyo, Gunma, Japan; Liebherr, Biberach an der Riß, Germany
Scales	Sartorius, Göttingen, Germany
Shakers	GFL, Burgwedel, Germany; Heidolph, Kelheim, Germany

Spectrophotometer	Eppendorf, Hamburg, Germany
Sterilization oven	Memmert, Schwabach, Germany
Ultramicrotome	Leica, Nussloch, Germany
UV documentation/ crosslinker	INTAS, Göttingen, Germany
Vibratome	Leica, Nussloch, Germany
Vortexer	IKA, Wilmington, NC, USA
Waterbaths	Julabo, Seelbach, Germany; Lauda, Lauda-Königshofen, Germany

2.1.8. Chemicals for morphological methods

Antifade mounting medium	Molecular probes, Eugene, OR, USA
0.2 M Sodium cacodylate buffer, pH 7	Electron Microscopy Siences, Hatfield, PA, USA
Cresyl violet	Sigma, Taufkirchen, Germany
Cryomatrix embedding medium	Thermo Scientific, Waltham, MA, USA
3,3-Diaminobenzidine (DAB)	Sigma, Taufkirchen, Germany
Diethylether	Roth, Karlsruhe, Germany
Entellan mounting medium	Merck, Darmstadt, Germany
Eosin B	Merck, Darmstadt, Germany
Ethanol for histology	Zentralapotheke der Universität Göttingen, Göttingen, Germany
Glutaraldehyde	Sigma, Taufkirchen, Germany; Electron Microscopy Siences, Hatfield, PA, USA
Hematoxylin solution Gill III	Merck, Darmstadt, Germany
Hydrogene peroxide 30%	Merck, Darmstadt, Germany
Lead citrate	Electron Microscopy Siences, Hatfield, PA, USA
Paraformaldehyde	Merck, Darmstadt, Germany
Poly-L-lysine	Sigma, Taufkirchen, Germany

Toluidine blue	Sigma, Taufkirchen, Germany
Uranyl acetate	Merck, Darmstadt, Germany
Vectashield mounting medium	Axxora Deutschland, Grünberg, Germany
Xylene	Roth, Karlsruhe, Germany

2.1.9. General chemicals

Acetic acid (glacial) 100%	Merck, Darmstadt, Germany
Agarose	Invitrogen, Groningen, The Netherlands
Alkaline phosphatase	Roche, Mannheim, Germany
Ampicillin, sodium salt	Amersham Pharmacia Biotech, Little Chalfont, UK
Bromophenol blue	Amersham Pharmacia Biotech, Little Chalfont, UK
Chloroform	Roth, Karlsruhe, Germany
[α-^{32}P]dCTP	Amersham Pharmacia Biotech, Little Chalfont, UK
Diethylpyrocarbonate (DEPC)	Sigma, Taufkirchen, Germany
Dimethylsulfoxide (DMSO)	Sigma, Taufkirchen, Germany
DNA standard	Roche, Mannheim, Germany
dNTPs	Invitrogen, Groningen, The Netherlands
EDTA·Na_2·$2H_2O$	Amersham Pharmacia Biotech, Little Chalfont, UK
Ethanol for molecular biology	Merck, Darmstadt, Germany
Ethidium bromide	Roche, Mannheim, Germany
Ficoll solution	Amersham Pharmacia Biotech, Little Chalfont, UK
Gelatin	Sigma, Taufkirchen, Germany
Glucose	Sigma, Taufkirchen, Germany
Glycerol	Roth, Karlsruhe, Germany
Hank's buffer salt solution (HBSS)	Invitrogen, Groningen, The Netherlands
Hydrochloric acid	Merck, Darmstadt, Germany

Isopropanol	Roth, Karlsruhe, Germany
Klenow enzyme and buffer	Roche, Mannheim, Germany
Kodak X-Ray developer Lx 24	INTAS, Göttingen, Germany
Kodak X-Ray fixer AL4	INTAS, Göttingen, Germany
LB broth base	Invitrogen, Groningen, The Netherlands
LB agar	Invitrogen, Groningen, The Netherlands
Liberase	Roche, Mannheim, Germany
Lysozyme	Roche, Mannheim, Germany
Magnesium chloride	Merck, Darmstadt, Germany
Magnesium sulfate	Merck, Darmstadt, Germany
Methanol	Roth, Karlsruhe, Germany
Nickel chloride	Merck, Darmstadt, Germany
Normal goat serum (NGS)	Invitrogen, Groningen, The Netherlands
NZY$^+$ broth	Sigma, Taufkirchen, Germany
Phenol/Chloroform/Isoamyl alcohol	Amersham Pharmacia Biotech, Little Chalfont, UK
Proteinase K	Roche, Mannheim, Germany
QuickHyb buffer	Stratagene, La Jolla, CA, USA
Restriction endonucleases, buffers	Roche, Mannheim, Germany; New England Biolabs, Ipswich, MA, USA
RNAzolB	WAK-Chemie, Steinbach, Germany
Sodium acetate	Merck, Darmstadt, Germany
Sodium chloride	Merck, Darmstadt, Germany
Sodium dihydrophosphate	Merck, Darmstadt, Germany
Sodium dodecyl sulfate (SDS)	Amersham Pharmacia Biotech, Little Chalfont, UK
Sodium hydrodiphosphate	Merck, Darmstadt, Germany
Sodium hydroxide	Merck, Darmstadt, Germany
Sucrose	Sigma, Taufkirchen, Germany

SYBR Green PCR Master Mix	Applied Biosystems, Foster City, CA, USA
T4 DNA ligase and buffer	Roche, Mannheim, Germany
Tris	Amersham Pharmacia Biotech, Little Chalfont, UK
Trisodium citrate dihydrate	Calbiochem, San Diego, CA, USA
Triton X100	Eurobio, Paris, France

2.1.10. Chemicals for cell culture

dH_2O cell culture grade	Invitrogen, Groningen, The Netherlands
DMEM powder	Invitrogen, Groningen, The Netherlands
D-PBS	Invitrogen, Groningen, The Netherlands
Fetal calf serum (for ES cell culture)	Hyclone, Logan, UT, USA
Ganciclovir	Sigma, Taufkirchen, Germany
G418 sulfate	Invitrogen, Groningen, The Netherlands
Hygromycin B	Invitrogen, Groningen, The Netherlands
LIF (ESGRO)	Chemicon, Temecula, CA, USA
MEM-non essential amino acids	Invitrogen, Groningen, The Netherlands
Mineral oil	Sigma, Taufkirchen, Germany
Mitomycin C	Sigma, Taufkirchen, Germany
N-Lauroylsarcosine	Sigma, Taufkirchen, Germany
Penicillin/Streptomycin	Invitrogen, Groningen, The Netherlands
Sodium bicarbonate	Invitrogen, Groningen, The Netherlands
Trypsin/EDTA	Invitrogen, Groningen, The Netherlands

2.1.11. Consumables

Blotting paper	Whatman, Maidstone, UK
Cell culture plastic equipment	Corning, Acton, MA, USA

Copper and Nickel hexagonal mesh grids	Electron Microscopy Siences, Hatfield, PA, USA
Electroporation cuvettes, 0.2 cm and 0.4 cm	BioRad, Hercules, CA, USA
Falcon round-bottom tubes (14 ml)	Becton Dickinson, Franklin Lakes, NJ, USA
Filters	Corning, Acton, MA, USA; Sartorius, Göttingen, Germany; Schleicher & Schuell, Dassel, Germany
Glass coverslips	Menzel-Gläser, Braunschweig, Germany
Glass slides	Menzel-Gläser, Braunschweig, Germany
Hybond-XL, Hybond-N nylon membranes	Amersham Pharmacia Biotech, Little Chalfont, UK
Microcentrifuge tubes	Corning, Acton, MA, USA
Micro Spin S-300 Columns	Amersham Pharmacia Biotech, Little Chalfont, UK
Microtome blades	Sakura Finetek, Heppenheim, Germany
Needles	HSW, Tuttlingen, Germany
Optical adhesive covers (for real-time PCR)	Applied Biosystems, Foster City, CA, USA
Parafilm	Roth, Karlsruhe, Germany
Pasteur pipettes	Brand, Wertheim/Main, Germany; Rofa-Mavi, Beverwijk, The Netherlands
Plastic pipettes (1 ml, 5 ml, 10 ml, 25 ml)	Corning, Acton, MA, USA
Pipette tips	Brand, Wertheim/Main, Germany
Pipette filter tips (for PCR)	Brand, Wertheim/Main, Germany
Plastic tubes for bacterial centrifugations	Kendro, Asheville, NC, USA
Plastic tubes, sterile (15 ml, 50 ml)	Corning, Acton, MA, USA
Plates, for bacterial culture	Greiner, Nürtingen, Germany
PCR tubes	Sarstedt, Nümbrecht, Germany
Safe-lock microcentrifuge tubes	Eppendorf, Hamburg, Germany

Scalpels	Brand, Wertheim/Main, Germany
Spectrophotometry cuvettes	Brand, Wertheim/Main, Germany
Syringes	HSW, Tuttlingen, Germany
Ultracentrifuge tubes	Kendro, Asheville, NC, USA
96-well reaction plates (for real-time PCR)	Applied Biosystems, Foster City, CA, USA
X-ray films	Kodak, Rochester, NY, USA

2.1.12. Kits for molecular biology

Expand High Fidelity PCR System	Roche, Mannheim, Germany
Expand Long Template PCR System	Roche, Mannheim, Germany
GeneAmp Gold RNA PCR Core Kit	Applied Biosystems, Foster City, CA, USA
Megaprime Kit	Amersham Pharmacia Biotech, Little Chalfont, UK
Plasmid Maxi Kit	Qiagen, Hilden, Germany
Qiaex II Agarose Gel Extraction Kit	Qiagen, Hilden, Germany
QIAprep Spin Miniprep Kit	Qiagen, Hilden, Germany
QuickChange XL Site-Directed Mutagenesis Kit	Stratagene, La Jolla, CA, USA

2.1.13. Primary antibodies

Adrenocorticotrophic hormone, rabbit	1:20,000	Obtained from Dr. Parlow, NHPP, NIDDK
β-Endorphin, rabbit	1:500	Sigma, St. Louis, MO, USA
Follicle-stimulating hormone, rabbit	1:1000	Obtained from Dr. Parlow, NHPP, NIDDK
GAD65, rabbit	1:1000	Chemicon, Temecula, CA, USA
GAD67, rabbit	1:1000	Chemicon, Temecula, CA, USA

Growth hormone, rabbit	1:30,000	Obtained from Dr. Parlow, NHPP, NIDDK
Luteinizing hormone β-subinit, rabbit	1:20,000	Obtained from Dr. Parlow, NHPP, NIDDK
α-Melanocyte-stimulating hormone, rabbit	1:500	Peninsula Laboratories Inc., Belmont, CA, USA
Oxytocin, rabbit	1:500	Chemicon, Temecula, CA, USA
Parvalbumin, mouse	1:1000	Swant, Bellinzona, Switzerland
Prolactin, rabbit	1:30,000	Obtained from Dr. Parlow, NHPP, NIDDK
Proopiomelanocortin, rabbit	1:500	Phoenix Pharmaceuticals, Belmont, CA, USA
Synapsin EO28, rabbit	1:1000	Kindly provided by Dr. T.C. Südhof, UTSW, Dallas, Texas, USA
Synaptophysin, mouse	1:1000	DAKO, Glostrup, Denmark
Thyrotrophic hormone β-subunit, rabbit	1:3000	Obtained from Dr. Parlow, NHPP, NIDDK
Vasopressin, rabbit	1:500	Chemicon, Temecula, CA, USA
VGlu1, rabbit	1:10,000	Kindly provided by Dr. R. Jahn, MPIbpc, Göttingen, Germany
VGlu2, rabbit	1:1000	Kindly provided by Dr. R. Jahn, MPIbpc, Göttingen, Germany
VGAT, rabbit	1:1000	Synaptic Systems, Göttingen, Germany

2.1.14. Second and third antibodies

Goat-anti-rabbit Alexa Fluor 546	1:400	Molecular Probes, Eugene, OR, USA
Goat-anti-rabbit	1:100	Sternberger Monoclonals Inc., Baltimore, MD, USA
Goat-anti-mouse	1:100	Sternberger Monoclonals Inc., Baltimore, MD, USA
Mouse peroxydase-anti-peroxydase (PAP)	1:500	Sternberger Monoclonals Inc., Baltimore, MD, USA
Rabbit PAP	1:500	Sternberger Monoclonals Inc., Baltimore, MD, USA

2.2. Methods

2.2.1. Morphology

2.2.1.1. Histological analyses

6- to 8-week-old mice were anaesthetized with chloroform and perfused transcardially with PBS followed by 4% PFA in 0.1 PB. The brains or pituitary glands were dissected from the skull, left for 2 hours in 4% PFA to postfix, and cryoprotected by immersion into 25% solution of sucrose in 0.1 M PB overnight. Parts of the brain containing the regions of interest or whole pituitary glands were embedded in Cryomatrix medium and cut on a cryotome into 12-30 μm thick sections. For DAB staining, free-floating sections were collected in PBS. For all other methods, cryosections were thaw-mounted on poly-L-lysine-coated slides.

2.2.1.1.1. Nissl staining

Slides with 25 μm cryosections were immersed into a solution of chloroform:ether:ethanol 7:1:1 for 7-10 min, rehydrated in a series of ethanol dilutions (100%, 90%, 70%, water) and stained with cresyl violet for 5-6 min.

2.2.1.1.2. Hematoxylin-eosin staining

25 μm cryosections were treated with chloroform:ether:ethanol and graded ethanol dilutions as described above and stained with hematoxylin Gill III solution for 3 min, then rinsed very briefly in 0.1% HCl, followed by tap water for 3-5 min, and stained in eosin solution for 7 min.

2.2.1.1.3. DAB staining

30 μm free-floating brain sections were quenched with 10% methanol, 3% H_2O_2 in PBS for 15 min at room temperature (RT), permeabilized with 1% triton in PBS for 15 min and blocked in 50% NGS in PBS for 4 hours at RT. No triton was used when labeling cell bodies with the anti-GAD67 antibody. Sections were incubated with the first antibody diluted in blocking solution overnight at 4°C. Second antibody was applied for 30 min at 37°C, and third antibody for 1 hour at 37°C. The sections were DAB-stained with $NiCl_2$ enhancement (0.01 g DAB, 0.03 g $NiCl_2$, 20 ml PBS and 3.5 μl H_2O_2) for 5-7 min, mounted on gelatin-covered slides and dried at RT for at least 2 days.

After Nissl, hematoxylin-eosin or DAB staining, sections were dehydrated in ethanol solutions of increasing concentrations, cleared in xylene for 5 min, and covered with glass coverslips using Entellan medium.

2.2.1.1.4. Immunofluorescence

12 μm cryosections of the pituitary gland were permeabilized with 0.3% triton in PBS and incubated in blocking solution (5% NGS in PBS) for 1-2 hours at RT. Primary antibodies were applied overnight at 4°C, and secondary antibodies were applied for 45 min at RT. Sections were covered with glass coverslips using Vectashield or Antifade mounting medium.

Sections were examined at the Axioscope 2 epifluorescent microscope, and images were captured with the AxioCam HRc digital camera. Atlas of the mouse brain (Paxinos and Franklin 2001) was used for delineation of the areas of interest. Morphometric measurements were performed using AxioVision software (Zeiss, Oberkochen, Germany). Overviews of the brain (Fig. 5A-D) and pituitary gland (Fig. 13-16, 19) were composed of 40-50 and 4-8 individual images, respectively, using Adobe Photoshop SC. Contrast and brightness of the images were adjusted in Adobe Photoshop SC. Figures were assembled in Adobe Illustrator SC.

2.2.1.2. Electron microscopy

For *brain* fixation, mice were perfused with 0.1 M PB followed by 2.5% glutaraldehyde/ 2.5% PFA in 0.1 M PB. Brains were dissected, kept in fixative for 2 hours, and cut into 200 μm thick vibratome sections, from which small regions of the primary visual cortex were dissected with a scalpel.

For electron microscopy of the *pituitary gland*, mice were sacrificed by cervical dislocation, and fresh pituitary glands were dissected and immediately immersed into 2% glutaraldehyde in 0.1 M cacodylate buffer, pH 7.4.

After overnight incubation at 4°C in the respective fixative, samples were additionally fixed with 1% OsO_4 for 1 hour at RT, and preembedding-stained with uranyl acetate. After dehydration in a series of ethanol dilutions and propylene oxide, the samples were embedded in Agar 100 resin. Steps from OsO_4 fixation to embedding were performed by Dr. Dietmar Riedel at the electron microscopy facility, MPIbpc, Göttingen. Blocks were trimmed and sectioned on an ultramicrotome with a diamond knife. The region of interest was identified on toluidine blue-stained semithin sections (700 nm). Ultrathin sections (60 nm) on copper or

nickel meshed grids were counterstained with uranyl acetate for 10 min and lead citrate for 2 min, and examined at the Philips CM 120 electron microscope. Images were obtained with the 2048x2048 Tietz TemCam 224A camera. Images of melanotrophs were taken randomly at 8,400x magnification (~25 images for each animal). Electron micrographs of synapses were taken at constant ~30-40 nm intervals throughout the primary visual cortex at 3750x magnification for measuring synapse densities and at 27000x magnification for evaluating synaptic ultrastructure (40 images of each magnification from 2 different blocks for each animal). Measurements were made with the DigitalMicrograph 3.4 software (GATAN Inc., Pleasanton, CA, USA). Only vesicles/granules with a clearly visible membrane were taken for analysis. The size of a vesicle/granule was determined as the average of its shorter and longer diameters. For analysis of the vesicle/granule distribution, the shortest distance between the membrane of the granule and plasma membrane was measured in melanotrophs, and the shortest distance between the vesicle membrane and the active zone in synapses.

2.2.2. Molecular biology

2.2.2.1. Restriction enzyme digestion

Restriction enzyme digestions were performed in 15-20 μl total volume for ~3 hours for analytical purposes and in 60 μl total volume overnight for cloning purposes. The digestion mixtures were incubated at 37°C unless recommended otherwise by the manufacturer. Restriction enzyme buffers were chosen according to the compatibility table provided by the manufacturer.

2.2.2.2. Dephosphorylation

If the vector was digested with only one restriction enzyme and/or blunt-ended, dephosphorylation of the 5' ends was carried out to prevent re-ligation of the vector. 1 μl alkaline phosphatase was added to the restriction digest mixture followed by incubation for additional 30 min at 37°C.

2.2.2.3. Agarose gel electrophoresis

Fragments were separated by electrophoresis on a 0.8% agarose gel (2% for fragments <500 kb) with 1 μg/μl ethidium bromide at 100-120 V for 0.5-1 hour for analytical digests and 1.5-2 hours for preparative digests. The separated DNA fragments were visualized and documented under UV light. A DNA molecular weight marker was used as a standard to determine the size of the bands.

2.2.2.4. Purification of DNA

After restriction enzyme digestion, dephosphorylation and/or blunt-ending, DNA was purified by phenol-chloroform extraction and ethanol precipitation. Digest volume was brought to at least 100 μl, the digest was then mixed with an equal volume of phenol/chloroform/isoamyl alcohol (25:24:1) and centrifuged at 13,000 g for 10 min. The resulting supernatant was transferred to a new tube and mixed with an equal volume of chloroform, followed by further centrifugation for 10 min. 1/10 volume of sodium acetate (3.3 M) and 2.5 volumes of 100% ethanol were added to the collected supernatant to precipitate the DNA. The mixture was kept at -20°C for at least 30 min and centrifuged at 13,000 g for 15 min, resulting in a DNA pellet. The pellet was washed with ice-cold 70% ethanol, followed by a 5 min centrifugation. The pellet was then air-dried, dissolved in water and stored at -20°C.

If a preparative digest resulted in several fragments, they were separated by electrophoresis, then the desired bands were cut out from the gel and purified with the QIAEX II extraction kit according to the manufacturer's protocol.

2.2.2.5. Blunt-end cloning

To obtain blunt ends after a restriction digestion with an enzyme that produces "sticky ends", purified DNA was treated for 30 min at 37°C with 0.5 μl Klenow polymerase in the presence of 2.5 μl Klenow buffer, 0.5 μl 10 mM dNTPs and water added to a total volume of 25 μl.

2.2.2.6. Ligation

Ligation of the vector and fragment was performed in the presence of 1 μl T4 DNA ligase, 2.5 μl ligation buffer and water added up to a total volume of 25 μl. Vector and fragment were taken in the concentration ratio 1:5 for sticky-end ligations and 1:10 for blunt-end ligations. The ligation mixture was incubated overnight at 12°C.

2.2.2.7. Electrotransformation and plating

To amplify DNA, circular plasmids were electroporated into *E.coli* XL1-Blue MRF' competent bacteria. For electroporation, ligation products were diluted in TE 1:4, and mini- or maxipreps were diluted 1:300. 4 μl DNA solution was mixed with 40 μl thawed bacteria and incubated on ice for 1 min. The mixture was transferred to a cold 0.2 cm electroporation cuvette and a 2.5 kV pulse was applied by the *E.coli* pulser. The cells were resuspended in 1 ml RT-warm LB medium, transferred to a 14 ml round-bottom tube and incubated for

1 hour in the shaker at 37°C, 250 rpm. For minipreps, the cultures were then plated onto LB plates with 50 μg/ml Ampicillin and grown overnight at 37°C.

When amplifying DNA for a maxiprep, after 1 hour of incubation in the shaker, 4 ml LB medium were added to the miniculture, as well as Ampicillin to a final concentration of 50 μg/ml, and the cultures were incubated for 4 more hours at 37°C, 250 rpm. 500 ml LB medium with 50 μg/ml Ampicillin were then inoculated with 100 μl miniculture and incubated overnight in the shaker under the same conditions.

2.2.2.8. DNA plasmid miniprep

5 ml LB medium with 50 μg/ml Ampicillin were inoculated with a single colony from LB plates, and the cultures were grown overnight. DNA was extracted and purified with the QIAprep Spin Miniprep kit according to the manufacturer's instructions and dissolved in the EB buffer. The procedure is based on alkaline lysis of bacteria followed by adsorption of plasmid DNA onto a silica-gel membrane in the presence of high salt.

For screening purposes, express minipreps were made from 2 ml overnight cultures. The cultures were centrifuged for 1 min at 13,000 g, the bacterial pellets were briefly dried, resuspended in 300 μl STET buffer and lysed by incubating with 25 μl freshly prepared lysozyme (10 mg/ml in TE buffer) for 45 sec at 100°C. After centrifugation for 10 min at 13,000 g, the cellular debris were removed, and the DNA was precipitated from the lysate with 100 μl 3.3 M sodium acetate and 500 μl 100% ethanol. The mixture was centrifuged for 15 min at 13,000 g, the pellet was washed with 500 μl 70% ethanol, air-dried and resuspended in 100 μl TE.

Minipreps were analyzed by restriction enzyme digestion and stored at 4°C.

2.2.2.9. DNA plasmid maxiprep

Maxipreps were prepared from 500 ml overnight cultures with the Qiagen Plasmid Maxi Kit as recommended by the manufacturer. The DNA was dissolved in 500 μl TE buffer and stored at 4°C. Similar to the Qiagen miniprep, in this procedure bacteria are lysed in alkaline conditions, and plasmid DNA is bound to an anion-exchange resin.

2.2.2.10. Colony hybridization

To quickly screen for positive insertions in the cases when a ligation product yielded a low percentage of positive colonies, radioactive hybridization procedure was used. Hybond-N round nylon membranes labeled with several asymmetric holes for recognition were put on

LB agar plates with overnight-grown colonies and immediately lifted together with the colonies. The plates were returned to the incubator to allow further growth of the colonies for several hours. The membranes were treated with 10% SDS for 5 min to lyse the bacteria, followed by denaturing buffer for 5 min and then neutralizing buffer for 5 min by putting the membrane on pieces of Whatman paper soaked with the respective solutions. After shaking in 2x SSPE for 10 min, the membranes were crosslinked under UV light and washed with 2x SSC, 1% SDS for 30 min. A DNA probe representing a fragment of the ligation insert was radioactively labeled with [α-^{32}P]dCTP as described for Southern blotting (see 2.2.2.14), and the rest of the procedure was identical to the respective steps of Southern blotting.

2.2.2.11. PCR reaction

PCR-amplification of DNA fragments up to 1 kb in length was performed with the Expand High Fidelity PCR kit. For amplification of longer fragments, the Expand Long Template kit was used. Sequence-specific primers were designed using the DNASTAR software (DNASTAR, Madison, WI, USA). The following PCR reaction mixture was used:

1 μl	DNA (~10 ng)
1 μl	10 mM dNTPs
1 μl	forward primer, 5 OD_{260}
1 μl	reverse primer, 5 OD_{260}
2 μl	PCR buffer with $MgCl_2$
1 μl	enzyme mix (Taq DNA polymerase and Pfu DNA polymerase)
13 μl	H_2O

The following PCR program was used:

96°C	2 min	
96°C	30 sec	
58-70°C	30 sec	
72°C	1 min/1 kb DNA to be amplified	back to step 2, 30-40 cycles
72°C	5 min	

Annealing temperatures were set ~5°C below the melting temperature of the primers. PCR products were sequenced to test for possible PCR-caused mutations.

2.2.2.12. Quick-change site-directed mutagenesis

To perform substitutions of nucleotides in a DNA sequence, site-directed mutagenesis was carried out with the QuickChange XL Site-Directed Mutagenesis Kit essentially as recommended by the manufacturer, using 10-25 ng template DNA. The following reaction mixture was used:

5 μl	10x reaction buffer
2-5 μl	DNA (10-25 ng)
2 μl	forward primer, 500 ng/μl
2 μl	reverse primer, 500 ng/μl
1 μl	10 mM dNTPs
3 μl	Quick solution
up to 50 μl	H_2O
1 μl	Pfu polymerase

The following PCR program was used:

95°C	1 min	
95°C	50 sec	
60°C	50 sec	
68°C	1 min/kb of plasmid length	back to step 2, 18 cycles
68°C	7 min	

After amplification, 1 μl Dpn I restriction enzyme was added to the reaction mixture, followed by incubation for 1 hour at 37°C to digest the nonmutated template DNA.

The DNA was then transformed into 45 μl *E. coli* XL10-Gold ultracompetent cells by a heat pulse at 42°C for 30 sec according to the manufacturer's instructions. The cells were cultured in NZY^+ broth for 1 hour at 37°C, 250 rpm and plated onto LB plates with 50 μg/ml Ampicillin, followed by an overnight incubation at 37°C. Minipreps were made from single colonies and checked for successful mutation with restriction enzyme digestion and sequencing.

2.2.2.13. DNA sequencing and oligonucleotide synthesis

For sequencing of DNA inserts introduced into a vector, primers were used that anneal to the vector near the site of insertion. For longer inserts, additional inside primers with annealing sites at ~600 bp intervals were designed with the help of the DNASTAR software. Primer synthesis and DNA sequencing were performed with the ABI 5000 DNA/RNA Synthesizer

and Applied Biosystems 373 DNA sequencer at the Department of Molecular Neurobiology, MPI for Experimental Medicine, Göttingen. Sequences were then analyzed with the DNASTAR software.

2.2.2.14. Southern blotting

To screen for homologous recombination events in ES cells, genotyping was performed by Southern blotting after an overnight digestion with the appropriate restriction endonuclease. Digested ES cell DNA was loaded on a 0.8% agarose gel and electrophoresed overnight at ~30 mV. The gel was photographed for documentation, incubated in denaturing buffer for 30 min with gentle shaking, and rinsed in distilled water. After shaking the gel in neutralizing buffer for 30 min and rinsing it in distilled water again, DNA was transferred onto prewetted nylon membranes (Hybond-XL) by blotting in 20x SSC buffer overnight. The membranes were washed in 2x SSC for 1-2 min, then in 2x SSC, 1.5% SDS for 30 min with gentle shaking, and in 0.2x SSC, 1% SDS for 15 min with shaking. The membranes were prehybridized for 15-30 min at 65°C in glass tubes with 15 ml QuickHyb hybridization buffer.

Outside DNA probes were radioactively labeled using the Megaprime kit. 50 ng probe DNA dissolved in 5 μl water was mixed with 5 μl primer (random hexanucleotides), boiled at 95-100°C for 4 min and cooled down on ice for 1 min. The following components were then added:

10 μl	labeling buffer
24 μl	dH_2O
4 μl (40 μCi)	[α-^{32}P]dCTP
2 μl	Klenow enzyme

The mixture was incubated for 15 min at 37°C and loaded onto S-300 columns, followed by centrifugation for 2 min at 3000 rpm to elute the probe. The eluate was boiled in a waterbath at 95-100°C for 5 min, cooled down on ice and added to the hybridization buffer. After hybridizing for 16-20 hours at 65°C, the membranes were washed twice in 0.1x SSC, 0.1% SDS for 10 min at RT and for 30 min at 62°C. Autoradiographic images of the membranes were obtained with the phosphoimager after 4 hours exposure or on X-ray films after 2-3 days exposure.

2.2.2.15. RNA isolation and reverse-transcription

Wild type mice were sacrificed by cervical displacement, followed by immediate removal of the brain and/or pituitary gland from the skull, and total RNA was isolated with RNAzol B according to the manufacturer's protocol and dissolved in DEPC water. Pituitary glands from 6-8 animals were pooled together to obtain enough material for RNA isolation.

Isolation of pancreatic islets was performed with the help of Shibing Yang (Neuroendocrinology group, ENI Göttingen), essentially as described (Yang et al. 2004). Briefly, adult male NMRI mice were killed by cervical dislocation. Liberase was dissolved in Hank's buffer salt solution (HBSS) (0.3 mg/ml) and cooled down on ice to activate the enzyme. About 3 ml solution were injected into the pancreas via the bile duct. The expanded pancreas was then removed, incubated for 25–30 min at 37°C and gently triturated. Cold HBSS was added, and the mixture was centrifuged twice at 800, 4°C for 10 min. The pellet was mixed with 4 ml Ficoll solution, kept on ice for 10 min, added on the top of 6 ml Ficoll solution and centrifuged at 2500 rpm for 30 min. The supernatant containing the islets was mixed with 10 ml HBSS, the islets were enriched by centrifugation at 800 rpm for 30 sec and then hand-picked. Islets from 3 animals were pooled together, and RNA was isolated as described above.

2.2.2.16 Reverse transcription

The RNA was reverse-transcribed with the GeneAmp Gold RNA PCR Core Kit using oligo dT primer, with the following reaction mixture:

10 μl	5xPCR buffer
5 μl	$MgCl_2$
5 μl	dithiothreitol (DTT)
5 μl	dNTPs
1.25 μl	oligo dT_{16}
1.25 μl	RNAse inhibitor
1 μg	RNA
0.75 μl	reverse transcriptase
up to 50 μl	DEPC H_2O

The mixture was incubated for 10 min at 25°C (primer annealing), followed by 12 min at 42°C (DNA synthesis). The resulting cDNA was used as a template for PCR reaction.

2.2.2.17. Quantitative real-time PCR with SYBR Green

Real-time PCR was performed using SYBR Green PCR Master Mix in the ABI Prism 7000 Sequence Detection System, with the following reaction mixture:

25 μl	2x SYBR-Green mix
2.5 μl	cDNA
3 μl	forward primer, 100 nM
3 μl	reverse primer, 100 nM
16.5 μl	H_2O

PCR program was as follows:

95°	10 min	„hot start“ to activate AmpliTaq Gold DNA polymerase
95°	30 sec	
58°	30 sec	
72°	30 sec	back to step 2, 40 cycles

All reactions were performed in duplicates. β-Actin served as a reference gene, which was consistently amplified with similar threshold cycles in all experiments, indicating that the concentration of β-actin mRNA was similar in all conditions tested. Signals were analyzed by ABI Prism Sequence Detection Software (Applied Biosystems), and the $\Delta\Delta C_T$ method was used for relative quantification of neurexin transcripts (Pfaffl 2001). Briefly, the C_T (threshold cycle) values of the duplicate reactions for each gene were averaged. The mean C_T value of each gene of interest was first normalized to the β-actin mean C_T (giving ΔC_T). Then one of the genes (usually with the lowest expression level) was chosen to be a “calibrator” and all the rest were normalized to the calibrator, giving the $\Delta\Delta C_T$ value. The amount of each target gene was then calculated as $2^{-\Delta\Delta CT}$ (or $(E+1)^{-\Delta\Delta CT}$, if amplification efficiency was under 100%, see below). The values were expressed as % of β-actin amount.

Standard curves for all the isoform-specific reactions were generated with serial five-fold dilutions of cDNA in triplicates, and the efficiency of amplification was calculated from the slope of the standard curve as $E=10^{-1/k}$, where E is amplification efficieny and k is the slope. For all genes studies, the efficiency was between 79-100% and was taken into consideration when calculating the relative expression levels.

DNA melting curves were generated after each experiment to confirm the specificity of amplification.

2.2.2.18. DNA database search

DNA searches were performed using the National Center for Biotechnology Information database (http://www.ncbi.nlm.nih.gov). Sequence alignments were carried out with the Basic Local Alignment Search Tool (BLAST) available at the website.

2.2.3. Embryonic stem cell culture

2.2.3.1. Culturing MEF feeder layers

ES cells were grown on mouse embryonic fibroblasts (MEF cells) resistant to the appropriate antibiotic as feeder layers. The feeder cells were grown in 75 cm^2 flasks until they reached confluence, then split 1:4 and grown to confluence again. The cells were mitotically inactivated by incubating with 10 μg/ml mytomycin C for 2 hours at 37°C and plated onto 0.1% gelatin-covered 25 cm^2 flasks or 100 mm dishes.

2.2.3.2. Culturing ES cells on the feeder layers

E14.1 embryonic stem (ES) cells from the SV129 mouse strain at passage 8 were used. After thawing, ES cells were plated onto mitotically inactivated MEF feeder layers in 25 cm^2 flasks, grown to confluence and split once again. The medium for ES cells was changed daily, leaving behind 1 ml of preconditioned medium.

2.2.3.3. Preparation of DNA

Targeting vector DNA (60-100 µg) was linearized with the appropriate restriction enzyme, extracted twice with an equal volume of phenol/chloroform, twice with an equal volume of chloroform and precipitated with 1/10 volume of 3.3 M Sodium acetate and 2.5 volumes of 100% ethanol. The pellet was washed twice with 10 ml ice-cold 70% ethanol, dried in sterile conditions under the hood, stored at 4°C and resuspended in 0.5 ml of sterile D-PBS just before use.

2.2.3.4. Electroporation

On the next day after splitting, subconfluent ES cells from each 25 cm^2 flask were washed, treated with trypsin to detach from the flask, centrifuged and dissolved in 0.5 ml D-PBS. The cells were mixed with the linearized and purified vector DNA in D-PBS and pipetted into a 0.4 mm electroporation cuvette. Electroporation was carried out in the Gene Pulser Xcell electroporator, with the condensor set at 500 μF, 230 V. After the electroporation, the cells

were immediately transferred into a tube with 29 ml prewarmed ES cells medium and distributed onto two 100 mm dishes.

2.2.3.5. Selection of resistant clones

After letting the cells recover for 24 hours, positive selection was started with G 418 (190 μg/ml) and/or Hygromycin (50-100 μg/ml) and continued for 9 days. In addition, 0.25 μM Ganciclovir was added to the medium on days 3-5 for negative selection. Single clones started appearing on day 7-8 after electroporation. After 9 days of positive selection, the clones were grown in medium without any selective agent for an additional 1-2 days.

2.2.3.6. Picking and growing resistant clones

96 or 192 single clones were picked for each electroporated construct. The clones were first transferred into a 96-well plate with trypsin and then split into two 96-well plates with feeder layers. The cells were grown for 4-5 days until confluent, after that the cells in one of the plates (the "masterplate") were trypsinized, mixed with 2x freezing medium and overlaid with mineral oil. The plate was frozen and kept at -80°C, while the other one was split again 1:2, plating the cells onto gelatinized 96-well plates without feeder layers. These 2 plates were used to genotype the clones.

After reaching confluence, the cells were washed with D-PBS and lysed overnight at 60°C in lysis buffer. The DNA was precipitated with 100% cold ethanol and 5 M NaCl, washed three times with 70% ethanol, and dissolved in water. One of the plates was kept at -20°C as a backup, and in the other one, the ES clone DNA was digested overnight with the appropriate restriction enzyme and genotyped by Southern blotting (see 2.2.2.14).

2.2.4. Data analysis

Data are presented as means ± SEM. Statistical significance was assessed by two-tailed Student's *t*-test (when two groups were compared) or one-way ANOVA (when more than two groups were compared) using Prism software (GraphPad Software Inc., San Diego, CA, USA). The level of significance was set at $p \leq 0.05$.

3. Results

3.1. Structural effects of α-neurexin deletion in mature brain

3.1.1. Expression of neurexin isoforms in the postnatal brain

The developmental profile of neurexin expression has been previously investigated in mice by Northern blot and *in situ* hybridization, showing that neurexin transcripts appear in the nervous system as early as embryonic day 10 (E10), and their amount increases significantly during development. Neurexins were detected exclusively in postmitotic neurons, and the onset of their expression in particular regions shortly preceded synapse formation (Puschel and Betz 1995). In another study, where neurexin and neuroligin RNA was quantified by Northern blotting, a peak of expression was observed for both proteins between postnatal day 5 (P5) and P10, with a subsequent mild decline and stabilization of expression at adult levels (Irie et al. 1997). However, single isoforms have not been studied separately. Before addressing the structural role of α-neurexins in adult animals, we investigated the time course of expression of the principal neurexin isoforms during postnatal development in more detail and using a more quantitative approach.

Since no antibodies are available that are specific for individual neurexin isoforms, we detected neurexin transcripts at the RNA level by reverse-transcriptase real-time PCR with principal isoform-specific primers. All of the isoforms were detectable in the brain at P1, although the expression levels were mostly low, with the exception of Nrxn1β, which was already present in high amounts (Fig. 4). The expression levels rose prominently between P4 and P7, and remained high (Nrxn1α) or increased further (all other isoforms) in the second and third weeks of life, again with the exception of Nrxn1β, which showed no clear increase during this period (Fig. 4D). For most of the isoforms, the amounts continued to grow until adulthood, while for Nrxn2α the early postnatal elevation was only transient, and its amount decreased after P20 (Fig. 4B), making this isoform the least abundant in adults (Fig. 4H). Nrxn3α and 1β transcripts, on the other hand, were detectable in especially high amounts in adult brains (Fig. 4H).

The rise in expression that most of the isoforms displayed during the 1st-3rd postnatal weeks coincides with the time of extensive synaptogenesis (Steward and Falk 1991), and high levels of neurexins in adult animals are consistent with a role of these molecules at mature synapses. The different temporal profile observed for Nrxn1β may be explained by the presence of this variant at synapses in early maturing regions of the brain, where synapse formation is prominent before birth.

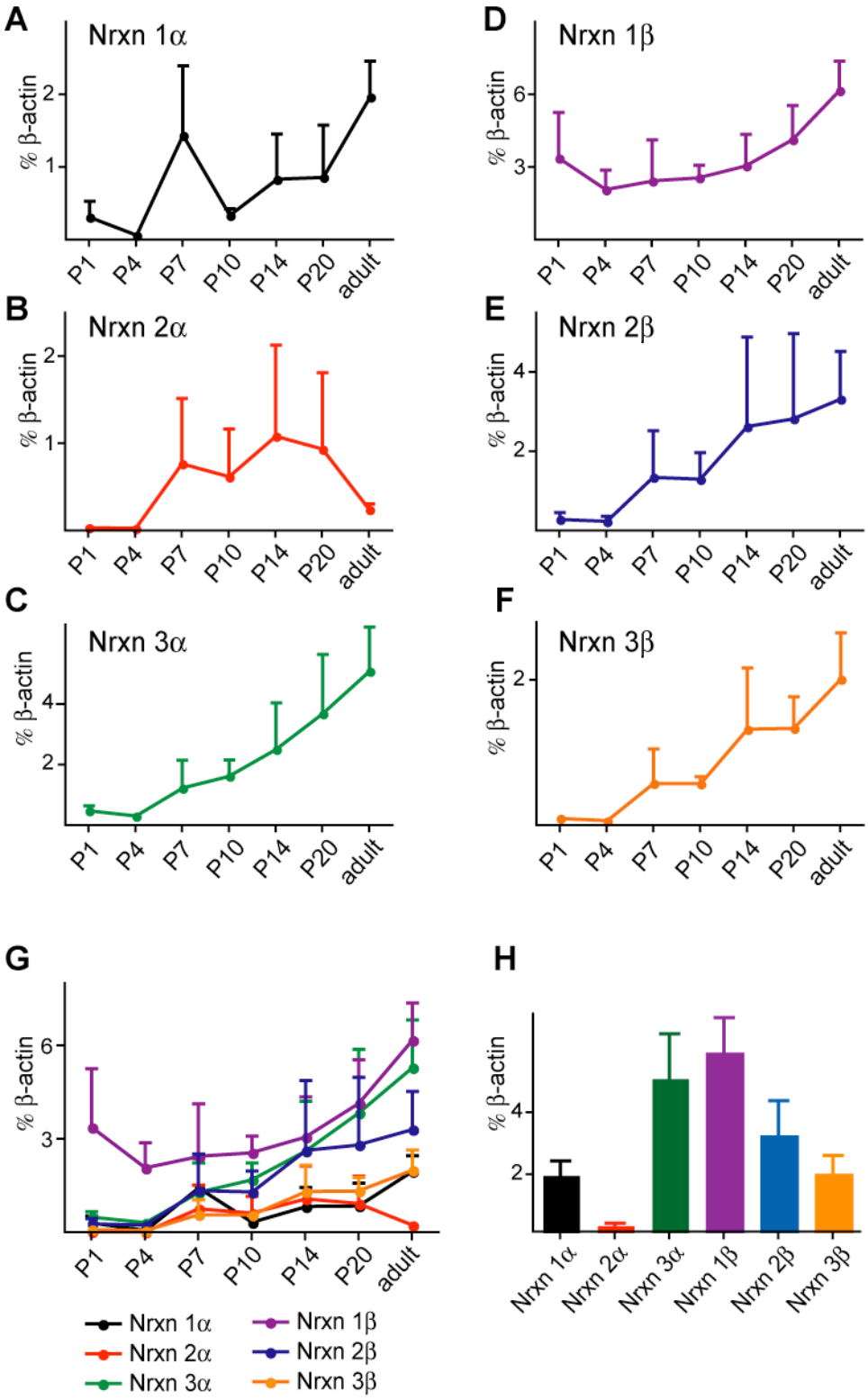

Figure 4. Expression of neurexin isoforms in the postnatal brain quantified with real-time PCR. Total brain RNA was isolated at the indicated developmental stages, reverse-transcribed and amplified with isoforms-specific primers. The values are normalized to β-actin as a reference gene. **A-F**: Developmental expression profiles of individual neurexin isoforms. **G**: The individual graphs are overlaid for comparison. **H**: Expression levels of the principal isoforms in the adult brain. Data are from 3-5 animals for each age. P – postnatal day.

The increase in expression during postnatal period suggested that the absence of α-neurexins might cause more pronounced defects in synapse and brain structure at a later stage, than those observed previously in newborn animals (Missler et al. 2003).

3.1.2. Adult α-neurexin DKO mice have a reduced neuropil

To evaluate the overall brain structure in adult α-neurexin mutants, we performed Nissl staining of whole brain serial sections from 6-8-week-old DKO and control mice. Part of the Nissl staining data from the DKO2/3 and SKO2 mice were collected during my MSc project. As DKO1/2 mutants have very low surviving rates (see Fig. 3A), they could not be obtained in sufficient numbers during the limited time of that study. In the PhD project, we included DKO1/2 mutants into the study, and also increased the number of animals in the other two experimental groups. SKO2 mice were used as a control group, since they display the least severe phenotype among all α-neurexin mutants in most of the aspects studied so far (e.g., survival rates, see Fig. 3A), and can be obtained as littermates of DKOs in our breeding scheme. However, we have observed that Nrxn2α is expressed at relatively high levels during early postnatal development (see Fig. 4B), and therefore SKO2 mice may already be considerably affected by the loss of one α-neurexin. In order to detect the full extent of morphological changes in the DKOs, wild type (WT) animals from a separate mouse line of the same genetic background were also included into the study as an additional control group.

In agreement with the intact brain morphology of newborn α-neurexin mutants (Missler et al. 2003), we did not find any apparent abnormalities in the gross anatomy of the adult DKO brains (Fig. 5A-D). However, upon closer examination we noticed a reduction in the thickness of some neocortical areas and in the size of several subcortical structures, which were accompanied by an increase in the area density of cell bodies. Among the most affected regions was the primary visual cortex, where higher cell densities were especially notable in layer II and in sublayers Va and VIa, while in control brains cell bodies were sparser in these layers (Fig. 5E-H). Similar, albeit smaller changes occurred in more rostral neocortical areas, such as the primary somatosensory cortex. Several subcortical regions were affected too, among them the caudate-putamen, lateral septal and thalamic nuclei. In the olfactory bulb, the glomeruli were reduced in size, and the external plexiform layer was thinner, than in controls (MSc thesis, see Fig. 2 and Table 2 in Dudanova et al. 2007, App. 1).

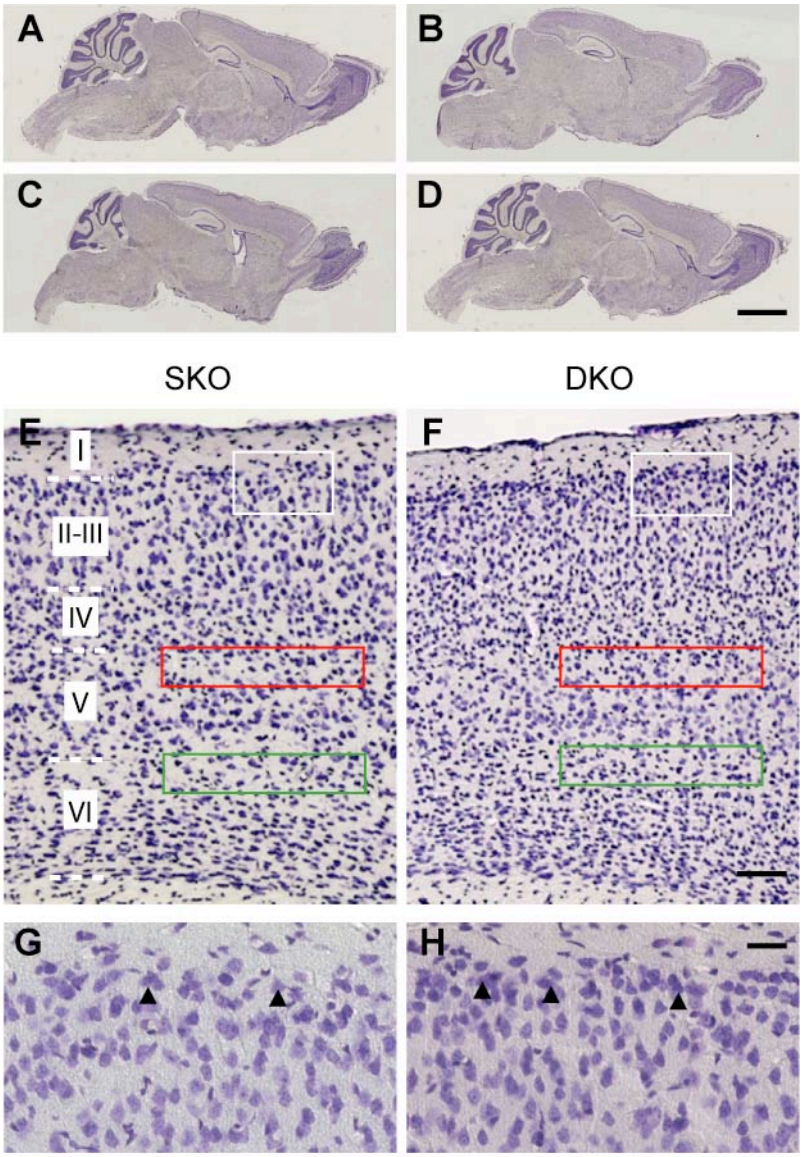

Figure 5. Reduced brain neuropil in adult α-neurexin DKO mutants. **A-D**: Nissl-stained parasaggital brain sections from WT (A), SKO2 (B), DKO1/2 (C) and DKO2/3 (D) mice. No obvious abnormalities can be observed in the DKO brains. **E-F**: Primary visual cortex in SKO2 (E) and DKO2/3 (F) brains. Cells densities are higher in the DKO, especially in layers II, Va (red boxes) and VIa (green boxes). Cortical layers are labeled in E with roman numerals. **G-H**: Higher magnification images of the areas indicated by white boxes in E-F, showing increased density of cell bodies in cortical layer II (arrowheads). Scale bars: 2 mm in A-D, 100 μm in E-F, and 25 μm in G-H.

We quantified the morphological alterations in the primary visual cortex by measuring the area density of cells in layers Va and VIa, and the proportion of cell bodies vs. intercellular space in layer II, where cell density measurements were difficult because of the thinness of this cortical layer. The changes amounted to an ~20% increase in the densities of cell bodies in the DKOs (Table 1). Although moderate, the alterations were statistically significant, and were consistently observed in all the DKO animals examined.

Table 1. Analysis of cell densities in the primary visual cortex of α-neurexin DKO and control mice

	Genotype				
	WT (n = 5)	SKO2 (n = 9)	DKO1/2 (n = 6)	DKO2/3 (n = 7)	P
Layer II, % cells [a, b]	36.3 ± 1.9	42.6 ± 1.6	54.1 ± 2.0* [c]	52.9 ± 1.3*	<0.001
Layer Va, cell density [cells/mm^2] [a]	3772 ± 165	4386 ± 171	5139 ± 264*	5566 ± 347*	<0.001
Layer VIa, cell density [cells/mm^2] [a]	3777 ± 100	4319 ± 157	5127 ± 243*	5493 ± 264*	<0.001
	SKO (n = 2)		DKO (n = 3)		
GAD65-positive neuron density, [cells/mm^2] [a]	273.8 ± 2.5		347.0 ±15.2		<0.05

Data are means ± SEM; *n* = number of animals. Measurements were made on images of Nissl-stained sections as in Fig. 5. Statistical analysis was performed with t-test (where two groups are compared) or with one-way ANOVA with Tukey's post-test (where more than two groups are compared).
[a] 4-12 sections from each animal were used for data collection.
[b] The proportion of cell bodies vs. neuropil was measured along a horizontal line in layer II.
[c] Asterisks indicate significant difference from WT and SKO2 according to pairwise comparisons with Tukey's test: *p<0.05.

Since the morphometric analysis (Table 1) did not reveal any significant differences between WT and SKO mice in any of the parameters measured, we used only SKO animals as controls in the rest of this study. The degree of the changes was also similar between DKO1/2 and DKO2/3 mice, so we did not distinguish between these two types of mutants in further experiments, and they are hereafter collectively referred to as DKOs or α-neurexin-deficient animals.

The decrease in the size of brain regions and the corresponding increase in cell densities suggested a reduction of the neuropil in the DKOs. Neuropil represents the part of the nervous tissue which surrounds cell bodies and blood vessels, and is comprised of neuronal and glial cell processes, dendritic spines and synaptic contacts. However, the reduction of brain volume could be partly caused by a decrease in cell numbers in addition to the neuropil defect. Several experiments were carried out in my MSc project to address the possibility of cell loss contributing to the overall reduction in the size of the affected regions. DAPI (4',6-Diamidino-2-phenylindole-hydrochlorid) staining demonstrated the absence of apoptotic signs in the DKOs. Furthermore, the pattern of immunolabeling produced by antibodies against neuronal

and glial cellular markers was not changed (see Fig. 3 in Dudanova et al. 2007, App. 1). These findings, together with the increased density of cell bodies observed in Nissl-stained sections, excluded cell loss in the mutants and pointed instead to the paucity of neuropil as a likely reason for the smaller size of the affected structures.

Although we observed neuropil reduction in many regions of the brain, for a more detailed investigation of the structural changes we focused on the primary visual cortex, a morphologically well-defined cortical area, which was among the most prominently affected regions according to the initial histological analysis.

3.1.3. Decreased number and normal ultrastructure of synapses in α-neurexin-deficient mouse brains

To investigate which components of the neuropil contribute to the reduction of its volume, we previously performed a Golgi impregnation of the DKO and control mouse brains to visualize dendritic arbors and dendritic spines (MSc thesis). Dendritic architecture and spine numbers were analyzed in pyramidal neurons in layers III and V of the primary visual cortex. While there were no obvious changes in the cellular morphology and dendrite orientation, we found that the higher-order branches of both apical and basal dendritic trees were reduced in length in the DKO neurons, and the number of dendritic spines on these segments was correspondingly decreased, while their density remained unaltered (see Fig. 4 and Table 3 in Dudanova et al. 2007, App. 1). Since the majority of excitatory synapses are situated on dendritic spines, the reduced number of spines provided evidence for a loss of excitatory synapses in the absence of α-neurexins.

Building upon these results, in the current work we addressed the possible changes in synapse numbers by studying the distribution of several synaptic proteins in the control and mutant brains with immunohistochemistry. DAB-staining of brain sections was performed using antibodies against the general synaptic markers synapsin and synaptophysin, the excitatory synapse-specific vesicle glutamate transporters 1 and 2 (VGlu1, VGlu 2), and the inhibitory synapse-specific vesicle GABA transporter (VGAT). The GABA-synthesizing enzyme glutamic acid decarboxilase of 67 kDa (GAD67) served as an additional marker for inhibitory synapses. With all the antibodies we observed the punctate neuropil labeling characteristic for synaptic proteins (Fig. 6-8). We paid special attention to the staining pattern in layers II and V of the visual cortex, where more prominent changes could be expected considering our findings in Nissl-stained sections (see 3.1.2). No obvious differences could be detected in the immunoreactivity pattern of the general (Fig. 6) or excitatory (Fig. 7) synaptic

markers, confirming normal assembly of the brain in α-neurexin-deficient animals. Antibodies against the inhibitory synaptic markers produced the typical perisomatic staining, but the labeling intensity was on average slightly lower in the DKOs, than in the controls (Fig. 8). This difference, albeit subtle, suggested a decrease in the number of inhibitory synapses in the mutants.

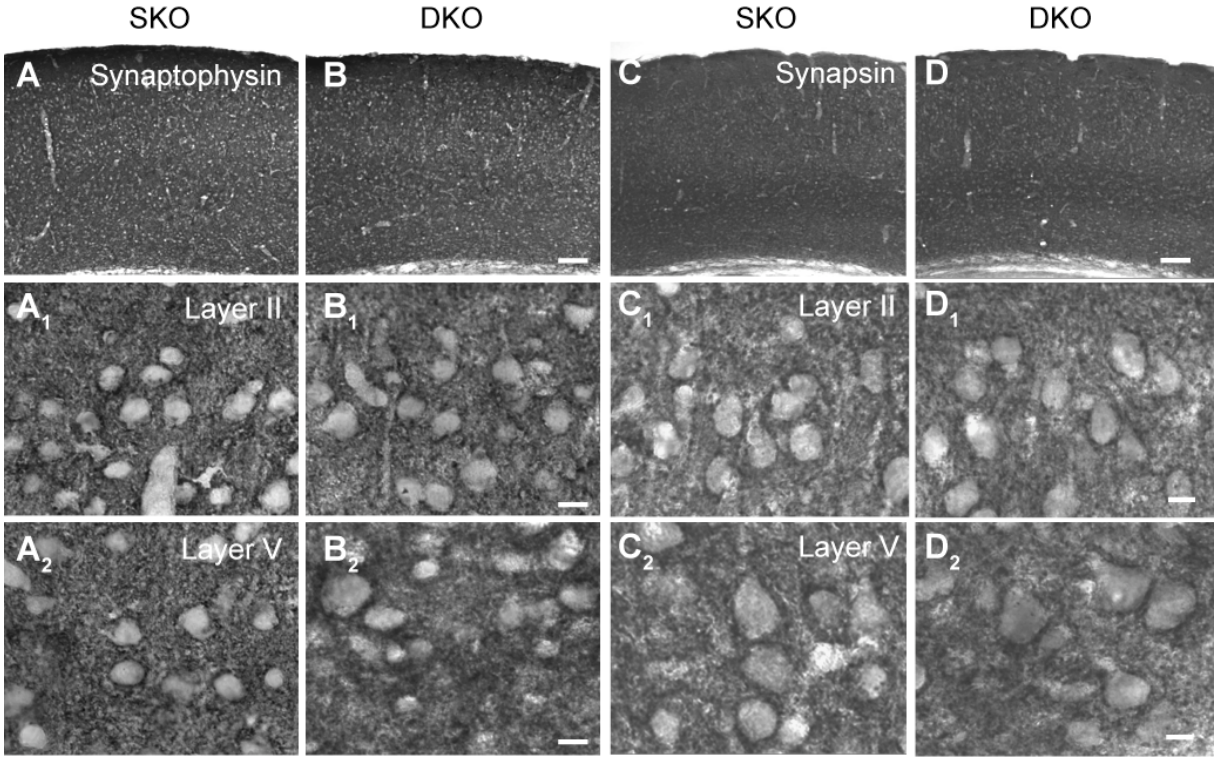

Figure 6. Unchanged distribution of pansynaptic markers in the neocortex of α-neurexin DKO mice. Brain sections of control (**A, C**) and DKO (**B, D**) mice were immunolabeled with anti-synaptophysin (A-B) and anti-synapsin (C-D) antibodies. Layer II (A_1-D_1) and layer V (A_2-D_2) are shown at a higher magnification, demonstrating a similar labeling pattern of the neuropil. Scale bars: 100 μm in the overviews and 10 μm in the higher magnification images.

We next used quantitative electron microscopy to reliably determine synapse densities and to study synaptic ultrastructure in the visual cortex. Since light microscopy revealed changes in several different layers, electron micrographs of the neuropil were obtained at regular intervals throughout the cortex, from layer I to the border with the white matter. There were no obvious ultrastructural defects in adult DKOs (Fig. 9A-B). In line with the ultrastructural data from newborn TKO mutants (Missler et al. 2003), we observed a selective ~30% decrease in the area density of Gray type II (inhibitory) contacts in the DKOs, which similarly affected all cortical layers, while the density of Gray type I (excitatory) synapses was not altered (Table 2). It should be noted, however, that the overall volume of the cortex was mildly reduced, as revealed by the histological examination. The decreased volume,

together with the unchanged excitatory synapse densities, would imply a proportional reduction in the absolute number of excitatory contacts. We separately quantified the area density of axo-spinous synapses (synaptic junctions formed between an axon and a dendritic spine) and also observed no changes in this parameter (Table 2). Moreover, we detected a higher number of perforated synapses (with two separate parts of the postsynaptic density apposed to one presynaptic terminal) in the mutants, although this difference did not reach a statistically significant level.

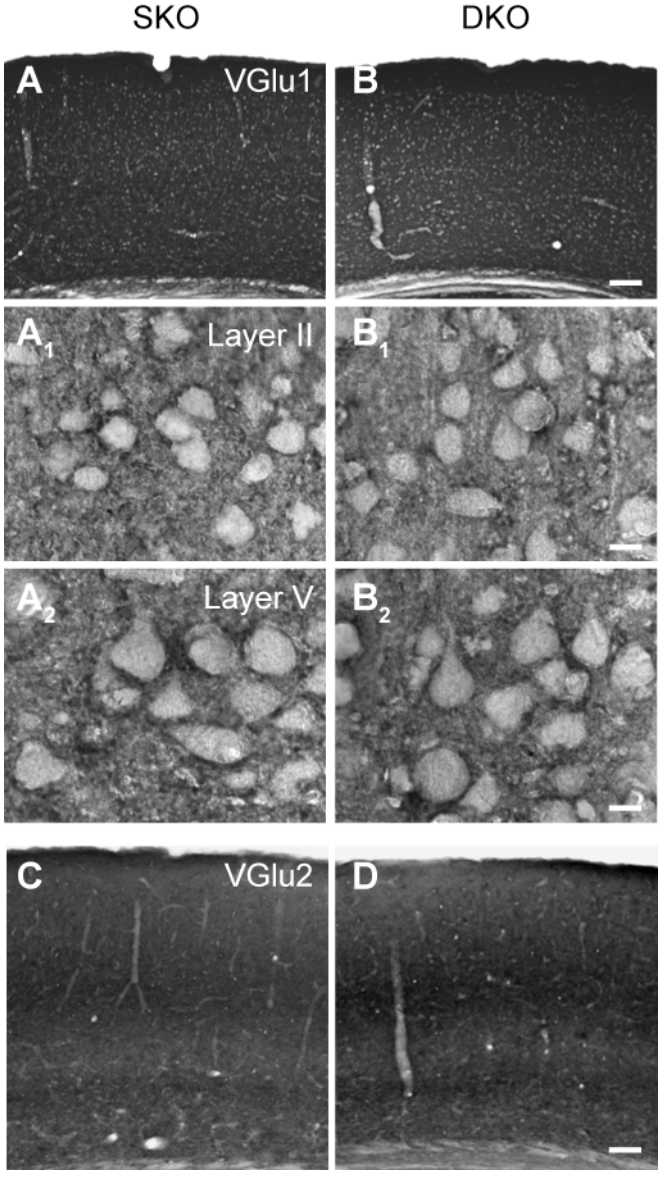

Figure 7. Unchanged distribution of excitatory synaptic markers in the neocortex of α-neurexin mutants. Brain sections from control (**A, C**) and DKO (**B, D**) mice were labeled with antibodies against the vesicle glutamate transporters VGlu1 (A-B) and VGlu2 (C-D), producing similar intensity and pattern of labeling in the neuropil of both genotypes. Cortical layer II (A_1-B_1) and layer V (A_2-B_2) labeled with VGlu1 are shown at a higher magnification. Scale bars: 100 μm in the overviews and 10 μm in the higher magnification images.

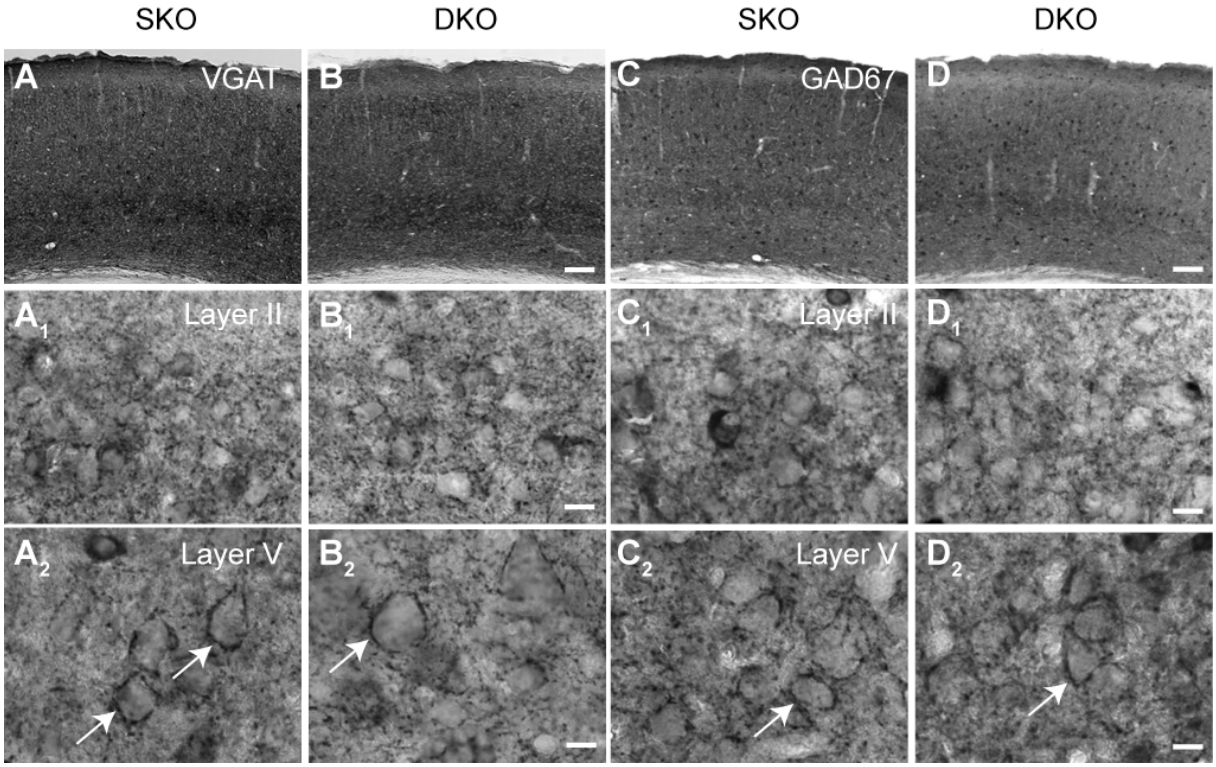

Figure 8. Distribution of inhibitory synaptic markers in the neocortex of α-neurexin DKO mice. Brain sections from control (**A, C**) and DKO (**B, D**) mice were labeled with antibodies against the vesicle GABA transporter VGAT (A-B) and the GABA-synthesizing enzyme GAD67. The labeling is slightly weaker in the mutants (compare C and D), while the perisomatic pattern (arrows) is preserved, as can be seen in higher magnification images of layer II (A_1-D_1) and layer V (A_2-D_2). Scale bars: 100 μm in the overviews and 10 μm in the higher magnification images.

Synaptic ultrastructure appeared normal in the DKOs, as can be seen on higher magnification electron micrographs (Fig. 9C-F), and none of the parameters of synaptic ultrastructure that we quantified (active zone length, vesicle size, area density of vesicles in the synaptic terminal, distribution of vesicles in relation to the active zone, width of the synaptic cleft) showed any differences between the genotypes (Table 2), in line with the previous observations in newborn TKO mutants (Missler et al. 2003).

The decrease in the amount of inhibitory synapses could be caused by a reduction in the number of inhibitory neurons or by a reduction in the number of synaptic terminals formed by a single neuron. To differentiate between the two possibilities, we labeled brain sections with the GABAergic neuron markers parvalbumin and GAD65. In order to obtain primarily somatic GAD65 staining, triton permeabilization was omitted in the immunohistochemistry procedure. There were no apparent differences in the immunoreactivity pattern between the genotypes (Fig. 10). Counts of GAD65-positive cells showed no reduction, but a slight increase in GABAergic cell density in the DKOs (Table 1). The change was proportional to

the overall increase in cell densities in the affected brain regions (~20%), therefore the absolute number of GAD65-positive cells is probably similar in the DKO and control animals. This result excluded inhibitory neuron loss as a cause of the lower inhibitory synapse density, and suggested that the number of synaptic contacts formed by each inhibitory neuron is reduced in α-neurexin mutants.

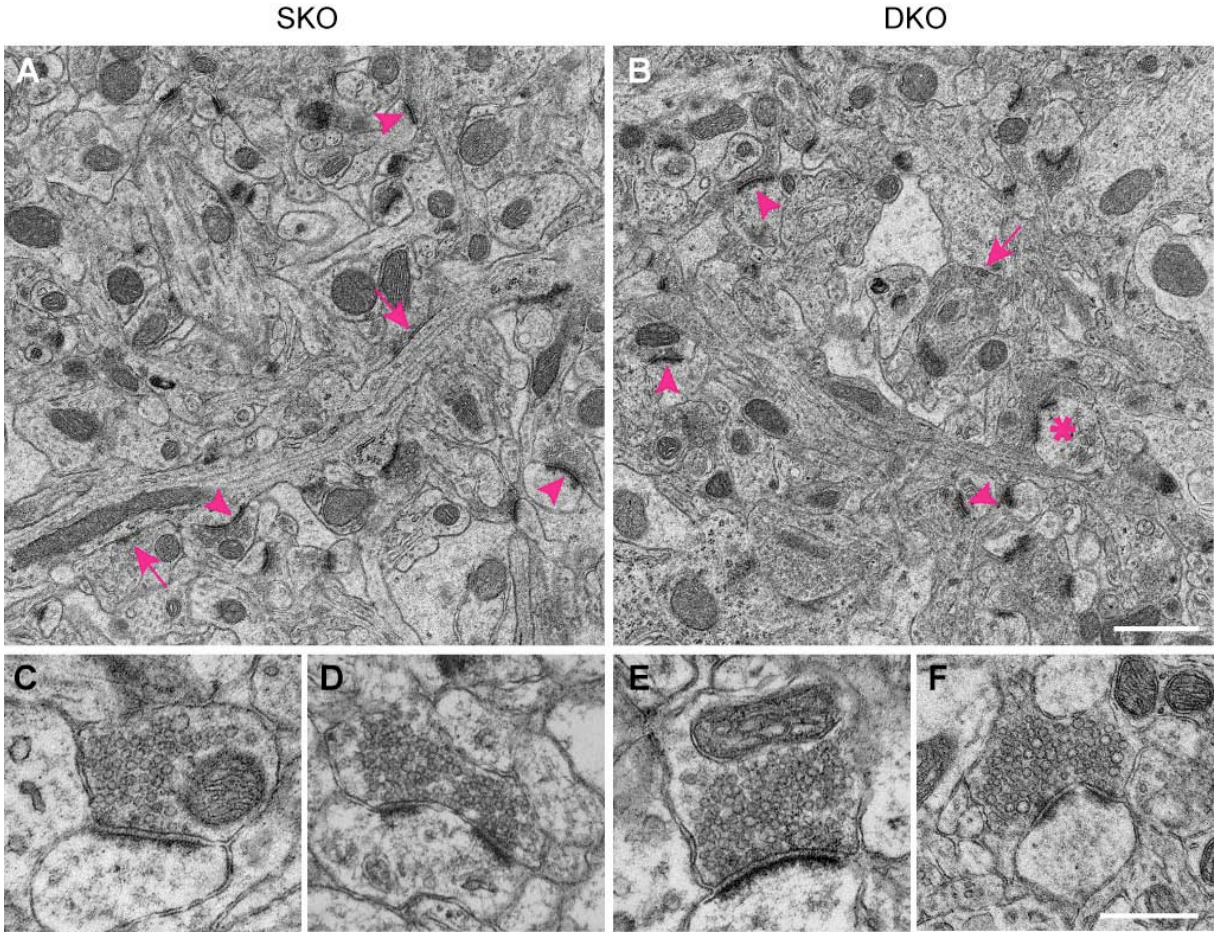

Figure 9. Neuropil ultrastructure in the primary visual cortex of α-neurexin DKO mice. **A-B**: No obvious ultrastructural defects can be seen in the mutants. Several examples of Gray type I (arrowheads) and Gray type II (arrows) synapses are shown. Type I synapses can be distinguished by thicker postsynaptic densities. A perforated synapse is marked with an asterisk in B. **C-F**: Examples of type I (C, E) synapses and perforated synapses (D, F) in control (C, D) and DKO (E,F) animals. Synaptic ultrastructure appears intact in the mutants. Scale bars: 1 μm in A-B, 500 nm in C-F.

Table 2. Synapse densities and synaptic ultrastructure in the primary visual cortex of α-neurexin DKO and control mice

	Genotype		
	SKO2 (n = 3)	DKO (n = 3)	P
Synapse densites [1/1000 μm^2] [a]			
Type I synapses	131.1 ± 2.8	124.6 ± 5.6	n.s.
Axospinous synapses	65.0 ± 2.4	62.5 ± 4.2	n.s.
Perforated synapses	5.2 ± 1.0	7.3 ± 0.7	n.s.
Type II synapses	17.9 ± 0.3	12.6 ± 0.1	<0.001
Synaptic ultrastructure [b]			
Vesicle diameter [nm] [c]	42.2 ± 0.6	41.8 ± 0.4	n.s.
Density of vesicles [1/μm^2]	59.6 ± 7.6	55.6 ± 11.4	n.s.
Length of the active zone [nm]	345.2 ± 8.6	334.5 ± 4.8	n.s.
Width of the synaptic cleft [nm]	15.1 ± 0.3	14.6 ± 0.5	n.s.
Relative distribution of synaptic vesicles [d]			
<40 nm	0.12 ± 0.01	0.13 ± 0.01	n.s.
40-100 nm	0.21 ± 0.01	0.23 ± 0.01	n.s.
>100 nm	0.67 ± 0.02	0.64 ± 0.02	n.s.

Data are means ± SEM; *n* = number of animals. Measurements were made on electron micrographs of the primary visual cortex taken at equal intervals (~30-40 μm) in layers I to VI as those shown in Fig. 9. Statistical analysis was performed with t-test; n.s. – not significant.

[a] A total number of 1491 (SKO) and 1397 (DKO) synapses were evaluated for the analysis of synapse densities.

[b] A total number of 110 (SKO) and 127 (DKO) type I synapses were evaluated for the analysis of synaptic ultrastructure.

[c] Vesicle diameter was determined as the average of the shorter and longer diameters.

[d] The distribution of vesicles in the synaptic terminal was analyzed by determining their relative frequency in 3 classes of shortest distances from the synaptic active zone.

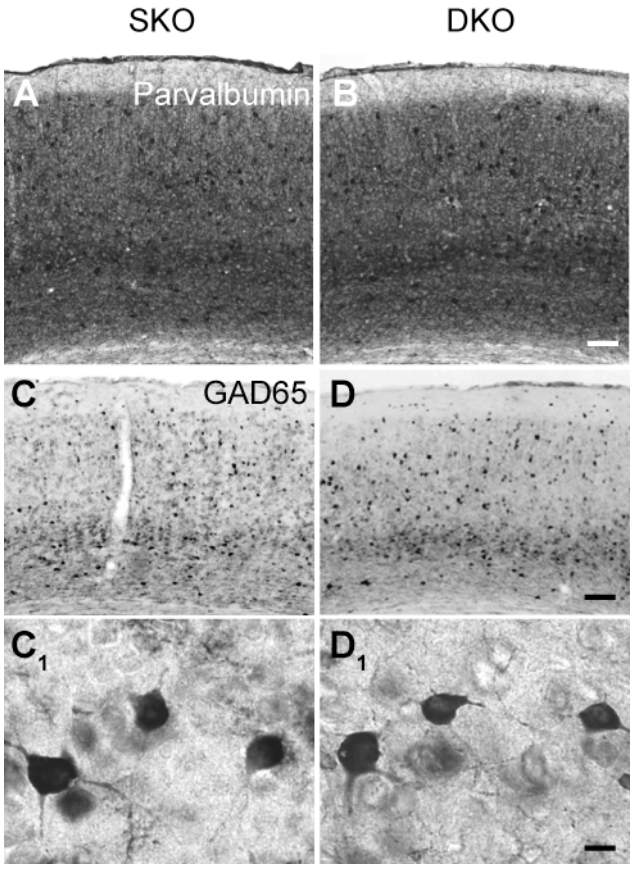

Figure 10. Staining of GABAergic neurons in the cortex of α-neurexin mutants. Brain sections from control (**A, C**) and DKO (**B, D**) mice were labeled with antibodies against the inhibitory neuron markers parvalbumin (A-B) and GAD65 (C-D). No obvious changes in inhibitory neuron number, distribution and morphology can be observed in the DKOs. Scale bars: 100 μm in the overviews and 10 μm in the higher magnification images.

3.1.4. Initial steps towards deleting the whole *Nrxn1*αβ locus in the mouse

The morphological alterations found in the neuropil of α-neurexin mouse mutants were quite mild (Missler et al. 2003 and this study). One possible explanation for this could be that β-neurexins are preserved in these mutants and could compensate for the absence of α-isoforms. The synaptogenic function of β-neurexins has been postulated based on *in vitro* findings (Dean et al. 2003; Graf et al. 2004), but still awaits confirmation in a genetic mouse model.

To start addressing the functions of β-neurexins *in vivo*, as well as the question of functional redundancy of α- and β-isoforms, we set out to generate a mouse mutant lacking both Nrxn1α and Nrxn1β. Previous attempts to ablate both principal isoforms of Nrxn1 by conventionally replacing most of the gene with a neomycin resistance cassette were unsuccessful (Markus Missler, personal communication), presumably because of the exceptionally large size of the gene (1.1 Mb in the mouse). It also seems impractical to make separate mutations by deleting α- and β-specific exons and crossing the resulting mutants,

since both α- and β-specific sequences lie in close proximity on the same chromosome, so the probability of a recombination event between the two sites would be extremely low. Therefore, to perform a deletion of the whole *Nrxn1*αβ locus in the mouse we devised a conditional knockout strategy based on a large-scale rearrangement. The 5' and 3' ends of the gene are targeted with two LoxP site-containing vectors, which will then allow the removal of the floxxed gene by Cre-mediated recombination (Fig. 11A).

For the 5' end of the gene, we made use of the vector targeting the first coding exon of the *Nrxn1* gene, which was previously generated in the laboratory by Mohiuddin Ahmad. For the 3' end we generated two alternative constructs, targeting exons 21 and 24 (Fig. 11B, C). As the initiation codon of *Nrxn1*β is situated in exon 18 (Tabuchi and Sudhof 2002), in both cases at least the first four coding exons of *Nrxn1*β would be removed in addition to *Nrxn1*α deletion. While the 5' targeting vector contains a Neomycin resistance gene, we included a Hygromycin resistance cassette into the 3' constructs to allow for two rounds of positive selection after two different recombination events. The constructs have been electroporated into mouse embryonic stem cells, but no positive recombinants have been obtained during the time frame of the PhD.

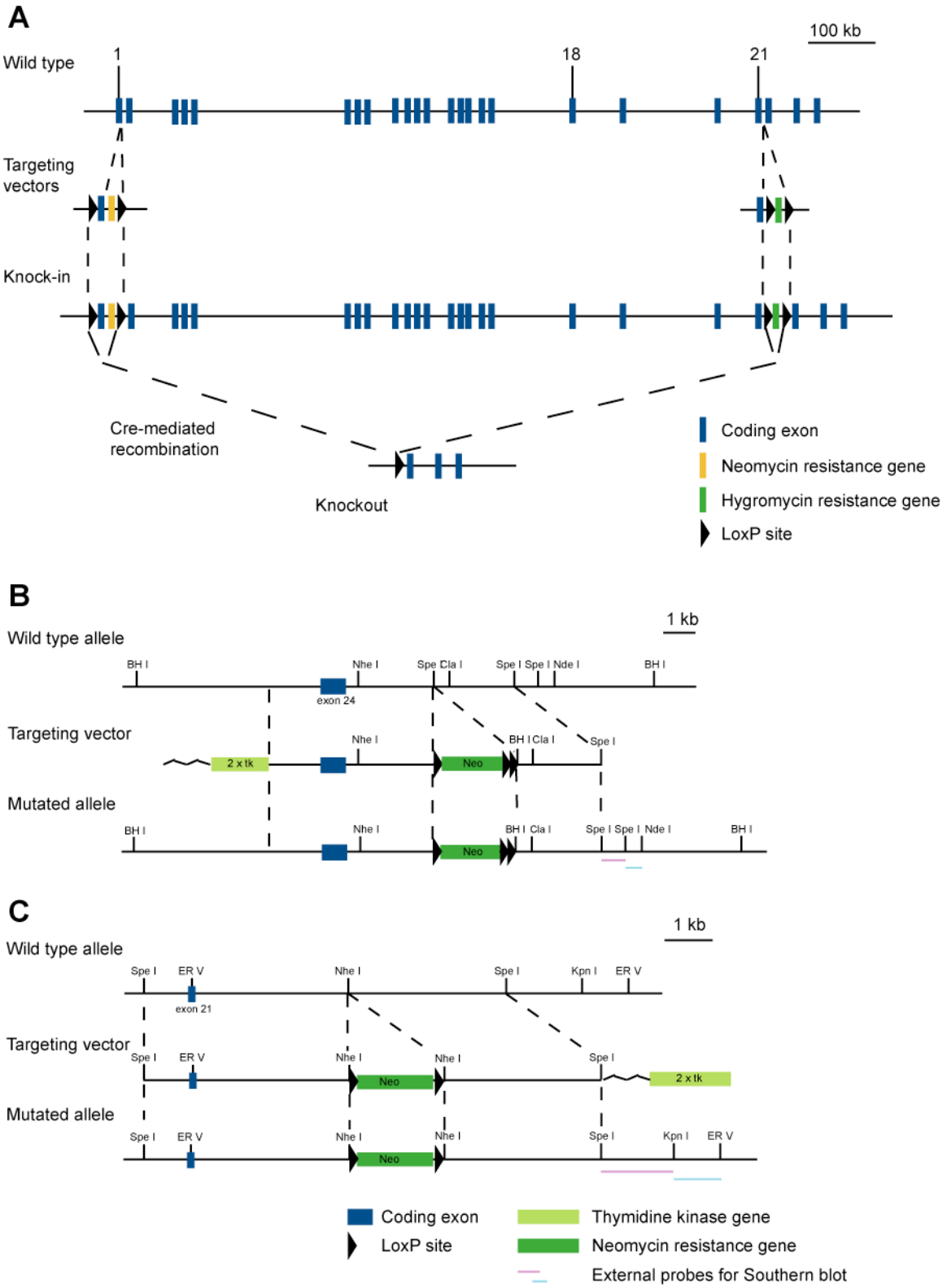

Figure 11. Knockout strategy for deleting the whole *Nrxn1*αβ locus. **A**: Large-scale deletion of the *Nrxn1* locus. The gene is targeted with two vectors at the 5' and 3' ends; Cre-recombination results in the excision of the antibiotic resistance genes and all the coding exons lying between the loxP sites. The recombination scheme is similar when exon 24 is targeted at the 3' end. Exons are not drawn to scale. **B, C**: Targeting strategies for the 3' end of the *Nrxn1* gene. Homologous recombination results in a knock-in where the Hygromycin resistance gene flanked with LoxP sites is inserted into the intron downstream of exon 24 (B) or exon 21 (C).

3.2. α-Neurexins are required for Ca^{2+}-dependent exocytosis in endocrine cells

3.2.1. Neurexins are expressed in endocrine tissues

To screen for other structural alterations in the mutants that possibly remained uncovered in our morphological analyses, manganese-enhanced MRI scans of adult WT and DKO mouse brains were performed (experiments carried out by Dr. Frank Angenstein, IfN, Magdeburg). In this method, Mn^{2+} ions serve as a contrast agent, which is taken up by cells depending on their activity (Angenstein et al. 2007; Pautler et al. 1998). The analysis of the MRI images confirmed the essentially normal gross brain architecture in the α-neurexin mutants and did not reveal additional alterations in the brain, but surprisingly demonstrated a reduced size of the pituitary gland (arrow in Fig. 12A-B). In addition, the intensity of the signal from this region was markedly weaker in the DKOs, suggesting a difference in the functional activity. This observation seemed interesting in view of such aspects of the α-neurexin DKO phenotype as impaired body growth and poor breeding abilities, which are indicators of endocrine disturbances. We therefore wished to explore the morphology and function of the pituitary gland in more detail.

It should be kept in mind that the changes in the pituitary gland of α-neurexin mutants could be brought about by an impaired function of the hypothalamus, which exerts extensive control over pituitary functions. Neurexins have so far been considered neuron-specific (Ushkaryov et al. 1992, but see Occhi et al. 2002), while the defect observed in the pituitary suggested that they may be present in endocrine cells as well. To address this possibility, we studied the expression of the principal neurexin isoforms in endocrine tissues with RT-PCR. Two α-neurexin (Nrxn1α and Nrxn3α) and two β-neurexin (Nrxn1β and Nrxn2β) isoforms were detected at notable levels in the pituitary gland (Fig. 12C). The same isoforms were also present in the pancreatic islets (Fig. 12D). In addition, a similar combination of isoforms (Nrxn1α, 3α and 2β) was found in the adrenal gland (Mohiuddin Ahmad, personal communication). Furthermore, quantitative real-time PCR showed that the relative quantities of α-neurexin mRNA transcripts in the pituitary gland were comparable to or even exceeded those in the brain (Fig. 12E). The relation between the amounts of α-isoforms was also conserved in the brain and pituitary gland, Nrxn1α and 3α being expressed at a higher level, and Nrxn2α being the least abundant α-variant in both tissues.

The presence of neurexins in endocrine cells suggested that the putative defect in the pituitary gland of the DKO mice could be a direct consequence of α-neurexin deletion, and not merely a result of disturbed hypothalamic regulation.

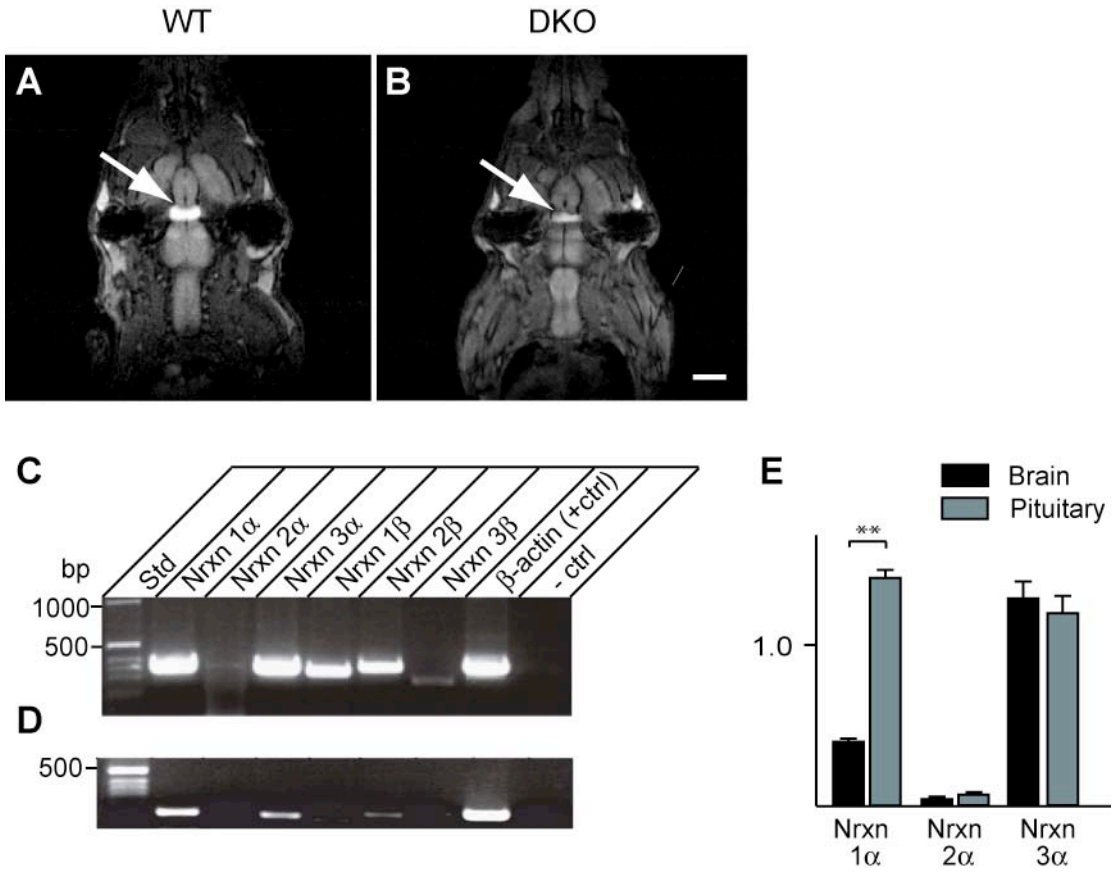

Figure 12. Neurexins are expressed in endocrine tissues. **A-B**: Manganese-enhanced T_1-weighted MRI scans of WT (**A**) and α-neurexin DKO (**B**) mouse brains reveal reduced Mn^{2+} uptake by the pituitary gland (arrows) in the DKO, while brain structure appears unchanged. *Images courtesy of Dr. F. Angenstein, IfN Magdeburg*. **C-D**: Expression of neurexin isoforms in endocrine cells. Total RNA was isolated from the pituitary gland (C) and from purified pancreatic islets (D) and reverse-transcribed. RT-PCR was performed with isoform-specific primers, and amplification products were visualized on an agarose gel. Different pairs of isoform-specific primers were used in the reactions, leading to the different size of the products in C and D. Note the very faint band in the Nrxn1β lane in D. **E**: Quantification of α-neurexin expression in the brain and pituitary gland with real-time PCR. The values are normalized to β-actin as a reference gene. Statistical significance is indicated above the bars: *p<0.01. + ctrl – positive control, - ctrl – negative control. Scale bar: 3 mm in A-B.

3.2.2. Adult α-neurexin knockout mice have a hypomorphic pituitary gland

To find out which parts of the pituitary are affected in the KOs, we next performed a histological analysis of the gland. The pituitary gland in rodents consists of three lobes (Fig. 13A): (i) the anterior lobe (adenohypophysis), which harbors several cell types, producing a

number of trophic hormones; (ii) the intermediate lobe, which is represented by a homogenous population of melanotrophs, mainly producing α-melanocyte-stimulating hormone (α-MSH); (iii) the posterior lobe (neurohypophysis), where the neurohormones oxytocin and vasopressin are released into the bloodstream from the axonal terminals of the magnocellular hypothalamic neurons.

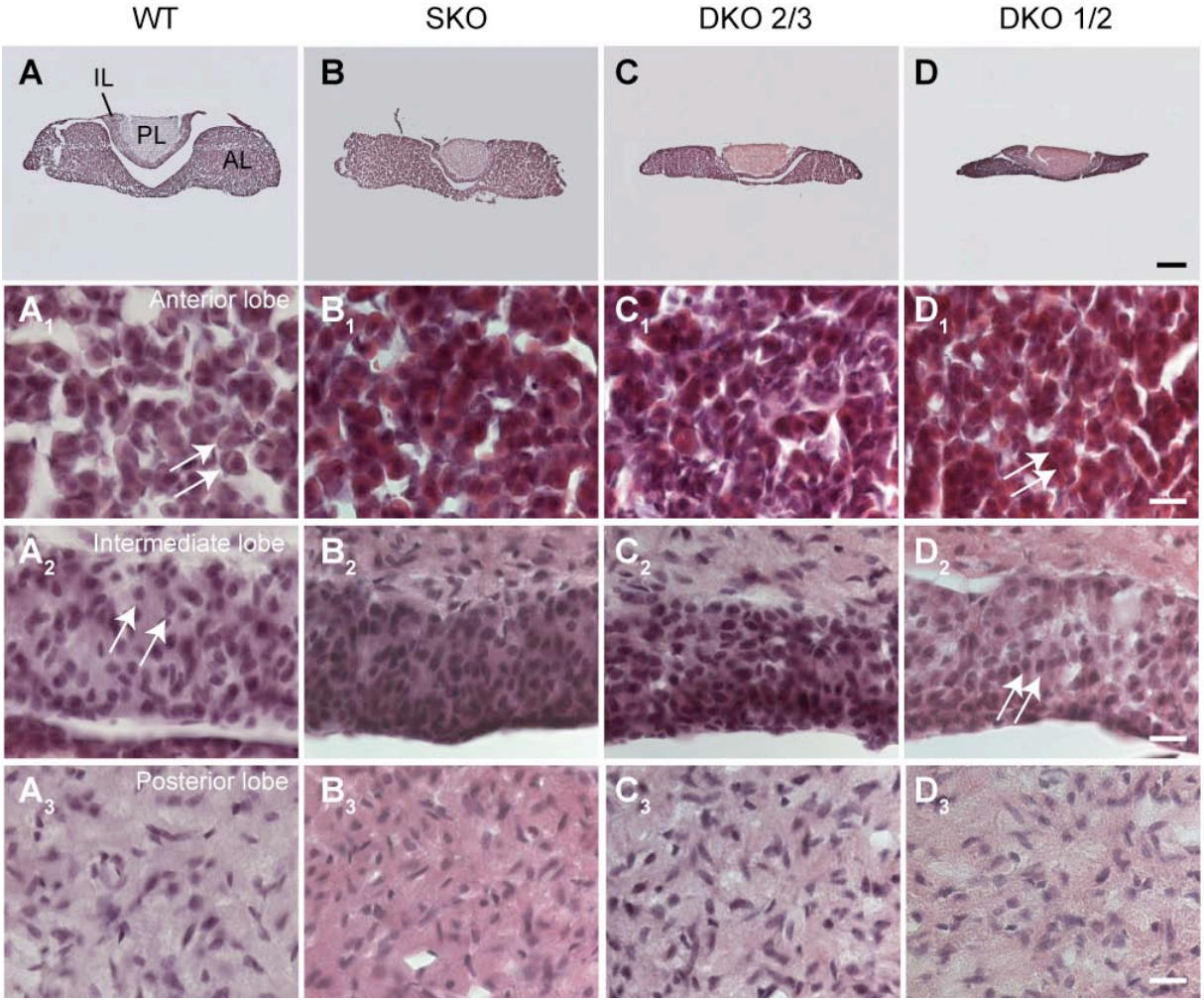

Figure 13. Hypomorphic pituitary gland in α-neurexin mutants. **A-D**: Frontal hematoxylin-eosin-stained sections of the pituitary gland from WT (A), SKO2 (B), DKO2/3 (C) and DKO1/2 (D) mice. Lobes of the pituitary gland are indicated in A: AL – anterior lobe, IL – intermediate lobe, PL – posterior lobe. Higher magnification images of the anterior (A_1-D_1), intermediate (A_2-D_2) and posterior (A_3-D_3) lobes are shown. Note the smaller size and higher density of endocrine cells in the anterior and intermediate lobes of the DKOs (arrows in A_1, A_2 and D_1, D_2). Scale bars: 200 μm in the overviews and 20 μm in the higher magnification images.

Morphometric evaluation of hematoxylin-eosin-stained pituitary sections validated the hypomorphic phenotype of the pituitary gland in the mutants (Fig. 13 A-D) and revealed that the anterior and intermediate lobes of the gland mainly contributed to the decrease in size,

whereas the posterior lobe was less affected (Table 3). In contrast to the moderate morphological changes in the brain (see above), the alterations in the pituitary gland were more dramatic: the affected lobes were much smaller in the DKOs than in the control animals, with the area of the anterior lobe being reduced by over 50%. Higher magnification images showed that this was due to the smaller size of the endocrine cells in the anterior and intermediate lobes of the DKOs (Fig. 13A_1-D_1 and A_2-D_2). The uneven changes in the various lobes of the pituitary suggested a defect specific to endocrine cells, since the posterior lobe, which consists of glial cells and hypothalamic axonal terminals, remained structurally intact, while the anterior and intermediate lobes, composed of endocrine cells, were affected.

Table 3. Morphometric analysis of the pituitary gland in α-neurexin-deficient and control mice

	Genotype				
	WT (n = 3)	SKO2 (n = 6)	DKO1/2 (n = 5)	DKO2/3 (n = 6)	P
Anterior lobe [mm^2] [a, b]	0.65 ± 0.08	0.48 ± 0.04	0.34 ± 0.02* [c]	0.3 ± 0.05*	<0.01
Intermediate lobe [μm] [a, b]	91 ± 6	68 ± 2*	56 ± 3*	58 ± 3*	<0.001
Posterior lobe [mm^2] [a, b]	0.24 ± 0.03	0.19 ± 0.01	0.21 ± 0.01	0.2 ± 0.01	n.s.

Data are means ± SEM; *n* = number of animals. Measurements were made on hematoxylin-eosin-stained section as those shown in Fig. 13A-D. Statistical analysis was performed with one-way ANOVA with Tukey's post-test; n.s. – not significant.
[a] 3-10 sections from each animal were used for data collection.
[b] For anterior and posterior lobes, the values represent the area, for intermediate lobes the thickness.
[c] Asterisks indicate significant difference from WT according to pairwise comparisons with Tukey's test: *p<0.05

We next investigated the distribution of the various pituitary hormones by labeling pituitary sections with hormone-specific antibodies. In the anterior lobe, growth hormone, adrenocorticotrophic hormone and other trophic hormones were detected (Fig. 14). The hormone precursor proopiomelanocortin (POMC) and its cleavage products, α-MSH and β-endorphin were used as markers of the intermediate lobe (Fig. 15). We observed a normal distribution pattern for all these markers. The percentage of cells containing each hormone, the intensity of labeling of individual cells and the distribution of these cells within the lobes were indistinguishable between the mutants and control animals, demonstrating that the cellular composition of the gland and the synthesis of pituitary peptide hormones are preserved in α-neurexin mutants.

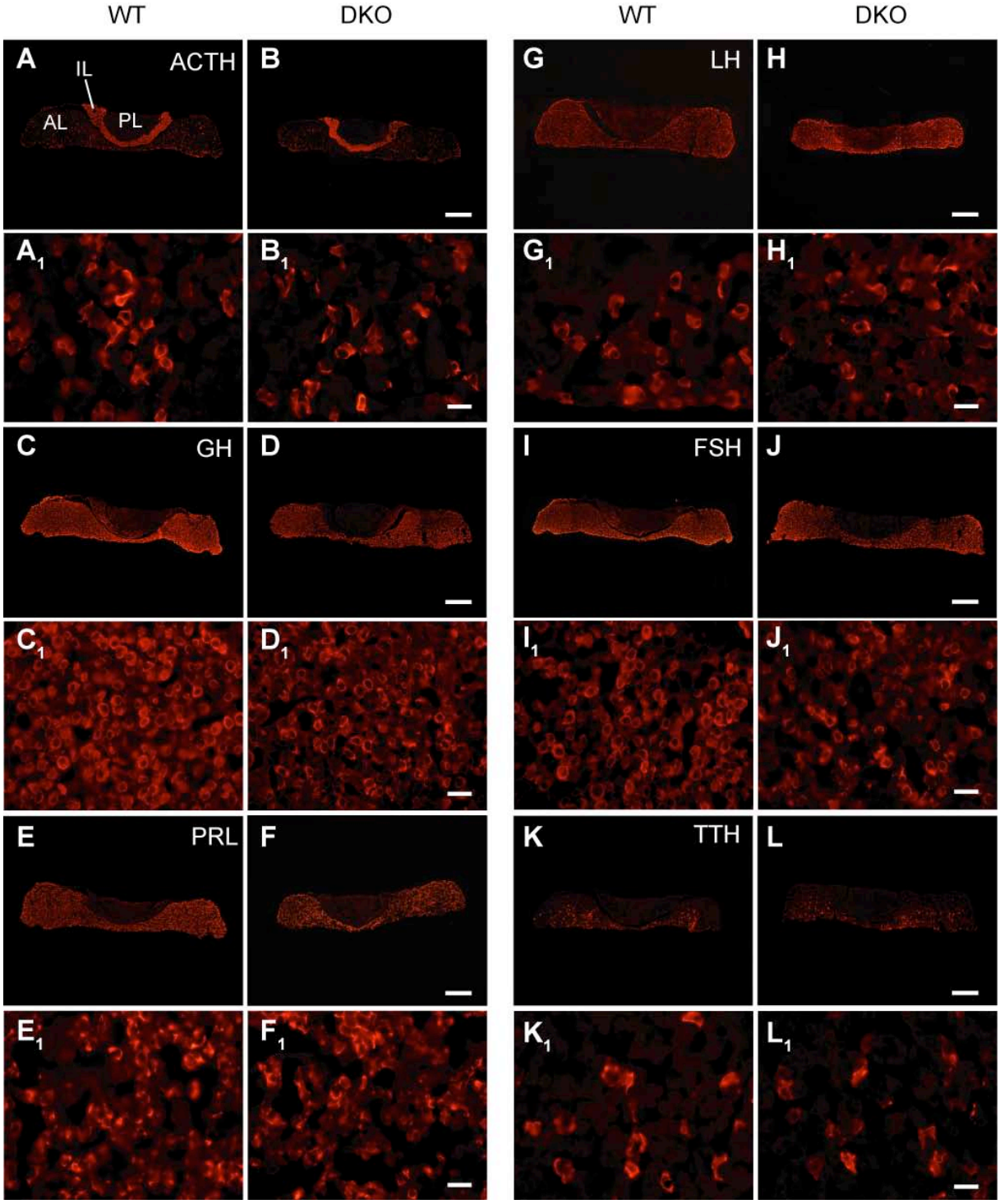

Figure 14. Unchanged distribution of peptide hormones in the anterior lobe of the pituitary gland. Frontal sections of the pituitary gland from WT (**A, C, E, G, I, K**) and α-neurexin DKO mice (**B, D, F, H, J, L**) were immunolabeled with antibodies against the trophic hormones: adrenocorticotrophic hormone (ACTH, A-B), growth hormone (GH, C-D), prolactin (PRL, E-F), luteinizing hormone (LH, G-H), follicle-stimulating hormone (FSH, I-J) and thyrotrophic hormone (TTH, K-L). Higher magnification images are shown for all the markers (A_1-L_1). Anti-ACTH antibody also reacts with POMC in the intermediate lobe (A-B), as ACTH is a product of POMC cleavage. Lobes of the pituitary gland are indicated in A: AL – anterior lobe, IL – intermediate lobe, PL – posterior lobe. Scale bars: 200 μm in the overviews and 20 μm in the higher magnification images.

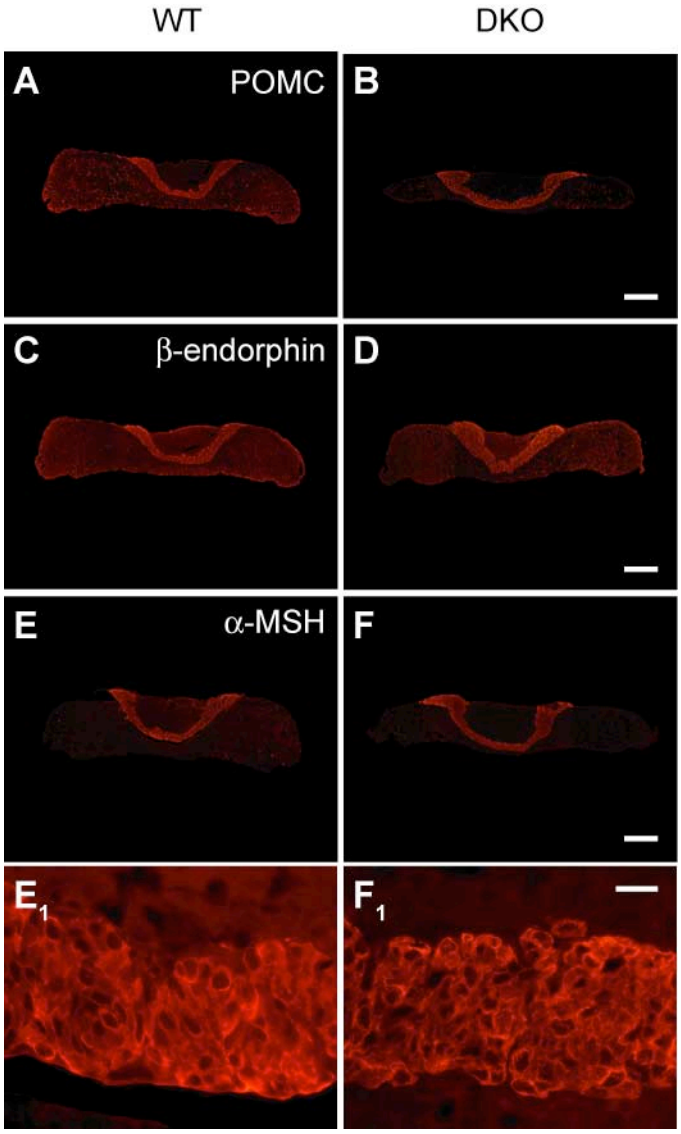

Figure 15. Unchanged distribution of peptide hormones in the intermediate lobe of the pituitary gland in α-neurexin mutants. Frontal sections of the pituitary gland from control (**A, C, E**) and DKO mice (**B, D, F**) were labeled with antibodies against the intermediate lobe marker proopiomelanocortin (POMC, A-B) and its cleavage products β-endorphin (C-D) and α-melanocyte-stimulating hormone (α-MSH, E-F). Higher magnification images of anti-α-MSH-labeled sections demonstrate staining of melanotrophs (E_1, F_1). Scale bars: 200 μm in the overviews and 20 μm in the higher magnification images.

Finally, to label the posterior lobe we used antisera against vasopression and oxytocin, which in both genotypes produced a similar punctate staining surrounding blood vessels (arrows in Fig. 16), indicating that the transport of neurohormones along hypothalamic axons into the posterior lobe is also intact in α-neurexin KOs.

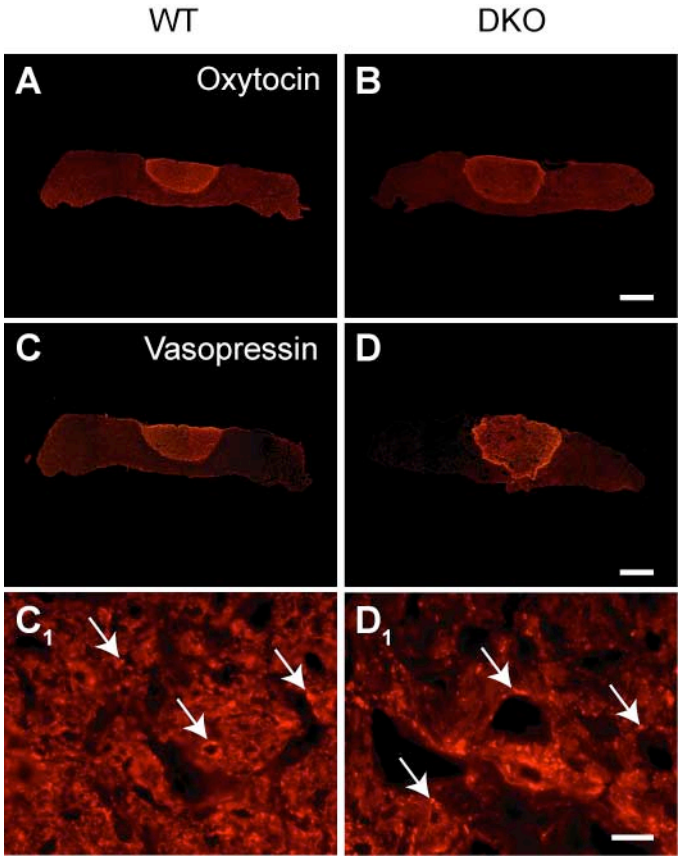

Figure 16. Unchanged distribution of posterior lobe markers in the pituitary gland of α-neurexin DKOs. Frontal sections of the pituitary gland from control (**A, C**) and DKO (**B, D**) mice were immunostained for oxytocin (A-B) and vasopressin (C-D). Higher magnification images of vasopressin-labeled sections (C_1, D_1) show the punctate staining of hypothalamic axonal terminals (arrows) surrounding blood vessels. Scale bars: 200 μm in the overviews and 20 μm in the higher magnification images.

3.2.3. Impaired Ca^{2+}-dependent secretion and intact ultrastructure of α-neurexin-deficient melanotrophs

To investigate the functional activity of the hypomorphic pituitary endocrine cells in α-neurexin mutants, whole-cell patch clamp measurements of membrane capacitance and Ca^{2+}-currents were carried out in melanotrophs in acute pituitary slices. All electrophysiological recordings described here were performed by Dr. Simon Sedej (Neuroendocrinology group, ENI Göttingen). Melanotrophs in the intermediate lobe were chosen for the analysis of secretory activity, because these cells are well characterized electrophysiologically and represent a homogeneous population that can be easily recognised in unstained tissue (Sedej et al. 2004). Besides, in contrast to the situation in other widely studied endocrine cells (chromaffin and pancreatic β-cells), N-, P/Q-, and L-type HVA Ca^{2+} channels are all coupled to the exocytosis of secretory granules in melanotrophs (Mansvelder and Kits 2000; Sedej et al. 2004). This enabled us to further investigate the effect of α-neurexins on Ca^{2+} channel

function, as it was presumed to be specific to N- and P/Q-types of Ca^{2+} channels (Missler et al. 2003; Zhang et al. 2005).

The resting membrane capacitance of melanotrophs was greatly reduced in the DKO mutants (see Fig. 3A-B in Dudanova et al. 2006, App. 2), confirming smaller cell size (membrane capacitance is proportional to the area of the cell membrane and can be used as a measure of cell size). Therefore, in further analyses capacitance and current measurements were normalized to the resting membrane capacitance. As no significant differences were observed between the phenotypes of DKO1/2 and DKO2/3 mutants in the analysis of the histological (Table 3) and electrophysiological data, the two types of DKOs were pooled into one group in further experiments.

Depolarization-evoked Ca^{2+}-dependent exocytosis was severely reduced in the DKOs, mostly due to the fast phase of secretion, while the sustained component was not greatly affected (Fig. 3C-F in Dudanova et al. 2006, App. 2). The fast component of secretion was investigated in more detail by determining the size and release kinetics of the immediately releasable pool (IRP) of secretory granules. The IRP is a part of the readily releasable pool in endocrine cells, which includes a small population of granules docked in the immediate vicinity of Ca^{2+} channels (Moser and Neher 1997; Parsons et al. 1995; Thomas et al. 1993a; Voets et al. 1999). This pool is most tightly coupled to Ca^{2+} influx and characterized by very fast release kinetics in the low millisecond range, approaching the rapid kinetics of synaptic vesicle fusion. Measurements of capacitance responses to a pair of short depolarizing pulses (Gillis et al. 1996) and to depolarizing pulses of increasing duration (Horrigan and Bookman 1994) both demonstrated a two-fold reduction of the IRP in the mutants (Fig. 5 in Dudanova et al. 2006, App. 2).

Based on the previous observations in neurons (Missler et al. 2003), we hypothesized that the defect in secretion could be caused by reduced HVA Ca^{2+} currents. However, whole-cell HVA Ca^{2+} current densities did not differ between the genotypes. Furthermore, pharmacological separation of HVA Ca^{2+} currents did not reveal any changes in the contribution of the different channel types to the whole-cell currents (Fig. 6 in Dudanova et al. 2006, App. 2).

To test whether the reduction of secretion is a consequence of changes in the size, number and/or localization of secretory granules, we performed an ultrastructural study of pituitary melanotrophs. α-Neurexin-deficient cells had no obvious ultrastructural defects and showed a normal packing density of secretory granules. The granule size and the distribution of granules relative to the plasma membrane were also similar to the control cells (Fig. 17A-

D, Table 4) and in agreement with previously published data (Zupancic et al. 1994). The small shift in the distribution of secretory granules towards the plasma membrane in the DKOs (Table 4, Fig. 17E) in fact indicated that a larger number of granules are situated close to the membrane in the DKOs, so the impaired secretion cannot be explained by a reduced availability of secretory granules.

Table 4. Ultrastructural analysis of secretory granules in melanotrophs of α-neurexin DKO and control mice

	Genotype		
	SKO2 (n = 3)	DKO (n = 3)	P
Diameter [nm] [a, b]	299 ± 30	261 ± 17	n.s.
Density [granules/µm] [a]	1.0 ± 0.09	1.0 ± 0.04	n.s.
Relative distribution [a,c]			
0-50 nm	0.22 ± 0.03	0.25 ± 0.03	n.s.
50-150 nm	0.11 ± 0.01	0.15 ± 0.01	n.s.
150-250 nm	0.12 ± 0.01	0.14 ± 0.01	n.s.
250-350 nm	0.11 ± 0.01	0.12 ± 0.01	n.s.
>350 nm	0.44 ± 0.06	0.34 ± 0.04	n.s.

Data are means ± SEM; *n* = number of animals. Measurements were made on randomly sampled electron microscopic pictures of melanotrophs such as shown in Fig. 17A-D. Statistical analysis was performed with *t*-test; n.s. – not significant.
[a] A total number of 1504 (SKO2) and 1564 (DKO) granules were evaluated.
[b] The granule diameter was determined as the average of the shorter and longer diameters.
[c] The distribution of granules within the cytoplasm was analyzed by determining their relative frequency in 5 classes of shortest distances between the granule membrane and the plasma membrane.

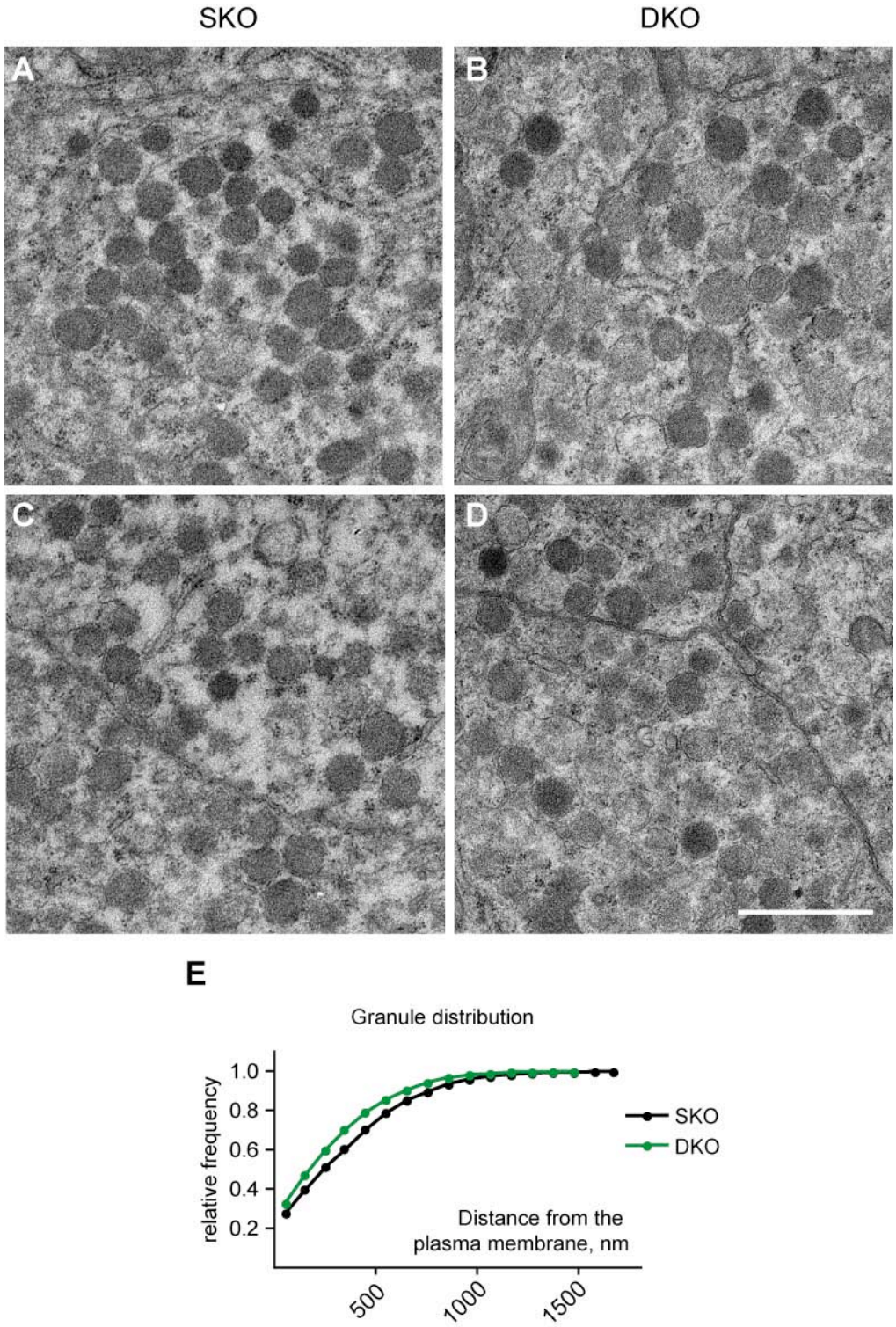

Figure 17. Unchanged ultrastructure of melanotrophs in α-neurexin DKO mice. **A-D**: Examples of electron micrographs of melanotrophs from control (A, C) and DKO (B, D) mice. **E**: Cumulative frequency distribution plot of the shortest distances between the granule membrane and plasma membrane in control (black) and DKO (green) animals. The data are displayed in 50 nm bins. A small shift of the granule distribution towards the membrane in evident in the DKOs. Scale bar: 1 μm in A-D.

3.2.4. Reduced secretion and unchanged morphology of melanotrophs in newborn α-neurexin mutants

We extended our morphological and functional analyses to newborn mice, which allowed us to include TKOs into the study and to observe the full extent of the changes in the pituitary gland caused by α-neurexin deletion. Interestingly, in contrast to the findings in adults, we did not detect any morphological alterations in the size of the gland, its individual lobes or cell size at this early age (Fig. 18). The thickness of the intermediate lobe was 29.5 ± 0.6 µm in controls (n = 3) and 30.6 ± 1.0 µm in DKO and TKO mutants (n = 3, n.s.).

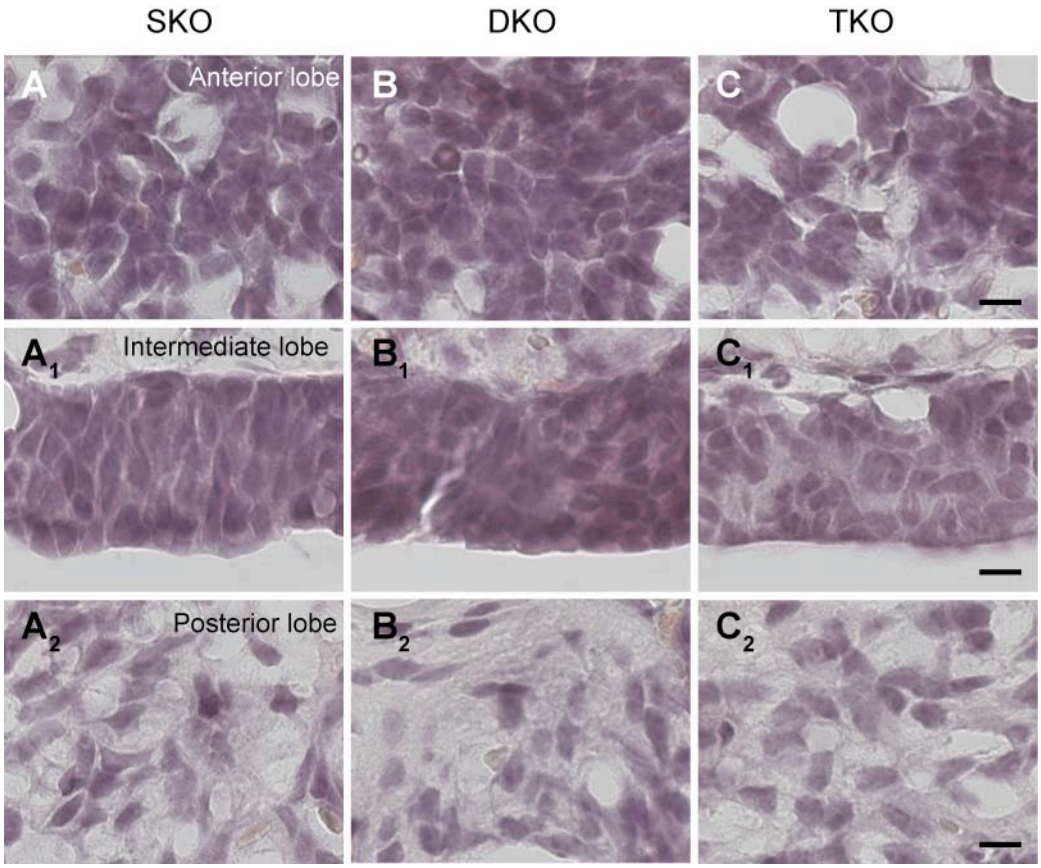

Figure 18. Intact morphology of the pituitary gland in newborn α-neurexin null mutants. Cell size and cell density do not differ in any of the pituitary lobes in newborn SKO2 (**A**), DKO (**B**) and TKO (**C**) mice, as can be seen in frontal hematoxylin-eosin-stained sections. Scale bar: 10 μm in A-C.

The unchanged cell size was confirmed by measurements of the resting membrane capacitance in melanotrophs (Electrophysiological recordings performed by Dr. Simon Sedey, see Fig. 4C in Dudanova et al. 2006, App. 2). However, the secretory defect was already fully present in the newborn DKO mutants (Fig. 4D-F in Dudanova et al. 2006, App. 2), and the impairment was even more severe in the TKOs, in agreement with the previous findings in

neurons (Missler et al. 2003). As in the adult mice, the density of HVA Ca^{2+} currents was not statistically different between α-neurexin-deficient and control melanotrophs (Fig. 6B in Dudanova et al. 2006, App. 2).

3.2.5. Hypothalamic innervation of the pituitary gland in α-neurexin mutants

Hormone secretion in melanotrophs is known to be under the control of inhibitory GABA- and dopaminergic inputs from the hypothalamus (Baumgarten et al. 1972; Oertel et al. 1982; Tomiko et al. 1983; Taraskevich and Douglas 1990). Therefore, secretory defects in melanotrophs could, at least in part, be a consequence of disturbed hypothalamic regulation. To explore this possibility, we visualized hypothalamic axonal terminals in the intermediate pituitary lobe by labeling them with the general synaptic marker synapsin and the GABAergic synaptic marker GAD65. Both markers produced a dispersed punctate staining, with occasional strings of punctae, representing diffuse innervation by hypothalamic fibers, which form synapses *en passant*. The punctae were of a similar size and fluorescence intensity, but much sparser in the DKOs, than in the control animals (Fig. 19), suggesting that hypothalamic innervation is present, but greatly reduced in the mutants. Electrophysiological recordings of spontaneous postsynaptic activity in melanotrophs revealed an ~50% decrease in the frequency of spontaneous postsynaptic currents (Recordings performed by Dr. Simon Sedey, see Fig. 7A-B in Dudanova et al. 2006, App. 2), probably reflecting the lower density of synaptic inputs (Fig. 19) as well as impaired spontaneous release from individual boutons (Missler et al. 2003). Application of 500 mM hypertonic sucrose, which mechanically evokes the release of all readily releasable vesicles in a Ca^{2+}-independent manner (Rosenmund and Stevens 1996), elicited postsynaptic responses which were ~30% smaller in the mutants, than in controls (Fig. 7C-D in Dudanova et al. 2006, App. 2). This decrease is presumably also due to the reduced synapse numbers (Fig. 19). Therefore, reduced innervation might contribute to the impairment of secretion in adult α-neurexin KOs. However, no postsynaptic activity was detected in newborn mice of any genotype, even after the application of α-latrotoxin, which is known to induce massive synaptic vesicle exocytosis (Tzeng et al. 1978). This is in agreement with the observation that hypothalamic innervation of melanotrophs is not established until the first postnatal week (Makarenko et al. 2005). The impaired exocytosis in newborn DKO and TKO mice lacking hypothalamic inputs (Fig. 4D-F in Dudanova et al. 2006, App. 2) provides evidence for a primary, cell-autonomous defect in the pituitary gland, which is independent of hypothalamic influences.

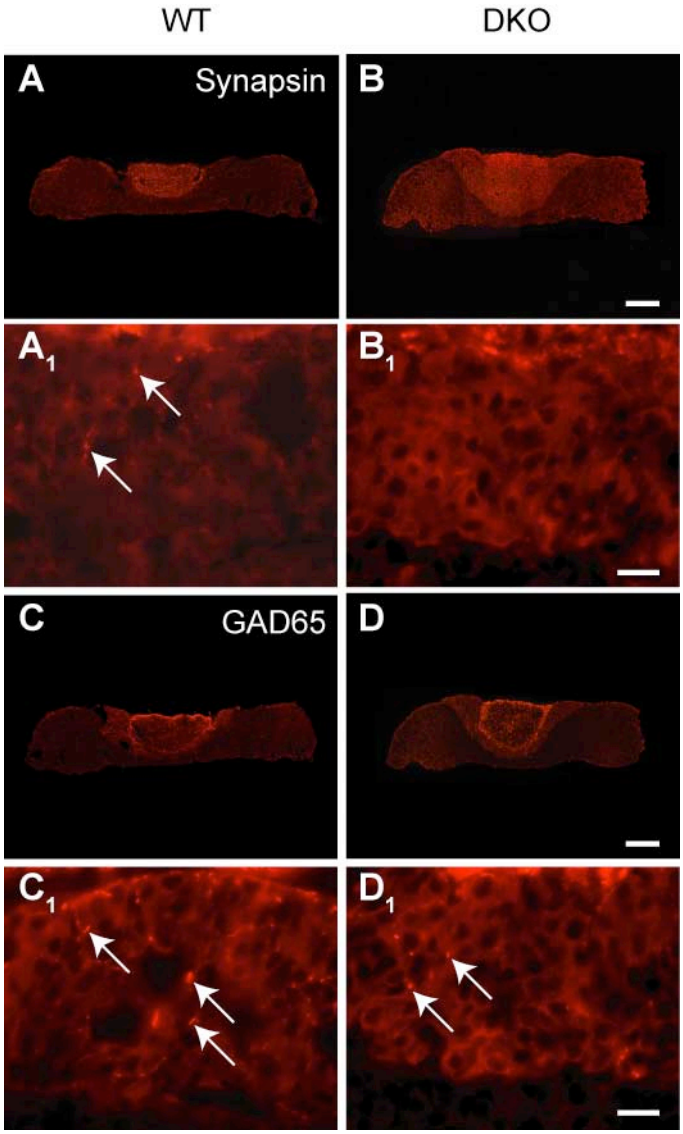

Figure 19. Sparse hypothalamic innervation of the intermediate pituitary lobe in α-neurexin KO mutants. Frontal sections of the pituitary gland from control (**A, C**) and α-neurexin DKO (**B, D**) mice were labeled with antibodies against the general synaptic marker synapsin (A-B) and the inhibitory synaptic marker GAD65 (C-D). Each of the antibodies produces a similar punctate staining pattern in both genotypes, but the number of fluorescently labeled punctae (arrows) is much lower in the DKOs, as can be seen in the higher magnification images. Scale bars: 200 μm in the overviews and 20 μm in the higher magnification images.

4. Discussion

In this study we show that (i) α-neurexins do not play a prominent role in the formation of the majority of synapses *in vivo*, but are required for the normal development of the neuropil, (ii) α-neurexins are expressed in endocrine tissues and are important for Ca^{2+}-dependent release of peptide hormones from endocrine cells.

4.1. α-Neurexins contribute to normal neuropil structure, but do not play a major role in synaptogenesis

The morphometric analysis of α-neurexin DKO brains revealed a moderate reduction in the size of brain structures and a corresponding increase in cell density (Fig. 5, Table 1). These structural changes were not restricted to a particular part of the brain, but their degree of severity varied across different areas. Based on the absence of any signs of increased apoptosis or alterations of the immunoreactivity to cellular markers (Dudanova et al. 2007), we attributed the observed reduction in the size of the affected brain structures to a paucity of neuropil components. Although it is not clear why there were local differences in the degree of neuropil reduction, one of the reasons may be the differential expression of the remaining α-neurexin isoforms in the DKOs. Previous experiments demonstrated a shortening of dendritic branches and a loss of spines at the peripheral segments of the dendritic trees (Dudanova et al. 2007), pointing a possible source of neuropil reduction in the mutants.

The immunoreactivity pattern of excitatory and pan-synaptic markers was not changed in the DKO brains (Fig. 6, 7), and electron microscopy did not show any decrease in the density of asymmetric contacts in general or axospinous contacts (Table 2). However, these data do not contradict our observations in Golgi-impregnated brains, because the staining intensity of immunolabeled sections reflects only the *density* of synapses, which was unaltered according to the measurements in Golgi-stained neurons, rather than the *absolute number* of synapses, which is most likely reduced. The same argument applies to the unchanged density of type I and axospinous synapses measured with electron microscopy.

Surprisingly, we also detected a notably higher density of perforated synapses in the DKOs. Although the origin and functional correlates of these synapses have not been clearly established, an increase in perforated synapses has often been associated with synaptic plasticity (Buchs and Muller 1996; Calverley and Jones 1990; Lynch et al. 1994; Toni et al. 2001). Interestingly, enhanced long-term potentiation has been observed at the Schaffer collateral – CA1 synapses of α-neurexin DKO mice (Ahmad et al., submitted).

For inhibitory synapse markers, we noticed a lower staining intensity of brain sections from the DKO mutants (Fig. 8), indicating a reduction in the area density of inhibitory synapses, which was confirmed by quantitative electron microscopy (Table 2).

The neuropil changes we observed are consistent with some involvement of α-neurexins in synapse formation, as also suggested by cell culture-based experiments (Chih et al. 2006; Graf et al. 2004). However, the degree of structural alterations is very mild in comparison to the dramatic consequences of α-neurexins deletion on survival and synaptic release (Missler et al. 2003; Zhang et al. 2005). While α-neurexins clearly play an important role in synaptic function, their contribution to synaptogenesis *in vivo* seems to be less significant.

The recently reported findings in KO mice deficient in multiple neuroligins, the putative partners of neurexins in mediating synapse formation (Graf et al. 2004), also do not support any prominent role of the neurexin-neuroligin complex in synaptogenesis. Similar to α-neurexin mutants, neuroligin KOs display a severe impairment of synaptic transmission, while the total synapse numbers in their brains are unchanged, with only a small shift in the ratio between excitatory and inhibitory contacts (Varoqueaux et al. 2006).

It should be kept in mind that one α-neurexin gene is still intact in the DKO mutants, providing some degree of compensation for the two deleted genes, since α-neurexins are likely to be functionally redundant (Zhang et al. 2005). Furthermore, the majority of DKO mice, which are presumably more heavily affected by the mutation, perish within the first 2-3 weeks of life, so in studying adults we were restricted to a sample of surviving DKOs biased towards a better compensation for the deletion-caused defects. Finally, β-neurexins are also preserved in α-neurexin knockouts, and could partially take over the synaptogenic function of α-neurexins. However, protein levels of β-isoforms are not elevated in the mutant animals (Missler et al. 2003), and the expression patterns of α- and β-isoforms do not entirely overlap (Ullrich et al. 1995).

A reduction of neuropil has also been observed in some other mouse models such as the Semaphorin 3A (Sema 3A) KO mice (Behar et al. 1996) and heterozygous reeler mice (Liu et al. 2001). Compared to α-neurexin knockouts, neuropil hypoplasia is more severe in these mutants and is accompanied by additional defects. For example, in the reeler mutant, spine densities are also decreased (Liu et al. 2001). The phenotype of the Sema3A KO also includes axonal pathfinding errors and aberrant dendritic orientation (Behar et al. 1996). In addition, reduced dendritic complexity throughout the whole length of the dendritic arbor was observed in cortical cultures from Sema3A KOs, and a pronounced loss of spines was revealed in the

neocortical pyramidal neurons by Golgi staining of the KO brains (Fenstermaker et al. 2004; Morita et al. 2006). In contrast to the severe consequences of these genetic manipulations, the defect of dendritic architecture in α-neurexin mutants is mild and periphery-restricted, suggesting normal dendrite growth and secondary retraction of the terminal branches. The differences between α-neurexin KOs and mutants of other molecules involved in neuronal development again corroborate our hypothesis that α-neurexins are not necessary for the initial brain assembly, but might participate in later stages of development.

4.2. The role of α-neurexins at inhibitory synapses: Specific or coincidental?

In our *in vivo* study, the most pronounced morphological change was the significant decrease in the area density of type II (presumably inhibitory) synapses in all the layers of the primary visual cortex in the DKO mice (Table 2), supported by the reduced intensity of immunohistochemical stainings with GABAergic markers (Fig. 8). These findings extend the previous observations of a decrease in type II synapse density in newborn α-neurexin TKOs (Missler et al. 2003) and suggest that this decrease is permanent and does not represent a delay in development, a possibility that could not be excluded in the newborns. The less pronounced reduction in adult DKO mice compared to newborn TKOs (30% vs. 50%) is probably due to the fact that one α-neurexin isoform is still preserved in the DKOs. In addition, the overall "compression" of the neuropil in the adult DKOs leads to some overestimation of synapse numbers when compared to newborn mice with unchanged volume of the neuropil. Thus, inhibitory synapses indeed seem more affected by the absence of α-neurexins, their number being clearly reduced, while that of excitatory synapses is marginally different from the control brains. Along this line, evoked inhibitory neurotransmission is also dramatically reduced at inhibitory synapses in the mutants, while excitatory transmission is less severely affected (Missler et al. 2003).

As no reduction in the number of GABAergic neurons could be detected in the cortex (Fig. 10, Table 1), the decrease in the area density of type II synapses must be due to a reduction in the number of inhibitory contacts formed by each GABAergic neuron, so it is conceivable that α-neurexins are important for inducing inhibitory synapses, while being dispensable for excitatory ones.

Based on the evidence provided by *in vitro* studies (Chih et al. 2006; Graf et al. 2004, 2006) neuroligin seems to be the most likely postsynaptic partner for mediating synaptogenic effects of α-neurexins. In neuroligin-deficient mice the overall number of synapses was not changed, but there was a small shift in the excitatory/inhibitory synapse ratio, with inhibitory

contacts being slightly reduced. Functional defects in neuroligin KOs were also mostly found at inhibitory synapses. Another possible adhesion partner of α-neurexins at the postsynapse is dystroglycan (Sugita et al. 2001). However, deletion of dystroglycan in mice did not cause a reduction of presynaptic neurotransmitter release (Moore et al. 2002). Graf et al. (2004) also showed that heterologously expressed neurexins do not cluster α- or β-dystroglycan in contacting dendrites. Moreover, the late accumulation of dystroglycan at synapses, which lags behind the accumulation of receptors and scaffolding proteins, and the unchanged numbers of GABAergic synapses formed by dystroglycan-deficient neurons in culture (Levi et al. 2002), both argue against its role in synaptogenesis. In addition to neuroligin and dystroglycan, neurexins may engage in transsynaptic interactions with other, as yet unknown, binding partners.

Although inhibitory synapses appear to be more severely affected by the deletion of α-neurexins, it nevertheless seems unlikely that α-neurexins might be restricted to and have specialized functions at this type of synapse, as has been suggested recently (Chih et al. 2006; Craig and Kang 2007). A number of observations point against this hypothesis: (i) *In situ* hybridization demonstrated localization of α- and β-neurexins in both excitatory and inhibitory neurons (Ullrich et al. 1995); (ii) The deletion of α-neurexins in mice causes dramatic defects of neurotransmitter release and long-term structural alterations that are present at both GABAergic and glutamatergic synapses (Missler et al. 2003 and this study); (iii) In a number of *in vitro* assays, manipulations of presumably unselective neurexin isoforms also produced stronger effects on inhibitory synapses. For example, Graf et al. (2006) demonstrated a higher potency of neurexin 1β in inducing GABAergic, than glutamatergic, synapses. Along this line, Levinson et al. (2005) reported a reduction of both excitatory and inhibitory miniature postsynaptic current (mEPSC and mIPSC) frequencies, with mIPSCs being more severely affected, when soluble β-neurexin was used to block the transsynaptic neurexin-neuroligin interaction. Importantly, these studies employed the splice insert 4-*lacking* isoform of β-neurexin, presumably *not* selective for synapse types. Similarly, Chih et al. (2005) described higher vulnerability of inhibitory synapse function to disruption of neurexin-neuroligin binding by RNAi knockdown of *all* neuroligins.

Therefore, the fact that the density of inhibitory synapses is affected in the knockouts, while that of excitatory synapses is not, might have something to do with the properties of these synapses, rather than with selective effects of neurexin isoforms. Most of the adhesion molecules and postsynaptic scaffolding proteins described so far are localized at excitatory synapses (McGee and Bredt 2003; Waites et al. 2005), and at the moment there are only a few

candidates for mediating inhibitory synaptogenesis (e.g., Paradis et al. 2007). While it is possible that our knowledge about the molecules involved in inhibitory synapse assembly is still very limited (Fritschy and Brunig 2003) and more adhesion molecules remain to be discovered at inhibitory contacts in the future, it may also be that inhibitory synapses actually dispose of fewer transsynaptic adhesion systems and therefore rely more heavily on neurexins for their structural integrity. In addition, inhibitory synapses may be generally more vulnerable to developmental disturbances (e.g., Ramakers et al. 1994), possibly because of their early onset of activity and their particular role in the establishment of neuronal networks (Ben-Ari 2001). An ~30% decrease in the density of inhibitory synapses in the hippocampus, accompanied by a reduction of inhibitory synaptic transmission, was observed in mice with a deletion of the cell adhesion molecule L1 (Saghatelyan et al. 2004). However, L1 is expressed by both excitatory and inhibitory neurons (Horinouchi et al. 2005), and it is not able to initiate pre- or postsynaptic differentiation in co-culture assays (Graf et al. 2004; Scheiffele et al. 2000), suggesting that a selective reduction of inhibitory contacts in the mutant does not necessarily imply a specific role of the deleted molecule in inhibitory synapse formation.

Therefore, restricted localization and activity of neurexin isoforms at excitatory and inhibitory synapses observed *in vitro* may not truly represent the physiological function of these molecules. The effects observed in culture might vary depending on experimental conditions such as cell type and degree of overexpression (Sara et al. 2005; Fairless 2006). The pending analysis of β-neurexin null mutants will be necessary to resolve the issue of specialized or overlapping functions of α- and β-neurexins. We have now started generating a Nrxn1αβ null-mutant to address the question of functional redundancy of neurexin isoforms. It would be interesting to see whether an additional deletion of β-neurexin on the α-neurexin KO background would aggravate the structural defects observed in this study. As with α-neurexins, it will probably be necessary to ablate multiple β-neurexins to get an insight into their *in vivo* function, due to extensive functional redundancy.

4.3. Synapse stabilization by α-neurexins

In contrast to inhibitory contacts, excitatory synapse numbers are not changed at birth in α-neurexin KOs (Missler et al. 2003), but decrease slightly during the course of postnatal development. Moreover, the changes in excitatory synapses are rather small and restricted to the terminal dendritic ramifications. It therefore seems likely that elimination of neuronal connections, rather than a primary defect in synaptogenesis, underlies this decrease.

What might cause these changes in α-neurexin DKOs? As α-neurexins have been implicated in both synapse formation and regulation of synaptic transmission, it is hard to distinguish between the possible causes of the observed morphological alterations. Multiple scenarios can be proposed for the involvement of α-neurexins in synapse maintenance.

First, activity may play a crucial role in stabilizing neuronal connections. A commonly held view on the relationship between synaptic function and structure is that activity is dispensable for the initial synapse formation, which is predetermined genetically, but is important for the stabilization and refinement of neuronal connections in the long term (Benson et al. 2001; Craig and Boudin 2001; Katz and Shatz 1996; Waites et al. 2005). The issue of relationship between synaptic activity and brain structure has been addressed in multiple studies of synaptic protein KOs. Normal brain assembly and neuronal wiring were usually observed in these mutants, in spite of severe defects or even a complete shutdown of neurotransmission. As for the maintenance of the correctly established connections, the present evidence from genetic models is more contradictory. In Munc18-1 KO brains, which are completely devoid of synaptic activity, extensive neurodegeneration starts long before birth (Verhage et al. 2000), and synapse formation and maturation are impaired (Bouwman et al. 2004). On the contrary, Munc13-1/2 DKOs are born with electrically silent, but morphologically normal brains (Varoqueaux et al. 2002). Unaltered brain morphology was also reported in other synaptic protein mutants, such as Mint 1/2 DKOs (Ho et al. 2006), Synaptotagmin 1 (Geppert et al. 1994), Synaptobrevin 2 (Schoch et al. 2001) and SNAP-25 KOs (Washbourne et al. 2002). However, the brain is largely immature at birth, and synaptogenesis extends long into postnatal life. Interestingly, when hippocampal neurons of SNAP-25 mutants are maintained in culture, they initially form synaptic connections, which then undergo early degeneration before reaching maturation (Washbourne et al. 2002). The early postnatal lethality of the majority of synaptic protein mutants prevents investigating the long-term effects of the mutation on brain structure. α-Neurexin DKOs represent a convenient model to study such effects, since these mutants show an impairment of synaptic function which is mild enough to allow the survival of some of the animals for several weeks. This enabled us to observe rather subtle, but widespread structural alterations in the brain that accumulate over a long period and could not be detected in the newborn animals. Since excitatory synaptic transmission in the mutants is already impaired at birth, while morphological alterations of excitatory synapses appear only later, these changes may at least in part be activity-dependent. Retraction of spines has been observed after pharmacological blockade of neurotransmission, suggesting a trophic role of synaptic activity in maintaining

synapses and spines (McKinney et al. 1999). The greatly decreased synaptic activity in α-neurexin mutants could therefore lead to synapse elimination (Goda and Davis 2003). Furthermore, local synaptic signaling appears to actively support dendritic structure (Lohmann et al. 2002; McAllister 2000; Niell et al. 2004). So the elimination of synapses would destabilize dendrites and lead to retraction of inactive dendritic branches in the long term. The loss of a proportion of synaptic inputs to a neuron may in turn have a substantial effect on neuronal circuitry (Whitford et al. 2002). Synaptic activity is also important for the normal formation and functional maturation of inhibitory synapses, as demonstrated in a number of *in vitro* (Colin-Le Brun et al. 2004; Marty et al. 2000; Rosato-Siri et al. 2002; Seil and Drake-Baumann 1994) and *in vivo* (Micheva and Beaulieu 1995) preparations. However, additional long-term changes in inhibitory contacts would probably be difficult to detect in α-neurexin mutants because of the pronounced decrease in the number of these contacts observed already at birth.

Another possible explanation for the described morphological changes is based on the properties of α-neurexins as classical adhesion molecules, which keep the pre- and postsynaptic membranes in close apposition by interacting with postsynaptic cell-surface molecules, presumably neuroligins. In one of the *in vitro* studies, the splice variant of neuroligin which binds α-neurexins was much more potent in increasing the size of presynaptic boutons and dendritic spines, than in inducing new contacts, suggesting a role for the α-neurexin-neuroligin pair in synapse maturation and expansion (Boucard et al. 2005). Furthermore, it has been shown by *in vivo* time-lapse imaging that bigger spines (and presumably synapses) are usually more stable and have longer lifetimes (Holtmaat et al. 2005). The absence of α-neurexins may thus hinder synapse growth and stabilization. As with the previous explanation, it seems likely that these processes also affect inhibitory synapses, but putative changes on top of the initial decrease in inhibitory contacts would be quite small.

Finally, a more indirect explanation of excitatory synapse loss involves homeostatic compensatory reactions which take place at the level of neural circuits and adjust their overall activity, keeping it at a certain optimal set-point value (Turrigiano and Nelson 2004). The decrease in inhibitory synapse number and function probably causes reduced inhibitory tone in the mutants (Ahmad et al., submitted), leading potentially to overexcitation. Homeostatic mechanisms may exist that act to prevent this dangerous condition and stabilize neural circuits by changing the level of excitation accordingly. This may occur by silencing and subsequent elimination of a proportion of excitatory synapses in order to re-establish the excitation/inhibiton balance.

In conclusion, the overall mild degree and late development of morphological changes in α-neurexin mutants suggest that these molecules are largely dispensable for initial synapse formation, but contribute to long-term stability of synapses. Further experiments will show whether this function of α-neurexins depends on their properties as cell adhesion molecules, or on their role as regulators of synaptic transmission.

4.4. α-Neurexins belong to the general machinery for Ca^{2+}-triggered exocytosis

We have shown here that neurexins, previously regarded as neuron-specific molecules, are also expressed in endocrine tissues. Only synapse-specific functions have been known or suggested for neurexins so far, such as heterophylic synaptic adhesion, organization of active zones and regulation of neurotransmission (Dean et al. 2003; Graf et al. 2004; Missler et al. 2003; Ushkaryov et al. 1992). It is therefore unexpected that neurexins are also present in significant amounts in endocrine cells, which have no postsynaptic adhesion partners and no specialized release sites similar to active zones. This finding suggested that neurexins may have a more general role in secretory cells than previously believed.

A severe defect of secretion was found in melanotrophs of α-neurexin mutants (Dudanova et al. 2006), demonstrating that α-neurexins are required for Ca^{2+}-triggered release in endocrine cells as well as in neurons. Interestingly, electrophysiological measurements revealed no differences between WT and SKO2, probably because of the very low level of expression of Nrxn2α in the pituitary (Fig. 12E). The two types of DKOs also did not differ significantly from each other in any of the parameters. This is in contrast to the previous findings, where deletion of Nrxn1α and 2α isoforms generally had more severe consequences than deletion of Nrxn2α and 3α, i.e., much lower survival rates and a greater impairment of synaptic transmission (Missler et al. 2003). The level of Nrxn1α in the pituitary was actually higher, than in the brain (Fig. 12E), while the consequences of its absence were less severe, suggesting a certain degree of functional specialization between α-neurexin isoforms.

It should be noted that expression of neurexins was not investigated in the intermediate lobe separately. However, a number of observations suggest the presence of neurexins in melanotrophs. First, neurexins are not known to be expressed in glia, so it seems unlikely that the posterior lobe pituicytes, which have a glial origin, could contribute significantly to the detected amounts of RNA. The morphological changes rather suggest that endocrine cells of the anterior and intermediate lobe are specifically affected by the deletion of α-neurexins. This is further supported by the detection of neurexin isoforms in other

populations of endocrine cells (pancreatic islets, adrenal gland). Finally, the cell-autonomous nature of the secretory defect observed in newborn mutant melanotrophs confirmed that this defect is a direct consequence of α-neurexin deletion.

Analyses of several genetic mouse models have shown that other synaptic proteins also perform similar functions at synapses and in endocrine cells. Deletion of synaptotagmin 1 gene selectively abolished the fast phase of secretion in both hippocampal neurons (Geppert et al. 1994) and chromaffin cells (Voets et al. 2001a), establishing the role of synaptotagmin 1 as the Ca^{2+} sensor for both types of release. A similar effect was observed in melanotrophs upon acute block of synaptotagmin I expression (Kreft et al. 2003). Furthermore, the same SNARE proteins are involved in mediating vesicle fusion in both cell types. For example, SNAP25-deficient neurons (Washbourne et al. 2002) and chromaffin cells (Sorensen et al. 2003) exhibited a similar phenotype with a block of regulated Ca^{2+}-dependent exocytosis. Ablation of Munc18-1 resulted in a complete arrest of neurotransmission in the brain (Verhage et al. 2000) and a dramatic reduction of endocrine secretion in chromaffin cells (Voets et al. 2001b) and pituitary somatotrophs (Korteweg et al. 2005).

What distinguishes α-neurexins from these proteins with well-established roles in synaptic vesicle exocytosis is their additional function as synaptic cell adhesion molecules. It is surprising that these molecules can also regulate secretion in cells that have no postsynaptic partners. Several other cell adhesion molecules have also been implicated in regulating endocrine release. For example, deletion of neural cell adhesion molecule (NCAM) led to a pronounced impairment in Ca^{2+}-dependent secretion and reduced IRP in chromaffin cells (Chan et al. 2005), along with the defects at central and neuromuscular synapses (Cremer et al. 1998; Muller et al. 1996; Polo-Parada et al. 2001; Polo-Parada et al. 2004; Rafuse et al. 2000). Furthermore, both NCAM- and N-cadherin-mediated homophylic adhesion was shown to stimulate secretion of growth hormone from cultured anterior pituitary cells (Rubinek et al. 2003). These few studies and our data from α-neurexin KOs reported here add synaptic cell adhesion molecules to the general components and modulators of the secretory machinery that are shared between neuronal and endocrine cells. No extracellular binding partner for neurexins has been detected in the pituitary gland so far, so it remains unclear whether the action of α-neurexins on release has any relation to their adhesive properties.

4.5. The impairment of secretion in α-neurexin-deficient melanotrophs is primary and cell-autonomous

The impairment of exocytosis was accompanied by pronounced morphological changes in the anterior and intermediate pituitary lobes of α-neurexin KO mice (Fig. 13, Table 3). To answer the question whether the structural changes represent the cause or the consequence of the reduction in release, we turned to newborn animals. This allowed us to reveal a clear temporal difference between the structural and functional defects: Newborn melanotrophs were still morphologically intact, but displayed a pronounced decrease in evoked secretion (Fig. 18 and Dudanova et al. 2006). Therefore, it seems likely that the hypomorphic changes in the adult pituitary gland are a consequence of its insufficient functional activity.

Interestingly, the structural effects of α-neurexin deletion found in the pituitary gland (Fig. 13, Table 3) were much more severe than those in the brain (Fig. 5, and Dudanova et al. 2007). This may be explained by the ability of endocrine cells to undergo rapid structural changes depending on the state of their secretory activity. For example, treatment with dopaminergic drugs, stress and other conditions which affect peptide secretion from melanotrophs were reported to cause considerable alterations of melanotroph morphology in rodents (Back and Rechardt 1985; Chronwall et al. 1988; Moriarty et al. 1975; Saland 1978; Saland et al. 1982; Santolaya and Ciocca 1981).

In spite of the reduction in the size of endocrine cells, the synthesis of pituitary hormones and biogenesis and membrane targeting of secretory granules in melanotrophs were not affected in the mutants (Fig. 14, 15, 17, Table 4). The slightly shifted distribution of granules in melanotrophs (Fig. 17E) could probably represent a consequence of reduced secretion, with granules accumulating in the docked state at the membrane due to the reduced number of fusion events. The change in distribution was rather small, and no similar accumulation of granules could be found at neocortical synapses (Table 2), which also display an impairment of release. This discrepancy may result from the differences in biogenesis of synaptic vesicles and secretory granules (Morgan and Burgoyne 1997; Sudhof 2004). Synaptic vesicles undergo activity-dependent recycling, which should slow down accordingly when release is reduced. In contrast, the generation of new secretory granules is not directly coupled to their release, which may lead to a slight imbalance of granule generation in release-defective cells.

Since α-MSH secretion is regulated by the hypothalamus, several experiments were performed to test the state of hypothalamic inputs in the intermediate lobe. We did observe a pronounced reduction in the number and activity of hypothalamic axonal terminals in α-

neurexin mutants (Fig. 19 and Dudanova et al. 2006). However, the impairment of secretion was also present in newborn mice before the arrival of the hypothalamic terminals to the intermediate lobe, and was as severe as in the adult animals of the same genotype (Dudanova et al. 2006). These observations clearly point to a cell-automonous defect in melanotrophs. Even if reduced innervation does play some role in the changes that we observed in the adult mice, its contribution is not very prominent, since there is no significant aggravation of the secretory defect in the DKOs after the onset of hypothalamic regulation.

In three different systems studied so far, i.e., brain, pituitary gland and the neuromuscular junction (Missler et al. 2003; Sons et al. 2006 and this study), functional defects were more severe and appeared earlier, than morphological alterations. These data show that α-neurexins are primarily involved in the function of excitable cells, while playing a secondary role in their structure. Furthermore, our results support the hypothesis that functional activity has a significant impact on the morphological aspects of the nervous and other excitable tissues (Katz and Shatz 1996, Chronwall et al. 1998).

4.6. α-Neurexins as organizers of release sites

Several observations indicate that α-neurexins may be important for Ca^{2+} triggering of release at synapses as well as in endocrine cells: (i) The weak effect of Ca^{2+} channel blockers in α-neurexin-deficient neurons, which could be rescued by the transgenic expression of Nrxn1α (Missler et al. 2003; Zhang et al. 2005); (ii) The severely affected fast kinetic component of release in α-neurexin DKO melanotrophs (Dudanova et al. 2006). During the fast component, primed and release-ready granules undergo fusion, and their release is only dependent on the Ca^{2+} concentration in the immediate vicinity of the vesicle (Neher 2006; Wadel et al. 2007). During the sustained component, more granules undergo recruitment and reach fusion competence (Voets et al. 1999), and their release kinetics are mostly determined by docking and priming rates, which do not seem to be affected in α-neurexin mutants. Once a sufficient Ca^{2+} concentration has built up in the cytoplasm, fusion can proceed at a normal rate. (iii) The normal ultrastructure of synapses and melanotrophs (Missler et al. 2003 and this study), which excluded any defects in the early steps of exocytosis, such as biogenesis of granules, their transport to the membrane and morphological docking. This is in contrast to the observations in release-deficient somatotrophs and chromaffin cells from Munc18-1 mutants, where electron microscopy releaved a clear docking defect with markedly larger distances between the vesicles and plasma membrane (Korteweg et al. 2005; Toonen et al. 2006; Voets et al. 2001b).

What could be the molecular mechanism of α-neurexins involvement in the Ca^{2+} triggering of release? Based on the previous observations in neurons, we first hypothesized that the function of HVA Ca^{2+} channels might be directly regulated by α-neurexins. But, in contrast to neurons, whole-cell Ca^{2+} current densities were not decreased in α-neurexin-deficient melanotrophs (Dudanova et al. 2006). Since several types of HVA Ca^{2+} channels participate with equal efficiency in triggering release in melanotrophs, a selective reduction of a certain Ca^{2+} current component and compensation by an increase in other components still remained a possibility. However, application of Ca^{2+} channel-specific toxins demonstrated intact function of all the Ca^{2+} channels. Thus, at least in melanotrophs the role of α-neurexins appears to be more general than regulating particular types of Ca^{2+} channels. The selective impairment of N- and P/Q-type channels described at central synapses might be due to spatial reasons (i.e., the synaptic localization of these channel types), rather than their specific interaction with α-neurexins.

Measurements of the IRP in melanotrophs demonstrated that there were less vesicles colocalized with Ca^{2+} channels in α-neurexin-deficient cells. These data are compatible with the role of neurexins as a link between Ca^{2+} channel clusters and the vesicle release apparatus. Both in neurons and in endocrine cells, α-neurexins may play a role in the organization of release sites by anchoring Ca^{2+} channels within their "slots" (Cao et al. 2004) and providing the spatial proximity of the channels and the molecular components involved in exocytosis (Fig. 20). Because of the heterogeneity of Ca^{2+} concentration near the membrane (Meinrenken et al. 2002; Neher 1998) and the non-linear dependence of release on Ca^{2+} concentration, the release of a vesicle critically depends on its position with respect to Ca^{2+} entry sites (Wadel et al. 2007), so mislocalization of Ca^{2+} channels is expected to have a great impact on release probability. In the absence of α-neurexins, the average distance between Ca^{2+} channels and release-ready vesicles would be increased, leading to a less efficient coupling between Ca^{2+} influx and vesicle exocytosis. This hypothesis can explain many of the aspects of α-neurexin KO phenotype: (i) the impaired basal synaptic transmission and lower sensitivity to Ca^{2+} channel blockers at central synapses (Missler et al. 2003); (ii) the reduced transmission and disturbed Ca^{2+}-dependent homeostasis at the neuromuscular junction (Sons et al. 2006); (iii) the defect of secretion in melanotrophs without any change in ultrastructure or Ca^{2+} current densities (this study, Dudanova et al. 2006); (iv) increased short-term and long-term plasticity at the Schaffer collateral – CA1 synapses in the DKOs (Ahmad et al., submitted). At present, it is difficult to provide a definitive proof for this hypothesis, because the lack of suitable antibodies for both neurexins and Ca^{2+} channels precludes ultrastructural localization studies.

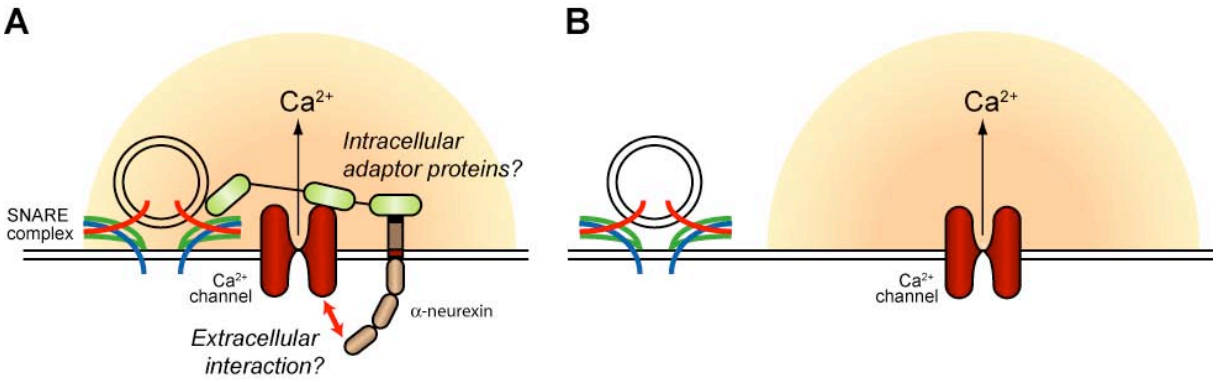

Figure 20. Proposed role of α-neurexins in anchoring Ca^{2+} channels at release sites. **A**: In order to be released, vesicles not only need to be docked and primed for release, but also be situated close to Ca^{2+} channels to experience a high enough local Ca^{2+} concentration (orange cloud) that would trigger fusion. α-Neurexins may be involved in ensuring the spatial proximity of vesicles and Ca^{2+} channels, by binding to intracellular adaptor proteins and/or via an extracellular interaction. **B**: In the absence of α-neurexins, the molecular link between Ca^{2+} channels and vesicle proteins is disrupted, leading to larger distances between vesicles and Ca^{2+} channels, so that the same amount of Ca^{2+} entry may not be sufficient to trigger release of a primed and fusion-competent vesicle.

Since no direct interaction is known between α-neurexins and Ca^{2+} channels, other adaptor proteins may be involved in this link (Fig. 20). Among the candidates are the intracellular binding partners of neurexins, CASK and Mints, which interact and colocalize with Ca^{2+} channels at synapses and therefore have been proposed to target Ca^{2+} channels to presynaptic sites (Maximov and Bezprozvanny 2002; Maximov et al. 1999). However, deletion of CASK results in a phenotype very different from that of α-neurexin mutants (Atasoy et al. 2007), so it seems unlikely that this molecule might provide the connection to Ca^{2+} channels. In contrast, Mints are more promising candidates, since Mint 1/2 DKOs copy several aspects of the α-neurexin KO phenotype, such as reduced basal synaptic transmission and enhanced short-term plasticity at the Schaffer collateral - CA1 synapses (Ho et al. 2006). Hormone release has not been investigated in these mutants, but since Mints are known to be expressed in at least one type of endocrine cells (Zhang et al. 2004), it is conceivable that they are a part of the same protein complex at the release sites in endocrine cells and in neurons. In addition, based on recent biochemical and cell biological evidence, the active zone protein RIM1α has emerged as a potential new intracellular interaction partner of neurexins (Mohiuddin Ahmad, Richard Fairless, Markus Missler, unpublished results), pointing to yet another possible neurexin-mediated link between Ca^{2+} channels and synaptic vesicles via

RIM1α. Binding partners of RIM1α include several active zone proteins, such as ELKS/CAST/ERC, Munc13 and α-liprins (Betz et al. 2001; Ohtsuka et al. 2002; Schoch et al. 2002; Wang et al. 2002), and synaptic vesicle proteins, such as synaptotagmin 1 and Rab3 (Coppola et al. 2001; Wang et al. 1997). Furthermore, RIM1α is known to be associated with Ca^{2+} channels, both by a direct interaction (Coppola et al. 2001) and via RIM binding proteins (Hibino et al. 2002). Therefore, this molecule appears to be a central component of the active zone, which coordinates multiple interactions between active zone and synaptic vesicle proteins. Accordingly, a number of studies have established an essential role of RIM1α in neurotransmitter release and synaptic plasticity (Calakos et al. 2004; Castillo et al. 2002; Dulubova et al. 2005; Schoch et al. 2002). Importantly, RIM1α KO mutants display functional defects partially resembling those in α-neurexin TKOs, such as reduced synaptic strength and similar changes in short-term plasticity at the Schaffer collateral - CA1 hippocampal synapses (Schoch et al. 2002).

However, all intracellular interactions are common to α- and β-neurexins, therefore if intracellular adaptors should provide the link between neurexins and Ca^{2+} channels, it remains unclear why β-isoforms are not able to compensate for the deletion of α-neurexins in mice (Zhang et al. 2005). As suggested by the latter study, additional, and as yet unknown, extracellular interactions of α-neurexins may be involved in regulating synaptic transmission. Further experiments are needed to resolve this issue.

In conclusion, although our experiments so far do not give a definitive answer, they strongly suggest that the tight coupling between Ca^{2+}-influx and exocytosis is disturbed in α-neurexin mutants and point to a possible role of α-neurexins in anchoring Ca^{2+} channels at release sites.

Interestingly, in our RT-PCR experiments, β-neurexins were also detected in endocrine cells in significant amounts (Fig. 12C-D). It is not clear at the moment which role β-neurexins might play in endocrine tissues. The intensively studied synaptogenic activity of β-neurexins does not seem relevant in this type of cells. One possibiltiy is that β-neurexins, similar to NCAM and N-cadherin (Rubinek et al. 2003), mediate non-synaptic cell adhesion, which might be important for efficient endocrine secretion. While NCAM and N-cadherins function as homophilic adhesion molecules (Hall et al. 1990; Koch et al. 1999), neurexins mediate heterophilic adhesion (Nguyen and Sudhof 1997), which seems appropriate for polarized structures such as synapses, but not for non-polarized endocrine cells. It is also conceivable that β-neurexins, like α-isoforms, may play a role in regulating exocytosis of secretory granules, possibly by organizing release sites. The only piece of evidence that β-

neurexins could be involved in regulating Ca^{2+}-triggered release comes from an *in vitro* study in hippocampal slices, where β-neurexin was proposed to mediate retrograde signaling from PSD-95 and neuroligin (Futai et al. 2007). However, this type of signaling can not take place in endocrine cells. Finally, β-neurexins may have a different, as yet unknown function, which could be general for various cell types or specific to endocrine cells.

5. Summary and conclusions

Here we have explored the morphological changes in the brains of surviving adult α-neurexin DKO mice in order to assess the *in vivo* contribution of α-neurexins to the formation and structure of central synapses. There were no obvious defects in the overall assembly of the brain in the DKOs. Quantitative analysis revealed a mild but widely spread ~20% reduction in the neuropil fraction, which was caused by a shortening of terminal dendritic branches and a loss of synapses. Electron microscopy demonstrated unaltered synapse ultrastructure and a decline in the density of type II synapses by ~30%. Since most of the defects uncovered in adult brains were not present in the newborns, α-neurexins probably contribute to the long-term maintenance of synaptic connections. However, the overall mild degree of structural changes in the mutants suggests that α-neurexins do not play a major role in synaptic structure *in vivo*.

In addition, we show here that neurexins are expressed in endocrine tissues. The pituitary gland was hypomorphic in adult α-neurexin DKOs, due to the reduced size of endocrine cells. While the expression of peptide hormones by the pituitary lobes was unchanged and the ultrastructure of pituitary melanotrophs appeared normal, a decrease of Ca^{2+}-dependent secretion by ~50% was found in melanotrophs of adult α-neurexin DKOs. The impairment of secretion was also observed in newborn DKO and TKO mutants, in spite of the unaltered morphology of the gland at this early age, demonstrating that the functional defect is independent of the hypomorphic changes. The impairment of secretion may be due to the loss of tight coupling between Ca^{2+} channels and release-competent vesicles, implicating α-neurexins in the organization of release sites. Our results show that α-neurexins belong to the general components of Ca^{2+}-dependent exocytotic machinery, which are involved in regulated secretion in both neurons and endocrine cells.

References

Angenstein F, Niessen HG, Goldschmidt J, Lison H, Altrock WD, Gundelfinger ED, Scheich H (2007) Manganese-enhanced MRI reveals structural and functional changes in the cortex of Bassoon mutant mice. Cereb Cortex 17:28-36

Atasoy D, Schoch S, Ho A, Nadasy KA, Liu X, Zhang W, Mukherjee K, Nosyreva ED, Fernandez-Chacon R, Missler M, Kavalali ET, Sudhof TC (2007) Deletion of CASK in mice is lethal and impairs synaptic function. Proc Natl Acad Sci U S A 104:2525-2530

Back N, Rechardt L (1985) The effect of reserpine on the pars intermedia of the rat pituitary. An electron-microscopic, fluorescence-histochemical and immunohistochemical study. Cell Tissue Res 241:1-8

Baumgarten HG, Bjorklund A, Holstein AF, Nobin A (1972) Organization and ultrastructural identification of the catecholamine nerve terminals in the neural lobe and pars intermedia of the rat pituitary. Z Zellforsch Mikrosk Anat 126:483-517

Becherer U, Moser T, Stuhmer W, Oheim M (2003) Calcium regulates exocytosis at the level of single vesicles. Nat Neurosci 6:846-853

Behar O, Golden JA, Mashimo H, Schoen FJ, Fishman MC (1996) Semaphorin III is needed for normal patterning and growth of nerves, bones and heart. Nature 383:525-528

Ben-Ari Y (2001) Developing networks play a similar melody. Trends Neurosci 24:353-360

Benson DL, Colman DR, Huntley GW (2001) Molecules, maps and synapse specificity. Nat Rev Neurosci 2:899-909

Betz A, Thakur P, Junge HJ, Ashery U, Rhee JS, Scheuss V, Rosenmund C, Rettig J, Brose N (2001) Functional interaction of the active zone proteins Munc13-1 and RIM1 in synaptic vesicle priming. Neuron 30:183-196

Biederer T, Sudhof TC (2000) Mints as adaptors. Direct binding to neurexins and recruitment of munc18. J Biol Chem 275:39803-39806

Boeckers TM (2006) The postsynaptic density. Cell Tissue Res 326:409-422

Boucard AA, Chubykin AA, Comoletti D, Taylor P, Sudhof TC (2005) A splice code for trans-synaptic cell adhesion mediated by binding of neuroligin 1 to alpha- and beta-neurexins. Neuron 48:229-236

Bouwman J, Maia AS, Camoletto PG, Posthuma G, Roubos EW, Oorschot VM, Klumperman J, Verhage M (2004) Quantification of synapse formation and maintenance in vivo in the absence of synaptic release. Neuroscience 126:115-126

Buchs PA, Muller D (1996) Induction of long-term potentiation is associated with major ultrastructural changes of activated synapses. Proc Natl Acad Sci U S A 93:8040-8045

Butz S, Okamoto M, Sudhof TC (1998) A tripartite protein complex with the potential to couple synaptic vesicle exocytosis to cell adhesion in brain. Cell 94:773-782

Calakos N, Schoch S, Sudhof TC, Malenka RC (2004) Multiple roles for the active zone protein RIM1alpha in late stages of neurotransmitter release. Neuron 42:889-896

Calverley RK, Jones DG (1990) Contributions of dendritic spines and perforated synapses to synaptic plasticity. Brain Res Brain Res Rev 15:215-249

Cao YQ, Piedras-Renteria ES, Smith GB, Chen G, Harata NC, Tsien RW (2004) Presynaptic Ca2+ channels compete for channel type-preferring slots in altered neurotransmission arising from Ca2+ channelopathy. Neuron 43:387-400

Castillo PE, Schoch S, Schmitz F, Sudhof TC, Malenka RC (2002) RIM1alpha is required for presynaptic long-term potentiation. Nature 415:327-330

Chan SA, Polo-Parada L, Landmesser LT, Smith C (2005) Adrenal chromaffin cells exhibit impaired granule trafficking in NCAM knockout mice. J Neurophysiol 94:1037-1047

Chih B, Engelman H, Scheiffele P (2005) Control of excitatory and inhibitory synapse formation by neuroligins. Science 307:1324-1328

Chih B, Gollan L, Scheiffele P (2006) Alternative splicing controls selective trans-synaptic interactions of the neuroligin-neurexin complex. Neuron 51:171-178

Chronwall BM, Hook GR, Millington WR (1988) Dopaminergic regulation of the biosynthetic activity of individual melanotropes in the rat pituitary intermediate lobe: a morphometric analysis by light and electron microscopy and in situ hybridization. Endocrinology 123:1992-2002

Colin-Le Brun I, Ferrand N, Caillard O, Tosetti P, Ben-Ari Y, Gaiarsa JL (2004) Spontaneous synaptic activity is required for the formation of functional GABAergic synapses in the developing rat hippocampus. J Physiol 559:129-139

Comoletti D, Flynn RE, Boucard AA, Demeler B, Schirf V, Shi J, Jennings LL, Newlin HR, Sudhof TC, Taylor P (2006) Gene selection, alternative splicing, and post-translational processing regulate neuroligin selectivity for beta-neurexins. Biochemistry 45:12816-12827

Coppola T, Magnin-Luthi S, Perret-Menoud V, Gattesco S, Schiavo G, Regazzi R (2001) Direct interaction of the Rab3 effector RIM with Ca2+ channels, SNAP-25, and synaptotagmin. J Biol Chem 276:32756-32762

Craig AM, Boudin H (2001) Molecular heterogeneity of central synapses: afferent and target regulation. Nat Neurosci 4:569-578

Craig AM, Kang Y (2007) Neurexin-neuroligin signaling in synapse development. Curr Opin Neurobiol 17:43-52

Cremer H, Chazal G, Carleton A, Goridis C, Vincent JD, Lledo PM (1998) Long-term but not short-term plasticity at mossy fiber synapses is impaired in neural cell adhesion molecule-deficient mice. Proc Natl Acad Sci U S A 95:13242-13247

Dalva MB, McClelland AC, Kayser MS (2007) Cell adhesion molecules: signalling functions at the synapse. Nat Rev Neurosci 8:206-220

Dean C, Scholl FG, Choih J, DeMaria S, Berger J, Isacoff E, Scheiffele P (2003) Neurexin mediates the assembly of presynaptic terminals. Nat Neurosci 6:708-716

Dudanova I (2004) Discrete abnormalities in the brains of adult α-neurexin double knockout mice may reflect long term consequences of impaired synaptic transmission. MSc thesis. University of Göttingen

Dudanova I, Sedej S, Ahmad M, Masius H, Sargsyan V, Zhang W, Riedel D, Angenstein F, Schild D, Rupnik M, Missler M (2006) Important contribution of alpha-neurexins to Ca2+-triggered exocytosis of secretory granules. J Neurosci 26:10599-10613

Dudanova I, Tabuchi K, Rohlmann A, Sudhof TC, Missler M (2007) Deletion of alpha-neurexins does not cause a major impairment of axonal pathfinding or synapse formation. J Comp Neurol 502:261-274

Dulubova I, Lou X, Lu J, Huryeva I, Alam A, Schneggenburger R, Sudhof TC, Rizo J (2005) A Munc13/RIM/Rab3 tripartite complex: from priming to plasticity? Embo J 24:2839-2850

Fairless R, Reissner C, Missler M (2006) The role of neuroligin binding to neurexins in synaptic organization. In: Molecular Mechanisms of Synaptogenesis. Dityatev A, El-Husseini A (eds). Springer, New York, 111-124

Feng J, Schroer R, Yan J, Song W, Yang C, Bockholt A, Cook EH, Jr., Skinner C, Schwartz CE, Sommer SS (2006) High frequency of neurexin 1beta signal peptide structural variants in patients with autism. Neurosci Lett 409:10-13

Fenstermaker V, Chen Y, Ghosh A, Yuste R (2004) Regulation of dendritic length and branching by semaphorin 3A. J Neurobiol 58:403-412

Fritschy JM, Brunig I (2003) Formation and plasticity of GABAergic synapses: physiological mechanisms and pathophysiological implications. Pharmacol Ther 98:299-323

Fu Z, Washbourne P, Ortinski P, Vicini S (2003) Functional excitatory synapses in HEK293 cells expressing neuroligin and glutamate receptors. J Neurophysiol 90:3950-3957

Futai K, Kim MJ, Hashikawa T, Scheiffele P, Sheng M, Hayashi Y (2007) Retrograde modulation of presynaptic release probability through signaling mediated by PSD-95-neuroligin. Nat Neurosci 10:186-195

Geppert M, Goda Y, Hammer RE, Li C, Rosahl TW, Stevens CF, Sudhof TC (1994) Synaptotagmin I: a major Ca2+ sensor for transmitter release at a central synapse. Cell 79:717-727

Geppert M, Ushkaryov YA, Hata Y, Davletov B, Petrenko AG, Sudhof TC (1992) Neurexins. Cold Spring Harb Symp Quant Biol 57:483-490

Gillis KD, Mossner R, Neher E (1996) Protein kinase C enhances exocytosis from chromaffin cells by increasing the size of the readily releasable pool of secretory granules. Neuron 16:1209-1220

Goda Y, Davis GW (2003) Mechanisms of synapse assembly and disassembly. Neuron 40:243-264

Graf ER, Kang Y, Hauner AM, Craig AM (2006) Structure function and splice site analysis of the synaptogenic activity of the neurexin-1 beta LNS domain. J Neurosci 26:4256-4265

Graf ER, Zhang X, Jin SX, Linhoff MW, Craig AM (2004) Neurexins induce differentiation of GABA and glutamate postsynaptic specializations via neuroligins. Cell 119:1013-1026

Gray EG (1963) Electron microscopy of presynaptic organelles of the spinal cord. J Anat 97:101-106

Hall AK, Nelson R, Rutishauser U (1990) Binding properties of detergent-solubilized NCAM. J Cell Biol 110:817-824

Hata Y, Butz S, Sudhof TC (1996) CASK: a novel dlg/PSD95 homolog with an N-terminal calmodulin-dependent protein kinase domain identified by interaction with neurexins. J Neurosci 16:2488-2494

Heidelberger R, Heinemann C, Neher E, Matthews G (1994) Calcium dependence of the rate of exocytosis in a synaptic terminal. Nature 371:513-515

Hibino H, Pironkova R, Onwumere O, Vologodskaia M, Hudspeth AJ, Lesage F (2002) RIM binding proteins (RBPs) couple Rab3-interacting molecules (RIMs) to voltage-gated Ca(2+) channels. Neuron 34:411-423

Ho A, Morishita W, Atasoy D, Liu X, Tabuchi K, Hammer RE, Malenka RC, Sudhof TC (2006) Genetic analysis of Mint/X11 proteins: essential presynaptic functions of a neuronal adaptor protein family. J Neurosci 26:13089-13101

Holtmaat AJ, Trachtenberg JT, Wilbrecht L, Shepherd GM, Zhang X, Knott GW, Svoboda K (2005) Transient and persistent dendritic spines in the neocortex in vivo. Neuron 45:279-291

Horinouchi K, Nakamura Y, Yamanaka H, Watabe T, Shiosaka S (2005) Distribution of L1cam mRNA in the adult mouse brain: In situ hybridization and Northern blot analyses. J Comp Neurol 482:386-404

Horrigan FT, Bookman RJ (1994) Releasable pools and the kinetics of exocytosis in adrenal chromaffin cells. Neuron 13:1119-1129

Ichtchenko K, Hata Y, Nguyen T, Ullrich B, Missler M, Moomaw C, Sudhof TC (1995) Neuroligin 1: a splice site-specific ligand for beta-neurexins. Cell 81:435-443

Ichtchenko K, Nguyen T, Sudhof TC (1996) Structures, alternative splicing, and neurexin binding of multiple neuroligins. J Biol Chem 271:2676-2682

Irie M, Hata Y, Takeuchi M, Ichtchenko K, Toyoda A, Hirao K, Takai Y, Rosahl TW, Sudhof TC (1997) Binding of neuroligins to PSD-95. Science 277:1511-1515

Jacobsson G, Bean AJ, Scheller RH, Juntti-Berggren L, Deeney JT, Berggren PO, Meister B (1994) Identification of synaptic proteins and their isoform mRNAs in compartments of pancreatic endocrine cells. Proc Natl Acad Sci U S A 91:12487-12491

Jacobsson G, Meister B (1996) Molecular components of the exocytotic machinery in the rat pituitary gland. Endocrinology 137:5344-5356

Jahn R, Lang T, Sudhof TC (2003) Membrane fusion. Cell 112:519-533

Jamain S, Quach H, Betancur C, Rastam M, Colineaux C, Gillberg IC, Soderstrom H, Giros B, Leboyer M, Gillberg C, Bourgeron T (2003) Mutations of the X-linked genes encoding neuroligins NLGN3 and NLGN4 are associated with autism. Nat Genet 34:27-29

Kattenstroth G, Tantalaki E, Sudhof TC, Gottmann K, Missler M (2004) Postsynaptic N-methyl-D-aspartate receptor function requires alpha-neurexins. Proc Natl Acad Sci U S A 101:2607-2612

Katz B (1969) The release of neural transmitter substances. Liverpool: Liverpool University Press

Katz LC, Shatz CJ (1996) Synaptic activity and the construction of cortical circuits. Science 274:1133-1138

Kennedy MB (2000) Signal-processing machines at the postsynaptic density. Science 290:750-754

Kim E, Niethammer M, Rothschild A, Jan YN, Sheng M (1995) Clustering of Shaker-type K+ channels by interaction with a family of membrane-associated guanylate kinases. Nature 378:85-88

Klingauf J, Neher E (1997) Modeling buffered Ca2+ diffusion near the membrane: implications for secretion in neuroendocrine cells. Biophys J 72:674-690

Koch AW, Bozic D, Pertz O, Engel J (1999) Homophilic adhesion by cadherins. Curr Opin Struct Biol 9:275-281

Kornau HC, Schenker LT, Kennedy MB, Seeburg PH (1995) Domain interaction between NMDA receptor subunits and the postsynaptic density protein PSD-95. Science 269:1737-1740

Korteweg N, Maia AS, Thompson B, Roubos EW, Burbach JP, Verhage M (2005) The role of Munc18-1 in docking and exocytosis of peptide hormone vesicles in the anterior pituitary. Biol Cell 97:445-455

Kreft M, Kuster V, Grilc S, Rupnik M, Milisav I, Zorec R (2003) Synaptotagmin I increases the probability of vesicle fusion at low [Ca2+] in pituitary cells. Am J Physiol Cell Physiol 284:C547-554

Laumonnier F, Bonnet-Brilhault F, Gomot M, Blanc R, David A, Moizard MP, Raynaud M, Ronce N, Lemonnier E, Calvas P, Laudier B, Chelly J, Fryns JP, Ropers HH, Hamel BC, Andres C, Barthelemy C, Moraine C, Briault S (2004) X-linked mental retardation and autism are associated with a mutation in the NLGN4 gene, a member of the neuroligin family. Am J Hum Genet 74:552-557

Leonard AS, Davare MA, Horne MC, Garner CC, Hell JW (1998) SAP97 is associated with the alpha-amino-3-hydroxy-5-methylisoxazole-4-propionic acid receptor GluR1 subunit. J Biol Chem 273:19518-19524

Levi S, Grady RM, Henry MD, Campbell KP, Sanes JR, Craig AM (2002) Dystroglycan is selectively associated with inhibitory GABAergic synapses but is dispensable for their differentiation. J Neurosci 22:4274-4285

Levinson JN, Chery N, Huang K, Wong TP, Gerrow K, Kang R, Prange O, Wang YT, El-Husseini A (2005) Neuroligins mediate excitatory and inhibitory synapse formation: involvement of PSD-95 and neurexin-1beta in neuroligin-induced synaptic specificity. J Biol Chem 280:17312-17319

Levinson JN, El-Husseini A (2005) Building excitatory and inhibitory synapses: balancing neuroligin partnerships. Neuron 48:171-174

Liu WS, Pesold C, Rodriguez MA, Carboni G, Auta J, Lacor P, Larson J, Condie BG, Guidotti A, Costa E (2001) Down-regulation of dendritic spine and glutamic acid

decarboxylase 67 expressions in the reelin haploinsufficient heterozygous reeler mouse. Proc Natl Acad Sci U S A 98:3477-3482

Lohmann C, Myhr KL, Wong RO (2002) Transmitter-evoked local calcium release stabilizes developing dendrites. Nature 418:177-181

Lynch MA, Voss KL, Rodriguez J, Bliss TV (1994) Increase in synaptic vesicle proteins accompanies long-term potentiation in the dentate gyrus. Neuroscience 60:1-5

Makarenko IG, Ugrumov MV, Calas A (2005) Axonal projections from the hypothalamus to the pituitary intermediate lobe in rats during ontogenesis: DiI tracing study. Brain Res Dev Brain Res 155:117-126

Mansvelder HD, Kits KS (2000) Calcium channels and the release of large dense core vesicles from neuroendocrine cells: spatial organization and functional coupling. Prog Neurobiol 62:427-441

Marqueze B, Boudier JA, Mizuta M, Inagaki N, Seino S, Seagar M (1995) Cellular localization of synaptotagmin I, II, and III mRNAs in the central nervous system and pituitary and adrenal glands of the rat. J Neurosci 15:4906-4917

Marty S, Wehrle R, Sotelo C (2000) Neuronal activity and brain-derived neurotrophic factor regulate the density of inhibitory synapses in organotypic slice cultures of postnatal hippocampus. J Neurosci 20:8087-8095

Maximov A, Bezprozvanny I (2002) Synaptic targeting of N-type calcium channels in hippocampal neurons. J Neurosci 22:6939-6952

Maximov A, Sudhof TC, Bezprozvanny I (1999) Association of neuronal calcium channels with modular adaptor proteins. J Biol Chem 274:24453-24456

McAllister AK (2000) Cellular and molecular mechanisms of dendrite growth. Cereb Cortex 10:963-973

McGee AW, Bredt DS (2003) Assembly and plasticity of the glutamatergic postsynaptic specialization. Curr Opin Neurobiol 13:111-118

McKinney RA, Capogna M, Durr R, Gahwiler BH, Thompson SM (1999) Miniature synaptic events maintain dendritic spines via AMPA receptor activation. Nat Neurosci 2:44-49

Meinrenken CJ, Borst JG, Sakmann B (2002) Calcium secretion coupling at calyx of held governed by nonuniform channel-vesicle topography. J Neurosci 22:1648-1667

Micheva KD, Beaulieu C (1995) An anatomical substrate for experience-dependent plasticity of the rat barrel field cortex. Proc Natl Acad Sci U S A 92:11834-11838

Missler M, Fernandez-Chacon R, Sudhof TC (1998) The making of neurexins. J Neurochem 71:1339-1347

Missler M, Sudhof TC (1998) Neurexins: three genes and 1001 products. Trends Genet 14:20-26

Missler M, Zhang W, Rohlmann A, Kattenstroth G, Hammer RE, Gottmann K, Sudhof TC (2003) Alpha-neurexins couple Ca2+ channels to synaptic vesicle exocytosis. Nature 423:939-948

Moore SA, Saito F, Chen J, Michele DE, Henry MD, Messing A, Cohn RD, Ross-Barta SE, Westra S, Williamson RA, Hoshi T, Campbell KP (2002) Deletion of brain dystroglycan recapitulates aspects of congenital muscular dystrophy. Nature 418:422-425

Morgan A, Burgoyne RD (1997) Common mechanisms for regulated exocytosis in the chromaffin cell and the synapse. Semin Cell Dev Biol 8:141-149

Moriarty GC, Halmi NS, Moriarty M (1975) The effect of stress on the cytology and immunocytochemistry of pars intermedia cells in the rat pituitary. Endocrinology 96:1426-1436

Morita A, Yamashita N, Sasaki Y, Uchida Y, Nakajima O, Nakamura F, Yagi T, Taniguchi M, Usui H, Katoh-Semba R, Takei K, Goshima Y (2006) Regulation of dendritic

branching and spine maturation by semaphorin3A-Fyn signaling. J Neurosci 26:2971-2980

Moser T, Neher E (1997) Rapid exocytosis in single chromaffin cells recorded from mouse adrenal slices. J Neurosci 17:2314-2323

Muller D, Wang C, Skibo G, Toni N, Cremer H, Calaora V, Rougon G, Kiss JZ (1996) PSA-NCAM is required for activity-induced synaptic plasticity. Neuron 17:413-422

Murthy VN, De Camilli P (2003) Cell biology of the presynaptic terminal. Annu Rev Neurosci 26:701-728

Nam CI, Chen L (2005) Postsynaptic assembly induced by neurexin-neuroligin interaction and neurotransmitter. Proc Natl Acad Sci U S A 102:6137-6142

Neher E (1998) Vesicle pools and Ca2+ microdomains: new tools for understanding their roles in neurotransmitter release. Neuron 20:389-399

Neher E (2006) A comparison between exocytic control mechanisms in adrenal chromaffin cells and a glutamatergic synapse. Pflugers Arch 453:261-268

Nguyen T, Sudhof TC (1997) Binding properties of neuroligin 1 and neurexin 1beta reveal function as heterophilic cell adhesion molecules. J Biol Chem 272:26032-26039

Niell CM, Meyer MP, Smith SJ (2004) In vivo imaging of synapse formation on a growing dendritic arbor. Nat Neurosci 7:254-260

Occhi G, Rampazzo A, Beffagna G, Antonio Danieli G (2002) Identification and characterization of heart-specific splicing of human neurexin 3 mRNA (NRXN3). Biochem Biophys Res Commun 298:151-155

Oertel WH, Mugnaini E, Tappaz ML, Weise VK, Dahl AL, Schmechel DE, Kopin IJ (1982) Central GABAergic innervation of neurointermediate pituitary lobe: biochemical and immunocytochemical study in the rat. Proc Natl Acad Sci U S A 79:675-679

Ohtsuka T, Takao-Rikitsu E, Inoue E, Inoue M, Takeuchi M, Matsubara K, Deguchi-Tawarada M, Satoh K, Morimoto K, Nakanishi H, Takai Y (2002) Cast: a novel protein of the cytomatrix at the active zone of synapses that forms a ternary complex with RIM1 and munc13-1. J Cell Biol 158:577-590

Okamoto M, Sudhof TC (1997) Mints, Munc18-interacting proteins in synaptic vesicle exocytosis. J Biol Chem 272:31459-31464

Olsen O, Moore KA, Fukata M, Kazuta T, Trinidad JC, Kauer FW, Streuli M, Misawa H, Burlingame AL, Nicoll RA, Bredt DS (2005) Neurotransmitter release regulated by a MALS-liprin-alpha presynaptic complex. J Cell Biol 170:1127-1134

Palay SL (1956) Synapses in the central nervous system. J Biophys Biochem Cytol 2:193-202

Paradis S, Harrar DB, Lin Y, Koon AC, Hauser JL, Griffith EC, Zhu L, Brass LF, Chen C, Greenberg ME (2007) An RNAi-based approach identifies molecules required for glutamatergic and GABAergic synapse development. Neuron 53:217-232

Parsons TD, Coorssen JR, Horstmann H, Almers W (1995) Docked granules, the exocytic burst, and the need for ATP hydrolysis in endocrine cells. Neuron 15:1085-1096

Pautler RG, Silva AC, Koretsky AP (1998) In vivo neuronal tract tracing using manganese-enhanced magnetic resonance imaging. Magn Reson Med 40:740-748

Paxinos G, Franklin KB.J (2001) The mouse brain in stereotaxic coordinates. 2nd ed. Academic press, San Diego and London

Perin MS (1994) The COOH terminus of synaptotagmin mediates interaction with the neurexins. J Biol Chem 269:8576-8581

Petrenko AG, Ullrich B, Missler M, Krasnoperov V, Rosahl TW, Sudhof TC (1996) Structure and evolution of neurexophilin. J Neurosci 16:4360-4369

Pfaffl MW (2001) A new mathematical model for relative quantification in real-time RT-PCR. Nucleic Acids Res 29:e45

Piechotta K, Dudanova I, Missler M (2006) The resilient synapse: insights from genetic interference of synaptic cell adhesion molecules. Cell Tissue Res 326:617-642

Polleux F, Lauder JM (2004) Toward a developmental neurobiology of autism. Ment Retard Dev Disabil Res Rev 10:303-317

Polo-Parada L, Bose CM, Landmesser LT (2001) Alterations in transmission, vesicle dynamics, and transmitter release machinery at NCAM-deficient neuromuscular junctions. Neuron 32:815-828

Polo-Parada L, Bose CM, Plattner F, Landmesser LT (2004) Distinct roles of different neural cell adhesion molecule (NCAM) isoforms in synaptic maturation revealed by analysis of NCAM 180 kDa isoform-deficient mice. J Neurosci 24:1852-1864

Prange O, Wong TP, Gerrow K, Wang YT, El-Husseini A (2004) A balance between excitatory and inhibitory synapses is controlled by PSD-95 and neuroligin. Proc Natl Acad Sci U S A 101:13915-13920

Puschel AW, Betz H (1995) Neurexins are differentially expressed in the embryonic nervous system of mice. J Neurosci 15:2849-2856

Rafuse VF, Polo-Parada L, Landmesser LT (2000) Structural and functional alterations of neuromuscular junctions in NCAM-deficient mice. J Neurosci 20:6529-6539

Ramakers GJ, van Galen H, Feenstra MG, Corner MA, Boer GJ (1994) Activity-dependent plasticity of inhibitory and excitatory amino acid transmitter systems in cultured rat cerebral cortex. Int J Dev Neurosci 12:611-621

Rettig J, Neher E (2002) Emerging roles of presynaptic proteins in Ca++-triggered exocytosis. Science 298:781-785

Rosales CR, Osborne KD, Zuccarino GV, Scheiffele P, Silverman MA (2005) A cytoplasmic motif targets neuroligin-1 exclusively to dendrites of cultured hippocampal neurons. Eur J Neurosci 22:2381-2386

Rosato-Siri M, Grandolfo M, Ballerini L (2002) Activity-dependent modulation of GABAergic synapses in developing rat spinal networks in vitro. Eur J Neurosci 16:2123-2135

Rosenmund C, Rettig J, Brose N (2003) Molecular mechanisms of active zone function. Curr Opin Neurobiol 13:509-519

Rosenmund C, Stevens CF (1996) Definition of the readily releasable pool of vesicles at hippocampal synapses. Neuron 16:1197-1207

Rowen L, Young J, Birditt B, Kaur A, Madan A, Philipps DL, Qin S, Minx P, Wilson RK, Hood L, Graveley BR (2002) Analysis of the human neurexin genes: alternative splicing and the generation of protein diversity. Genomics 79:587-597

Rubinek T, Yu R, Hadani M, Barkai G, Nass D, Melmed S, Shimon I (2003) The cell adhesion molecules N-cadherin and neural cell adhesion molecule regulate human growth hormone: a novel mechanism for regulating pituitary hormone secretion. J Clin Endocrinol Metab 88:3724-3730

Saghatelyan AK, Nikonenko AG, Sun M, Rolf B, Putthoff P, Kutsche M, Bartsch U, Dityatev A, Schachner M (2004) Reduced GABAergic transmission and number of hippocampal perisomatic inhibitory synapses in juvenile mice deficient in the neural cell adhesion molecule L1. Mol Cell Neurosci 26:191-203

Saland LC (1978) Effects of reserpine administration on the fine structure of the rat pars intermedia. Cell Tissue Res 194:115-123

Saland LC, Ortiz E, Munger AT (1982) Effects of acute opiate-peptide administration on pro-opiomelanocortin cells of the intermediate lobe of the rat pituitary. Cell Tissue Res 225:217-222

Santolaya RC, Ciocca D (1981) Effects of pimozide on the ultrastructure of the pars intermedia in the rat. Cell Tissue Res 217:397-403

Sara Y, Biederer T, Atasoy D, Chubykin A, Mozhayeva MG, Sudhof TC, Kavalali ET (2005) Selective capability of SynCAM and neuroligin for functional synapse assembly. J Neurosci 25:260-270

Scheiffele P, Fan J, Choih J, Fetter R, Serafini T (2000) Neuroligin expressed in nonneuronal cells triggers presynaptic development in contacting axons. Cell 101:657-669

Schoch S, Castillo PE, Jo T, Mukherjee K, Geppert M, Wang Y, Schmitz F, Malenka RC, Sudhof TC (2002) RIM1alpha forms a protein scaffold for regulating neurotransmitter release at the active zone. Nature 415:321-326

Schoch S, Deak F, Konigstorfer A, Mozhayeva M, Sara Y, Sudhof TC, Kavalali ET (2001) SNARE function analyzed in synaptobrevin/VAMP knockout mice. Science 294:1117-1122

Sedej S, Tsujimoto T, Zorec R, Rupnik M (2004) Voltage-activated Ca(2+) channels and their role in the endocrine function of the pituitary gland in newborn and adult mice. J Physiol 555:769-782

Seil FJ, Drake-Baumann R (1994) Reduced cortical inhibitory synaptogenesis in organotypic cerebellar cultures developing in the absence of neuronal activity. J Comp Neurol 342:366-377

Song JY, Ichtchenko K, Sudhof TC, Brose N (1999) Neuroligin 1 is a postsynaptic cell-adhesion molecule of excitatory synapses. Proc Natl Acad Sci U S A 96:1100-1105

Sons MS, Busche N, Strenzke N, Moser T, Ernsberger U, Mooren FC, Zhang W, Ahmad M, Steffens H, Schomburg ED, Plomp JJ, Missler M (2006) alpha-Neurexins are required for efficient transmitter release and synaptic homeostasis at the mouse neuromuscular junction. Neuroscience 138:433-446

Sorensen JB, Nagy G, Varoqueaux F, Nehring RB, Brose N, Wilson MC, Neher E (2003) Differential control of the releasable vesicle pools by SNAP-25 splice variants and SNAP-23. Cell 114:75-86

Steward O, Falk PM (1991) Selective localization of polyribosomes beneath developing synapses: a quantitative analysis of the relationships between polyribosomes and developing synapses in the hippocampus and dentate gyrus. J Comp Neurol 314:545-557

Sudhof TC (2004) The synaptic vesicle cycle. Annu Rev Neurosci 27:509-547

Sugita S, Saito F, Tang J, Satz J, Campbell K, Sudhof TC (2001) A stoichiometric complex of neurexins and dystroglycan in brain. J Cell Biol 154:435-445

Szatmari P et al. (2007) Mapping autism risk loci using genetic linkage and chromosomal rearrangements. Nat Genet 39:319-328

Tabuchi K, Sudhof TC (2002) Structure and evolution of neurexin genes: insight into the mechanism of alternative splicing. Genomics 79:849-859

Taraskevich PS, Douglas WW (1990) Dopamine (D2) or gamma-aminobutyric acid (GABAB) receptor activation hyperpolarizes rat melanotrophs and pertussis toxin blocks these responses and the accompanying fall in [Ca2+]i. Neurosci Lett 112:205-209

Thomas P, Surprenant A, Almers W (1990) Cytosolic Ca2+, exocytosis, and endocytosis in single melanotrophs of the rat pituitary. Neuron 5:723-733

Thomas P, Wong JG, Almers W (1993a) Millisecond studies of secretion in single rat pituitary cells stimulated by flash photolysis of caged Ca2+. Embo J 12:303-306

Thomas P, Wong JG, Lee AK, Almers W (1993b) A low affinity Ca2+ receptor controls the final steps in peptide secretion from pituitary melanotrophs. Neuron 11:93-104

Tomiko SA, Taraskevich PS, Douglas WW (1983) GABA acts directly on cells of pituitary pars intermedia to alter hormone output. Nature 301:706-707

Toni N, Buchs PA, Nikonenko I, Povilaitite P, Parisi L, Muller D (2001) Remodeling of synaptic membranes after induction of long-term potentiation. J Neurosci 21:6245-6251

Toonen RF, Kochubey O, de Wit H, Gulyas-Kovacs A, Konijnenburg B, Sorensen JB, Klingauf J, Verhage M (2006) Dissecting docking and tethering of secretory vesicles at the target membrane. Embo J 25:3725-3737

Turrigiano GG, Nelson SB (2004) Homeostatic plasticity in the developing nervous system. Nat Rev Neurosci 5:97-107

Tzeng MC, Cohen RS, Siekevitz P (1978) Release of neurotransmitters and depletion of synaptic vesicles in cerebral cortex slices by alpha-latrotoxin from black widow spider venom. Proc Natl Acad Sci U S A 75:4016-4020

Ullrich B, Ushkaryov YA, Sudhof TC (1995) Cartography of neurexins: more than 1000 isoforms generated by alternative splicing and expressed in distinct subsets of neurons. Neuron 14:497-507

Ushkaryov YA, Hata Y, Ichtchenko K, Moomaw C, Afendis S, Slaughter CA, Sudhof TC (1994) Conserved domain structure of beta-neurexins. Unusual cleaved signal sequences in receptor-like neuronal cell-surface proteins. J Biol Chem 269:11987-11992

Ushkaryov YA, Petrenko AG, Geppert M, Sudhof TC (1992) Neurexins: synaptic cell surface proteins related to the alpha-latrotoxin receptor and laminin. Science 257:50-56

Varoqueaux F, Aramuni G, Rawson RL, Mohrmann R, Missler M, Gottmann K, Zhang W, Sudhof TC, Brose N (2006) Neuroligins determine synapse maturation and function. Neuron 51:741-754

Varoqueaux F, Sigler A, Rhee JS, Brose N, Enk C, Reim K, Rosenmund C (2002) Total arrest of spontaneous and evoked synaptic transmission but normal synaptogenesis in the absence of Munc13-mediated vesicle priming. Proc Natl Acad Sci U S A 99:9037-9042

Verhage M, Maia AS, Plomp JJ, Brussaard AB, Heeroma JH, Vermeer H, Toonen RF, Hammer RE, van den Berg TK, Missler M, Geuze HJ, Sudhof TC (2000) Synaptic assembly of the brain in the absence of neurotransmitter secretion. Science 287:864-869

Voets T, Moser T, Lund PE, Chow RH, Geppert M, Sudhof TC, Neher E (2001a) Intracellular calcium dependence of large dense-core vesicle exocytosis in the absence of synaptotagmin I. Proc Natl Acad Sci U S A 98:11680-11685

Voets T, Neher E, Moser T (1999) Mechanisms underlying phasic and sustained secretion in chromaffin cells from mouse adrenal slices. Neuron 23:607-615

Voets T, Toonen RF, Brian EC, de Wit H, Moser T, Rettig J, Sudhof TC, Neher E, Verhage M (2001b) Munc18-1 promotes large dense-core vesicle docking. Neuron 31:581-591

Wadel K, Neher E, Sakaba T (2007) The Coupling between Synaptic Vesicles and Ca(2+) Channels Determines Fast Neurotransmitter Release. Neuron 53:563-575

Waites CL, Craig AM, Garner CC (2005) Mechanisms of vertebrate synaptogenesis. Annu Rev Neurosci 28:251-274

Wang Y, Liu X, Biederer T, Sudhof TC (2002) A family of RIM-binding proteins regulated by alternative splicing: Implications for the genesis of synaptic active zones. Proc Natl Acad Sci U S A 99:14464-14469

Wang Y, Okamoto M, Schmitz F, Hofmann K, Sudhof TC (1997) Rim is a putative Rab3 effector in regulating synaptic-vesicle fusion. Nature 388:593-598

Washbourne P, Thompson PM, Carta M, Costa ET, Mathews JR, Lopez-Bendito G, Molnar Z, Becher MW, Valenzuela CF, Partridge LD, Wilson MC (2002) Genetic ablation of the t-SNARE SNAP-25 distinguishes mechanisms of neuroexocytosis. Nat Neurosci 5:19-26

Whitford KL, Dijkhuizen P, Polleux F, Ghosh A (2002) Molecular control of cortical dendrite development. Annu Rev Neurosci 25:127-149

Yamagata M, Sanes JR, Weiner JA (2003) Synaptic adhesion molecules. Curr Opin Cell Biol 15:621-632

Yang SB, Proks P, Ashcroft FM, Rupnik M (2004) Inhibition of ATP-sensitive potassium channels by haloperidol. Br J Pharmacol 143:960-967

Zhang W, Lilja L, Bark C, Berggren PO, Meister B (2004) Mint1, a Munc-18-interacting protein, is expressed in insulin-secreting beta-cells. Biochem Biophys Res Commun 320:717-721

Zhang W, Rohlmann A, Sargsyan V, Aramuni G, Hammer RE, Sudhof TC, Missler M (2005) Extracellular domains of alpha-neurexins participate in regulating synaptic transmission by selectively affecting N- and P/Q-type Ca2+ channels. J Neurosci 25:4330-4342

Zupancic G, Kocmur L, Veranic P, Grilc S, Kordas M, Zorec R (1994) The separation of exocytosis from endocytosis in rat melanotroph membrane capacitance records. J Physiol 480 (Pt 3):539-552

Acknowledgements

I am indebted to many people whose help and advice I was lucky to receive during the years of my PhD. First of all, I would like to express my gratitude to my supervisor Prof. Markus Missler for continuous support, guidance, and the right proportion of encouragement and criticism. I am thankful to my PhD committee members Prof. Kerstin Krieglstein and Prof. Stephan Sigrist, and also to Dr. Michael Rickmann for helpful discussions during the PhD committee meetings.

Next, I would like to acknowledge the people we have collaborated with or received practical advice from during these studies. When carrying out the electron microscopy experiments, I relied on the generous help of Dr. Dietmar Riedel, who performed the embedding, introduced me to working with an electron microscope and provided continuous assistance and advice. It was a pleasure to work in a collaboration with Prof. Marjan Rupnik and Dr. Simon Sedej, who were always open for discussion and willing to share ideas. I am thankful to Konstantin Glebov for introducing me to the real-time PCR technique, and Dr. Evgeni Ponimaskin for his advice on this method.

Daily work in the lab was fun thanks to my friendly and helpful colleagues Eva Eismann, Martin Klose, Henriette Masius, Carsten Reissner and Dr. Astrid Rohlmann. I am especially grateful to my nearest "bench neighbours" Dr. Kerstin Piechotta and Dr. Richard Fairless for the enjoyable working environment, exciting conversations and helpful practical tips, and also for reading and correcting my manuscripts. Sincere thanks to Dr. Mohiuddin Ahmad for insightful scientific discussions and for readily sharing his expertise whenever I asked for advice. I appreciate the help of Sandra Gerke, most skillful and reliable technical assistant, who makes work in the lab much easier.

I am grateful to my parents, Olga Dudanova and Ivan Dudanov, whose example inspired me to start doing research. Finally, I wish to thank my boyfriend Matthias Küntzel, whose patience, understanding, encouragement and sense of humor were a great help.

Curriculum Vitae

Name	Irina Dudanova
Date of birth	February 27, 1981
Place of birth	Petrozavodsk, Russia
Current address	Nonnenstieg 25 37075 Göttingen Germany
Phone	+49-551-3893617 +49-176-23234017
Email	idudano@gwdg.de, idudanova@gmx.net

Education

Since March 2004	PhD in the laboratory of Prof. Missler, Institute for Physiology and Pathophysiology, Göttingen, Germany
Since September 2002	International MSc/PhD program in Neurosciences, Göttingen
October 2003 - March 2004	Master's thesis in the laboratory of Prof. Missler, Institute for Physiology and Pathophysiology, Göttingen "Discrete structural abnormalities in the brains of adult α-neurexin double knockout mice may reflect long-term consequences of impaired synaptic transmission"
September 1998 – July 2002	Petrozavodsk State University, medical faculty, Petrozavodsk, Russia

List of publications

1. Piechotta K, **Dudanova I**, and Missler M (2006) The resilient synapse: insights from genetic interference of synaptic cell adhesion molecules. Cell Tissue Res 326: 617-42
2. **Dudanova I***, Sedej S*, Ahmad M*, Masius H, Sargsyan V, Zhang W, Riedel D, Angenstein F, Schild D, Rupnik M, and Missler M (2006) Important contribution of α-neurexins to Ca^{2+}-triggered exocytosis of secretory granules. J Neurosci 26: 10599-10613
*There authors contributed equally to this work.
3. **Dudanova I**, Tabuchi K, Rohlmann A, Südhof T, and Missler M (2007) Deletion of α-neurexins does not cause a major impairment of axonal pathfinding or synapse formation. J Comp Neurol 502: 261-274

Poster abstracts

1. Dudanova I, Sedej S, Rupnik M, and Missler M. Structural alterations in the brains of adult α-neurexin double knockout mice may be a long-term concequence of impaired synaptic transmission. Presented at: **30th Göttingen Neurobiology Conference**, Febr 17-20, 2005, Göttingen, Germany
2. Dudanova I, Sedej S, Rupnik M, Missler M. α-Neurexins are required for Ca^{2+} - dependent release of secretory granules and contribute to the stabilization of synaptic contacts. Program No. 961.10. *2005 Abstract Viewer/Itinerary Planner*. Washington, DC: Society for Neuroscience. Presented at: **SfN 35th Annual Meeting**, Nov 12-16, 2005, Washington DC, USA
3. Dudanova I, Sedej S, Rupnik M, Missler M. α-Neurexins are required for Ca^{2+}-dependent release of secretory granules from neuroendocrine cells. *FENS Abstr., vol.3, A190.7, 2006*. Presented at: **5th Forum of European Neuroscience**, July 8-12, 2006, Vienna, Austria

Appendix 1

Deletion of α-Neurexins Does Not Cause a Major Impairment of Axonal Pathfinding or Synapse Formation

IRINA DUDANOVA,[1,2] KATSUHIKO TABUCHI,[3] ASTRID ROHLMANN,[1,2] THOMAS C. SÜDHOF,[3] AND MARKUS MISSLER[1,2]

[1]Department of Anatomy and Molecular Neurobiology, Westfälische Wilhelms-Universität, D-48149 Münster, Germany

[2]Center for Physiology and Pathophysiology, Georg-August University, D-37073 Göttingen, Germany

[3]Center for Basic Neuroscience & HHMI, The University of Texas Southwestern Medical Center, Dallas, Texas 75390

ABSTRACT

α-Neurexins are synaptic cell-surface molecules that are required for Ca^{2+}-triggered exocytosis. Mice lacking all three α-neurexins show drastically reduced neurotransmitter release at excitatory and inhibitory synapses and die early postnatally. Although previous histological analysis of newborn α-neurexin triple mutants revealed only a moderate reduction in the density of type II synapses in the brainstem, cell culture studies proposed that neurexins are prominently involved in synapse formation. To assess the contribution of α-neurexins to the formation and structural properties of synapses in vivo, we performed a detailed morphological analysis of the brains from surviving adult double knockout mice lacking two of the three α-neurexins. Despite their impaired neurotransmission, we did not observe any gross anatomical defects or changes in the distribution of synaptic proteins in adult mutants. Only mild structural alterations were found: a ~20% reduction of neuropil area in many brain regions, resulting predominantly from shortened distal dendritic branches and fewer spines, as demonstrated by Golgi impregnation of pyramidal neurons. Quantitative electron microscopy revealed ultrastructurally normal type I and II terminals and a ~30% decrease in the density of type II synapses in the neocortex. To exclude errors in pathfinding, we investigated axonal projections in the olfactory bulb of newborn knockouts and did not observe any changes. Therefore, α-neurexins are not essential for the formation of the vast majority of synapses in vivo but rather regulate the function of these synapses. J. Comp. Neurol. 502:261–274, 2007.

Indexing terms: synaptogenesis; cell adhesion molecules; dendritic architecture; knockout mice; electron microscopy; neurotransmission

Assembly of neuronal networks includes the initial guidance of axons to the appropriate regions, target recognition within the region, and establishment of synaptic contacts with partner cells, all of which occur largely independently of electrical activity. Later in development, stabilization and refinement of neuronal connections depend more strongly on synaptic activity (Waites et al., 2005). Consequently, synaptogenesis requires the coordinated action of many guidance and cell-adhesion molecules as well as components regulating neurotransmitter release (Piechotta et al., 2006).

Neurexins constitute a family of highly variable cell-adhesion molecules expressed in the nervous system that have been proposed to function in synapse formation (Missler and Sudhof, 1998). Each of the three vertebrate neurexin genes encodes two principal types of neurexin

Grant sponsor: Deutsche Forschungsgemeinschaft (DFG); Grant number: SFB 406-TPC9; Grant sponsor: Georg Christoph Lichtenberg Stipend from the Ministry for Science and Culture of Lower Saxony, Germany (to I.D.).

*Correspondence to: Prof. Markus Missler, Department of Anatomy and Molecular Neurobiology, UKM, Westfälische Wilhelms-University, Vesaliusweg 2-4, Münster D-48149, Germany. E-mail: mmissle1@gwdg.de

Received 29 September 2007; Revised 30 November 2007; Accepted 22 December 2007

DOI 10.1002/cne.21305

Published online in Wiley InterScience (www.interscience.wiley.com).

proteins, which differ in length and domain composition. The extracellular sequences of the longer α-neurexins contain six laminin-like LNS domains (also called *LG domains*), whereas only the last LNS domain is found in β-neurexins following a short N-terminal β-specific sequence. The transmembrane and intracellular regions are common to α and β isoforms (Missler et al., 1998). All neurexins undergo extensive alternative splicing at several conserved sites (Rowen et al., 2002; Tabuchi and Sudhof, 2002), resulting in an enormous number of isoforms distributed in the brain with partially differential and partially overlapping expression patterns (Ullrich et al., 1995). All six principal isoforms are found in the cortex, but different cortical layers display specific combinations of neurexin variants; e.g., in layer II, all isoforms are present, whereas layer V lacks neurexins 1β, 2α, and 3α. In the olfactory bulb, periglomerular cells express predominantly 1α, 2β, and 3β isoforms; mitral cells neurexin 1β; and granule cells neurexins 2β, 3α, and 3β (Ullrich et al., 1995).

The similarity of molecular structure of α- and β-neurexins (Missler et al., 1998; Ushkaryov et al., 1992, 1994) and their common intracellular (Biederer and Sudhof, 2000, 2001; Butz et al., 1998; Hata et al., 1996) and extracellular binding partners (Boucard et al., 2005; Ichtchenko et al., 1995; Sugita et al., 2001) suggest that their functions could at least partially overlap. Recently, it has been shown that α-neurexins can bind certain splice variants of neuroligins that previously appeared to be a specific interaction partner for β-neurexin isoforms (Boucard et al., 2005).

Analysis of α-neurexin null mutant mice showed that α-neurexins are essential for efficient neurotransmitter release at synapses (Missler et al., 2003). Ablation of multiple α-neurexin genes leads to perinatal lethality of the triple knockout (TKO) and most of the double knockout (DKO) mutants, with only 5–10% of neurexin 1α/2α DKO and 40% of neurexin 2α/3α DKO mice (DKO1/2 and DKO2/3, respectively) reaching the age of 1 month. The most striking feature of the triple knockout phenotype is the dramatic reduction in spontaneous and evoked neurotransmission at both glutamatergic and GABAergic synapses, which is also observed, albeit in a milder form, in double knockouts and presumably is due to an impaired function of high-voltage-activated Ca^{2+} channels. Transgenic rescue experiments on the null mutant background confirmed that α-neurexins perform a nonredundant role in Ca^{2+}-dependent neurotransmitter release, which requires their long extracellular domains and cannot be undertaken by the shorter β-neurexins (Zhang et al., 2005). In spite of the dramatic functional defects, only subtle morphological changes were found in the brains of newborn TKOs, limited to a moderate decrease in area density of type II (presumably inhibitory) synapses (Missler et al., 2003). In addition to their role at central synapses, α-neurexins also affect transmission at the neuromuscular junction (Sons et al., 2006) and contribute substantially to Ca^{2+}-triggered release of secretory granules from endocrine cells (Dudanova et al., 2006).

Recently, a major role in the initiation of synapse formation has been proposed for α- and β-neurexins based on in vitro studies. Synapse-inducing activity was first demonstrated for β-neurexins (Chih et al., 2005; Dean et al., 2003; Graf et al., 2004; Sara et al., 2005; Scheiffele et al., 2000), which are known to form a Ca^{2+}-dependent transsynaptic adhesion complex with postsynaptically localized neuroligins (Ichtchenko et al., 1995; Nguyen and Sudhof, 1997; Song et al., 1999). In vitro overexpression and RNAi knock-down experiments pointed to the function of the β-neurexin–neuroligin complex as a potent bidirectional inducer of pre- and postsynaptic specializations (Graf et al., 2004; Scheiffele et al., 2000). These observations were then extended to α-neurexins, which were also shown to contribute to synaptogenesis in culture (Boucard et al., 2005). Surprisingly, another study suggested a functional specialization of neurexin isoforms according to the neurotransmitter phenotype: heterologously expressed α-neurexins and a subset of β-neurexins with an insert in splice site 4 exclusively triggered GABAergic postsynaptic specializations in contacting dendrites, whereas excitatory contacts could be initiated only by β-neurexins lacking this splice insert (Chih et al., 2006). Similarly, when soluble neurexins were applied to disrupt the endogenous neurexin–neuroligin complexes, α-neurexin and splice site 4-positive β-neurexin selectively reduced the number of inhibitory synaptic specializations (Chih et al., 2006), whereas splice-site-4-lacking β-isoform interfered with the formation and function of both types of contacts (Chih et al., 2006; Levinson et al., 2005). Thus, the results of in vitro assays point to a major contribution of α- and β-neurexins to synaptogenesis and even suggest exclusive roles of particular isoforms at excitatory or inhibitory synapses. This is in contrast to the in vivo findings in α-neurexin and neuroligin null mutant mice, which show dramatic functional impairments at both types of synapses but no significant defects in synaptogenesis (Missler et al., 2003; Varoqueaux et al., 2006). Moreover, the proposed neurotransmitter-specific role of neurexin splice variants is difficult to reconcile with their expression patterns in the brain (Ichtchenko et al., 1995; Ullrich et al., 1995).

Here, we addressed this controversy by performing a quantitative morphological analysis of the brain structure in α-neurexin mutants. We investigated axonal projections to the olfactory glomeruli in newborn mice and did not detect any pathfinding errors in the mutants. For adult double-knockout mice, we observed essentially normal brain architecture, unchanged synaptic ultrastructure, and only mildly reduced type II synapse densities, in line with the findings in newborn mutants. In addition, adult mutants demonstrated a moderate decrease in neuropil and shortening of dendritic ramifications and a corresponding reduction in overall numbers of dendritic spines. Our present data show that α-neurexins are not essential for the formation or ultrastructure of the vast majority of synapses in vivo.

MATERIALS AND METHODS

Animals

The generation and maintenance of α-neurexin knockout mice in a hybrid C57Bl6 × SV129 background have been described previously (Missler et al., 2003; Zhang et al., 2005). Except where stated otherwise, littermates lacking only a single neurexin gene (Nrxn2α single KO) served as control animals for double and triple knockouts. For experiments on olfactory projections, α-neurexin knockout mice were crossed with P2-IRES-tau-LacZ knockin (KI) mice (Mombaerts et al., 1996; generous gift

from Dr. Richard Axel, Colombia University) to generate mutant mice for the three α-neurexin KO alleles and the P2-IRES-tau-LacZ KI allele. All experiments were performed in accordance with institutional guideline for animal welfare.

Histological analyses

Six- to eight-week-old mice were anesthetized and perfused transcardially with phosphate-buffered saline (PBS), followed by 4% paraformaldehyde (PFA) in 0.1 phosphate buffer (PB; pH 7.4), the brains were dissected and left for 2 hours in 4% PFA to postfix. P1 mouse heads were immersion fixed in 2% PFA for 2 hours. The brains were cryoprotected by immersion in a 25% solution of sucrose in 0.1 M PB overnight. For morphometric analysis, whole brains were serially sectioned, and every fifth 25-μm-thick cryosection was thaw mounted on poly-L-lysine-coated slides and stained with cresyl violet (Nissl). For DAPI staining, 12-μm cryosections were treated with 1 μm/ml 4′,6-diamidino-2-phenylindole (DAPI)-hydrochloride solution. For immunofluorescence, 12-μm cryosections were permeabilized with 0.3% Triton in PBS and incubated in blocking solution (5% normal goat serum in PBS) for 1–2 hr at room temperature (RT). For P1 brains, the sections were 30 μm thick, and permeabilization was omitted. Primary antibodies were applied overnight at 4°C: anti-MAP2 1:500, SMI32 1:500, GFAP 1:500, synaptophysin 1:50, GAP 43 1:200. Secondary antibodies were goat anti-rabbit or goat anti-mouse Alexa 488 or Alexa 546 (Invitrogen, Eugene, OR), applied at 1:400 for 45 minutes at RT. For DAB staining, 30-μm free-floating brain sections were quenched with 10% methanol, 3% H_2O_2 in PBS, Triton-permeabilized and blocked in 5% normal goat serum (NGS) in PBS. No Triton was used when labelling cell bodies with the anti-GAD67 antibody. First antibody diluted in blocking solution was applied overnight at 4°C: anti-VGlu1 1:10,000, VGAT 1:1,000, GAD67 1:1,000, synaptophysin 1:1,000. Second antibody was applied for 30 minutes at 37°C: goat anti-rabbit or goat anti-mouse 1:100 (Sternberger Monoclonals Inc., Baltimore, MD) and third antibody for 1 hour at 37°C: rabbit peroxidase-antiperoxidase (PAP) or mouse PAP, 1:500 (Sternberger Monoclonals Inc.). The sections were diaminobenzidine (DAB) stained and mounted on gelatin-covered slides. The sections were examined at an Axioscope 2 epifluorescent microscope, and images were captured with the AxioCam HRc digital camera (Zeiss, Oberkochen, Germany). Images of brain sections immunolabelled with cellular markers were obtained by using a confocal laser scanning microscope LSM 510 (Zeiss) with a ×63 water-immersion objective. Morphometric measurements were performed in AxioVision software (Zeiss). Overviews of the brain (see Fig. 2A–D) are composed of up to 40–50 individual higher magnification images in Adobe Photoshop CS. The brightness and contrast of the images were adjusted in Adobe Photoshop SC; red-green images were converted to magenta-green.

Primary antibodies

Mouse monoclonal anti-MAP2 antibody (Sternberger Monoclonals Inc.; No. SMI52) was raised against full-length bovine MAP2 protein (manufacturer's information). It produced a somatodendritic staining identical to that previously described for MAP2 (see Fig. 3C,D; Bernhardt and Matus, 1984). On immunoblots of brain cytoskeletal preparations, the antibody reacts with MAP2a and MAP2b and an additional double band of 68 kDa, presumably representing MAP2c (Kaufmann et al., 1997). The SMI32 mouse monoclonal antibody (Sternberger Monoclonal Inc.) resulted from immunization with hypothalamus and recognizes nonphosphorylated neurofilament H (manufacturer's information). On a Western blot of a rat brain, it labels two bands of ~195 and ~160 kDa (Pennypacker et al., 1991). The antibody produced a staining pattern indentical to the one previously described (Sternberger and Sternberger, 1983). Anti-GFAP rabbit antiserum (Dako, Glostrup, Denmark; No. Z0334) was raised against GFAP isolated from cow spinal cord (manufacturer's information) and labelled cells with typical astrocyte morphology (Fig. 3G,H). Mouse monoclonal antisynaptophysin antibody (Dako; No. MO776) was obtained by immunization with coated vesicles of bovine brain tissue (Wiedenmann and Franke, 1985) and recognizes a region between amino acids 269 and 289 in the cytoplasmic domain of synaptophysin (Knaus and Betz, 1990). On a Western blot of synaptic vesicle fraction from the mouse brain, it recognizes a single band of 38 kDa (Wiedenmann and Franke, 1985). The antibody produced a punctate staining of brain sections, as previously described (Wiedenmann and Franke, 1985). Rabbit polyclonal anti-GAP 43 (Chemicon, Temecula, CA; No. AB5220) was raised against recombinant rat GAP 43, including the complete protein sequence (manufacturer's information). The pattern of immunoreactivity produced by the antibody in the olfactory bulb was identical to that previously reported (Ramakers et al., 1992). Anti-VGlu1 rabbit antiserum (Synaptic Systems, Göttingen, Germany; No. 135302) was raised against a Strep-tag fusion protein containing amino acid residues 456–560 of rat VGlu1 and recognizes a band of 60 kb on a Western blot (manufacturer's information). When used on mouse brain sections, it produced a pattern of staining identical to the one previously described for VGlu1 in rat brain (Fujiyama et al., 2001). Anti-VGAT rabbit antiserum (Synaptic Systems; No.131002) was raised against a synthetic peptide including amino acid residues 75–87 of rat VGAT. It recognizes two bands of 57 and 50 kDa on a Western blot of a brain homogenate (Takamori et al., 2000). On brain sections, the antiserum showed the same pattern of VGAT immunoreactivity as reported previously (Chaudhry et al., 1998). Anti-GAD67 rabbit polyclonal antibody (Chemicon; No. AB5992) was raised against recombinant feline GAD. On a Western blot, the antibody preferentially recognizes the larger 67-kDa isoform of GAD protein, and has a weaker reactivity to GAD 65 (manufacturer's information). The immunoreactivity pattern observed on mouse brain sections was identical to the previous description in the rat brain (Esclapez et al., 1994).

Golgi-Cox impregnation

Unfixed brains were removed from the skull and immersed into Golgi impregnation solution (1% $K_2Cr_2O_7$, 1% $HgCl_2$ and 0.83% K_2CrO in dH_2O) for 14 days. The brains were then slowly dehydrated, embedded in celloidin, and cut into 150-μm-thick frontal sections. The sections were developed by using a modified Golgi-Cox technique (Glaser and Van der Loos, 1981). Neurons recognized morphologically as pyramidal cells were traced in Neurolucida software (MicroBrightField Inc., Colchester, VT). In each cerebral hemisphere, cells in layer III and layer V were

analyzed. Dendritic branches were followed over the live picture up to their natural terminations, adjusting for changes in depth continuously. Dendritic branches were numbered from proximal to distal, as shown in Figure 4D. The density of spines was calculated by dividing the number of spines by the length of the dendritic segment.

β-Galactosidase staining of olfactory bulbs

Newborn mice carrying the three α-neurexin deletions and in addition the P2-IRES-tau-LacZ KI allele (quadruple mutant animals) were decapitated, and sagittal halfheads were fixed with 4% paraformaldehyde, 2 mM $MgSO_4$, and 5 mM EGTA in 100 mM PB (pH 7.4) for 30 minutes on ice. Samples were then washed in 100 mM PB (pH 7.4) with 2 mM $MgSO_4$ for 30 minutes at room temperature, followed by 100 mM PB (pH 7.4) with 2 mM $MgCl_2$, 0.01% sodium deoxycholate, and 0.02% Triton X-100 twice for 5 minutes each at RT. For β-galactosidase staining, whole mounts were incubated in 100 mM PB (pH 7.4) with 2 mM $MgCl_2$, 0.01% sodium deoxycholate, 0.02% Triton X-100, 5 mM potassium ferricyanide, 5 mM potassium ferrocyanide, and 1 mg/ml X-gal at 37°C.

Electron microscopy

Mice were perfused with 0.1 M PB, followed by 2.5% glutaraldehyde, 2.5% PFA in 0.1 M PB. Brains were dissected, kept in fixative for 2 hours, and cut into 200-μm-thick vibratome sections, from which small regions of the primary visual cortex were dissected. After overnight incubation at 4°C in the same fixative, samples were additionally fixed with 1% OsO_4 for 1 hour at RT, and preembedding stained with uranyl acetate. After dehydration with a consecutive series of ethanol and propylene oxide, the samples were embedded in Agar 100 resin. The region of interest was identified on toluidine blue-stained semithin sections (700 nm). Ultrathin sections (60 nm) were counterstained with uranyl acetate for 10 minutes and lead citrate for 2 minutes and examined at a Philips CM 120 electron microscope (Philips Inc., Eindhoven, The Netherlands). Images of synapses were taken with a 2,048 × 2,048 Tietz TemCam 224A camera (TVIPS, Gauting, Germany) at constant intervals throughout the primary visual cortex at ×3,750 magnification for measuring synapse densities and at ×27,000 magnification for studying synaptic ultrastructure. Measurements were made with DigitalMicrograph 3.4 software (Gatan Inc.).

Data analysis

Data are presented as means ± SEM. Statistical significance was assessed by one-way ANOVA or two-tailed Student's *t*-test in Prism software (GraphPad). The level of significance was set at $P \leq 0.05$.

RESULTS

Olfactory sensory projections are normal but glomerular size is reduced in newborn α-neurexin mutants

We first studied the role of α-neurexins in axonal pathfinding and the initial establishment of synaptic connections in the olfactory bulb of newborn TKO mutants. This area was chosen because it is already quite mature at birth and has a defined layered structure and a precise topographic organization of sensory inputs. The overall size of the olfactory bulb did not differ between genotypes (Table 1), and neuronal layering was preserved in the knockouts. We investigated the targeting and sorting of olfactory cell axons into glomeruli in α-neurexin-deficient animals, making use of a knockin mouse strain where the P2 odorant receptor is coexpressed with a LacZ reporter gene (Mombaerts et al., 1996). P2-IRES-tau-LacZ KI mice were crossed with α-neurexin knockout mice, and P2-positive axons were visualized with X-gal staining. As in control animals, the axons of P2-expressing olfactory neurons in α-neurexin knockouts were routed to one glomerulus on the medial side of the olfactory bulb, which also preserved its correct position (Fig. 1A,B). Thus deletion of α-neurexins does not prevent normal axonal pathfinding by odorant receptor axons, nor does it impair the spatial arrangement of glomeruli in the olfactory bulb.

TABLE 1. Quantitative Assessment of the Olfactory Bulb in Newborn Mice[1]

	Genotype		
	WT (n = 3)	TKO (n = 3)	*P*
Olfactory bulb, area (mm^2)	1.13 ± 0.07	1.12 ± 0.06	n.s.
Glomeruli, area (μm^2)	795 ± 20	623 ± 33	<0.02
ML, thickness (μm)	37.0. ± 3.8	37.7 ± 3.2	n.s.
EPL, thickness (μm)	34.0 ± 1.3	32.6 ± 4.1	n.s.
GL, thickness (μm)	50.0 ± 4.6	42.7 ± 4.1	n.s.

[1]Data are means ± SEM. n = Number of animals used. Three to six sections from each animal were used for data collection. On each section, between 10 (thickness) and 25 (area of glomeruli) measurements were taken with NIH Image 1.61 software. Statistical analysis was performed via *t*-test (Prism software; GraphPad); n.s., Not significant. ML, mitral cell layer; EPL, external plexiform layer; GL, glomerular layer.

To test the integrity of the entire population of glomeruli, sections of the bulb were doubly labeled with antibodies against the axonal marker GAP 43 and the synaptic marker synaptophysin. Olfactory glomeruli, where incoming axons of olfactory sensory neurons make synaptic contacts with the dendrites of mitral and tufted cells, were colabeled with both markers (Fig. 1C–F). Quantitative analysis demonstrated that olfactory glomeruli were ~20% smaller in α-neurexin mutants, whereas no differences were found in any other layer of the olfactory bulb (Table 1). Axonal projections to the glomeruli were intact, so the reduced size of these structures may reflect a decrease in the number of synaptic contacts.

Adult α-neurexin knockout mice reveal a reduced neuropil compartment

Because the olfactory bulb morphology exhibited discrete changes in newborn mutants, whereas other, more immature regions were not affected (Missler et al., 2003), we hypothesized that the structural consequences of deleting α-neurexins would be more obvious in older brains. Therefore, morphological changes in the brains of surviving DKO animals at the age of 6–8 weeks were investigated.

To evaluate general brain architecture of adult α-neurexin mutants, we first examined whole-brain serial Nissl-stained sections from mutant and littermate control mice. In addition to wild-type mice of the same genetic background, we used neurexin 2α single knockout (SKO 2) littermates as controls, because they display the least severe phenotype among all α-neurexin null mutants. Similarly to the case in newborn α-neurexin TKO mice (Missler et al., 2003), there were no overt anatomical

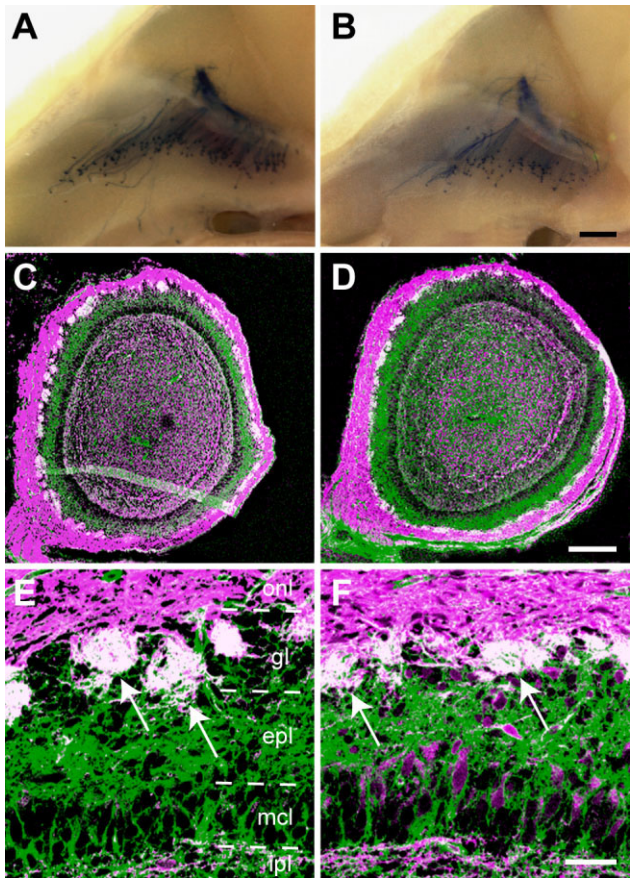

Fig. 1. Morphological changes in the olfactory bulb of newborn α-neurexin triple knockout mutants. **A,B:** X-gal-stained olfactory sensory fibers are normally targeted to a single olfactory glomerulus in newborn α-neurexin triple knockout mice (B), similar to control animals (A). **C,D:** Overviews of the olfactory bulb from newborn wild type (C) and α-neurexin triple knockout mice (D), double-labelled with GAP 43, an axonal growth cone marker (magenta), and synaptophysin, a synaptic marker (green). Olfactory glomeruli appear white in the overlay. **E,F:** Olfactory glomeruli (arrows) are smaller in α-neurexin triple knockout mice (F) than in control animals (E). Layers of the olfactory bulb are indicated. onl, Olfactory nerve layer; gl, glomerular layer; epl, external plexiform layer; mcl, mitral cell layer; ipl, internal plexiform layer. Scale bars = 500 μm in B (applies to A,B); 200 μm in D (applies to C,D); 30 μm in F (applies to E,F).

abnormalities in adult DKO mutants (Fig. 2A–D). However, upon closer examination, many brain regions appeared to be smaller and to have higher cell densities. For example, the primary visual cortex was slightly reduced in thickness, and higher cell densities could be observed in layer II as well as in sublayers Va and VIa, where cells were sparse in controls (Fig. 2E–H). More rostral cortical areas displayed similar, albeit less pronounced, alterations (data not shown). Several subcortical structures, such as caudate-putamen and thalamic nuclei, also showed higher cell densities. In the olfactory bulb, the glomeruli were smaller, similar to newborn TKOs (see Fig. 1C–F), and in addition the thickness of the external plexiform layer was decreased (Fig. 2I,J). In the affected regions, the changes typically amounted to an ~20% reduction of area or an equivalent increase in area density of cells (Table 2). Despite being relatively mild, these alterations were observed consistently in all animals that were analyzed. The effect included most of the brain areas, with a few notable exceptions, such as the hippocampus, that remained morphologically unchanged (Fig. 2K,L, Table 2). Because the defect was quantitatively similar in the two types of double knockout mutants (DKO 1/2 and DKO 2/3), we pooled them together into one group and collectively refer to them as *double knockouts*.

A reduction in the volume of brain structures could be due to cell loss or to the paucity of neuropil, the acellular part of nervous tissue, which includes neuronal and glial cell processes, spines, and synaptic contacts. We first tested whether increased cell death contributes to the reduction in the size of affected brain regions in the knockouts. Staining of brain sections from two pairs of adult DKO and control mice with DAPI hydrochloride did not reveal nuclear fragmentation or other features characteristic of apoptosis (Fig. 3A,B, and data not shown). We then labelled brain sections with markers of the dendritic (MAP2) and axonal (SMI32) compartments as well as a glial cell marker (GFAP). The intensity and pattern of labelling did not differ between the genotypes (Fig. 3C–H, and data not shown). The absense of apoptotic signs, the unchanged distribution of cellular markers, and the increased density of cell bodies observed in Nissl-stained sections exclude the possibility of cell loss and suggest instead that a decrease in neuropil probably underlies the overall smaller size of the affected brain areas.

Changes in dendritic architecture of cortical pyramidal neurons in α-neurexin double knockout mice

We asked which of the components that build up the neuropil might contribute to the defect in α-neurexin knockouts. To investigate dendritic morphology in the mutants, we performed a Golgi impregnation of brain sections. With this technique, a small percentage of neurons are randomly stained, and their entire dendritic trees can be visualized up to the terminal branches, including dendritic spines. The overall impregnation pattern was similar in control and mutant animals (Fig. 4A,B). We chose pyramidal neurons in layers III and V of the primary visual cortex for analysis because these cells are abundant and easily recognizable morphologically. In addition, the apical dendrites of these neurons form their terminal ramifications in layer II, whereas the basal dendrites of layer V cells ramify in layer V, the very layers where neuropil reduction was observed in Nissl-stained sections (Fig. 2E,F).

The impregnated pyramidal neurons in double knockouts displayed normal cellular morphology and dendritic orientation. We evaluated dendritic architecture in detail by measuring dendritic length, the number of dendritic spines, and the density of spines on the dendrites. In each neuron, the apical dendrite with its horizontal branches and two basal dendrites up to their third-order ramifications were traced, because the majority of dendritic arbors did not ramify further (Fig. 4C,D). The length of the apical dendrites and their horizontal branches was significantly decreased in layer III pyramidal cells of double-knockout mice, as was the total length of the basal dendrites (Table 3). Measurements of the segments of different branching orders of basal dendrites showed that the proximal

branches were similar in length in both genotypes, whereas the third-order branches were significantly shorter in the double knockouts. The reduction of dendritic length correlated with the changes in the number of dendritic spines: the overall number of spines on the apical and basal dendrites was reduced, and the changes were found mainly on the distal branches of the dendritic arbors and were roughly proportional to the decrease in length. The density of spines remained unchanged in all dendritic segments analyzed (Table 3). Similar alterations were found in layer V pyramidal neurons of the knockouts (data not shown). Thus, the analysis of dendritic architecture in single Golgi-stained neurons revealed shorter dendritic branches and lower spine numbers at the periphery of dendritic trees in α-neurexin DKOs. Because the majority of excitatory synapses are formed on spines, the loss of dendritic spines in pyramidal neurons is indicative of a reduction in total excitatory synapse number in the absence of α-neurexins.

Synapse achitecture in the cortex of α-neurexin knockout mice

To address directly the possible changes in synapse numbers, we next studied the distribution of several marker proteins in the control and mutant brains, focusing again on layers II and V of the primary visual cortex. We tested synaptophysin, a synaptic vesicle protein, as a general synaptic marker, and vesicle glutamate transporter 1 (VGlu1) and vesicle GABA transporter (VGAT) as markers specific for excitatory and inhibitory synapses, respectively. The GABA-synthetizing enzyme glutamic acid decarboxilase (GAD67) served as an additional marker for inhibitory synapses. All the antibodies used produced the punctate staining pattern characteristic for synaptic proteins. We did not detect any notable differences in the immunoreactivity pattern or intensity of the general (Fig. 5A,B) or excitatory (Fig. 5C,D) synaptic markers, confirming the normal overall brain assembly in α-neurexin null mutants. For the inhibitory synaptic markers, however, the staining intensity was somewhat lower in the double knockouts (Fig. 5E–H), although this difference was rather subtle and did not include a change in the perisomatic distribution pattern.

To assess synapse densities more reliably and to analyze synaptic ultrastructure, electron microscopy was performed in the primary visual cortex of mutant and control animals, essentially as described by Missler et al. (1993). Electron micrographs of neuropil were taken at equal intervals throughout the cortex, so that all cortical layers were represented in the analysis, because light microscopy revealed changes in several cortical layers. We did not observe any overt ultrastructural defects in the neuropil of α-neurexin mutants (Fig. 6A,B). Quantitative analysis revealed that the density of Gray type I (presum-

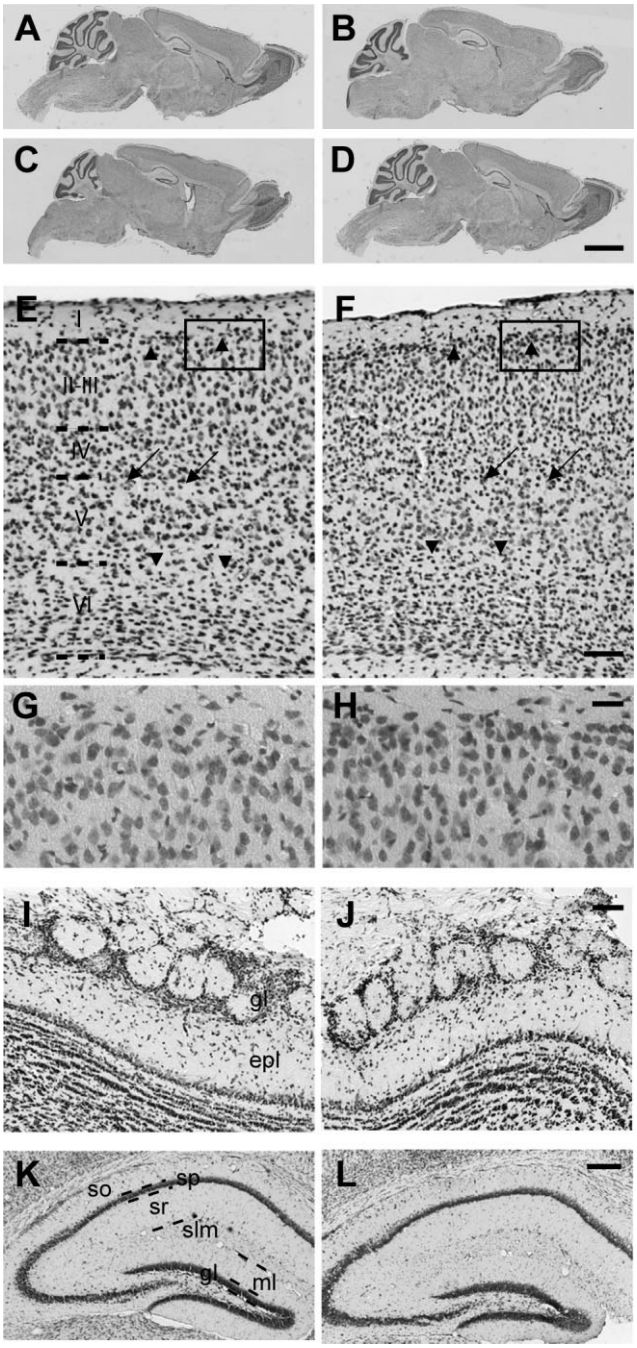

Fig. 2. Adult α-neurexin double knockout mutants have reduced brain neuropil. **A–D:** Overviews of Nissl-stained parasaggital sections show no overt anatomical defects in the brains of neurexin 1α/2α (C) and neurexin 2α/3α (D) knockout mice, as compared with wild-type (A) and neurexin 2α single knockout (B) controls. **E,F:** In the primary visual cortex, the cell density is higher in the double knockout mice (F) than in controls (E), shown in layer II (arrowheads pointing upward), layer Va (arrows), and layer VIa (arrowheads pointing downward). Cortical layers are indicated by roman numerals. **G,H:** Higher magnification images of the areas boxed in (E,F) showing increased density of cell bodies in layer II of the primary visual cortex in the double knockout mutants (H) compared with control mice (G). **I,J:** In the olfactory bulb, the glomeruli appear smaller in diameter in α-neurexin mutants (J) compared with control animals (I). **K,L:** No differences can be observed in the hippocampus morphology between control (K) and double knockout (L) mice. gl, Glomerular layer; epl, external plexiform layer; so, stratum oriens; sp, stratum pyramidale; sr, stratum radiatum; slm, stratum lacunosum moleculare; ml, molecular layer of the dentate gyrus; gl, granular layer of the dentate gyrus. Scale bars = 2 mm in D (applies to A–D); 100 μm in F (applies to E,F); 25 μm in H (applies to G,H); 100 μm in J (applies to I,J) 200 μm in L (applies to K,L).

TABLE 2. Quantitative Assessment of the Neuropil in α-Neurexin Double Knockout and Control Mice[1]

	Genotype				
	WT (n = 5)	SKO 2 (n = 9)	DKO 1/2 (n= 6)	DKO 2/3 (n= 7)	*P*
V1 cortex					
Layer II, % cells[2,3]	36.3 ± 1.9	42.6 ± 1.6	54.1 ± 2.0	52.9 ± 1.3	<0.001
Layer Va, cell density (cells/mm^2)[2]	3,772 ± 165	4,386 ± 171	5,139 ± 264	5,566 ± 347	<0.001
Layer VIa, cell density (cells/mm^2)[2]	3,777 ± 100	4,319 ± 157	5,127 ± 243	5,493 ± 264	<0.001
	SKO 2 (n)	DKO (n)			
Subcortical structures, cell density (cells/mm^2)					
Caudate-putamen	4,794 ± 119 (4)	5,771 ± 285 (4)			<0.05
Lateral septal nucleus	3,977 ± 222 (3)	4,223 ± 135 (4)			n.s.
Ventrolateral thalamic nucleus	3,212 ± 228 (3)	3,852 ± 165 (4)			n.s.
Olfactory bulb					
Glomeruli, area (μm^2)	7,573 ± 186 (4)	5,916 ± 255 (4)			<0.01
EPL, thickness (μm)	184 ± 5 (4)	160 ± 5 (4)			<0.05
MCL, thickness (μm)	27.4 ± 1.1 (4)	25.3 ± 0.7 (4)			n.s.
Hippocampus, layer thickness (μm)					
SO	107.7 ± 3.0 (4)	125.1 ± 3.7 (4)			<0.05
SP (CA1)	36.5 ± 1.1 (4)	37.0 ± 1.3 (4)			n.s.
SR	172.9 ± 2.9 (4)	182.9 ± 8.7 (4)			n.s.
SLM	94.9 ± 3.3 (4)	108.2 ± 6.9 (4)			n.s.
Dentate gyrus, layer thickness (μm)					
ML	136.9 ± 3.3 (4)	138.5 ± 7.0 (4)			n.s.
GL	50.4 ± 1.2 (4)	43.5 ± 2.3 (4)			<0.05

[1]Data are means ± SEM; *n* = number of animals used. Measurements were made with Axiovision software (Zeiss). Statistical analysis was performed via one-way ANOVA (where more than two groups of animals were compared) or *t*-test (Prism software; GraphPad). n.s., Not significant. EPL, external plexiform layer; MCL, miral cell layer; SO, stratum oriens; SP, stratum pyramidale; SR, stratum radiatum; SLM, stratum lacunosum moleculare; ML, molecular layer of the dentate gyrus; GL, granular layer of the dentate gyrus.
[2]Four to ten sections from each animal were used for data collection.
[3]The proportion of cell bodies vs. neuropil was measured along a horizontal line in layer II.

ably excitatory) synapses was not changed, whereas the density of Gray type II (presumably inhibitory) synaptic contacts was diminished by ~30% in the mutants (Table 4). The changes in type II synapses were distributed evenly throughout the cortex, with all the layers similarly affected. In line with the finding that spine densities in cortical neurons were unchanged, the density of axospinous synapses, i.e., synapses between an axon terminal and a dendritic spine, measured on electron micrographs did not differ between the genotypes. In addition, we observed a slightly higher density of perforated synapses in the DKOs.

Although electron microscopy demonstrated a decrease in area density of only inhibitory synapses, the total number of excitatory synapses in a brain region is probably also decreased, as suggested by the smaller numbers of spines in Golgi-stained pyramidal neurons and total reduction of the volume, e.g., of the primary visual cortex together with unchanged excitatory synapse densities in this region. Evaluation of synaptic ultrastructure did not reveal any changes in the size, area density, or distribution of synaptic vesicles; length of the active zone; or width of the synaptic cleft in α-neurexin mutants (Fig. 6C–F, Table 4), which is consistent with our earlier study in the brainstem of newborn triple knockout mice (Missler et al., 2003).

The loss of inhibitory synapses throughout the cortex of α-neurexin mutants (Table 4) could be caused by a decrease in the number of inhibitory neurons or a reduction in the number of synapses formed by each inhibitory neuron. To test whether the number of GABAergic inhibitory cells is altered in the knockout brains, we labelled brain sections with antibodies against GAD67, omitting the Triton permeabilization step to obtain prominent cell body staining of GABAergic interneurons. We observed a similar distribution of immunoreactive cells in both genotypes (Fig. 7A–D). Quantification of GAD-positive cells in the visual cortex showed that the area density of GABAergic neurons was not reduced but mildly increased in the double knockouts (347 ± 15.2 cells/mm^2) compared with control mice (273.8 ± 2.5 cells/mm^2, $P = 0.03$). Because the total area of the cortex is slightly reduced in the double knockout brains and the area density of inhibitory neurons slightly increased, the absolute number of inhibitory cells is likely to be similar in the mutant and control mice. Thus, our data exclude a loss of inhibitory neurons as the primary cause of lower type II synapse densities found in double knockout mice and suggest that the reduced total numbers of excitatory and inhibitory contacts represent a defect of synapse formation and/or destabilization of individual synapses in the absence of α-neurexins.

DISCUSSION

In the present study, we have investigated the brain structure of knockout mice lacking multiple α-neurexins at the light- and electron-microscopic level. We show that α-neurexins are not essential for the initial formation and ultrastructural properties of the majority of synapses and are not required for axonal pathfinding in the olfactory bulb but play a role at later stages of synapse development and contribute to the normal neuropil structure.

α-Neurexins do not play a major role in primary synaptogenesis but contribute to normal neuropil structure

As cell-adhesion molecules with a function at synapses, neurexins may regulate multiple steps in the establishment of neuronal connections, from axonal guidance and target recognition to the final validation of appropriate contacts (Waites et al., 2005). To estimate the contribution of α-neurexins to these consecutive developmental processes, we first investigated the targeting and sorting of

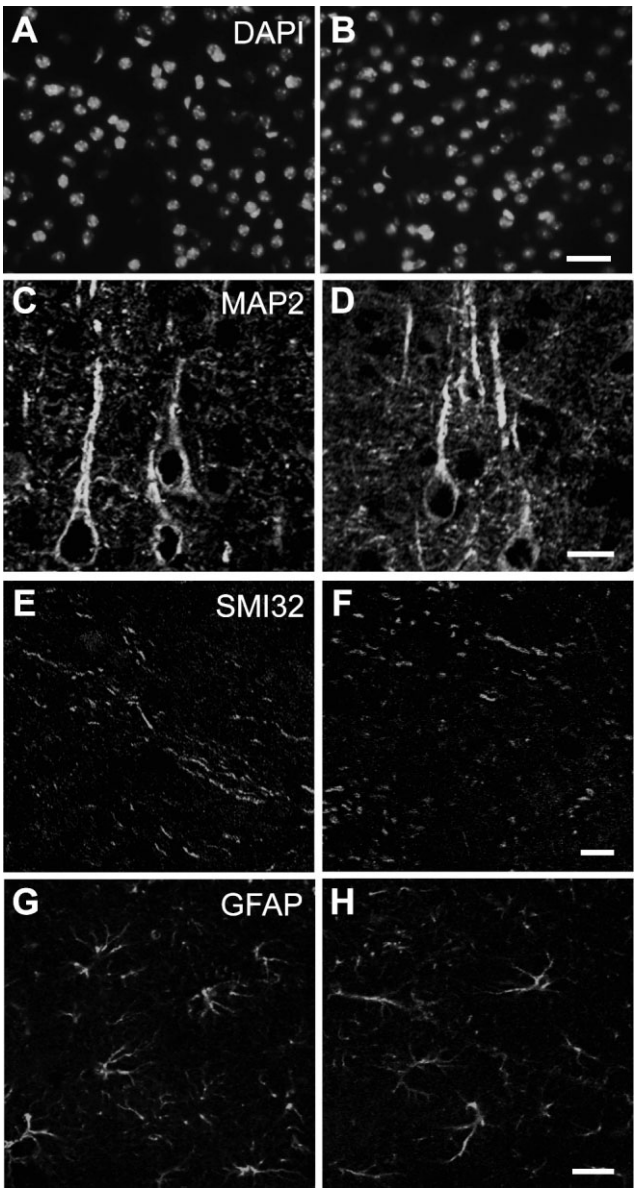

Fig. 3. The distribution of cellular markers is not changed in α-neurexin double knockout mutants. **A,B:** DAPI staining shows no increased apoptosis in the cortex of α-neurexin double knockout mice (B) compared with control animals (A). **C,D:** Labelling of the somatodendritic compartment of cortical pyramidal neurons with MAP2 in control (C) and double knockout (D) animals. **E,F:** Labelling of axons in the white matter with the neurofilament marker SMI32 in control (E) and knockout (F) animals. **G,H:** Labelling of astroglia in the subcortical structures with glial fibrillary acidic protein (GFAP) in control (G) and knockout (H) animals. Scale bars = 25 μm in A (applies to A,B); 10 μm in D (applies to C,D); 10 μm in F (applies to E,F); 10 μm in H (applies to G,H).

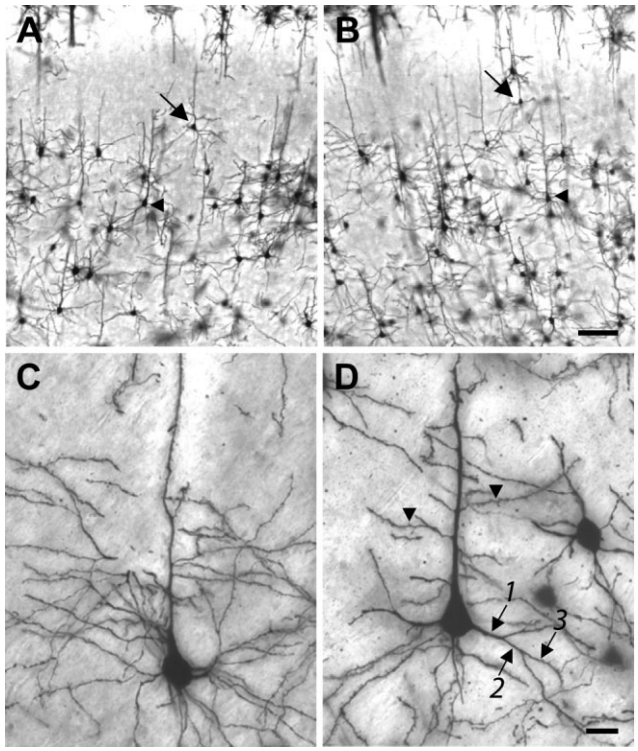

Fig. 4. Golgi impregnation of double knockout and control mouse brains. **A,B:** Pyramidal neurons in layer III (arrows) and layer V (arrowheads) of the visual cortex were used for the analysis of dendritic architecture in control (A) and double knockout (B) mice. **C,D:** Examples of layer V pyramidal neurons in control (C) and double knockout (D) animals. Basal dendrites (arrows) and horizontal branches of apical dendrites (arrowheads) are marked; numbers indicate the branching orders of basal dendrites. Scale bars = 100 μm in B (applies to A,B); 20 μm in D (applies to C,D).

olfactory receptor cell axons in newborn TKO mice. The normal routing of axons, their convergence into one glomerulus, and the unchanged position of the glomerulus in the medial half of the bulb (Fig. 1 A,B) confirmed that the early steps of axonal guidance and target recognition do not require α-neurexins. This is in contrast to findings in several other mutants deficient in axon guidance (see, e.g., Cloutier et al., 2004; Schwarting et al., 2000, 2004; Taniguchi et al., 2003; Walz et al., 2002) or cell-adhesion molecules (Cremer et al., 1994; Montag-Sallaz et al., 2002; Tomasiewicz et al., 1993), in which the projections and/or layering of the bulb are affected. In spite of the absence of these types of defects in α-neurexin knockouts, olfactory glomeruli were reduced in size (Fig. 1C–F), suggesting an abnormality in synapse formation and/or stabilization.

The neuropil changes were further investigated in adult brains, where we found a moderate reduction in the size of brain structures and a corresponding increase in cell density, which were not restricted to a particular area but affected most of the brain, with only a few exceptions, such as the hippocampus (Fig. 2, Table 2). Although it is not clear why these specific regions remained morphologically intact, one of the reasons may be the differential expression of the remaining α-neurexin isoforms in the double knockouts. Similarly to the absence of apoptotic changes in newborn mutants, we did not find any signs of increased apoptosis or alterations of immunoreactivity to cellular markers in adult animals (Fig. 3) and attributed the observed reduction in the size of brain structures to a paucity of neuropil components. The reduction in neuropil was validated at the single-cell level in Golgi-stained cortical neurons, which displayed changes in the dendritic

TABLE 3. Quantitative Analysis of Dendritic Architecture in Layer III Pyramidal Neurons of α-Neurexin Double Knockout and Control Mice[1]

	Genotype		
	SKO 2 (n[2])	DKO (n[3])	*P*
Length of dendritic branches (μm)			
Apical dendrite			
Main shaft	330 ± 27 (12)	269 ± 10 (24)	<0.05
First-order horizontal branches	66 ± 8 (11)	51 ± 4 (24)	n.s.
Second-order horizontal branches	81 ± 14 (8)	35 ± 4 (16)	<0.001
Horizontal branches total	102 ± 13 (12)	74 ± 5 (24)	<0.05
Basal dendrites			
First-order branches	19 ± 2 (12)	16 ± 1 (24)	n.s.
Second-order branches	53 ± 21 (12)	49 ± 5 (24)	n.s.
Third-order branches	62 ± 4 (10)	45 ± 5 (21)	<0.05
Basal dendrites total	332 ± 48 (12)	201 ± 19 (24)	<0.01
Number of dendritic spines			
Apical dendrite			
Main shaft	207 ± 21 (12)	160 ± 8 (24)	<0.05
First-order horizontal branches	126 ± 22 (12)	110 ± 16 (24)	n.s.
Second-order horizontal branches	67 ± 13 (9)	40 ± 6 (16)	<0.05
Horizontal branches total	183 ± 32 (12)	144 ± 16 (24)	n.s.
Basal dendrites			
First-order branches	4 ± 2 (12)	7 ± 2 (24)	n.s.
Second-order branches	67 ± 14 (12)	53 ± 5 (24)	n.s.
Third-order branches	102 ± 13 (11)	56 ± 11 (21)	<0.05
Basal dendrites total	179 ± 16 (12)	108 ± 8 (23)	<0.001
Density of dendritic spines (1/μm)			
Apical dendrite			
Main shaft	0.62 ± 0.04 (12)	0.61 ± 0.03 (24)	n.s.
First-order horizontal branches	0.45 ± 0.05 (12)	0.45 ± 0.03 (24)	n.s.
Second-order horizontal branches	0.41 ± 0.04 (9)	0.42 ± 0.04 (16)	n.s.
Horizontal branches total	0.45 ± 0.04 (12)	0.45 ± 0.03 (24)	n.s.
Basal dendrites			
First-order branches	0.08 ± 0.03 (12)	0.15 ± 0.02 (24)	n.s.
Second-order branches	0.25 ± 0.02 (12)	0.31 ± 0.02 (24)	n.s.
Third-order branches	0.34 ± 0.03 (11)	0.33 ± 0.02 (21)	n.s.
Basal dendrites total	0.27 ± 0.02 (12)	0.32 ± 0.03 (24)	n.s.

[1]Data are means ± SEM. Measurements were performed in Golgi-stained sections of the primary visual cortex in Neurolucida software (MicroBrightField Inc.) for dendrite tracing. Statistical analysis was via *t*-test (Prism software; GraphPad); n.s., not significant.
[2]*n* = Number of cells in four hemispheres of two animals.
[3]*n* = Number of cells in eight hemispheres of four animals.

architecture and a loss of spines at the peripheral segments of the dendritic trees (Table 3). This finding provided evidence for a decrease in excitatory synapse numbers.

The immunoreactivity pattern of excitatory and pansynaptic markers was not changed in DKO brains (Fig. 5); however, the staining intensity of immunolabeled sections reflects only the density of synapses, which was unaltered according to the measurements in Golgi-stained neurons, rather than the absolute number of synapses, which is likely reduced. For inhibitory synapse markers, a lower staining intensity was observed, consistent with the reduced area density of inhibitory synapses, which was confirmed by quantitative electron microscopy (Table 4).

The changes of neuropil in the mutants are consistent with an involvement of α-neurexins in synapse formation, as also suggested by cell culture-based studies (Chih et al., 2006; Graf et al., 2004). However, the mild degree of structural alterations is in contrast to the dramatic consequences of α-neurexins deletion on survival and synaptic release (Missler et al., 2003; Zhang et al., 2005). Whereas α-neurexins clearly play an important role in synaptic function, their contribution to synaptogenesis in vivo seems to be less significant.

It should be noted that one α-neurexin gene is intact in double-knockout mutants, providing some degree of compensation for the deleted ones, because α-neurexins are likely to be functionally redundant (Zhang et al., 2005). Besides, we focused on the small group of surviving mice, which are probably less affected by the mutation, than the majority of animals, which die in the first few weeks of life. Finally β-neurexins are also preserved in α-neurexin knockouts and could partially overtake the synaptogenic function of α-neurexins, although protein levels of β-isoforms are not elevated in the mutant animals (Missler et al., 2003), and the expression patterns of α- and β-isoforms do not entirely overlap (Ullrich et al., 1995).

It remains possible that β-neurexins have a more prominent role in synaptogenesis than the α-isoforms, although the recently reported findings in knockout mice deficient in multiple neuroligins do not support this hypothesis. Neuroligins are believed to be the binding partners of β-neurexins that mediate their synaptogenic effects (Graf et al., 2004). Similar to α-neurexin mutants, neuroligin knockouts display a severe impairment of synaptic transmission, whereas the total synapse numbers are unchanged, with only a small shift in the ratio between the excitatory and the inhibitory contacts (Varoqueaux et al., 2006).

A reduction of neuropil has also been observed in the Sema 3A knockout mice (Behar et al., 1996) and in heterozygous reeler mice (Liu et al., 2001). Compared with the case in α-neurexin knockouts, neuropil hypoplasia is more severe in these mutants and is accompanied by changes in axonal pathfinding and dendritic orientation in the case of Sema3A knockout (Behar et al., 1996), or decreased spine densities in the reeler mutant (Liu et al., 2001). The absence of such defects in α-neurexin knockouts again confirms that α-neurexins are not necessary for the initial brain assembly but might participate in later stages of synapse development. The advancement of structural defects over time observed in the mutants suggests

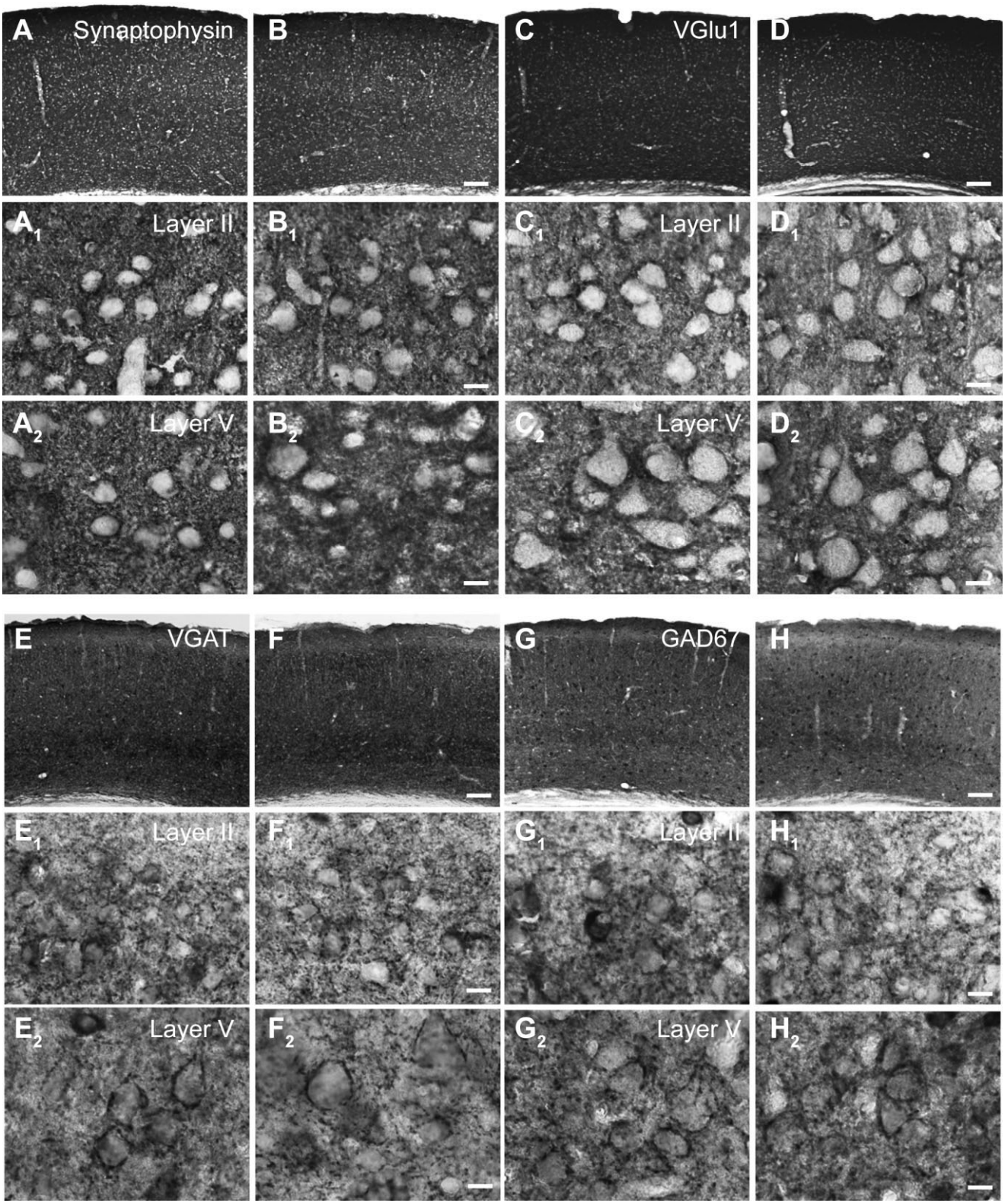

Fig. 5. Synaptic markers have a normal distribution pattern in the brains of α-neurexin double knockout mice. Brain sections from control (**A,C,E,G**) and α-neurexin double knockout mutant mice (**B,D,F,H**) were labeled with antibodies against pan-synaptic marker synaptophysin (A,B), exitatory synaptic marker VGlu1 (C,D), and markers of inhibitory synapses VGAT (E,F) and GAD 67 (G,H) and stained with DAB. For each of the markers, higher magnification images of cortical layer II (A1–H1) and layer V (A2–H2) are shown. Scale bars = 100 μm (A–H); 10 μm (A1–H1,A2–H2).

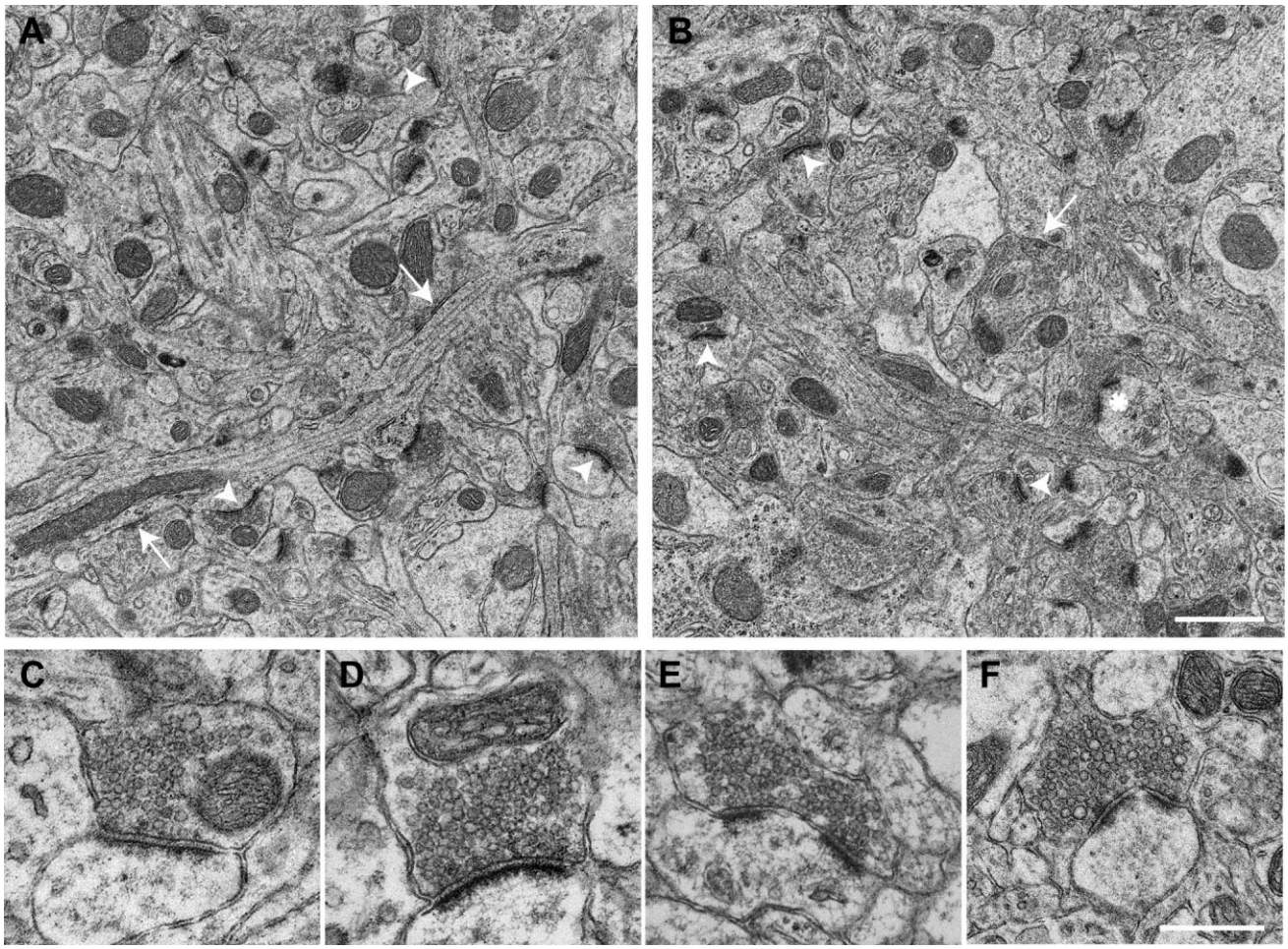

Fig. 6. Normal synapse ultrastructure in α-neurexin double knockout mice. **A,B:** Electron micrographs of the primary visual cortex neuropil in control (A) and double knockout (B) mice. Examples of type I (arrowheads) and type II (arrows) synapses are shown. Type I synapses can be distinguished by thicker postsynaptic densities. A perforated synapse, with two separate parts of the postsynaptic density apposed to one presynaptic terminal, is marked with an asterisk in B. **C,D:** Examples of type I synapses in control (C) and double knockout (D) animals. No differences can be observed in the synaptic ultrastructure. **E,F:** Examples of perforated synapses in control (E) and double knockout (F) mice. Scale bars = 1 μm in B (applies to A,B); 500 nm in F (applies to C–F).

that α-neurexins contribute to the long-term maintenance of synaptic connections.

Is there a more pronounced role for α-neurexins at inhibitory synapses?

Recent in vitro findings suggested that certain types of neurexins might be restricted to and have specialized functions at excitatory or inhibitory synapses. Thus α-neurexins exclusively induced inhibitory postsynaptic specializations in cultured neurons via their interaction with specific neuroligin isoforms (Chih et al., 2006).

In our in vivo study, synapse counts in all layers of the visual cortex revealed a significant reduction in the area density of type II (presumably inhibitory) synapses (Table 4), and immunohistochemical stainings with GABAergic markers appeared less intense in the double knockout mice (Fig. 5E–H). This finding extends previous observations in newborn α-neurexin triple knockouts (Missler et al., 2003). The change was less pronounced in adult DKO mice compared with newborn TKOs (30% vs. 50%), possibly reflecting the fact that one α-neurexin isoform is still preserved in the DKOs. There was no reduction in the number of GABAergic neurons in the cortex (Fig. 7), so the decrease in area density of type II synapses must be due to a reduction in the number of actual inhibitory contacts formed by each GABAergic neuron, suggesting a nonredundant function of α-neurexins in the formation and/or stabilization of inhibitory synapses. An important role of α-neurexins at inhibitory synapses is further supported by the greatly impaired inhibitory neurotransmission in α-neurexin knockout mice (Missler et al., 2003).

Although inhibitory synapses appear to be more severely affected by the deletion of α-neurexins, it seems unlikely that α-neurexins might be restricted to this type of synapses. A number of observations argue against exclusive localization and functions of neurexin isoforms with respect to neurotransmitter phenotype: 1) in situ hybridization demonstrated localization of α- and β-neurexins at both excitatory and inhibitory synaptic contacts (Ullrich et al., 1995); 2) the deletion of

TABLE 4. Synapse Densities and Synaptic Ultrastructure in the V1 Cortical Area of α-Neurexin Double Knockout and Control Mice[1]

	Genotype		
	SKO 2 (n = 3)	DKO (n = 3)	*P*
Synapse densites (1/1,000 μm²)[2]			
Type I synapses	131.1 ± 2.8	124.6 ± 5.6	n.s.
Axospinous synapses	65.0 ± 2.4	62.5 ± 4.2	n.s.
Perforated synapses	5.2 ± 1.0	7.3 ± 0.7	n.s.
Type II synapses	17.9 ± 0.3	12.6 ± 0.1	<0.001
Synaptic ultrastructure[3]			
Vesicle diameter	42.2 ± 0.6	41.8 ± 0.4	n.s.
Density of vesicles (1/μm²)	59.6 ± 7.6	55.6 ± 11.4	n.s.
Length of the active zone	345.2 ± 8.6	334.5 ± 4.	n.s.
Width of the synaptic cleft	15.1 ± 0.3	814.6 ± 0.5	n.s.
Distribution of synaptic vesicles[4]			
<40 nm	0.12 ± 0.01	0.13 ± 0.01	n.s.
40-100 nm	0.21 ± 0.01	0.23 ± 0.01	n.s.
>100 nm	0.67 ± 0.02	0.64 ± 0.02	n.s.

[1]Data are means ± SEM; *n* = number of animals used. Statistical analysis was via *t*-test (Prism software; GraphPad); n.s., not significant.
[2]In total 1,491 (SKO) and 1,397 (DKO) synapses were evaluated for the analysis of synapse densities.
[3]In total 110 (SKO) and 127 (DKO) type I synapses were evaluated for the analysis of synaptic ultrastructure. The size (average of shorter and longer diameters), area density, and distribution of synaptic vesicles; the length of the synaptic active zone; and the width of the synaptic cleft were determined on electron micrographs of the V1 cortical area taken at equal intervals (~50 μm) in layers I–VI, in DigitalMicrograph 3.4 software (Gatan Inc.).
[4]The distribution of vesicles in the synaptic terminal was analyzed by determining their relative frequency in three classes of shortest distances from the synaptic active zone.

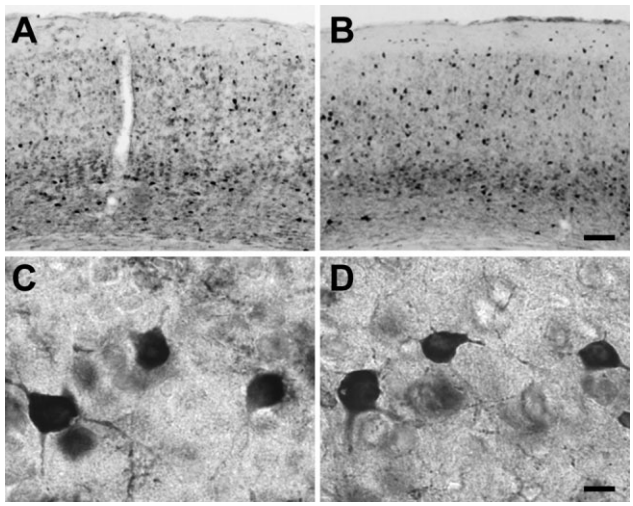

Fig. 7. The number of inhibitory neurons is not decreased in α-neurexin double knockout mice. **A,B:** Sections of the primary visual cortex of control (A) and double knockout (B) mice labelled with the inhibitory neuron marker GAD67. **C,D:** Examples of GAD-positive inhibitory interneurons in the primary visual cortex of control (C) and double knockout mice (D). Scale bars = 100 μm in A (applies to A,B); 10 μm in D (applies to C,D).

α-neurexins in mice causes dramatic defects of neurotransmitter release at both GABAergic and glutamatergic synapses (Missler et al., 2003); and 3) in a number of in vitro assays, manipulations of presumably unselective neurexin isoforms also produced stronger effects on inhibitory synapses. Thus, Graf et al. (2006) demonstrated a higher potency of neurexin 1β in inducing GABAegric, than glutaminergic synapses. Along this line, Levinson et al. (2005) showed a reduction of both excitatory and inhibitory miniature postsynaptic current (mEPSC and mIPSC) frequency, with mIPSCs being more severely affected, when soluble α-neurexin was used to block the transsynaptic neurexin–neuroligin interaction. These studies employed the splice insert-*lacking* isoform of β-neurexin, presumably not selective for synapse types. Similarly, Chih et al. (2005) described higher vulnerability of inhibitory synapse function to the disruption of neurexin–neuroligin binding by the RNAi knockdown of *all* neuroligins. Therefore, the fact that the density of inhibitory synapses is mildly affected in the knockouts, whereas that of excitatory synapses is not, might have to do with the properties of these synapses rather than with selective effects of neurexin isoforms. Inhibitory synapses might rely more heavily on neurexins for their structural integrity, because they dispose of fewer transsynaptic adhesion systems, which would be able to compensate for the absence of α-neurexins. Alternatively, they may be generally more sensitive to developmental disturbances (Rico et al., 2002), possibly because of their early onset of activity and their particular role in the establishment of neuronal networks (Ben-Ari, 2001).

The exclusive effects observed in vitro may critically depend on technical conditions such as the degree of overexpression (Levinson et al., 2005) and may not truly represent the physiological function of these molecules. The pending analysis of β-neurexin null mutants will be necessary to resolve the issue of specialized or overlapping functions of α- and β-neurexins.

Neurexins, brain structure, and synaptic activity

Unlike the pronounced reduction in inhibitory synapse numbers, the decrease in excitatory synapses observed in this study is rather small, appears postnatally, and is restricted to the terminal dendritic ramifications. It is therefore likely caused by elimination of neuronal connections rather than by a primary defect in synaptogenesis. Excitatory synaptic transmission in α-neurexin knockouts is already impaired at birth, whereas morphological changes of excitatory synapses appear later, so these changes may at least in part be activity dependent and caused by a chronic decrease in neurotransmitter secretion (Goda and Davis, 2003). The elimination of synapses may in turn lead to destabilization and retraction of terminal dendritic branches in the absence of local synaptic activity (Lohmann et al., 2002; Niell et al., 2004).

The influence of synaptic activity on brain structure has been investigated in several synaptic protein mutants, leading to some conflicting results. In a number of genetic mouse models, such as Munc13 (Augustin et al., 1999; Varoqueaux et al., 2002) or synaptotagmin 1 (Geppert et al., 1994) knockouts, normal brain structure and synaptogenesis have been reported in spite of an impairment or even a shutdown of neurotransmission. In contrast, electrically silent brains of Munc18-1 mutants, albeit normally assembled, start undergoing severe neurodegeneration before birth (Verhage et al., 2000) and show defects of synapse formation and maturation (Bouwman et al., 2004). Most of the mutants that have reduced neurotransmission die shortly after birth, precluding morphological analysis in older animals, whereas milder functional impairments in α-neurexin DKOs enabled us to study these mutants at an adult age. We show that subtle, but widespread, activity-dependent changes accumulate over time

in the knockout brains. Similarly, small structural alterations observed at the peripheral neuromuscular synapse of α-neurexin mutants were also proposed to be secondary to the impairment of neuromuscular transmission (Sons et al., 2006).

Impaired electrical activity is not the only possible explanation for synapse loss. The reduced stability of synapses might also result from impaired α-neurexin-mediated cell adhesion. In one of the in vitro studies, the splice variant of neuroligin that interacts with α-neurexins was much more potent in increasing the size of presynaptic boutons and postsynaptic spines than in inducing new contacts, suggesting a role for the α-neurexin–neuroligin pair in synapse maturation and expansion (Boucard et al., 2005). Furthermore, it has been shown by in vivo time-lapse imaging that bigger spines (and presumably synapses) are usually more stable and have longer lives (Holtmaat et al., 2005). The absence of α-neurexins may thus hinder synapse growth and stabilization. A similar destabilization of inhibitory synapses seems likely but would probably be difficult to detect because of the much more pronounced initial decrease in inhibitory synapse numbers. As an alternative explanation, the loss of a fraction of excitatory synapses might also represent a secondary compensatory reaction of neuronal networks to the reduction in inhibitory synapse numbers. As the inhibitory tone is lower in the adult knockouts (Mohiuddin Ahmad and Markus Missler, unpublished observations), excitatory inputs must be downscaled accordingly to maintain a normal level of neuronal activity and prevent excessive excitation.

The overall mild degree and late development of morphological changes in α-neurexin knockouts suggest that these molecules are largely dispensable for initial synapse formation but contribute to long-term stability of synapses. Further experiments will show whether this function of α-neurexins depends on their properties as cell-adhesion molecules or on their role as regulators of synaptic transmission.

ACKNOWLEDGMENTS

We thank Dr. D. Riedel for generous help with electron microscopy, Dr. C. Helmeke for advice on Golgi staining, Dr. M. Rickmann for the GFAP antibody, and S. Gerke and U. Kreher for excellent technical assistance.

LITERATURE CITED

Augustin I, Rosenmund C, Sudhof TC, Brose N. 1999. Munc13–1 is essential for fusion competence of glutamatergic synaptic vesicles. Nature 400:457–461.

Behar O, Golden JA, Mashimo H, Schoen FJ, Fishman MC. 1996. Semaphorin III is needed for normal patterning and growth of nerves, bones and heart. Nature 383:525–528.

Ben-Ari Y. 2001. Developing networks play a similar melody. Trends Neurosci 24:353–360.

Bernhardt R, Matus A. 1984. Light and electron microscopic studies of the distribution of microtubule-associated protein 2 in rat brain: a difference between dendritic and axonal cytoskeletons. J Comp Neurol 226: 203–221.

Biederer T, Sudhof TC. 2000. Mints as adaptors. Direct binding to neurexins and recruitment of munc18. J Biol Chem 275:39803–39806.

Biederer T, Sudhof TC. 2001. CASK and protein 4.1 support F-actin nucleation on neurexins. J Biol Chem 276:47869–47876.

Boucard AA, Chubykin AA, Comoletti D, Taylor P, Sudhof TC. 2005. A splice code for trans-synaptic cell adhesion mediated by binding of neuroligin 1 to alpha- and beta-neurexins. Neuron 48:229–236.

Bouwman J, Maia AS, Camoletto PG, Posthuma G, Roubos EW, Oorschot VM, Klumperman J, Verhage M. 2004. Quantification of synapse formation and maintenance in vivo in the absence of synaptic release. Neuroscience 126:115–126.

Butz S, Okamoto M, Sudhof TC. 1998. A tripartite protein complex with the potential to couple synaptic vesicle exocytosis to cell adhesion in brain. Cell 94:773–782.

Chaudhry FA, Reimer RJ, Bellocchio EE, Danbolt NC, Osen KK, Edwards RH, Storm-Mathisen J. 1998. The vesicular GABA transporter, VGAT, localizes to synaptic vesicles in sets of glycinergic as well as GABAergic neurons. J Neurosci 18:9733–9750.

Chih B, Engelman H, Scheiffele P. 2005. Control of excitatory and inhibitory synapse formation by neuroligins. Science 307:1324–1328.

Chih B, Gollan L, Scheiffele P. 2006. Alternative splicing controls selective trans-synaptic interactions of the neuroligin–neurexin complex. Neuron 51:171–178.

Cloutier JF, Sahay A, Chang EC, Tessier-Lavigne M, Dulac C, Kolodkin AL, Ginty DD. 2004. Differential requirements for semaphorin 3F and Slit-1 in axonal targeting, fasciculation, and segregation of olfactory sensory neuron projections. J Neurosci 24:9087–9096.

Cremer H, Lange R, Christoph A, Plomann M, Vopper G, Roes J, Brown R, Baldwin S, Kraemer P, Scheff S, et al. 1994. Inactivation of the N-CAM gene in mice results in size reduction of the olfactory bulb and deficits in spatial learning. Nature 367:455–459.

Dean C, Scholl FG, Choih J, DeMaria S, Berger J, Isacoff E, Scheiffele P. 2003. Neurexin mediates the assembly of presynaptic terminals. Nat Neurosci 6:708–716.

Dudanova I, Sedej S, Ahmad M, Masius H, Sargsyan V, Zhang W, Riedel D, Angenstein F, Schild D, Rupnik M, Missler M. 2006. Important contribution of alpha-neurexins to Ca^{2+}-triggered exocytosis of secretory granules. J Neurosci 26:10599–10613.

Esclapez M, Tillakaratne NJ, Kaufman DL, Tobin AJ, Houser CR. 1994. Comparative localization of two forms of glutamic acid decarboxylase and their mRNAs in rat brain supports the concept of functional differences between the forms. J Neurosci 14:1834–1855.

Fujiyama F, Furuta T, Kaneko T. 2001. Immunocytochemical localization of candidates for vesicular glutamate transporters in the rat cerebral cortex. J Comp Neurol 435:379–387.

Geppert M, Goda Y, Hammer RE, Li C, Rosahl TW, Stevens CF, Sudhof TC. 1994. Synaptotagmin I: a major Ca^{2+} sensor for transmitter release at a central synapse. Cell 79:717–727.

Glaser EM, Van der Loos H. 1981. Analysis of thick brain sections by obverse-reverse computer microscopy: application of a new, high clarity Golgi-Nissl stain. J Neurosci Methods 4:117–125.

Goda Y, Davis GW. 2003. Mechanisms of synapse assembly and disassembly. Neuron 40:243–264.

Graf ER, Zhang X, Jin SX, Linhoff MW, Craig AM. 2004. Neurexins induce differentiation of GABA and glutamate postsynaptic specializations via neuroligins. Cell 119:1013–1026.

Graf ER, Kang Y, Hauner AM, Craig AM. 2006. Structure function and splice site analysis of the synaptogenic activity of the neurexin-1 beta LNS domain. J Neurosci 26:4256–4265.

Hata Y, Butz S, Sudhof TC. 1996. CASK: a novel dlg/PSD95 homolog with an N-terminal calmodulin-dependent protein kinase domain identified by interaction with neurexins. J Neurosci 16:2488–2494.

Holtmaat AJ, Trachtenberg JT, Wilbrecht L, Shepherd GM, Zhang X, Knott GW, Svoboda K. 2005. Transient and persistent dendritic spines in the neocortex in vivo. Neuron 45:279–291.

Ichtchenko K, Hata Y, Nguyen T, Ullrich B, Missler M, Moomaw C, Sudhof TC. 1995. Neuroligin 1: a splice site-specific ligand for beta-neurexins. Cell 81:435–443.

Kaufmann WE, Taylor CV, Lishaa NA. 1997. Immunoblotting patterns of cytoskeletal dendritic protein expression in human neocortex. Mol Chem Neuropathol 31:235–244.

Knaus P, Betz H. 1990. Mapping of a dominant immunogenic region of synaptophysin, a major membrane protein of synaptic vesicles. FEBS Lett 261:358–360.

Levinson JN, Chery N, Huang K, Wong TP, Gerrow K, Kang R, Prange O, Wang YT, El-Husseini A. 2005. Neuroligins mediate excitatory and inhibitory synapse formation: involvement of PSD-95 and neurexin-1beta in neuroligin-induced synaptic specificity. J Biol Chem 280: 17312–17319.

Liu WS, Pesold C, Rodriguez MA, Carboni G, Auta J, Lacor P, Larson J,

Condie BG, Guidotti A, Costa E. 2001. Down-regulation of dendritic spine and glutamic acid decarboxylase 67 expressions in the reelin haploinsufficient heterozygous reeler mouse. Proc Natl Acad Sci U S A 98:3477–3482.

Lohmann C, Myhr KL, Wong RO. 2002. Transmitter-evoked local calcium release stabilizes developing dendrites. Nature 418:177–181.

Missler M, Sudhof TC. 1998. Neurexins: three genes and 1001 products. Trends Genet 14:20–26.

Missler M, Wolff A, Merker HJ, Wolff JR. 1993. Pre- and postnatal development of the primary visual cortex of the common marmoset. II. Formation, remodelling, and elimination of synapses as overlapping processes. J Comp Neurol 333:53–67.

Missler M, Fernandez-Chacon R, Sudhof TC. 1998. The making of neurexins. J Neurochem 71:1339–1347.

Missler M, Zhang W, Rohlmann A, Kattenstroth G, Hammer RE, Gottmann K, Sudhof TC. 2003. Alpha-neurexins couple Ca^{2+} channels to synaptic vesicle exocytosis. Nature 423:939–948.

Mombaerts P, Wang F, Dulac C, Chao SK, Nemes A, Mendelsohn M, Edmondson J, Axel R. 1996. Visualizing an olfactory sensory map. Cell 87:675–686.

Montag-Sallaz M, Schachner M, Montag D. 2002. Misguided axonal projections, neural cell adhesion molecule 180 mRNA upregulation, and altered behavior in mice deficient for the close homolog of L1. Mol Cell Biol 22:7967–7981.

Nguyen T, Sudhof TC. 1997. Binding properties of neuroligin 1 and neurexin 1beta reveal function as heterophilic cell adhesion molecules. J Biol Chem 272:26032–26039.

Niell CM, Meyer MP, Smith SJ. 2004. In vivo imaging of synapse formation on a growing dendritic arbor. Nat Neurosci 7:254–260.

Pennypacker K, Fischer I, Levitt P. 1991. Early in vitro genesis and differentiation of axons and dendrites by hippocampal neurons analyzed quantitatively with neurofilament-H and microtubule-associated protein 2 antibodies. Exp Neurol 111:25–35.

Piechotta K, Dudanova I, Missler M. 2006. The resilient synapse: insights from genetic interference of synaptic cell adhesion molecules. Cell Tissue Res (in press).

Ramakers GJ, Verhaagen J, Oestreicher AB, Margolis FL, van Bergen en Henegouwen PM, Gispen WH. 1992. Immunolocalization of B-50 (GAP-43) in the mouse olfactory bulb: predominant presence in preterminal axons. J Neurocytol 21:853–869.

Rico B, Xu B, Reichardt LF. 2002. TrkB receptor signaling is required for establishment of GABAergic synapses in the cerebellum. Nat Neurosci 5:225–233.

Rowen L, Young J, Birditt B, Kaur A, Madan A, Philipps DL, Qin S, Minx P, Wilson RK, Hood L, Graveley BR. 2002. Analysis of the human neurexin genes: alternative splicing and the generation of protein diversity. Genomics 79:587–597.

Sara Y, Biederer T, Atasoy D, Chubykin A, Mozhayeva MG, Sudhof TC, Kavalali ET. 2005. Selective capability of SynCAM and neuroligin for functional synapse assembly. J Neurosci 25:260–270.

Scheiffele P, Fan J, Choih J, Fetter R, Serafini T. 2000. Neuroligin expressed in nonneuronal cells triggers presynaptic development in contacting axons. Cell 101:657–669.

Schwarting GA, Kostek C, Ahmad N, Dibble C, Pays L, Puschel AW. 2000. Semaphorin 3A is required for guidance of olfactory axons in mice. J Neurosci 20:7691–7697.

Schwarting GA, Raitcheva D, Crandall JE, Burkhardt C, Puschel AW. 2004. Semaphorin 3A-mediated axon guidance regulates convergence and targeting of P2 odorant receptor axons. Eur J Neurosci 19:1800–1810.

Song JY, Ichtchenko K, Sudhof TC, Brose N. 1999. Neuroligin 1 is a postsynaptic cell-adhesion molecule of excitatory synapses. Proc Natl Acad Sci U S A 96:1100–1105.

Sons MS, Busche N, Strenzke N, Moser T, Ernsberger U, Mooren FC, Zhang W, Ahmad M, Steffens H, Schomburg ED, Plomp JJ, Missler M. 2006. alpha-Neurexins are required for efficient transmitter release and synaptic homeostasis at the mouse neuromuscular junction. Neuroscience 138:433–446.

Sternberger LA, Sternberger NH. 1983. Monoclonal antibodies distinguish phosphorylated and nonphosphorylated forms of neurofilaments in situ. Proc Natl Acad Sci U S A 80:6126–6130.

Sugita S, Saito F, Tang J, Satz J, Campbell K, Sudhof TC. 2001. A stoichiometric complex of neurexins and dystroglycan in brain. J Cell Biol 154:435–445.

Tabuchi K, Sudhof TC. 2002. Structure and evolution of neurexin genes: insight into the mechanism of alternative splicing. Genomics 79:849–859.

Takamori S, Riedel D, Jahn R. 2000. Immunoisolation of GABA-specific synaptic vesicles defines a functionally distinct subset of synaptic vesicles. J Neurosci 20:4904–4911.

Taniguchi M, Nagao H, Takahashi YK, Yamaguchi M, Mitsui S, Yagi T, Mori K, Shimizu T. 2003. Distorted odor maps in the olfactory bulb of semaphorin 3A-deficient mice. J Neurosci 23:1390–1397.

Tomasiewicz H, Ono K, Yee D, Thompson C, Goridis C, Rutishauser U, Magnuson T. 1993. Genetic deletion of a neural cell adhesion molecule variant (N-CAM-180) produces distinct defects in the central nervous system. Neuron 11:1163–1174.

Ullrich B, Ushkaryov YA, Sudhof TC. 1995. Cartography of neurexins: more than 1000 isoforms generated by alternative splicing and expressed in distinct subsets of neurons. Neuron 14:497–507.

Ushkaryov YA, Petrenko AG, Geppert M, Sudhof TC. 1992. Neurexins: synaptic cell surface proteins related to the alpha-latrotoxin receptor and laminin. Science 257:50–56.

Ushkaryov YA, Hata Y, Ichtchenko K, Moomaw C, Afendis S, Slaughter CA, Sudhof TC. 1994. Conserved domain structure of beta-neurexins. Unusual cleaved signal sequences in receptor-like neuronal cell-surface proteins. J Biol Chem 269:11987–11992.

Varoqueaux F, Sigler A, Rhee JS, Brose N, Enk C, Reim K, Rosenmund C. 2002. Total arrest of spontaneous and evoked synaptic transmission but normal synaptogenesis in the absence of Munc13-mediated vesicle priming. Proc Natl Acad Sci U S A 99:9037–9042.

Varoqueaux F, Aramuni G, Rawson RL, Mohrmann R, Missler M, Gottmann K, Zhang W, Sudhof TC, Brose N. 2006. Neuroligins determine synapse maturation and function. Neuron 51:741–754.

Verhage M, Maia AS, Plomp JJ, Brussaard AB, Heeroma JH, Vermeer H, Toonen RF, Hammer RE, van den Berg TK, Missler M, Geuze HJ, Sudhof TC. 2000. Synaptic assembly of the brain in the absence of neurotransmitter secretion. Science 287:864–869.

Waites CL, Craig AM, Garner CC. 2005. Mechanisms of vertebrate synaptogenesis. Annu Rev Neurosci 28:251–274.

Walz A, Rodriguez I, Mombaerts P. 2002. Aberrant sensory innervation of the olfactory bulb in neuropilin-2 mutant mice. J Neurosci 22:4025–4035.

Wiedenmann B, Franke WW. 1985. Identification and localization of synaptophysin, an integral membrane glycoprotein of Mr 38,000 characteristic of presynaptic vesicles. Cell 41:1017–1028.

Zhang W, Rohlmann A, Sargsyan V, Aramuni G, Hammer RE, Sudhof TC, Missler M. 2005. Extracellular domains of alpha-neurexins participate in regulating synaptic transmission by selectively affecting N- and P/Q-type Ca^{2+} channels. J Neurosci 25:4330–4342.

Appendix 2

Cellular/Molecular

Important Contribution of α-Neurexins to Ca^{2+}-Triggered Exocytosis of Secretory Granules

Irina Dudanova,[1]* Simon Sedej,[2]* Mohiuddin Ahmad,[1]* Henriette Masius,[1] Vardanush Sargsyan,[1] Weiqi Zhang,[1] Dietmar Riedel,[3] Frank Angenstein,[4] Detlev Schild,[1,5] Marjan Rupnik,[2] and Markus Missler[1,6]

[1]Center for Physiology and Pathophysiology, Georg-August University, Göttingen D-37073, Germany, [2]European Neuroscience Institute Göttingen, Göttingen D-37073, Germany, [3]Department of Neurobiology, Max Planck Institute for Biophysical Chemistry, Göttingen D-37077, Germany, [4]Leibniz Institute for Neurobiology, Magdeburg D-39118, Germany, [5]German Research Foundation-Research Center of Molecular Physiology of Brain, Göttingen D-37073, Germany, and [6]Institute of Anatomy, Westfälische Wilhelms-University, Münster D-48149, Germany

α-Neurexins constitute a family of neuronal cell surface molecules that are essential for efficient neurotransmission, because mice lacking two or all three α-neurexin genes show a severe reduction of synaptic release. Although analyses of α-neurexin knock-outs and transgenic rescue animals suggested an involvement of voltage-dependent Ca^{2+} channels, it remained unclear whether α-neurexins have a general role in Ca^{2+}-dependent exocytosis and how they may affect Ca^{2+} channels. Here we show by membrane capacitance measurements from melanotrophs in acute pituitary gland slices that release from endocrine cells is diminished by >50% in adult α-neurexin double knock-out and newborn triple knock-out mice. There is a reduction of the cell volume in mutant melanotrophs; however, no ultrastructural changes in size or intracellular distribution of the secretory granules were observed. Recordings of Ca^{2+} currents from melanotrophs, transfected human embryonic kidney cells, and brainstem neurons reveal that α-neurexins do not affect the activation or inactivation properties of Ca^{2+} channels directly but may be responsible for coupling them to release-ready vesicles and metabotropic receptors. Our data support a general and essential role for α-neurexins in Ca^{2+}-triggered exocytosis that is similarly important for secretion from neurons and endocrine cells.

Key words: **neuroendocrine cells; exocytosis; neurohormones; pituitary gland; melanotrophs; cell adhesion molecules; Ca^{2+} channels**

Introduction

Understanding the mechanisms of Ca^{2+}-triggered exocytosis has emerged as a central problem in neurobiology, because it provides insights into the foundations of our cognitive abilities as well as the regulation of endocrine functions. Secretory activity of neurons and endocrine cells shares many characteristics, including the machinery that mediates the steep $[Ca^{2+}]$ dependence of release and stimulus–secretion coupling (Rettig and Neher, 2002; Sudhof, 2004). We previously showed that the presynaptic transmembrane proteins neurexins (Missler et al., 1998a) perform an essential role in synaptic transmission. Knock-out mice that lack two or all three α-neurexins displayed a severe reduction in neurotransmitter release, causing premature death of all triple knock-out and most of the double knock-out animals (Missler et al., 2003).

All three neurexin genes include independent promoters for α- and β-neurexins (Rowen et al., 2002; Tabuchi and Sudhof, 2002). α-Neurexins contain more extracellular sequences than β-neurexins, but they share with β-neurexins the C-terminal extracellular domain, transmembrane region, and intracellular tail (Missler and Sudhof, 1998). Although biochemistry revealed shared intracellular partners for α- and β-neurexins (Hata et al., 1996; Butz et al., 1998; Biederer and Sudhof, 2000, 2001), their mostly distinct extracellular interactions (Ichtchenko et al., 1995; Missler et al., 1998b; Sugita et al., 2001; Boucard et al., 2005) are likely responsible for their different proposed roles at synapses (Missler et al., 2003; Graf et al., 2004).

As an explanation for the inefficient exocytosis in α-neurexin-deficient mice, we have suggested previously that α-neurexins regulate the function of voltage-dependent Ca^{2+} channels (VDCCs), because specific Ca^{2+} channel inhibitors such as ω-conotoxin and agatoxin were less efficient in blocking synaptic transmission between knock-out neurons when compared with control cells and because peak Ca^{2+} current amplitudes were decreased in mutant brainstem neurons (Missler et al., 2003; Zhang et al., 2005). Transgenic rescue experiments, furthermore,

Received May 4, 2006; revised Sept. 1, 2006; accepted Sept. 5, 2006.

This work was supported by German Research Foundation (DFG) Grants Mi479/3-1 and SFB 406 (to M.M. and W.Z.) and by the DFG-Research Center for Molecular Physiology of the Brain (to D.S.). The European Neuroscience Institute Göttingen is funded jointly by the University of Göttingen Medical School, the Max Planck Society, and Schering AG (to M.R.). I.D. and M.A. were recipients of a Georg Christoph Lichtenberg Stipend (Ministry for Science and Culture of Lower Saxony, Germany). We thank Gerald W. Zamponi (University of Calgary, Alberta, Canada) for generous support in establishing Ca^{2+} current measurements from heterologous cells; T. Snutch (University of British Columbia, British Columbia, Canada) for rat cDNA clones of α1B, β1b, and α2δ; Dr. Parlow (National Hormone and Peptide Program, National Institute of Diabetes and Digestive and Kidney Diseases, Bethesda, MD) for providing antibodies against pituitary hormones; and S. Gerke for excellent technical assistance.

*I.D., S.S., and M.A. contributed equally to this work.

Correspondence should be addressed to Dr. Markus Missler, Institute of Anatomy, Department of Anatomy and Molecular Neuroscience, Westfälische Wilhelms-University, Vesaliusweg 2-4, Münster D-48149, Germany. E-mail: mmissle1@gwdg.de.

S. Sedej and M. Rupnik's present address: Institute of Physiology, University of Maribor, Ljubljanska c.5, SI-2000 Maribor, Slovenia.

DOI:10.1523/JNEUROSCI.1913-06.2006

 0270-6474/06/2610599-15$15.00/0

showed that the effect on neurotransmission is specific for α-, but not β-neurexins, and mostly involves N-type ($Ca_V2.2$) and P/Q-type ($Ca_V2.1$) Ca^{2+} channels (Zhang et al., 2005). Although these studies demonstrated an essential role for α-neurexins in synaptic function, important open questions remained. Are α-neurexins also required for other forms of Ca^{2+}-dependent release such as exocytosis of secretory granules from endocrine cells? If high VDCCs are involved in the process, which aspect of their function is affected by α-neurexins?

Here we addressed these issues by studying secretory granule release from endocrine cells of α-neurexin knock-out mice and by analyzing the effects of α-neurexins on Ca^{2+} currents in melanotrophs, brainstem neurons, and transfected cell lines. For our purpose melanotrophs of the pituitary gland, when tested in an acute slice preparation, are an excellent model of endocrine exocytosis, because release from these cells is coupled tightly to several Ca^{2+} channel subtypes (Mansvelder and Kits, 2000; Sedej et al., 2004), resembling many central synapses. We found that α-neurexins play an important role in secretory granule release and that the effect of α-neurexins on Ca^{2+} channels may involve coupling the channels to release-ready vesicles rather than modulating their activity.

Materials and Methods

Mice. Knock-out mice lacking one, two, or all three α-neurexin isoforms were generated and genotyped as described previously (Missler et al., 2003). Mice were housed under a 12 h light/dark regimen with access to food and water *ad libitum*. Animal procedures were performed according to German laws and ethical guidelines set by the University of Göttingen. Experiments were performed with newborn triple knock-outs lacking neurexins 1α and 2α and 3α (TKO) and newborn and adult double knock-outs deficient for either neurexins 1α and 2α (DKO1/2) or neurexins 2α and 3α (DKO2/3). Littermate single knock-out mice deficient only for neurexin 2α (SKO2) and a wild-type (WT) line of the same genetic background served as controls, as described before (Missler et al., 2003; Zhang et al., 2005).

Reverse transcriptase-PCR. Total RNA was isolated with RNAzol B (WAK-Chemie, Steinbach, Germany) from brains and pituitary glands of wild-type mice. Pituitary glands from six to eight animals were pooled to obtain enough material for RNA isolation. The RNA was reverse-transcribed with the GeneAmp Gold RNA PCR Core Kit (Applied Biosystems, Foster City, CA), using Oligo-dT primer. The following primer pairs specific for neurexin (Nrxn) isoforms were used: Nrxn1α, 5′-CCACAACGGGCTACACGCAAGAAG-3′ (MM04–38) versus CAGGATGAGGCCATTTGGCTCCG (MM04–39); Nrxn2α, CTACCTTCTGCTGGACATGGGCTCC (MM04–40) versus CAGAAAGGAGCAACGCCCACAGCC (MM04–41); Nrxn3α, GCACCATCAAAGTGAAGGCCACTC (MM04–42) versus CTGCTTGGCGCTCATGCGTGAAC (MM04–43); Nrxn1β, CTGATCTGGATAGTCCCGCTCACC (MM04–44) versus GTGCAGCTCCAGGTAGTCACCCAG (MM04–45); Nrxn2β, GTCTCGTCCAGCCTCAGCACCACC (MM04–46) versus CTCACGATGGCGTTGGGCTCATC (MM04–47); Nrxn3β, CTCCGGGATCTCACTCTCAGCAGG (MM04–48) versus GTGAAGCTGGAGGAAGTCGCCAAG (MM04–49); synaptotagmin 1, GCTGCCCCTATCACCACTGTTG (MM04–50) versus GGGCTCCTCCTTTTCTTCTCCACT (MM04–51). The primers were placed in exons 8 and 9 for α-neurexins and in the β-specific exon and exon 18 (Nrxn1β) or 17 (Nrxn2β and Nrxn3β) for β-neurexins (Tabuchi and Sudhof, 2002). To quantitate the expression levels with real-time PCR, we used different pairs of primers that were located closer together: Nrxn1α, 5′-CCACAACGGGCTACACGCAAGAAG-3′ (MM04–38) versus GCAAGTCGCGATAATTCCAGCCT (MM05–11); Nrxn2α, CTACCTTCTGCTGGACATGGGCTCC (MM04–40) versus GCGTGCTGCGGCTGTTCACA (MM05–12); Nrxn3α, GCACCATCAAAGTGAAGGCCACTC (MM04–42) versus GCCCAGATACATGTCCCCCTCCA (MM05–13); Nrxn1β, CCATGGCAGCAGCAAGCATCATTCA (MM05–14) versus CGTGTACTGGGGCGGTCATTGGGA (MM05–15); Nrxn2β, GTCTCGTCCAGCCTCAGCACCACC (MM04–46) versus CGTGTCATGGGCCGGTCATTGGGA (MM05–16); Nrxn3β, CTCCGGGATCTCACTCTCAGCAGG (MM04–48) versus GATGAGGCCACCGCTTTTCCCAA (MM05–17); β-actin, CGTGCGTGACATCAAAGAGAAGCTG (MM05–03) versus GGATGCCACAGGATTCCATACCCAAG (MM05–04). Quantitative PCR was performed by using SYBR Green PCR Master Mix (Applied Biosystems) in an ABI Prism 7000 Sequence Detection System (Applied Biosystems), with all reactions performed in duplicate. Signals were analyzed by ABI Prism Sequence Detection software (Applied Biosystems), and the $\Delta\Delta C_t$ method was used for relative quantification of neurexin transcripts. Standard curves for all of the isoform-specific reactions were generated with serial fivefold dilutions of cDNA in triplicate. DNA melting curves were generated after each experiment to confirm the specificity of amplification.

Histology. Deeply anesthetized mice were perfused transcardially with PBS, followed by 4% paraformaldehyde in 0.1 M phosphate buffer. Pituitary glands were dissected, postfixed in 4% paraformaldehyde for 2 h, and cryoprotected with 25% sucrose in 0.1 M phosphate buffer overnight. For morphometric analysis 25 μm cryosections were thaw-mounted on poly-L-lysine-coated slides and stained with hematoxylin and eosin. For immunofluorescence 12 μm cryosections were permeabilized with 0.3% Triton X-100 in PBS and incubated in blocking solution (5% normal goat serum in PBS) for 1–2 h at room temperature. Primary antibodies were applied overnight at 4°C: anti-growth hormone, 1:30,000; adrenocorticotropic hormone, 1:20,000; follicle-stimulating hormone, 1:1000; luteinizing hormone β, 1:30,000; thyroid-stimulating hormone β, 1:30,000; prolactin, 1:20,000 (all from Dr. Parlow, National Hormone and Peptide Program, National Institute of Diabetes and Digestive and Kidney Diseases, Bethesda, MD); α-melanocyte-stimulating hormone (α-MSH), 1:500 (Peninsula Laboratories, Belmont, CA); pro-opiomelanocortin, 1:500 (Phoenix Pharmaceuticals, Belmont, CA); β-endorphin, 1:500 (Sigma, St. Louis, MO); vasopressin, 1:500 (Chemicon, Temecula, CA); and oxytocin, 1:500 (Chemicon). Secondary antibodies were goat anti-rabbit or goat anti-mouse Alexa 546 (Invitrogen, Carlsbad, CA) applied at 1:500 for 45 min. The sections were examined at an Axioscope 2 epifluorescent microscope, and images were captured with the AxioCam HRc digital camera (Zeiss, Oberkochen, Germany). The area of the anterior and posterior lobes and the thickness of the intermediate lobe were measured on corresponding frontal sections with AxioVision software (Zeiss). Overviews of the glands were composed of four to eight individual images, using Adobe Photoshop SC (Adobe Systems, Mountain View, CA).

Electron microscopy. Pituitary glands were dissected and immersed immediately in 2% glutaraldehyde in 0.1 M cacodylate buffer, pH 7.4. After overnight fixation at 4°C the samples were fixed additionally with 1% OsO_4 for 1 h at room temperature and were preembedding-stained with uranyl acetate. After dehydration with a consecutive series of ethanol and propylene oxide the samples were embedded in Agar 100 resin. The intermediate lobe was identified on toluidine blue-stained semithin sections (700 nm). Ultrathin sections (60 nm) were counterstained with uranyl acetate for 10 min and lead citrate for 2 min and then examined at a Philips CM 120 electron microscope (Philips, Eindhoven, The Netherlands). Images of melanotrophs were taken randomly with a 2048 × 2048 Tietz TemCam 224A camera (Tietz Video and Image Processing Systems, Gauting, Germany) at 8400× magnification. Measurements were made with DigitalMicrograph 3.4 software (Gatan, Munich, Germany). Only granules with a clearly visible membrane were included in the analysis (~400–600 granules on 25 different images for each animal).

Pituitary gland physiology. Pituitary glands were removed carefully from the skull and rinsed with ice-cold external solution one composed of the following (in mM): 125 NaCl, 2.5 KCl, 1.25 NaH_2PO_4, 2 Na-pyruvate, 3 myo-inositol, 0.5 ascorbic acid, 10 glucose, 26 $NaHCO_3$, 3 $MgCl_2$, 0.1 $CaCl_2$, 6 lactic acid. Then the glands were embedded in 2.5% low-melting agarose (Seaplaque GTG-agarose, BMA, Walkersville, MD), glued onto the sample plate of a vibrotome VT1000S (Leica, Nussloch, Germany), and sectioned in ice-cold external solution two composed of the following (in mM): 2.5 KCl, 1.25 NaH_2PO_4, 2 Na-pyruvate, 3 myo-inositol, 0.5 ascorbic acid, 250 sucrose, 10 glucose, 26 $NaHCO_3$, 3 $MgCl_2$, 0.1 $CaCl_2$, 6 lactic acid. Fresh 80 μm slices then were transferred to an incubation beaker containing oxygenated external solution one and kept

at 32°C for up to 8 h. Changes in cell membrane capacitance (ΔC_m) and Ca^{2+} currents were measured in single melanotrophs within intact clusters of the intermediate lobe, using the conventional whole-cell patch-clamp configuration essentially as described (Sedej et al., 2004). During measurements the slice was perfused continuously (1–2 ml/min) with external solution three composed of the following (in mM): 125 NaCl, 2.5 KCl, 1.25 NaH_2PO_4, 2 Na-pyruvate, 3 myo-inositol, 0.5 ascorbic acid, 10 glucose, 26 $NaHCO_3$, 1 $MgCl_2$, 2 $CaCl_2$, 6 lactic acid. The osmolality of the extracellular solution was 300 ± 10 mOsm/kg, except for the experiments with 500 mM hypertonic sucrose, and the solution was bubbled continuously with 95% O_2/5% CO_2 to keep the pH stable at 7.3. Patch pipettes were filled with intracellular solution as follows (in mM): 140 CsCl, 10 HEPES, 2 $MgCl_2$, 20 TEA-Cl, 2 Na_2ATP, and 0.05 EGTA. Whole-cell currents and capacitance changes were recorded at 30–32°C, measured with a lock-in patch-clamp amplifier (SWAM IIC, Celica, Ljubljana, Slovenia), low-pass filtered (3 kHz, –3 dB), and stored on a standard PC. The cells were voltage clamped at –80 mV, and Ca^{2+} currents were leak corrected. For pulse generation, data acquisition, and basic analysis we used WinWCP version 3.3.9. software from J. Dempster (Strathclyde University, Glasgow, UK). High-resolution capacitance measurements (in the fF range) were made by using the compensated technique as described previously (Sedej et al., 2004, 2005; Turner et al., 2005), using a sinusoidal voltage (1600 Hz; 10 mV peak-to-peak). To determine ΔC_m values, we first averaged membrane capacitance over the 30 ms preceding the depolarization to obtain a baseline value that was subtracted from the value estimated after the depolarization, averaged over a 40 ms window. The first 30 ms after the depolarization were excluded from the C_m measurement to avoid contamination by nonsecretory capacitative transients related to gating charge movement (Horrigan and Bookman, 1994). All chemicals were obtained from Sigma, unless otherwise stated. Signal processing and curve fitting were done by using Sigmaplot (SPSS, Chicago, IL) and MatLab (MathWorks, Natick, MA). Differences between samples were tested by using Student's paired *t* test and one-way ANOVA (SigmaSTAT, SPSS).

Transfected heterologous cells. A stable human embryonic kidney 293 (HEK293) cell line expressing three $Ca_V2.2$ calcium channel subunits was generated by using the Flp-In system (Invitrogen), following the manufacturer's suggestions (for a more detailed description, see supplemental text, available at www.jneurosci.org as supplemental material). Correct expression and targeting of all subunits that were introduced (hemagglutinin-tagged α1B, β3, and $\alpha2\delta$) were verified by immunoblots and immunohistochemistry (supplemental Fig. 6, available at www.jneurosci.org as supplemental material), using commercially available peptide antibodies (Chemicon and Alamone Labs, Jerusalem, Israel). HEK293_$Ca_V2.2$ cells were grown at 37°C in 5% CO_2 in DMEM supplemented with 10% fetal bovine serum, 2 mM L-glutamine, 100 μg/ml hygromycin B, and 100 μg/ml penicillin–streptomycin. Cells stably expressing Ca^{2+} channels then were transiently transfected with 4 μg of each plasmid containing full-length α-neurexin joined to a green fluorescent protein (GFP) tag via an internal ribosome entry site (IRES) (pCMVNrxn1α_IRESGFP) alone or in combination with expression vectors for calcium/calmodulin-dependent serine protein kinase (CASK) and munc18-interacting 1 (Mint1) [cytomegalovirus (pCMV)-CASK, pCMVMint1; both courtesy of T. C. Sudhof, Dallas, TX], using the calcium phosphate method (MBS mammalian transfection kit, Stratagene, La Jolla, CA). After 24 h the cells were trypsinized briefly and plated onto 16 mm glass coverslips.

Patch-clamp experiments were done on the second and third days after plating in a custom-made chamber with an external bath solution composed of the following (in mM): 140 NaCl, 10 $BaCl_2$, 1 $MgCl_2$, 10 HEPES, 10 glucose, pH 7.4 (312 mOsm/kg osmolality) at room temperature. Patch pipettes (borosilicate glass, 1.8 mm outer diameter; Hilgenberg, Malsfeld, Germany) were pulled by a two-stage electrode puller (Narishige, Tokyo, Japan) and fire polished; they showed resistances of 3–5 MΩ. The internal pipette solution contained the following (in mM): 125 Cs-methane sulfonate, 20 TEA-Cl, 5 EGTA, 2 $MgCl_2$, 10 HEPES, 4 Na_2-ATP, 0.5 Na-GTP, pH 7.4 (280 mOsm/ kg osmolality). Aliquots of pipette solution were stored at −80°C and kept on ice after thawing. Whole-cell Ca^{2+}current recordings were performed with an EPC7 patch-clamp amplifier (List, Darmstadt, Germany). The signals were filtered with a built-in Bessel filter at 3 kHz, digitized at 10 kHz by a custom-built analog-to-digital converter, and stored on a hard disc of the computer with an acquisition and evaluation program written in C. Cells were held at −80 mV in the whole-cell configuration. Leak currents and whole-cell membrane capacitance were determined by applying 50 ms pulses to −100 mV. Here whole-cell capacitance (C_m) was calculated by integrating the area under the whole-cell capacitance transient current (charge transfer, Q) divided by the voltage of the pulse (V), i.e., $C_m = Q/V$. Leak currents were subtracted off-line. Current–voltage (*I–V*) relationships were obtained by 20 ms voltage pulses from a holding potential of −80 to +50 mV in 10 mV increments. Currents were measured 15 ms after the onset of the test pulse as an average over 5 ms. *I–V* traces from individual cells were fit with a modified Boltzmann equation as follows: $I = G_{max}(V - V_{rev})/(1 + \exp[-(V - V_{1/2\ act})/k_{act}])$, where G_{max} is the maximum slope conductance, V_{rev} is the reversal potential, $V_{1/2\ act}$ is the half-activation potential, and k_{act} is the slope factor. Current densities were calculated as currents normalized to whole-cell capacitance. Steady-state inactivation properties were measured by evoking currents with a 20 ms test pulse to +10 mV after 2 s voltage displacement (prepulse) from –120 to +10 mV in 10 mV increments. Amplitudes of currents evoked by the test pulses were normalized to the maximum currents that were elicited and plotted against the prepulse potential. The data from individual cells were fit with a Boltzmann equation as follows: $I_{norm} = A1 + (A2 - A1)/(1 + \exp[(V - V_{1/2\ inact})/k_{inact}])$, where *A1* and *A2* are the noninactivating and inactivating fractions, respectively, $V_{1/2\ inact}$ is the half-inactivation potential, and k_{inact} is the slope factor. Initial analysis (measurements of current, leak resistance, and whole-cell capacitance) was done under LINUX, using a program written in C. Plotting and fitting of the data as well as statistical analysis were done in Prism (GraphPad Software, San Diego, CA). Statistical significance was evaluated by using an unpaired Student's *t* test and one-way ANOVA as appropriate.

Transfected tsA201 cells. Cells were grown at 37°C in 5% CO_2 in DMEM supplemented with 10% fetal bovine serum and penicillin–streptomycin. The tsA201 cells were plated onto 16 mm coverslips 1 d before transfection with α1B, β1b, and $\alpha2\delta$ subunits, using a standard calcium phosphate protocol. Then 3 μg of cDNA encoding for each calcium channel subunit was transfected together with 0.3 μg of cDNA for enhanced GFP (pEGFP-C1; Clontech, Cambridge, UK) and 3 μg of pCMV-Neurexin 1α or control vector (pCMV5). After 12 h the cells were provided with fresh medium and maintained at 37°C for another 12 h. Then the cells were moved to 30°C in 5% CO_2 and maintained for up to 6 d. Patch-clamp experiments were done on the fourth to sixth days after transfection, using a custom-made chamber with external bath solution composed of the following (in mM): 65 CsCl, 40 TEA-Cl, 20 $BaCl_2$ or 10 $CaCl_2$ (as indicated), 1 $MgCl_2$, 10 HEPES, 10 glucose, pH 7.2, at room temperature. The internal pipette solution contained the following (in mM): 108 Cs-methane sulfonate, 4 $MgCl_2$, 9 EGTA, 9 HEPES. The rest of the experimental conditions were the same as with HEK293_$Ca_v2.2$ cells except for the protocol for eliciting current–voltage (*I–V*) relationships, which were obtained by 150 ms voltage pulses from −40 to +50 mV in 10 mV increments.

Ca^{2+} currents in brainstem neurons. All electrophysiological analyses were performed on neurons of the pre-Bötzinger complex as described previously (Zhang et al., 1999, 2005; Missler et al., 2003). Briefly, acute slices from newborn (postnatal day 1) littermate mice were used for whole-cell recordings. The bath solution in all experiments consisted of the following (in mM): 118 NaCl, 3 KCl, 1.5 $CaCl_2$, 1 $MgCl_2$, 25 $NaHCO_3$, 1 NaH_2PO_4, 20 glucose, pH 7.4, which was aerated with 95% O_2/5% CO_2 and kept at 28–30°C. Voltage-activated Ca^{2+}currents were measured with electrodes containing the following (in mM): 110 $CsCl_2$, 30 TEA-Cl, 1 $CaCl_2$, 10 EGTA, 2 $MgCl_2$, 4 Na_3ATP, 0.5 Na_3GTP, 10 HEPES, pH 7.3, and with 0.5 μM tetrodotoxin (Alamone Labs) in the bath solution. Serial and membrane resistances were estimated from current transients induced by 20 mV hyperpolarization voltage commands from a holding potential of –70 mV. The serial resistance was compensated by 80%, and patches with a serial resistance of >20 MΩ, a membrane resistance of <0.8 GΩ, or leak currents of >150 pA were excluded. Currents were

recorded in response to voltage step changes from –70 mV holding potential to test potentials between –80 and +30 mV and were quantified as peak currents in response to voltage steps from –70 to 0 mV. Ca^{2+} current measurements were corrected by using the P/4 protocol. Baclofen (Research Biochemicals, Natick, MA) was prepared as a 10 mM stock solution and added to the bath to a final concentration as indicated in Results. Data acquisition and analysis were performed with commercially available software (pClamp 6.0 and AxoGraph 4.6, Molecular Devices, Union City, CA; Prism 3 software, GraphPad Software).

Results

Hypomorphic pituitary gland in adult α-neurexin double-mutant mice

Knock-out mice deficient for all three α-neurexin genes (*Nrxn1α*, *Nrxn2α*, *Nrxn3α*; triple knock-outs) and most of the double knock-out mutants die early postnatally because of respiratory dysfunction (Missler et al., 2003). Here we analyzed the small population of $Nrxn1\alpha^{-/-}$;$Nrxn2\alpha^{-/-}$ and $Nrxn2\alpha^{-/-}$;$Nrxn3\alpha^{-/-}$ double-mutant mice (DKO1/2 and DKO2/3) that survive into adulthood (~5–10 and 35–40%, respectively). Because the phenotype of DKOs is characterized by a hypomorphic appearance (Fig. 1*A*), an ~40% reduction in body weight (Fig. 1*B*), and an almost complete inability to breed (data not shown), we hypothesized that endocrine functions may be impaired in the absence of α-neurexins. Magnetic resonance imaging (MRI) of deeply anesthetized animals was performed to screen for structural alterations of brain areas regulating endocrine functions, using a manganese-enhanced T_1-weighted technique essentially as described (Angenstein et al., 2006) (for a brief description, see supplemental text, available at www.jneurosci.org as supplemental material). Quantitative evaluation of scan data revealed a 44% reduction of the total volume of the pituitary gland in DKOs as compared with control animals (Table 1; Fig. 1*C*,*D*), whereas the gross anatomy of other brain regions appeared normal, consistent with our earlier morphological observations in newborn triple knock-outs (Missler et al., 2003). To exclude the possibility that the defective pituitary gland is a mere consequence of a defect in the hypothalamus (Tomiko et al., 1983; Schneggenburger and Konnerth, 1992), we performed reverse transcriptase-PCR (RT-PCR) with neurexin isoform-specific primers (Fig. 1*E*), demonstrating that two α- and two β-neurexins are expressed prominently in the gland tissue at levels comparable to the brain or even higher (Fig. 1*F*). Because none of the morphological or physiological parameters examined in this study showed significant differences between the two surviving double knock-out populations (i.e., DKO1/2 represents $Nrxn1\alpha^{-/-}$;$Nrxn2\alpha^{-/-}$ and DKO2/3 represents $Nrxn2\alpha^{-/-}$;$Nrxn3\alpha^{-/-}$), we pooled the double knock-out data and henceforth refer to them collectively as DKOs. Similarly, we used two different types of control animals, littermate mice that are deficient for *Nrxn2α* alone (SKO2) and mice from a genetically matching WT background line. In agreement with the low expression of *Nrxn2α* in the pituitary gland (Fig. 1*F*), both WT and SKO2 genotypes showed virtually identical results in all of the parameters that were examined and are referred to collectively as controls.

To investigate which parts of the pituitary gland contribute to the overall diminished size detected in MRI scans, we performed a thorough histological analysis of the gland (Fig. 1*G–J*) (also, supplemental Fig. 1, available at www.jneurosci.org as supplemental material), revealing that the reduction is mostly attributable to smaller anterior and intermediate lobes (Table 1). Examination of high-magnification images suggested that smaller individual endocrine cells accounted for the reduced size of the anterior and intermediate lobes (Table 1, Fig. 1*I*,*J*). In contrast,

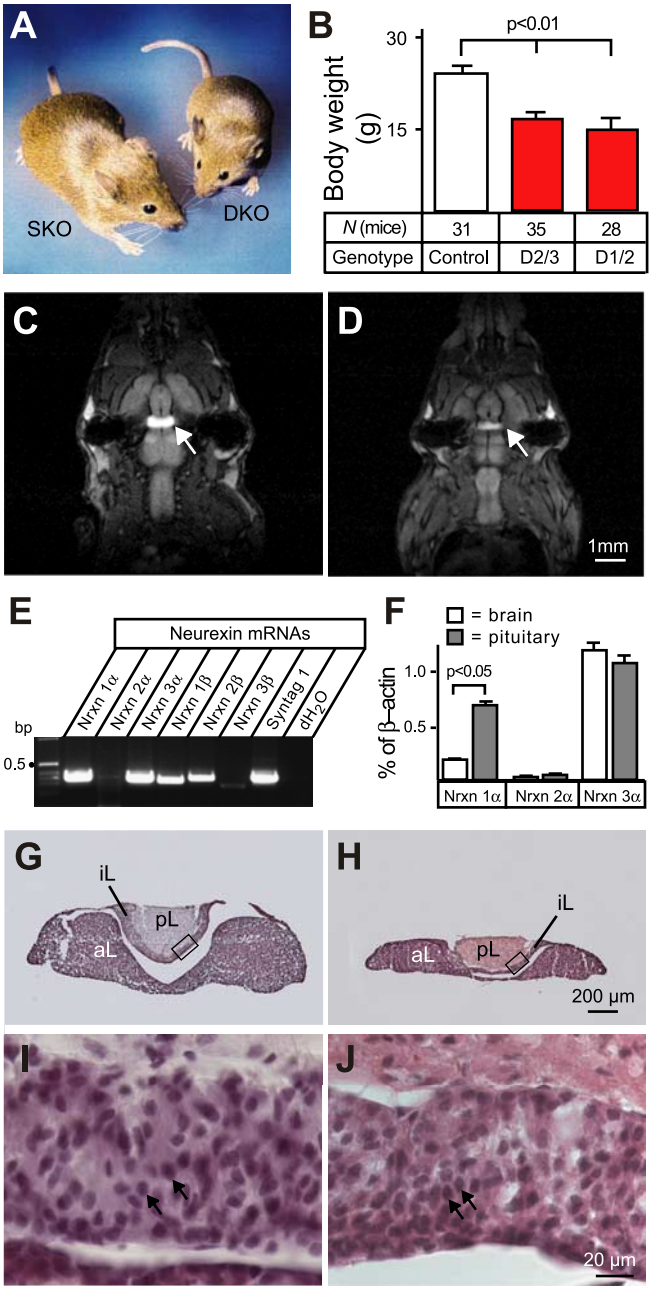

Figure 1. α-Neurexin-deficient mice exhibit a small pituitary gland. ***A***, Double knock-out mice (DKO; right) show a hypomorphic phenotype as compared with single knock-out littermate controls (SKO; left). ***B***, Body weight of 5- to 6-week-old female mice lacking *Nrxn2α* and *Nrxn3α* (D2/3), *Nrxn1α* and *Nrxn2α* (D1/2), or *Nrxn2α* alone (control). Error bars represent the mean ± SEM. ***C***, ***D***, Manganese-enhanced MRI of adult wild-type (***C***) and α-neurexin double knock-out mice (***D***). The sample images show horizontal T_1-weighted scans at the level of the base of the skull. Arrows point to the pituitary glands that highly enrich $MnCl_2$, indicating reduced uptake of $MnCl_2$ and/or size of the gland in mutant mice. ***E***, RT-PCR demonstrates the presence of two α-neurexins and two β-neurexins in the RNA from adult pituitary gland. Syntag1, Synaptotagmin 1 (positive control); dH_2O, distilled water. ***F***, α-Neurexin isoforms are expressed in the pituitary glands at levels comparable to or higher than their expression in the brain. The relative quantification was performed by SYBR Green-based real-time PCR with β-actin as a reference gene. Error bars represent the mean ± SEM. ***G***, ***H***, Hematoxylin and eosin-stained frontal sections of the pituitary glands from control (***G***) and double knock-out mice (***H***). aL, Anterior lobe; iL, intermediate lobe; pL, posterior lobe. ***I***, ***J***, High-magnification pictures of the intermediate lobe of control (***I***) and double knock-out animals (***J***). Cells appear to be packed more densely in the latter (arrows). Scale bars are as indicated; level of statistical significance is indicated above the bars.

Table 1. Quantitative morphological analysis of the pituitary gland in α-neurexin-deficient mice

	Genotype			
	Wild-type (*n*)	SKO2 (*n*)	DKO 2/3 (*n*)	DKO 1/2 (*n*)
Total volume[a] (mm^3)	1.6 ± 0.1 (5)	—	0.9 ± 0.1 (7)*	—
Anterior lobe[b] ($\times 10^5\ \mu m^2$)	6.5 ± 0.8 (3)	4.8 ± 0.4 (6)	3.4 ± 0.2 (6)**	3.0 ± 0.5 (5)**
Intermediate lobe (μm)	91 ± 6 (3)	68 ± 2 (6)***	56 ± 3 (6)*	58 ± 3 (4)*
Posterior lobe[b] ($\times 10^5\ \mu m^2$)	2.4 ± 0.3 (3)	1.9 ± 0.1 (6)[c]	2.1 ± 0.1 (6)[c]	2.0 ± 0.1 (5)[c]

Data are means ± SEM. *n* = number of animals used. All animals used in morphometric analysis were either littermate offspring from parents homozygous for *Nrxn2α* and double heterozygous for *Nrxn1α* and *Nrxn3α* or wild-type animals of the same genetic background. —, Not done. Statistical analysis was done using *t* test for total volume comparison and one-sided ANOVA with Tukey's post test for all other parameters (Prism Software; GraphPad Software); *$p < 0.001$; **$p < 0.01$; ***$p < 0.05$.

[a]Data derived from MRI scans as shown in Figure 1, *E* and *F*.

[b]Measurements were done on hematoxylin–eosin-stained sections as shown in Figure 1*G–J*. For anterior and posterior lobes, the values represent the mean area and for intermediate lobes the mean thickness.

[c]Not significant.

the posterior lobe, which consists of glial cells and hypothalamic neuronal terminals releasing oxytocin and vasopressin, was not affected significantly (Table 1). We next used immunocytochemistry to test whether the smaller pituitary lobes of knock-out animals contain the appropriate peptide hormones. Cryosections were labeled with antibodies against the intermediate lobe marker pro-opiomelanocortin (POMC) and its cleavage products, β-endorphin and α-MSH (Fig. 2). In addition, cells of the anterior lobe were probed with antibodies against growth hormone, prolactin, and other trophic hormones, and the posterior lobe was stained with antisera to vasopressin and oxytocin (supplemental Fig. 2, available at www.jneurosci.org as supplemental material) (data not shown). No differences in distribution pattern or staining intensity were detected among genotypes, suggesting that the mutant cells express all of the peptides normally.

Defective secretory activity from melanotrophs in adult α-neurexin double-mutant mice

To test directly whether the hypomorphic phenotype and smaller pituitary gland lobes are a sign of insufficient endocrine release, we monitored secretion from mutant and control melanotrophs by whole-cell patch-clamp measurements of membrane capacitance in fresh pituitary gland slices as characterized before (Sedej et al., 2004, 2005; Turner et al., 2005). Consistent with the morphological data reported above, the resting membrane capacitance (a parameter proportional to the membrane surface area) of adult double knock-out mice was reduced significantly as compared with wild-type and single knock-out control animals (Fig. 3*A*), indicating that DKO melanotrophs had a smaller calculated cell volume (assuming spherical shape and specific membrane capacitance of 10 $fF/\mu m^2$; control, 1359 ± 182 μm^3 and $n = 15$; DKO, 861 ± 63 μm^3 and $n = 54$) (Fig. 3*B*). Consequently, all recordings were normalized to the resting capacitance. Ca^{2+}-dependent secretion was triggered by a train of 200 depolarizing pulses from −80 to +10 mV for 40 ms at 10 Hz (Fig. 3*C*, top panel), which stimulated a rise in cytosolic $[Ca^{2+}]_i$ without significantly changing membrane conductance as defined by the real component of the admittance signal. The depolarization train reliably evoked secretory responses in melanotrophs from both DKO and control mice that were measured as a cumulative increase in membrane capacitance (ΔC_m) (Fig. 3*C*). However, in α-neurexin double-mutant cells the initial increase in ΔC_m was much slower (Fig. 3*D*) and did not reach control levels even after prolonged stimulation (Fig. 3*C*,*E*), indicating that the secretory activity in DKO pituitary gland is impaired. A single-pulse analysis of these recordings showed that membrane capacitance changes in response to the first 40 pulses were affected predominantly by the mutation while the ΔC_m changes during subsequent stimulations were similar (Fig. 3*F*). To distinguish whether the reduced secretion in double-mutant cells was attributable to an impaired release process or reflected alterations in the number, size, or distribution of secretory granules, we performed an ultrastructural analysis of DKO and control melanotrophs (for representative electron microscopic pictures, see supplemental Fig. 3, available at www.jneurosci.org as supplemental material). The size of the granules, the distance from the plasma membrane, and the area density of the granules in the cytoplasm were measured on randomly sampled sections from the intermediate lobe and were found to be similar to published data (Zupancic et al., 1994). No significant differences in ultrastructure were observed between α-neurexin double knock-out mice and littermate controls (Table 2), indicating that the defect in secretion was not caused by reduced size and/or availability of secretory granules.

Functional, but not morphological, defect is the primary phenotype in the pituitary gland

To address the question of whether the reduced size of the mutant anterior and intermediate lobes is a consequence of the defective release or, vice versa, the defective release is a manifestation of an impaired development of the pituitary gland in the absence of α-neurexins, we analyzed the morphology and secretory activity of the pituitary gland in newborn α-neurexin-deficient mice and littermate controls (Fig. 4). In contrast to the adult mutants, histology showed no differences in the size of the pituitary lobes or cell size in newborn mice (Fig. 4*A*,*B*) (also, supplemental Fig. 4, available at www.jneurosci.org as supplemental material). The average thickness of the intermediate lobe measured 29.5 ± 0.6 μm in controls ($n = 3$) and 30.6 ± 1.0 μm in mutant mice ($n = 3$, not significant). In line with the morphometric analysis, electrophysiological recordings in melanotrophs showed an almost identical resting membrane capacitance in these young animals (Fig. 4*C*), confirming that there is no difference in cell size. However, when we assessed the secretory activity in newborn melanotrophs, membrane capacitance measurements revealed a prominent defect in double knock-out cells (Fig. 4*D*--*F*, red lines) when compared with single knock-out controls (Fig. 4*D*–*F*, green). Consistent with our previous data on neurotransmission (Missler et al., 2003), the reduction in endocrine secretion was pronounced even more in newborn triple knock-outs lacking all three α-neurexin genes (Fig. 4*D*–*F*, gray). The early presence of the functional secretory phenotype and the normal gland structure of newborn mutants together suggest that the impairment of the secretory granule exocytosis is the cause of the morphological changes in the pituitary gland. The cell size in the endocrine system generally is related to the secretory activity of the cells. Therefore, hypoactive melanotrophs tend to show smaller volumes (Chronwall et al., 1988). Preliminary data on the function of β-cells in α-neurexin knock-out mice support the idea of a generalized defect in endocrine secretion. The DKO mice are hyperglycemic, their pancreatic β-cells are similarly hypomorph as melanotrophs, and stimulus–secretion experiments indicate that β-cells also may show an impaired responsiveness to depolarization protocols (M. Rupnik and M. Missler, unpublished observations). The generalized defect in endocrine

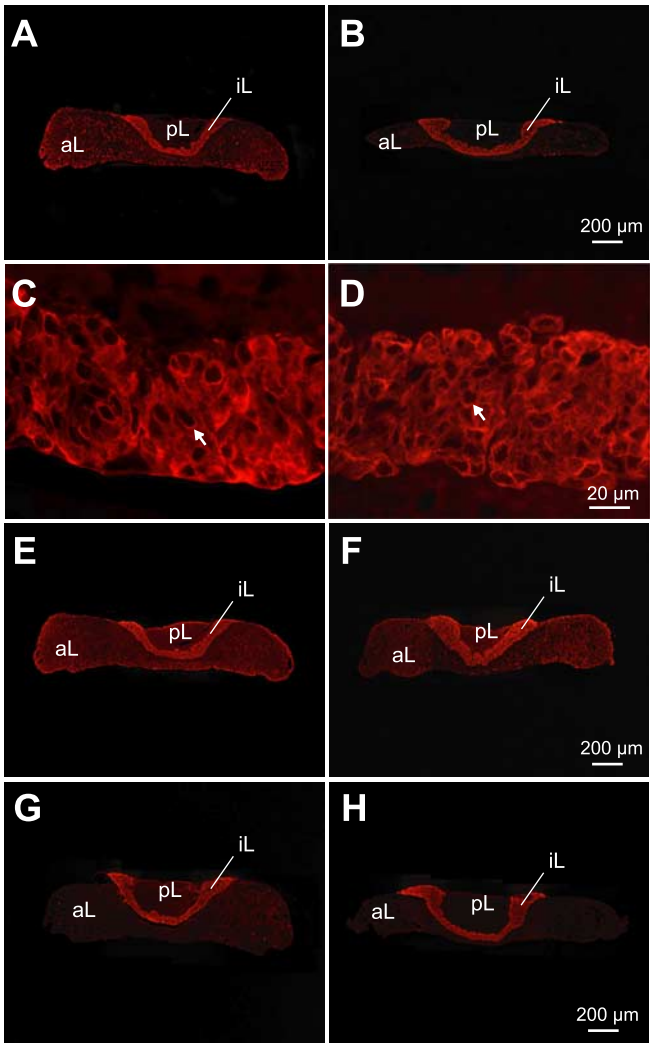

Figure 2. Melanotrophs show a normal expression of peptides in α-neurexin mutant mice. Control (***A***, ***C***, ***E***, ***G***) and double knock-out (***B***, ***D***, ***F***, ***H***) pituitaries were labeled with antibodies against intermediate lobe markers: POMC (***A–D***) and its cleavage products β-endorphin (***E***, ***F***) and α-MSH (***G***, ***H***), expressed by melanotrophs (arrows). aL, Anterior lobe; iL, intermediate lobe; pL, posterior lobe. Scale bars are as indicated.

secretion potentially underlies the overall hypomorphic phenotype and breeding difficulties observed in the surviving population of adult α-neurexin double-mutant mice.

Secretory activity during the early kinetic phase of secretion

In adult DKO and newborn TKO melanotrophs the responses to the early pulses of the depolarization train were reduced markedly (Figs. 3*D*, 4*E*). We next wanted to obtain an estimate of the pool size and secretion dynamics of the immediately releasable pool (IRP) of granules, which is the population of granules thought to colocalize with Ca^{2+} channels at release sites and thought to be equivalent to synaptic vesicles at the presynaptic active zone in terms of release kinetics (Thomas et al., 1993a; Parsons et al., 1995; Moser and Neher, 1997). We used two different approaches. First, we applied a dual-pulse protocol, adjusting the pulses to obtain two comparable charge injections (Gillis et al., 1996; Voets et al., 1999; Sedej et al., 2005) (Fig. 5*A*). The use of this assay is justified only when substantial pool depletion takes place and the ratio between the capacitance response after second and first depolarization ($r = \Delta C_{m2}/\Delta C_{m1}$) is <0.7 (Gillis et al., 1996; Voets et al., 1999; Sedej et al., 2005). Given that this criterion was fulfilled in less than one-half of the cells that were examined, we took instead the sum of capacitance responses ($S = \Delta C_{m1} + \Delta C_{m2}$) after both pulses as a measure of a release-ready vesicle pool size (Sedej et al., 2005). Significant differences were found in *S* value (Fig. 5*B*), indicating that the pool sizes differed in DKO (7.8 ± 2.0 fF, $n = 23$) and control (16.2 ± 2.8 fF; $n = 13$) melanotrophs. This result together with ultrastructural observation suggests that, although the proportion of "docked" (membrane-near) secretory granules is similar in all genotypes (Table 2), the number of immediately releasable vesicles is reduced by one-half in the DKOs. Second, we compared the kinetic properties of the IRP by using single depolarization pulses of different duration (Fig. 5*C*). Two rapid components of release could be distinguished as characterized before (Horrigan and Bookman, 1994; Gillis et al., 1996; Sedej et al., 2005). The fastest component (≤ 40 ms) was best fit by the following: $y(t) = y_0(1 - \exp(-t/\tau)^3)$, with $\tau = 4.1$ ms, and represents the fusion of IRP of vesicles. Measurements of the fastest component revealed membrane capacitance changes of ~ 13 fF in control ($n = 10$) and ~7 fF in DKO cells ($n = 20$), corresponding to the release of ~13 (control) and 7 (DKO) vesicles, respectively (conversion factor of 1 fF per vesicle) (Thomas et al., 1993b), indicating that during short depolarizations the mutant cells secrete only approximately one-half the number of immediately releasable vesicles. The actual size of vesicles in melanotrophs was measured previously by electron microscopy and compared with discrete steps in membrane capacitance (Zupancic et al., 1994). The slower component of secretory responses (depolarization pulses between 40 and 200 ms) was best fit by a linear function in control and mutant cells (Fig. 5*C*, dotted lines). Their corresponding *k* values, which display the slope of the linear fit, also revealed a 50% reduction in α-neurexin double knock-out melanotrophs as compared with littermate control animals. Because the IRP granules probably make the major contribution to basal release under physiological stimulation conditions (Voets et al., 1999), a twofold reduction of this pool can lead to significant exocytotic defects and, thereby, hormonal deficits in the knock-out animals.

Voltage-dependent Ca^{2+} currents in α-neurexin-deficient melanotrophs

We suggested earlier that the reduced neurotransmission at central synapses of newborn α-neurexin-deficient mice involves an impaired function of high VDCCs (Missler et al., 2003). We therefore examined whole-cell Ca^{2+} currents in melanotrophs of adult and newborn control and α-neurexin-deficient mice (Fig. 6*A*), using 300 ms voltage ramps to elicit currents as described previously (Sedej et al., 2004). We first investigated peak Ca^{2+} currents but failed to detect changes in current density when adult or newborn mutant mice were compared with their corresponding controls (Fig. 6*B*). To test that Ca^{2+} channel densities do not decline at different rates during whole-cell dialysis, we monitored the peak Ca^{2+} currents over 10 min, but they showed only little rundown in adult control and double knock-out cells (Fig. 6*C*). We next determined the contribution of different subtypes of VDCCs to the peak amplitude in mutant and control cells by applying specific N-type (1 μM ω-conotoxin GVIA), P/Q-type (100 nM of ω-agatoxin TK plus 100 nM ω-conotoxin MVIIC), and L-type blockers (10 μM nifedipine) in sequential order. No difference in Ca^{2+} current density was observed for any of the VDCCs (Fig. 6*D*), suggesting that, in contrast to brainstem neurons (Missler et al., 2003), no functional compensation among VDCCs takes place in DKO melanotrophs. We used the peak

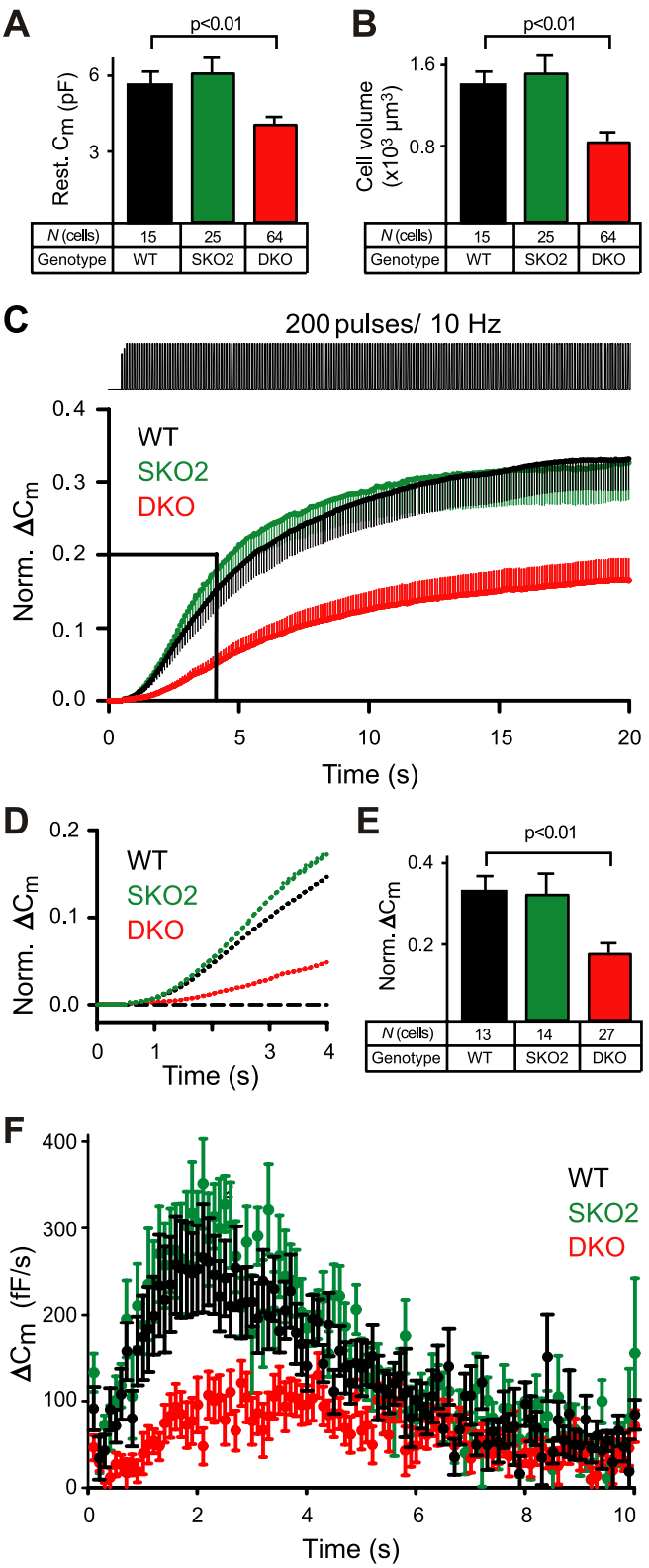

Figure 3. Release from pituitary gland melanotrophs is reduced in adult α-neurexin-deficient mice. ***A***, ***B***, Resting membrane capacitance was measured in melanotrophs of the intermediate lobes from adult wild-type (WT), single knock-out (SKO2), and double knock-out (DKO) pituitary glands (***A***), revealing that the average cell volume of DKO melanotrophs is reduced (***B***). ***C***, Ca^{2+}-dependent secretion was evoked by a train of 200 depolarizing pulses from −80 to +10 mV at 10 Hz. The secretory response was measured as ΔC_m in WT and SKO2 controls and in α-neurexin DKO cells and is shown as the mean ± SEM in the traces. ***D***, Higher-resolution plot of the first 4 s of capacitance change (boxed area in ***C***). ***E***, Cumulative membrane capacitance change normalized to the resting C_m in WT and SKO2 controls compared with α-neurexin DKO cells. ***F***, Membrane capacitance changes evoked by the single pulses of the depolarization train. Data are represented as the mean ± SEM (***A–C***, ***E***, ***F***) and have been normalized to the resting capacitance (***C–E***). Level of statistical significance is indicated above the bars.

Table 2. Ultrastructural analysis of secretory granules in melanotrophs

	Genotype		
	SKO2 (*n*)	DKO (*n*)	*p* value
Diameter[a] (nm)	299 ± 30 (3)	261 ± 17 (3)	0.37
Density[a] (μm^{-2})	1.0 ± 0.09 (3)	1.0 ± 0.04 (3)	0.69
Distribution[a,b]			
0–50 nm	0.22 ± 0.03 (3)	0.25 ± 0.03 (3)	0.45
50–150 nm	0.11 ± 0.01 (3)	0.15 ± 0.01 (3)	0.08
150–250 nm	0.12 ± 0.01 (3)	0.14 ± 0.01 (3)	0.11
250–350 nm	0.11 ± 0.01 (3)	0.12 ± 0.01 (3)	0.25
>350 nm	0.44 ± 0.06 (3)	0.34 ± 0.04 (3)	0.22

Data are means ± SEM. *n* = number of animals used. All animals used for quantitative electron microscopic analysis were littermate offspring from parents homozygous for *Nrxn2α* and double heterozygous for *Nrxn1α* and *Nrxn3α*. Statistical analysis was performed with *t* test (Prism Software; GraphPad Software), and *p* values are indicated.

[a]The size (average of shorter and longer diameters), area density, and distribution of secretory granules were determined on randomly sampled electron microscopic pictures of melanotrophs such as those shown in supplemental Fig. 3, available at www.jneurosci.org as supplemental material), using DigitalMicrograph 3.4 software (Gatan).

[b]The distribution of granules within the cytoplasm was analyzed by determining their relative frequency in five classes of shortest distances from the plasma membrane.

A total number of 1504 (control) and 1564 (DKO) granules was evaluated for the analysis.

amplitude of inward Ca^{2+}-activated Cl^- currents as an additional estimate of the amount of Ca^{2+} entering the cytosol via VDCCs (Turner et al., 2005) and observed similar Cl^- current densities in melanotrophs of both genotypes (Fig. 6*E*). We additionally compared Ca^{2+} current–voltage relationships by using the voltage ramp protocol that allows for the separation of low voltage-activated and high voltage-activated Ca^{2+} currents (Kocmur and Zorec, 1993). A difference was found in the *I–V* relation that corresponds to the activation of N and P/Q channels (Fig. 6*F*) (averaged from $n = 3$ sweeps; black trace was derived by subtracting SKO2−DKO), seen as a rightward shift in the peak voltage dependence from −10 mV (control; $n = 21$) to −4 mV (DKO; $n = 38$). These data suggest that a difference in VDCC function exists but is not large enough to explain the much lower release from melanotrophs on the basis of altered Ca^{2+} channel properties.

Expression of VDCCs is high in early postnatal melanotrophs and subsequently becomes downregulated by the gradual onset of their dopaminergic and GABAergic synaptic input (Gomora et al., 1996; Fass et al., 1999). Therefore, we also explored the innervation from hypothalamic neurons by recording spontaneous postsynaptic currents (SPCs) in melanotrophs of adult control and double knock-out mice (Fig. 7). Consistent with earlier data on miniature postsynaptic currents in α-neurexin-deficient neurons (Missler et al., 2003), the SPC frequency was ~65% lower in DKO cells (0.07 ± 0.02 Hz; $n = 15$) when compared with controls (0.2 ± 0.04 Hz; $n = 22$) (Fig. 7*A*,*B*). The addition of 60 pM α-latrotoxin into the external bath solution even aggravated this difference (control, 3.56 ± 0.63 Hz and $n = 17$; DKO, 0.07 ± 0.03 Hz and $n = 4$) (Fig. 7*A*,*B*), confirming and extending previous observations that α-neurexins act as a prominent receptor for this neurotoxin (Geppert et al., 1998; Sugita et al., 1999) and also play an important role at presynaptic terminals in the hypothalamo–hypophysial axis. To test whether the hypothalamic terminals in α-neurexin mutants are at all functional, we probed the Ca^{2+}-independent component of release with hypertonic so-

←

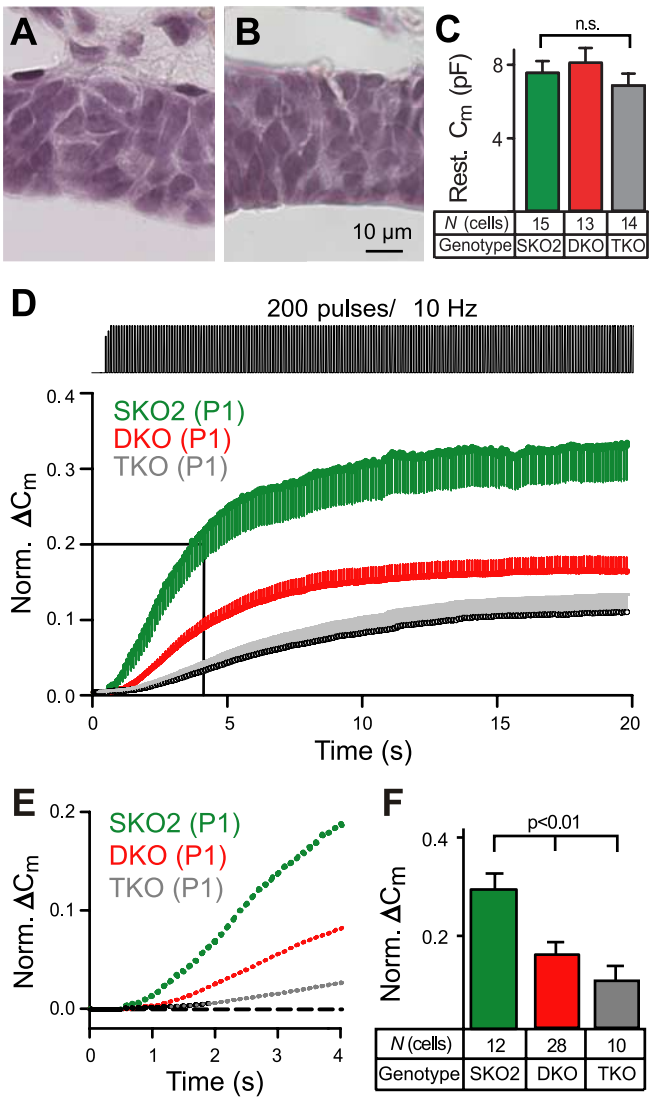

Figure 4. The functional defect, but not the structural phenotype, is present in the pituitary glands of newborn mutant mice. ***A***, ***B***, Representative sections of the pituitary gland from newborn control (***A***) and triple knock-out (***B***) mice stained with hematoxylin and eosin, showing intermediate lobes of similar thickness and cell density. ***C***, Resting membrane capacitance of melanotrophs from newborn double knock-out (DKO; red) and triple α-neurexin knock-out (TKO; gray) mice is not different from littermate control animals (SKO2; green). ***D***, Ca^{2+}-dependent secretion was evoked from melanotrophs of newborn control animals (SKO2; green trace) and α-neurexin double (DKO; red) and triple (TKO; gray) knock-out mice; responses are represented as changes in membrane capacitance, using the same protocol as for adult mice (see Fig. 3*C*). ***E***, Higher-resolution plot of the first 4 s of capacitance change (boxed area in ***D***). ***F***, Cumulative membrane capacitance change normalized to the resting C_m. Data are represented as the mean ± SEM (***C***, ***D***, ***F***) and have been normalized to the resting capacitance (***D–F***). Level of statistical significance is indicated above the bars; n.s., not significant. Scale bar (in ***B***) is as indicated.

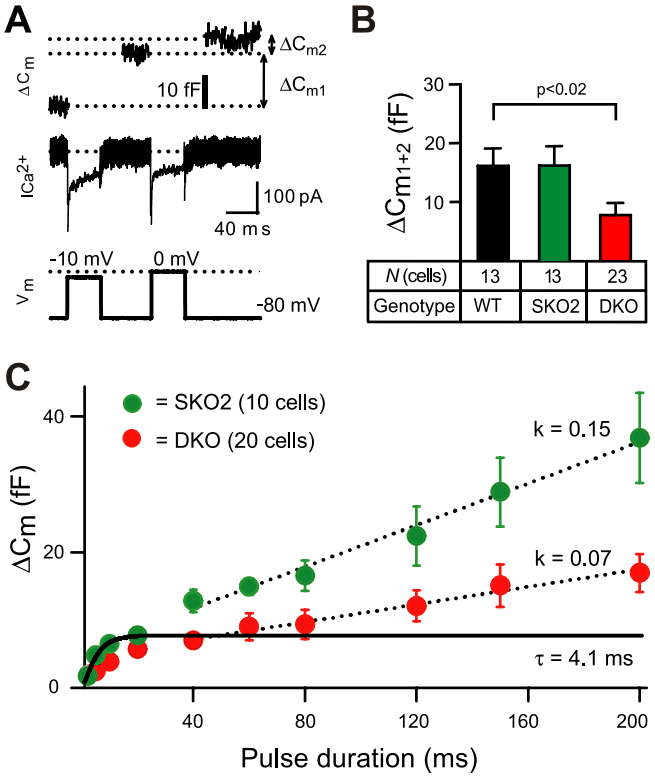

Figure 5. The impaired secretion from melanotrophs affects the release-ready pool of vesicles. ***A***, Dual-pulse protocol applied to elicit depletion of the IRP of vesicles. Paired pulses of 40 ms duration to −10 and 0 mV were applied 60 ms apart, and the voltage of the pulses was adjusted to give an equal amount of Ca^{2+} influx during both pulses. ***B***, Comparison of the IRP size among wild-type (WT) and α-neurexin single knock-out (SKO2) and double knock-out (DKO) mice by dual-pulse protocol as follows: $S = \Delta C_{m1} + \Delta C_{m2}$. Level of statistical significance is indicated above the bars. ***C***, Horrigan–Bookman plot identifies alterations in the IRP of vesicles. At 2 min after the beginning of whole-cell dialysis, single depolarization pulses of different duration (between 2 and 200 ms) from −80 to 0 mV were applied in random order. Then, 15 s was allowed for pool refilling after pulses shorter than 40 ms, and 30 s was allowed for longer pulses. Membrane capacitance changes were recorded from control (SKO2; green) and α-neurexin double knock-out (DKO; red) cells. Pulses <40 ms presumably evoke a release of vesicles from the IRP; this exponential phase reaches a plateau at ~20 ms, indicating pool depletion. τ represents the time constant for the exponential fit of control data, although knock-out data could not be fit satisfactorily with an exponential equation. The slower component of release was fit with a straight line; *k* indicates the slope of the linear fit. Data are represented as the mean ± SEM.

lution (but see Basarsky et al., 1994). Although lower sucrose concentrations (100 and 200 mM) (data not shown) appeared to be ineffective on the postsynaptic response of melanotrophs independent of their genotype, the addition of 500 mM sucrose evoked a significant increase in the presynaptic activity of both control (0 mM sucrose, 0.12 ± 0.02 Hz and $n = 3$; 500 mM sucrose, 4.14 ± 1.34 Hz and $n = 3$) and mutant cells (0 mM sucrose, 0.04 ± 0.02 Hz and $n = 6$; 500 mM sucrose, 2.56 ± 0.58 Hz and $n = 6$) (Fig. 7*C*,*D*). The slightly lower level of SPCs recorded from mutant cells after sucrose application (Fig. 7*D*) is consistent with our previous observations in neocortical neurons (Missler et al., 2003) and may indicate a reduction in the number of inhibitory synapses also seen before (Missler et al., 2003). To confirm whether this is also the case in the hypothalamo–hypophysial axis, we used immunofluorescence of synaptic markers to probe for the presence of GABAergic terminals in the vicinity of melanotrophs in control and mutant mice. Our data suggest that these terminals are present in the intermediate lobe but appear to be much sparser in mutant mice (supplemental Fig. 5, available at www.jneurosci.org as supplemental material). In contrast to the experiments on pituitary glands of adult mice, no postsynaptic activity was detected in melanotrophs from newborn mice of any genotype before or after the addition of latrotoxin or hypertonic sucrose solution (data not shown), reflecting the absence of hypothalamic innervation at this age (Gomora et al., 1996; Makarenko et al., 2005). Because the secretory phenotype is manifested fully in newborn mutant melanotrophs that lack hypothalamic regulation, the defect in secretory activity is attributable to the absence of α-neurexins in the pituitary gland and does not

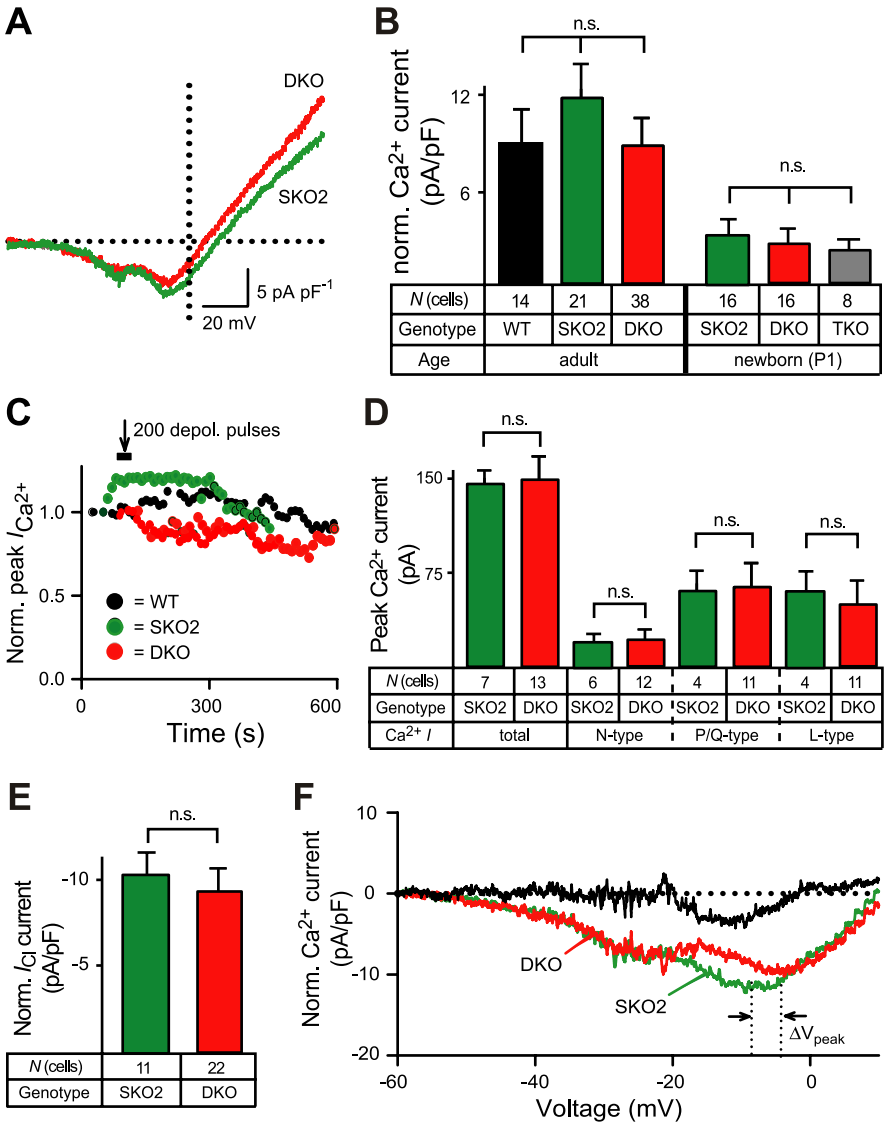

Figure 6. Whole-cell Ca^{2+} currents are not reduced in α-neurexin-deficient melanotrophs but show a small kinetic difference. ***A***, Representative Ca^{2+} current recordings evoked by 300 ms voltage ramps from −80 to +60 mV in melanotrophs of α-neurexin DKO (red), and littermate control (SKO2; green) mice. ***B***, Comparison of high voltage-activated peak Ca^{2+} current densities in melanotrophs of adult and newborn control (WT and SKO2) and α-neurexin DKO and TKO mice. ***C***, Rundown of normalized Ca^{2+} currents is similar among genotypes. ***D***, Ca^{2+} channel subtype contributions to Ca^{2+} currents were measured in 10 mM $[Ca^{2+}]_e$ by sequentially adding 1 μM ω-conotoxin GVIA, 100 nM of ω-agatoxin TK plus 100 nM ω-conotoxin MVIIC, and 10 μM nifedipine. ***E***, The densities of Ca^{2+}-activated Cl^- currents (Turner et al., 2005) are comparable between the genotypes. ***F***, Voltage dependence of the averaged Ca^{2+} current densities shows a shift in α-neurexin double knock-out cells (arrows; ΔV_{peak}). All data in bar histograms are represented as the mean ± SEM; n.s., not significant.

represent an indirect consequence of a completely dysfunctional release from hypothalamic terminals.

Effect of α-neurexins on Ca^{2+} channels

Two possible mechanisms can be proposed to explain the effect of α-neurexins on Ca^{2+}-dependent release: modulating the biophysical properties of Ca^{2+} channels or determining their localization at release sites. We took two independent approaches to distinguish between these possibilities: (1) VDCCs were coexpressed with α-neurexins in heterologous cells to study direct effects of α-neurexins on Ca^{2+} currents in this simple system, and (2) the interaction of a G-protein-coupled $GABA_B$ receptor with VDCCs was explored in α-neurexin triple knock-outs to reveal defects in anchoring or positioning of Ca^{2+} channels.

First, to test whether α-neurexins can regulate biophysical parameters of VDCCs directly, we generated a HEK293 cell line that stably expressed the α1B, β3, and α2δ1 subunits, conferring a recombinant $Ca_V2.2$ (N-type) calcium channel on a nonexcitable cell type that contains few endogenous high VDCCs (for a more detailed characterization of the stable cell line, see supplemental Fig. 6, available at www.jneurosci.org as supplemental material). The depolarization of HEK293_$Ca_V2.2$ cells with a voltage step protocol that used 10 mM Ba^{2+} as a charge carrier elicited inward VDCC-mediated currents of ~200–400 pA peak amplitude (average peak amplitude, −337.17 ± 33.62 pA; $n = 25$) (Fig. 8*A*). The currents could be blocked completely by adding the N-type Ca^{2+} channel inhibitor ω-conotoxin GVIA (1 μM) to the external solution, characterizing the currents as specific N-type Ca^{2+} currents (Fig. 8*B*). We then searched for alterations in these currents when full-length *Nrxn1α* was coexpressed in HEK293_$Ca_V2.2$ cells along with an EGFP reporter gene to select cells for patch-clamp experiments (Fig. 8*C*, top panel). Untransfected HEK293_$Ca_V2.2$ cells on the same coverslips were used as controls. Although *Nrxn1α* was expressed and targeted to the plasma membrane as predicted (Fig. 8*C*, bottom panel), no changes of current–voltage (*I–V*) relationship were observed in the presence of α-neurexin (Fig. 8*D*, red trace) when compared with control HEK293_$Ca_V2.2$ cells (Fig. 8*D*, black). VDCC current density in controls ($V_t = 10$ mV; I_{Ca} density = 24.8 ± 2.2 pA/pF) was not significantly different from that in HEK293_$Ca_V2.2$ cells expressing *Nrxn1α* cDNA ($V_t = 10$ mV; I_{Ca} density = 28.8 ± 2.6 pA/pF), suggesting that α-neurexin is not able to modulate directly the current density of VDCCs. Because the modular adaptor proteins CASK (Butz et al., 1998; Maximov et al., 1999; Maximov and Bezprozvanny, 2002) and Mint1 (Maximov et al., 1999; Biederer and Sudhof, 2000) are able to interact with both α-neurexins and $Ca_V2.2$ channels at least biochemically, we reasoned that their additional presence was necessary to reconstitute the functional link *in vitro*. However, no alterations in *I–V* relation or VDCC current density ($V_t = 10$ mV; $I_{Ca} = 29.7 \pm 3.8$ pA/pF) were detected in HEK293_$Ca_V2.2$ cells coexpressing full-length *Nrxn1α* together with CASK and Mint1 (Fig. 8*D*, blue trace). To investigate whether α-neurexin alone or in concert with the adaptor proteins affects the inactivation of VDCCs, we used a prepulse protocol to compare averaged steady-state inactivation curves, but no differences were observed between control and cotransfected cells (Fig. 8*E*). Table 3 summarizes all activation and inactivation parameters of Ca^{2+} currents recorded from control HEK293_$Ca_V2.2$, HEK293_$Ca_V2.2$ cotransfected with

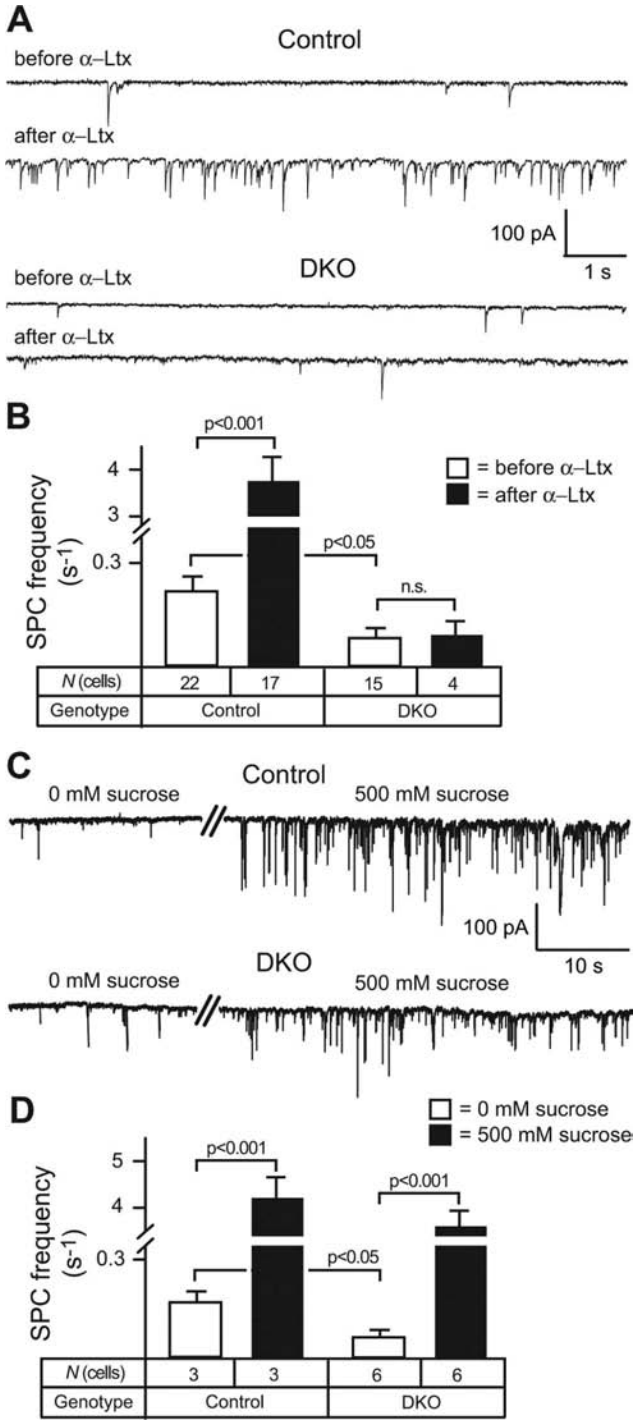

Figure 7. Melanotrophs in α-neurexin-deficient mice receive reduced synaptic inputs from hypothalamic neurons. ***A***, Representative current traces show GABA-mediated SPCs before and after the addition of 60 μM α-latrotoxin recorded under voltage clamp from adult melanotrophs of control and double knock-out mice (DKO). ***B***, Quantification of the SPC frequency demonstrates that synaptic release from hypothalamic neurons is reduced in mutant mice and cannot be stimulated by the neurotoxin as in controls. ***C***, Similar recording as in ***A*** before (0 mM sucrose) and after the addition of hypertonic solution (500 mM sucrose). ***D***, Quantification of the SPC frequency shows that the hypothalamic terminals on both control and mutant melanotrophs respond to sucrose stimulation. Data are represented as the mean ± SEM. Level of statistical significance is indicated above the bars; n.s., not significant.

Nrxn1α alone, and with *Nrxn1α* plus CASK and Mint1. Data were derived from *I–V* traces fit with a modified Boltzmann equation as described in Materials and Methods and did not reveal any differences among the groups.

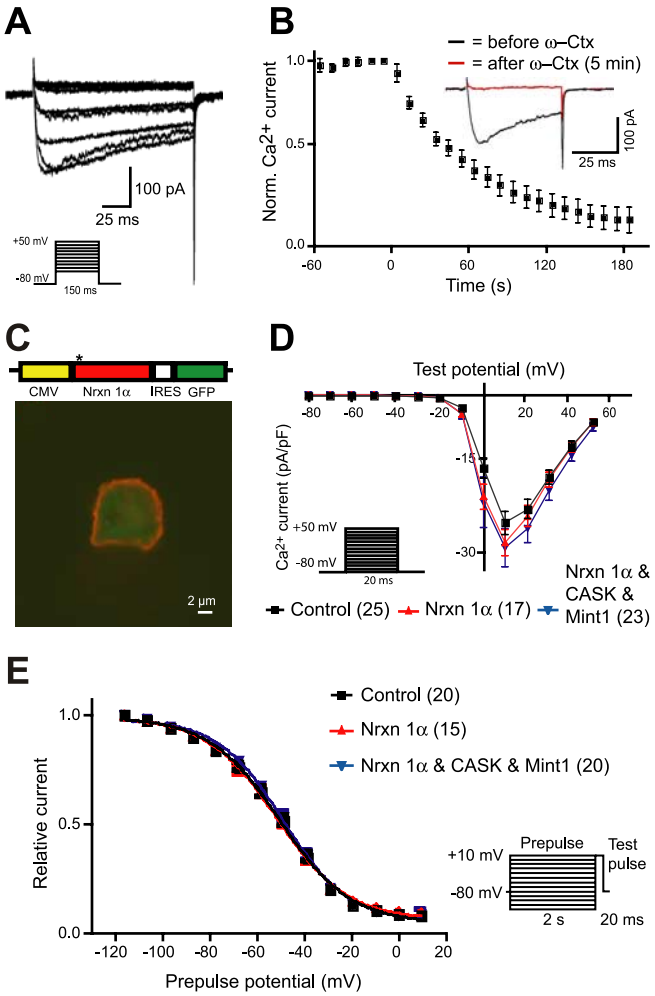

Figure 8. Neurexin 1α has no direct effect on biophysical parameters of recombinant N-type ($Ca_V2.2$) calcium channels. ***A***, Representative Ca^{2+} channel currents recorded from HEK293 cells stably expressing the α1B, β3, and α2δ subunits of high voltage-activated Ca^{2+} channels (HEK293_$Ca_V2.2$). Currents were induced by 150 ms pulses from −40 to +50 mV in 10 mV increments. ***B***, Ca^{2+} channel currents recorded from the stably transfected HEK293 cells can be blocked completely by 1 μM ω-conotoxin GVIA (ω-Ctx), suggesting that they are mediated specifically by the recombinant N-type ($Ca_V2.2$) channels. Time course was obtained by applying 50 ms voltage pulses to 0 mV every 10 s. The inset shows sample traces before (black) and 5 min after (red) the addition of ω-Ctx. ***C***, Cotransfection experiments of HEK293_$Ca_V2.2$ cells with *Nrxn1α* cDNA or *Nrxn1α* plus *CASK* and *Mint1* cDNAs. The diagram depicts the expression vector for *Nrxn1α* that coexpresses a reporter gene, GFP. A representative cell shows neurexin at the plasma membrane (red), and cytosolic GFP (green). ***D***, ***E***, Whole-cell voltage-clamp recordings reveal no differences in averaged current density–voltage relationships (***D***) and in averaged steady-state inactivation curves (***E***) in HEK293_$Ca_V2.2$ cells coexpressing *Nrxn 1α*, *Nrxn 1α* together with *CASK* and *Mint1*, or untransfected HEK293_$Ca_V2.2$ cells. Curves were generated from voltage-step protocols as indicated in the diagrams. The numbers of cells from more than three independent transfections are as indicated. Data are represented as the mean ± SEM.

In the recordings from stable cell lines Ba^{2+} had to be used as a charge carrier to produce quantifiable currents, raising the problem that certain aspects of Ca^{2+} channel function such as Ca^{2+}-dependent inactivation (Budde et al., 2002) could not be evaluated. To address these concerns, we repeated the experiments described above for HEK293_$Ca_V2.2$ cells but now compared responses with 10 mM Ca^{2+} and 20 mM Ba^{2+} as charge carriers by using transient transfections of tsA201 cells, a standard model to study the regulation of VDCCs *in vitro* (Zamponi and Snutch, 1998). Cells were transiently transfected with the α1B, β1b, and α2δ1 subunits of $Ca_V2.2$ with and without (con-

Table 3. Analysis of the effect of α-neurexins on $Ca_V2.2$ calcium channels in heterologous cells: stable HEK293_Ca_V 2.2 cell line

	Control	*Nrxn1α*	*Nrxn 1α* and CASK & Mint1	*p* value
Activation	$n = 25$	$n = 17$	$n = 23$	
$V_{1/2\ act}$ (mV)	1.46 ± 0.69	−0.812 ± 0.72	1.02 ± 0.98	0.16
k_{act} (mV)	3.53 ± 0.19	3.14 ± 0.21	3.42 ± 0.28	0.53
E_{rev} (mV)	56.12 ± 0.72	55.88 ± 0.70	56.37 ± 1.28	0.94
G_{max} (nS)	8.04 ± 0.68	8.47 ± 0.81	9.37 ± 1.07	0.52
Inactivation	$n = 20$	$n = 15$	$n = 20$	
$V_{1/2\ inact}$ (mV)	−52.65 ± 1.55	−53.73 ± 1.48	−50.50 ± 1.09	0.26
k_{inact} (mV)	14.86 ± 0.69	15.07 ± 0.69	13.72 ± 0.46	0.25

Data are means ± SEM. *n* = number of cells analyzed from at least three different transfections. Statistical analysis was done using Prism Software (GraphPad Software).

trol) the addition of *Nrxn1α*, as described in more detail in Materials and Methods. Independent of the charge carrier used, no major alterations of *I–V* relations, VDCC current densities, or inactivation profiles were detected (supplemental Fig. 7, available at www.jneurosci.org as supplemental material), with the notable exception of a statistically significant 2.5 mV leftward shift in half-activation potential when Ca^{2+} was used (Table 4). This leftward shift with the addition of α-neurexin in tsA201 cells is in agreement with the rightward shift in half-activation potential observed in melanotrophs with the deletion of α-neurexins (Fig. 6*F*). However, because the peak current density measured in 10 mM $[Ca^{2+}]_e$ in control cells ($V_t = 30$ mV; I_{Ca} density = 14.6 ± 2.8 pA/pF) was not different from cells coexpressing Nrxn1α ($V_t = 30$ mV; I_{Ca} density = 13.6 ± 2.9 pA/pF), it is unlikely that the small changes in voltage dependence of activation sufficiently explain the mostly reduced release at synapses or in endocrine cells. Table 4 summarizes all activation and inactivation parameters of Ca^{2+} channel currents recorded from transfected tsA201 cells, indicating that Nrxn1α is not able to modulate the biophysical properties of VDCCs considerably.

An alternative explanation of how α-neurexins affect Ca^{2+} channels could be that neurexins determine the correct spatial alignment between VDCCs and releasable vesicles, for example by anchoring VDCCs at their preferred slots within the active zone (Cao et al., 2004; Cao and Tsien, 2005). The microdomain hypothesis of Ca^{2+}-dependent exocytosis proposes the importance of the "subsynaptic" spatial arrangement of fusion-competent vesicles and the fusion machinery (Matthews, 1996; Klingauf and Neher, 1997; Neher, 1998). Because of the high $[Ca^{2+}]$ cooperativity of release (Bollmann et al., 2000; Schneggenburger and Neher, 2000) already small shifts (< 100 nm) in microdomains can have a large impact on the probability of release at synapses as well as in neuroendocrine cells (Becherer et al., 2003). Because usual strategies to test such a possibility, for example by ultrastructural immunogold labeling of endogenous or tagged channel subtypes in α-neurexin mutants versus control mice, currently are limited for technical reasons, we adopted a more indirect approach to address the issue.

We asked whether the link of an unrelated receptor molecule to VDCCs also might be impaired in α-neurexin knock-out mice, assuming that the absence of α-neurexins not only may weaken the link to docked vesicles but also weaken the link to other transmembrane proteins. The activation of G-protein-coupled $GABA_B$ receptors causes a reduction of release and VDCC-mediated Ca^{2+} current amplitudes (Pfrieger et al., 1994). $GABA_B$ receptors are expressed in brainstem neurons (Zhang et al., 1999) where our initial analysis of Ca^{2+} currents was performed (Missler et al., 2003), as well as in rodent melanotrophs (Purisai et al., 2005). We examined the regulation of Ca^{2+} channels by G-protein-coupled $GABA_B$ receptors in brainstem neurons of α-neurexin knock-outs. Ca^{2+} currents were evoked by 200 ms steps from a holding potential of −70 to +40 mV in 10 mV increments. Representative traces of Ca^{2+} currents from α-neurexin triple knock-out mice and control animals are shown in Figure 9, A_1 and $9B_1$. *I–V* relations show maxima at 0 mV (Fig. $9A_2$,$9B_2$), and averaged peak current densities were 18.6 ± 0.7 pA/pF in control (Fig. $9A_3$) as compared with 6.3 ± 0.2 pA/pF in knock-out mice (Fig. $9B_3$), validating with an independent set of experiments our previous finding of decreased VDCC-mediated Ca^{2+} currents in α-neurexin mutant mice (Missler et al., 2003; Zhang et al., 2005). Activation of the $GABA_B$ receptor by its specific agonist baclofen reduced the amplitude of Ca^{2+} currents in all neurons (Fig. 9*A*,*B*). However, although the averaged current density in control neurons was reduced by almost 60%, from 18.9 ± 0.7 to 8.0 ± 0.3 pA/pF with the application of baclofen (Fig. $9A_3$), in α-neurexin mutant neurons the current density was diminished by only 30%, from 6.1 ± 0.2 to 4.8 ± 0.2 pA/pF (Fig. $9B_3$). To exclude that the sensitivity of $GABA_B$ receptors for agonist-binding was changed in knock-out neurons, we plotted the effect of the bath application of baclofen against time (Fig. 9*C*). Ca^{2+} currents were evoked by a depolarizing step from −70 to 0 mV every 5 s. Baclofen developed its maximal effect within 1 min in both control and mutant neurons (Fig. 9*C*) ($n = 5$ mice for each genotype), and longer incubation with baclofen for up to 20 min did not enhance the effect in α-neurexin-deficient cells ($n = 3$ mice) (data not shown), revealing that the time course was similar in all of the genotypes that were tested. In addition, increasing baclofen concentration from 1 to 30 μM produced a similar dose–response relationship in both control ($n = 5$) and knock-out mice ($n = 5$) (Fig. 9*D*). The IC_{50} was determined as 2.4 μM in control and 4.2 μM in mutant neurons by fitting the data with the Hill equation, and baclofen concentrations higher than 30 μM did not cause any additional inhibition of Ca^{2+} currents (Fig. 9*D*). To test whether the difference in response to baclofen is attributable to changed expression of $GABA_B$ receptors in mutant brains, we used quantitative immunoblotting of $GABA_B$ receptor 1a and 1b subunits (Santa Cruz Biotechnology, Santa Cruz, CA) with ^{125}I-labeled secondary antibodies and PhosphoImager detection essentially as described (Kattenstroth et al., 2004). No differences were observed in brain and slice culture homogenates of control and triple knock-out mice (data not shown). Our results demonstrate that the deletion of α-neurexin genes abolishes $GABA_B$ receptor-mediated modulation of Ca^{2+} currents and may indicate an involvement of α-neurexin in anchoring and/or positioning of VDCCs close to receptor molecules such as $GABA_B$ receptors and fusion-ready vesicles.

Discussion

We show here that α-neurexins play an important role in Ca^{2+}-dependent release from endocrine cells. Furthermore, our data indicate that α-neurexins may function by coupling Ca^{2+} channels to components of the release machinery rather than by regulating Ca^{2+} channel activity directly.

α-Neurexins are general players in Ca^{2+}-triggered release

Neurexins were identified as a family of neuronal transmembrane proteins (Ushkaryov et al., 1992, 1994). Because of their

Table 4. Analysis of the effect of α-neurexins on $Ca_V2.2$ calcium channels in heterologous cells: tsA201 cells transiently transfected with $Ca_V2.2$ subunits and Nrxn1α or control

	20 mM Ba^{2+}			10 mM Ca^{2+}		
Charge carrier	Control	Nrxn 1α	*p* value	Control	Nrxn 1α	*p* value
Activation	$n = 23$	$n = 26$		$n = 25$	$n = 21$	
$V_{1/2\ act}$ (mV)	10.36 ± 0.76	9.55 ± 0.89	0.51	18.55 ± 0.59	15.97 ± 0.93	0.02
k_{act} (mV)	5.08 ± 0.22	5.07 ± 0.22	0.98	5.17 ± 0.17	5.11 ± 0.24	0.83
E_{rev} (mV)	59.18 ± 0.92	58.70 ± 0.93	0.71	68.28 ± 0.78	67.18 ± 0.71	0.31
G_{max} (nS)	11.83 ± 1.69	11.20 ± 1.38	0.77	9.55 ± 1.57	9.30 ± 1.86	0.92
Inactivation	$n = 19$	$n = 19$		$n = 17$	$n = 17$	
$V_{1/2\ inact}$ (mV)	−60.70 ± 1.92	−63.62 ± 2.28	0.33	−52.38 ± 2.09	−51.01 ± 1.99	0.64
k_{inact} (mV)	12.26 ± 0.86	13.49 ± 0.51	0.23	13.75 ± 0.54	14.24 ± 0.38	0.47

Data are means ± SEM. *n* = number of cells analyzed from at least three different transfections. Statistical analysis was done using Prism Software (GraphPad Software).

polymorphic structure and presumably synaptic localization, neurexins were proposed as synaptic cell adhesion molecules (Missler and Sudhof, 1998). Therefore, the discovery of an essential role for α-neurexins in synapse function rather than synapse formation came as a surprise (Missler et al., 2003). To reconcile their molecular composition with the finding of impaired synaptic transmission in knock-outs, we suggested that α-neurexins link synaptic cell adhesion to the organization of the release machinery (Missler et al., 2003).

We now studied endocrine release in α-neurexin knock-outs, using recordings from melanotrophs in an acute slice preparation of the pituitary gland, because melanotrophs provide a homogenous population of cells and release from these cells is coupled tightly to several Ca^{2+} channel subtypes (Mansvelder and Kits, 2000; Sedej et al., 2004), resembling many central synapses. The recordings from an acute slice are advantageous, because the slice shows a stronger stimulus–release coupling than cultured melanotrophs (Thomas et al., 1993a; Parsons et al., 1995; Mansvelder and Kits, 2000; Sedej et al., 2004, 2005). In addition to the physiological activation by VDCCs, the acute slice allows us to investigate perinatal tissue (Sedej et al., 2004) (Fig. 4) and to assess simultaneously both endocrine secretion (Figs. 3–6) and synaptic release function (Fig. 7).

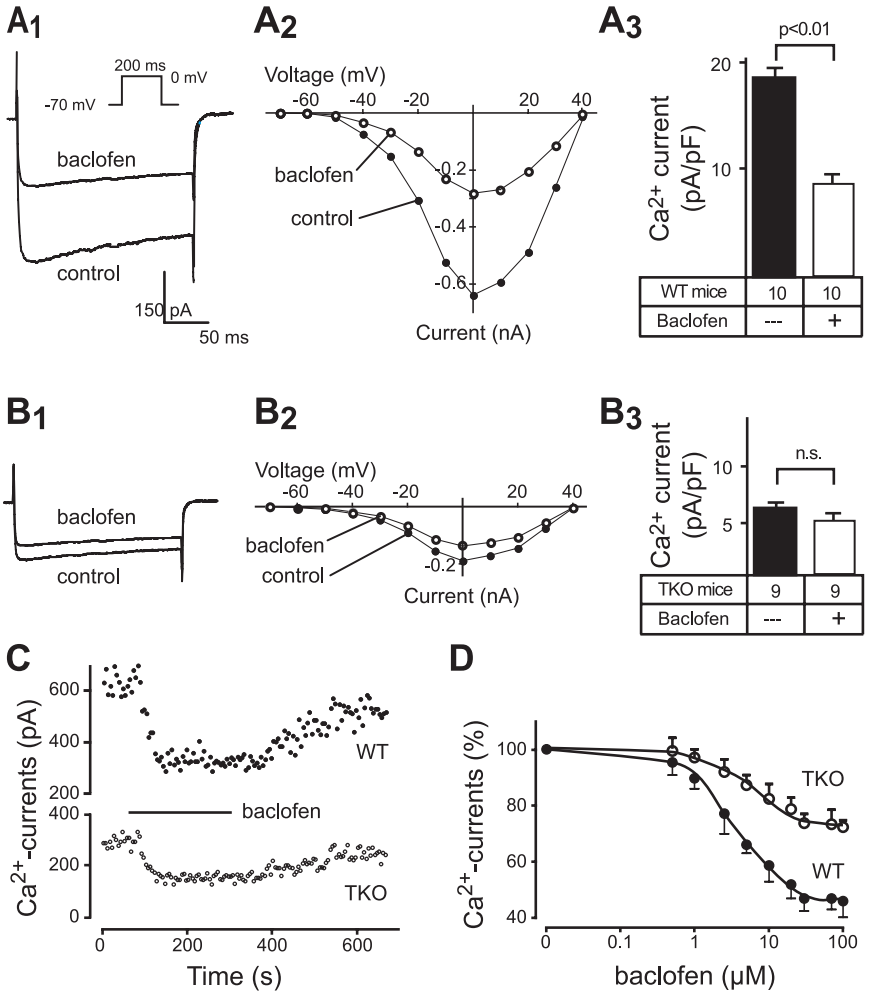

Figure 9. $GABA_B$ receptor modulation of Ca^{2+} currents is impaired in α-neurexin mutant mice. ***A***, ***B***, Ca^{2+} currents were recorded before and after the addition of 30 μM baclofen from brainstem neurons of newborn control (***A***; WT) and α-neurexin triple knock-out mice (***B***; TKO). Representative current traces (***A_1***, ***B_1***), current–voltage relationships (***A_2***, ***B_2***), and quantitated peak current densities (***A_3***, ***B_3***) show a decrease of Ca^{2+} currents in the presence of baclofen in control neurons, but not in mutant neurons. ***C***, Peak amplitude of high voltage-activated Ca^{2+} currents in response to 30 μM baclofen plotted against time in control (WT) and α-neurexin knock-out mice (TKO), demonstrating similar onset within <30 s. ***D***, Dose–response curve showing the concentration-dependent effect of baclofen in control (WT; $IC_{50} = 2.4$ μM; $n = 5$ mice) and α-neurexin knock-outs (TKO; $IC_{50} = 4.2$ μM; $n = 5$). Data are represented as the mean ± SEM. Level of statistical significance is indicated above the bars; n.s., not significant.

Although many components of the synaptic release machinery perform similar functions in (neuro)endocrine cells, only a few molecules reveal dramatic effects on both types of exocytosis when deleted. The vesicle protein synaptotagmin 1 is essential as the Ca^{2+} sensor of fast release, as demonstrated in hippocampal neurons (Geppert et al., 1994; Fernandez-Chacon et al., 2001) and endocrine cells (Voets et al., 2001b; Kreft et al., 2003). In the fusion complex the essential contribution of the soluble *N*-ethylmaleimide-sensitive factor attachment protein (SNAP) receptor (SNARE) proteins syntaxin, SNAP25, and synaptobrevin has been demonstrated in neurons by cleavage studies (Sakaba et al., 2005) and also in endocrine cells (Rupnik et al., 2000; Sorensen et al., 2003). Deletion of Munc18 protein silenced neurotransmission (Verhage et al., 2000) and reduced large dense-core vesicle release (Voets et al., 2001a). We now show a contribution of α-neurexins to release from melanotrophs, add-

ing them to the proteins that significantly affect Ca^{2+}-triggered exocytosis of both synaptic vesicles and secretory granules.

Our data on impaired exocytosis from mutant melanotrophs indicate that α-neurexins, putative synaptic cell adhesion molecules, influence secretion in cells that have no precisely organized active zones and no postsynaptic partners. Deletion of another adhesion molecule, neural cell adhesion molecule (NCAM), causes a secretory deficit in chromaffin cells (Chan et al., 2005) in addition to alterations of transmitter release (Rafuse et al., 2000; Polo-Parada et al., 2001, 2004) and impaired synaptic plasticity (Muller et al., 1996; Cremer et al., 1998). Both NCAM and N-cadherin were shown to affect secretion of growth hormone, because homophilic adhesion stimulated hormone release in cultured pituitary cells (Rubinek et al., 2003).

The relation between α-neurexins and Ca^{2+} channels

VDCCs mediate the presynaptic influx of Ca^{2+}, which triggers release, and may be connected physically to adaptor proteins (Maximov et al., 1999; Atlas, 2001; Coppola et al., 2001; Hibino et al., 2002) or components of the fusion complex (Bezprozvanny et al., 1995; Rettig et al., 1996; Zhong et al., 1999). VDCCs involved in presynaptic Ca^{2+} entry are usually of the N- and P/Q-type (Dunlap et al., 1995; Wu et al., 1999), but R- and L-type channels may be involved at synapses (Jensen and Mody, 2001; Dietrich et al., 2003) and in endocrine cells (Elhamdani et al., 1998; Mansvelder and Kits, 2000; Brandt, et al., 2003; Sedej et al., 2004). Because of the high Ca^{2+} cooperativity and Ca^{2+} sensitivity of release (Bollmann et al., 2000; Schneggenburger and Neher, 2000; Becherer et al., 2003) the regulation of VDCCs could have a great impact on synaptic strength, because little changes in Ca^{2+} influx lead to substantial effects on release.

Several lines of evidence indicate that the effect of α-neurexins on release of neurotransmitters involves the regulation of VDCCs: (1) the addition of Ca^{2+} channel inhibitors such as ω-conotoxin and agatoxin did not block synaptic transmission prominently in neocortical and brainstem knock-out neurons (Missler et al., 2003), (2) smaller whole-cell Ca^{2+} current peak amplitudes were observed in mutant brainstem neurons (Missler et al., 2003), (3) the effect of α-neurexins on neurotransmission specifically involved N-type ($Ca_V2.2$) and P/Q-type ($Ca_V2.1$) Ca^{2+} channels (Zhang et al., 2005), and (4) the synaptic homeostasis at neuromuscular junctions that is believed to require VDCCs was defective in the absence of α-neurexins (Sons et al., 2006). Our current study on endocrine release yielded additional support for an involvement of VDCCs because (5) a small shift in the voltage dependence of Ca^{2+} currents was present in mutant melanotrophs (Fig. 6*F*), (6) a corresponding shift in the half-activation potential was found in heterologous cells coexpressing VDCCs and α-neurexin (Table 4), and (7) $GABA_B$ receptor G-protein-mediated regulation of Ca^{2+} channels was impaired in α-neurexin knock-outs (Fig. 9). These findings raise the question of what property of VDCC function is regulated by α-neurexins?

First, we addressed the possibility that α-neurexins directly affect the biophysical properties of VDCCs such as activation or inactivation parameters. Several factors facilitate or inhibit VDCC-mediated currents, such as the $[Ca^{2+}]_i$ concentration itself (Budde et al., 2002), several EF-hand proteins (Weiss and Burgoyne, 2002), G-protein-coupled receptors (Herlitze et al., 1996; Zamponi and Snutch, 1998), components of the exocytotic machinery (Catterall, 1999; Atlas, 2001), or even lipid bilayer components (Wu et al., 2002). Unlike these regulations that could be demonstrated reliably in heterologous cell systems similar to the one used here (Fig. 8) (also, supplemental Figs. 6, 7, available at www.jneurosci.org as supplemental material), α-neurexin expressed in HEK293 cells alone or in combination with CASK and Mint1 did not affect the Ca^{2+} current parameters prominently when coexpressed with VDCCs (Table 3). Because the effect on the half-activation potential appears to be too small to explain the mostly reduced release and because the knock-out phenotype for α-neurexin is much stronger than those for many of the established VDCC regulators discussed above, it is unlikely that α-neurexins function by modulating VDCC-mediated currents directly. This conclusion is consistent with the finding that transgenic α-neurexin could rescue the phenotype when expressed in knock-out animals but did not enhance Ca^{2+} current density in wild-type neurons (Zhang et al., 2005). Although we did not observe prominent changes in whole-cell Ca^{2+} currents in melanotrophs, the reduction of whole-cell Ca^{2+} current amplitudes in mutant brainstem neurons is not an artifact, because the changes are robust and were validated in three independent sets of experiments (Missler et al., 2003; Zhang et al., 2005) (Fig. 7). According to our present data these lower somatodendritic Ca^{2+} currents represent a consequence of homeostatic reactions in α-neurexin knock-out mice. It is otherwise difficult to conceive how presynaptic α-neurexins could influence whole-cell Ca^{2+} current density, which is contributed mainly by somatodendritic Ca^{2+} channels.

The second possible explanation for an involvement of VDCCs is that the deletion of α-neurexins leads to an uncoupling between Ca^{2+} channels and components of the release machinery. α-Neurexins may be responsible, for example, for anchoring Ca^{2+} channels within the active zone close to releasable vesicles. Such a proximity is important, because the increase in $[Ca^{2+}]_i$ after action potentials is brief and spatially restricted (Meinrenken et al., 2002); consequently, the delay between Ca^{2+} influx and vesicle fusion is very short (Simon and Llinas, 1985; Borst and Sakmann, 1996). According to this concept of Ca^{2+} microdomains, any alterations in the positioning and/or coupling of VDCCs to vesicles would produce great effects on exocytosis. In our analyses of α-neurexin knock-out mice the reduced sensitivity of release to specific Ca^{2+} channel blockers, the predominantly affected N-type ($Ca_V2.2$) and P/Q-type ($Ca_V2.1$) Ca^{2+} channels, the inefficient Ca^{2+}-dependent upregulation of release at neuromuscular junctions with the blockage of postsynaptic receptors, and the impaired regulation by $GABA_B$ receptors all could be explained by such a mechanism. VDCCs could be targeted or anchored by α-neurexins via binding partners such CASK and Mints that associate with both α- and β-neurexins (Hata et al., 1996; Butz et al., 1998; Biederer and Sudhof, 2000). Because CASK and Mint also bind to intracellular sequences of recombinant N-type Ca^{2+} channel subunit α1B (Maximov et al., 1999; Maximov and Bezprozvanny, 2002), this complex represents a candidate to anchor VDCCs and neurexins at the active zone. Future studies will have to explore the molecular interactions that actually link α-neurexins to VDCCs and will have to address directly the targeting of different VDCCs at normal and α-neurexin mutant synapses.

References

Angenstein F, Niessen HG, Goldschmidt J, Lison H, Altrock WD, Gundelfinger ED, Scheich H (2006) Manganese-enhanced MRI reveals structural and functional changes in the cortex of bassoon mutant mice. Cereb Cortex, in press.

Atlas D (2001) Functional and physical coupling of voltage-sensitive calcium channels with exocytotic proteins: ramifications for the secretion mechanism. J Neurochem 77:972–985.

Basarsky TA, Parpura V, Haydon PG (1994) Hippocampal synaptogenesis

in cell culture: developmental time course of synapse formation, calcium influx, and synaptic protein distribution. J Neurosci 14:6402–6411.

Becherer U, Moser T, Stuhmer W, Oheim M (2003) Calcium regulates exocytosis at the level of single vesicles. Nat Neurosci 6:846–853.

Bezprozvanny I, Scheller RH, Tsien RW (1995) Functional impact of syntaxin on gating of N-type and Q-type calcium channels. Nature 378:623–626.

Biederer T, Sudhof TC (2000) Mints as adaptors. Direct binding to neurexins and recruitment of munc18. J Biol Chem 275:39803–39806.

Biederer T, Sudhof TC (2001) CASK and protein 4.1 support F-actin nucleation on neurexins. J Biol Chem 276:47869–47876.

Bollmann JH, Sakmann B, Borst JG (2000) Calcium sensitivity of glutamate release in a calyx-type terminal. Science 289:953–957.

Borst JG, Sakmann B (1996) Calcium influx and transmitter release in a fast CNS synapse. Nature 383:431–434.

Boucard AA, Chubykin AA, Comoletti D, Taylor P, Sudhof TC (2005) A splice code for *trans*-synaptic cell adhesion mediated by binding of neuroligin 1 to α- and β-neurexins. Neuron 48:229–236.

Brandt A, Striessnig J, Moser T (2003) $Ca_V1.3$ channels are essential for development and presynaptic activity of cochlear inner hair cells. J Neurosci 23:10832–10840.

Budde T, Meuth S, Pape HC (2002) Calcium-dependent inactivation of neuronal calcium channels. Nat Rev Neurosci 3:873–883.

Butz S, Okamoto M, Sudhof TC (1998) A tripartite protein complex with the potential to couple synaptic vesicle exocytosis to cell adhesion in brain. Cell 94:773–782.

Cao YQ, Tsien RW (2005) Effects of familial hemiplegic migraine type 1 mutations on neuronal P/Q-type Ca^{2+} channel activity and inhibitory synaptic transmission. Proc Natl Acad Sci USA 102:2590–2595.

Cao YQ, Piedras-Renteria ES, Smith GB, Chen G, Harata NC, Tsien RW (2004) Presynaptic Ca^{2+} channels compete for channel type-preferring slots in altered neurotransmission arising from Ca^{2+} channelopathy. Neuron 43:387–400.

Catterall WA (1999) Interactions of presynaptic Ca^{2+} channels and SNARE proteins in neurotransmitter release. Ann NY Acad Sci 868:144–159.

Chan SA, Polo-Parada L, Landmesser LT, Smith C (2005) Adrenal chromaffin cells exhibit impaired granule trafficking in NCAM knock-out mice. J Neurophysiol 94:1037–1047.

Chronwall B, Hook GR, Millington WR (1988) Dopaminergic regulation of the biosynthetic activity of individual melanotropes in the rat pituitary intermediate lobe: a morphometric analysis by light and electron microscopy and *in situ* hybridization. Endocrinology 123:1992–2002.

Coppola T, Magnin-Luthi S, Perret-Menoud V, Gattesco S, Schiavo G, Regazzi R (2001) Direct interaction of the Rab3 effector RIM with Ca^{2+} channels, SNAP-25, and synaptotagmin. J Biol Chem 276:32756–32762.

Cremer H, Chazal G, Carleton A, Goridis C, Vincent JD, Lledo PM (1998) Long-term but not short-term plasticity at mossy fiber synapses is impaired in neural cell adhesion molecule-deficient mice. Proc Natl Acad Sci USA 95:13242–13247.

Dietrich D, Kirschstein T, Kukley M, Pereverzev A, von der Brelie C, Schneider T, Beck H (2003) Functional specialization of presynaptic $Ca_V2.3$ Ca^{2+} channels. Neuron 39:483–496.

Dunlap K, Luebke JI, Turner TJ (1995) Exocytotic Ca^{2+} channels in mammalian central neurons. Trends Neurosci 18:89–98.

Elhamdani A, Zhou Z, Artalejo CR (1998) Timing of dense-core vesicle exocytosis depends on the facilitation L-type Ca channel in adrenal chromaffin cells. J Neurosci 18:6230–6240.

Fass DM, Takimoto K, Mains RE, Levitan ES (1999) Tonic dopamine inhibition of L-type Ca^{2+} channel activity reduces α1D Ca^{2+} channel gene expression. J Neurosci 19:3345–3352.

Fernandez-Chacon R, Konigstorfer A, Gerber SH, Garcia J, Matos MF, Stevens CF, Brose N, Rizo J, Rosenmund C, Sudhof TC (2001) Synaptotagmin I functions as a calcium regulator of release probability. Nature 410:41–49.

Geppert M, Goda Y, Hammer RE, Li C, Rosahl TW, Stevens CF, Sudhof TC (1994) Synaptotagmin I: a major Ca^{2+} sensor for transmitter release at a central synapse. Cell 79:717–727.

Geppert M, Khvotchev M, Krasnoperov V, Goda Y, Missler M, Hammer RE, Ichtchenko K, Petrenko AG, Sudhof TC (1998) Neurexin Iα is a major α-latrotoxin receptor that cooperates in α-latrotoxin action. J Biol Chem 273:1705–1710.

Gillis KD, Mossner R, Neher E (1996) Protein kinase C enhances exocytosis from chromaffin cells by increasing the size of the readily releasable pool of secretory granules. Neuron 16:1209–1220.

Gomora JC, Avila G, Cota G (1996) Ca^{2+} current expression in pituitary melanotrophs of neonatal rats and its regulation by D2 dopamine receptors. J Physiol (Lond) 492:763–773.

Graf ER, Zhang X, Jin SX, Linhoff MW, Craig AM (2004) Neurexins induce differentiation of GABA and glutamate postsynaptic specializations via neuroligins. Cell 119:1013–1026.

Hata Y, Butz S, Sudhof TC (1996) CASK: a novel dlg/PSD95 homolog with an N-terminal calmodulin-dependent protein kinase domain identified by interaction with neurexins. J Neurosci 16:2488–2494.

Herlitze S, Garcia DE, Mackie K, Hille B, Scheuer T, Catterall WA (1996) Modulation of Ca^{2+} channels by G-protein beta gamma subunits. Nature 380:258–262.

Hibino H, Pironkova R, Onwumere O, Vologodskaia M, Hudspeth AJ, Lesage F (2002) RIM binding proteins (RBPs) couple Rab3-interacting molecules (RIMs) to voltage-gated Ca^{2+} channels. Neuron 34:411–423.

Horrigan FT, Bookman RJ (1994) Releasable pools and the kinetics of exocytosis in adrenal chromaffin cells. Neuron 13:1119–1129.

Ichtchenko K, Hata Y, Nguyen T, Ullrich B, Missler M, Moomaw C, Sudhof TC (1995) Neuroligin 1: a splice site-specific ligand for beta-neurexins. Cell 81:435–443.

Jensen K, Mody I (2001) L-type Ca^{2+} channel-mediated short-term plasticity of GABAergic synapses. Nat Neurosci 4:975–976.

Kattenstroth G, Tantalaki E, Sudhof TC, Gottmann K, Missler M (2004) Postsynaptic *N*-methyl-D-aspartate receptor function requires α-neurexins. Proc Natl Acad Sci USA 101:2607–2612.

Klingauf J, Neher E (1997) Modeling buffered Ca^{2+} diffusion near the membrane: implications for secretion in neuroendocrine cells. Biophys J 72:674–690.

Kocmur L, Zorec R (1993) A new approach to separation of voltage-activated Ca currents in rat melanotrophs. Pflügers Arch 425:172–174.

Kreft M, Kuster V, Grilc S, Rupnik M, Milisav I, Zorec R (2003) Synaptotagmin I increases the probability of vesicle fusion at low $[Ca^{2+}]$ in pituitary cells. Am J Physiol Cell Physiol 284:C547–C554.

Makarenko IG, Ugrumov MV, Calas A (2005) Axonal projections from the hypothalamus to the pituitary intermediate lobe in rats during ontogenesis: DiI tracing study. Brain Res Dev Brain Res 155:117–126.

Mansvelder HD, Kits KS (2000) Calcium channels and the release of large dense-core vesicles from neuroendocrine cells: spatial organization and functional coupling. Prog Neurobiol 62:427–441.

Matthews G (1996) Neurotransmitter release. Annu Rev Neurosci 19:219–233.

Maximov A, Bezprozvanny I (2002) Synaptic targeting of N-type calcium channels in hippocampal neurons. J Neurosci 22:6939–6952.

Maximov A, Sudhof TC, Bezprozvanny I (1999) Association of neuronal calcium channels with modular adaptor proteins. J Biol Chem 274:24453–24456.

Meinrenken CJ, Borst JG, Sakmann B (2002) Calcium secretion coupling at calyx of Held governed by nonuniform channel–vesicle topography. J Neurosci 22:1648–1667.

Missler M, Sudhof TC (1998) Neurexins: three genes and 1001 products. Trends Genet 14:20–26.

Missler M, Fernandez-Chacon R, Sudhof TC (1998a) The making of neurexins. J Neurochem 71:1339–1347.

Missler M, Hammer RE, Sudhof TC (1998b) Neurexophilin binding to alpha-neurexins. A single LNS domain functions as an independently folding ligand-binding unit. J Biol Chem 273:34716–34723.

Missler M, Zhang W, Rohlmann A, Kattenstroth G, Hammer RE, Gottmann K, Sudhof TC (2003) Alpha-neurexins couple Ca^{2+} channels to synaptic vesicle exocytosis. Nature 423:939–948.

Moser T, Neher E (1997) Rapid exocytosis in single chromaffin cells recorded from mouse adrenal slices. J Neurosci 17:2314–2323.

Muller D, Wang C, Skibo G, Toni N, Cremer H, Calaora V, Rougon G, Kiss JZ (1996) PSA-NCAM is required for activity-induced synaptic plasticity. Neuron 17:413–422.

Neher E (1998) Vesicle pools and Ca^{2+} microdomains: new tools for understanding their roles in neurotransmitter release. Neuron 20:389–399.

Parsons TD, Coorssen JR, Horstmann H, Almers W (1995) Docked granules, the exocytotic burst, and the need for ATP hydrolysis in endocrine cells. Neuron 15:1085–1096.

Pfrieger FW, Gottmann K, Lux HD (1994) Kinetics of $GABA_B$ receptor-

mediated inhibition of calcium currents and excitatory synaptic transmission in hippocampal neurons *in vitro*. Neuron 12:97–107.

Polo-Parada L, Bose CM, Landmesser LT (2001) Alterations in transmission, vesicle dynamics, and transmitter release machinery at NCAM-deficient neuromuscular junctions. Neuron 32:815–828.

Polo-Parada L, Bose CM, Plattner F, Landmesser LT (2004) Distinct roles of different neural cell adhesion molecule (NCAM) isoforms in synaptic maturation revealed by analysis of NCAM 180 kDa isoform-deficient mice. J Neurosci 24:1852–1864.

Purisai MG, Sands SA, Davis TD, Price JL, Chronwall BM (2005) $GABA_B$ receptor subunit mRNAs are differentially regulated in pituitary melanotropes during development, and detection of functioning receptors coincides with completion of innervation. Int J Dev Neurosci 23:315–326.

Rafuse VF, Polo-Parada L, Landmesser LT (2000) Structural and functional alterations of neuromuscular junctions in NCAM-deficient mice. J Neurosci 20:6529–6539.

Rettig J, Neher E (2002) Emerging roles of presynaptic proteins in Ca^{2+}-triggered exocytosis. Science 298:781–785.

Rettig J, Sheng ZH, Kim DK, Hodson CD, Snutch TP, Catterall WA (1996) Isoform-specific interaction of the alpha1A subunits of brain Ca^{2+} channels with the presynaptic proteins syntaxin and SNAP-25. Proc Natl Acad Sci USA 93:7363–7368.

Rowen L, Young J, Birditt B, Kaur A, Madan A, Philipps DL, Qin S, Minx P, Wilson RK, Hood L, Graveley BR (2002) Analysis of the human neurexin genes: alternative splicing and the generation of protein diversity. Genomics 79:587–597.

Rubinek T, Yu R, Hadani M, Barkai G, Nass D, Melmed S, Shimon I (2003) The cell adhesion molecules N-cadherin and neural cell adhesion molecule regulate human growth hormone: a novel mechanism for regulating pituitary hormone secretion. J Clin Endocrinol Metab 88:3724–3730.

Rupnik M, Kreft M, Sikdar SK, Grilc S, Romih R, Zupancic G, Martin TFJ, Zorec R (2000) Rapid regulated dense-core vesicle exocytosis requires the CAPS protein. Proc Natl Acad Sci USA 97:5627–5632.

Sakaba T, Stein A, Jahn R, Neher E (2005) Distinct kinetic changes in neurotransmitter release after SNARE protein cleavage. Science 309:491–494.

Schneggenburger R, Konnerth A (1992) GABA-mediated synaptic transmission in neuroendocrine cells: a patch-clamp study in a pituitary slice preparation. Pflügers Arch 421:364–373.

Schneggenburger R, Neher E (2000) Intracellular calcium dependence of transmitter release rates at a fast central synapse. Nature 406:889–893.

Sedej S, Tsujimoto T, Zorec R, Rupnik M (2004) Voltage-activated Ca^{2+} channels and their role in the endocrine function of the pituitary gland in newborn and adult mice. J Physiol (Lond) 555:769–782.

Sedej S, Rose T, Rupnik M (2005) cAMP increases Ca^{2+}-dependent exocytosis through both PKA and Epac2 in mouse melanotrophs from pituitary tissue slices. J Physiol (Lond) 567:799–813.

Simon SM, Llinas RR (1985) Compartmentalization of the submembrane calcium activity during calcium influx and its significance in transmitter release. Biophys J 48:485–498.

Sons MS, Busche N, Strenzke N, Moser T, Ernsberger U, Mooren FC, Zhang W, Ahmad M, Steffens H, Schomburg ED, Plomp JJ, Missler M (2006) Alpha-neurexins are required for efficient transmitter release and synaptic homeostasis at the mouse neuromuscular junction. Neuroscience 138:433–446.

Sorensen JB, Nagy G, Varoqueaux F, Nehring RB, Brose N, Wilson MC, Neher E (2003) Differential control of the releasable vesicle pools by SNAP-25 splice variants and SNAP-23. Cell 114:75–86.

Sudhof TC (2004) The synaptic vesicle cycle. Annu Rev Neurosci 27:509–547.

Sugita S, Khvochtev M, Sudhof TC (1999) Neurexins are functional alpha-latrotoxin receptors. Neuron 22:489–496.

Sugita S, Saito F, Tang J, Satz J, Campbell K, Sudhof TC (2001) A stoichiometric complex of neurexins and dystroglycan in brain. J Cell Biol 154:435–445.

Tabuchi K, Sudhof TC (2002) Structure and evolution of neurexin genes: insight into the mechanism of alternative splicing. Genomics 79:849–859.

Thomas P, Wong JG, Almers W (1993a) Millisecond studies of secretion in single rat pituitary cells stimulated by flash photolysis of caged Ca^{2+}. EMBO J 12:303–306.

Thomas P, Wong JG, Lee AK, Almers W (1993b) A low-affinity Ca^{2+} receptor controls the final steps in peptide secretion from pituitary melanotrophs. Neuron 11:93–104.

Tomiko SA, Taraskevich PS, Douglas WW (1983) GABA acts directly on cells of pituitary pars intermedia to alter hormone output. Nature 301:706–707.

Turner J-E, Sedej S, Rupnik M (2005) Cytosolic Cl^- ions in the regulation of secretory and endocytotic activity in melanotrophs from mouse pituitary tissue slices. J Physiol (Lond) 566:443–453.

Ushkaryov YA, Petrenko AG, Geppert M, Sudhof TC (1992) Neurexins: synaptic cell surface proteins related to the alpha-latrotoxin receptor and laminin. Science 257:50–56.

Ushkaryov YA, Hata Y, Ichtchenko K, Moomaw C, Afendis S, Slaughter CA, Sudhof TC (1994) Conserved domain structure of beta-neurexins. Unusual cleaved signal sequences in receptor-like neuronal cell-surface proteins. J Biol Chem 269:11987–11992.

Verhage M, Maia AS, Plomp JJ, Brussaard AB, Heeroma JH, Vermeer H, Toonen RF, Hammer RE, van den Berg TK, Missler M, Geuze HJ, Sudhof TC (2000) Synaptic assembly of the brain in the absence of neurotransmitter secretion. Science 287:864–869.

Voets T, Neher E, Moser T (1999) Mechanisms underlying phasic and sustained secretion in chromaffin cells from mouse adrenal slices. Neuron 23:607–615.

Voets T, Toonen RF, Brian EC, de Wit H, Moser T, Rettig J, Sudhof TC, Neher E, Verhage M (2001a) Munc18-1 promotes large dense-core vesicle docking. Neuron 31:581–591.

Voets T, Moser T, Lund PE, Chow RH, Geppert M, Sudhof TC, Neher E (2001b) Intracellular calcium dependence of large dense-core vesicle exocytosis in the absence of synaptotagmin I. Proc Natl Acad Sci USA 98:11680–11685.

Weiss JL, Burgoyne RD (2002) Sense and sensibility in the regulation of voltage-gated Ca^{2+} channels. Trends Neurosci 25:489–491.

Wu L, Bauer CS, Zhen XG, Xie C, Yang J (2002) Dual regulation of voltage-gated calcium channels by PtdIns(4,5)P_2. Nature 419:947–952.

Wu LG, Westenbroek RE, Borst JG, Catterall WA, Sakmann B (1999) Calcium channel types with distinct presynaptic localization couple differentially to transmitter release in single calyx-type synapses. J Neurosci 19:726–736.

Zamponi GW, Snutch TP (1998) Modulation of voltage-dependent calcium channels by G-proteins. Curr Opin Neurobiol 8:351–356.

Zhang W, Elsen F, Barnbrock A, Richter DW (1999) Postnatal development of $GABA_B$ receptor-mediated modulation of voltage-activated Ca^{2+} currents in mouse brainstem neurons. Eur J Neurosci 11:2332–2342.

Zhang W, Rohlmann A, Sargsyan V, Aramuni G, Hammer RE, Sudhof TC, Missler M (2005) Extracellular domains of α-neurexins participate in regulating synaptic transmission by selectively affecting N- and P/Q-type Ca^{2+} channels. J Neurosci 25:4330–4342.

Zhong H, Yokoyama CT, Scheuer T, Catterall WA (1999) Reciprocal regulation of P/Q-type Ca^{2+} channels by SNAP-25, syntaxin, and synaptotagmin. Nat Neurosci 2:939–941.

Zupancic G, Kocmur L, Veranic P, Grilc S, Kordas M, Zorec R (1994) The separation of exocytosis from endocytosis in rat melanotroph membrane capacitance records. J Physiol (Lond) 480:539–552.